Exploring strategies to improve the reverse β-oxidation pathway in *Saccharomyces cerevisiae*

Dissertation

zur Erlangung des Doktorgrades

der Naturwissenschaften

Vorgelegt beim Fachbereich Biowissenschaften

der Johann Wolfgang Goethe-Universität

in Frankfurt am Main

von

John Fernando Garcés Daza

Aus Cali, Kolumbien

Frankfurt am Main, 2024

(D 30)

Vom Fachbereich Biowissenschaften
der Johann Wolfgang Goethe-Universität
als Dissertation angenommen.

Dekan:	Dr. Sven Klimpel
Gutacher:	Prof. Dr. Eckhard Boles Prof. Dr. Martin Grininger
Datum der Disputation:	

To my parents and my sister:

One more step in this beautiful adventure.

Contents

1 Summary

Microbes are the most diverse living organisms on Earth, with various metabolic adaptations that allow them to live in different conditions and produce compounds with different chemical complexity. Microbial biotechnology exploits the metabolic diversity of microorganisms to manufacture products for different industries. Today, the chemical industry is a significant energy consumer and carbon dioxide emitter, with processes that harm natural ecosystems, like the extraction of medium-chain fatty acids (MCFAs). MCFAs are used as precursors for biofuels, volatile esters, surfactants, or polymers in materials with enhanced properties. However, their current extraction process uses large, non-sustainable monocultures of coconut and palm trees. Therefore, the microbial production of MCFAs can help reduce the current environmental impact of obtaining these products and their derivatives.

In nature, fatty acids are mostly produced via fatty acid biosynthesis (FAB). However, the reverse β-oxidation (rBOX) is a more energy-efficient pathway compared to FAB. The rBOX pathway consists of four reactions, which result in the elongation of an acyl-CoA molecule by two carbon units from acetyl-CoA in each cycle. In this work we used *Saccharomyces cerevisiae*, an organism with a high tolerance towards toxic compounds, as the expression host of the rBOX pathway to produce MCFAs and medium-chain fatty alcohols (MCFOHs).

In the first part of this work, we expanded the length of the products from expressing the rBOX in the cytosol and increased the MCFAs titres. First, we deleted the major glycerol-3-phosphate dehydrogenase (*GPD2*). This resulted in a platform strain with significantly reduced glycerol fermentation and increased rBOX pathway activity, probably due to an increased availability of NADH. Then, we tested different combinations of rBOX enzymes to increase the length and titres of MCFA. Expressing the thiolase ^{Cn}*bktB* and β-hydroxyacyl-CoA dehydrogenase ^{Cn}*paaH1* from *Cupriavidus necator*, ^{Ca}*crt* from *Clostridium acetobutylicum* and the trans-enoyl-CoA reductase ^{Td}*ter* (*Treponema denticola*) resulted in hexanoic acid as the main product. Expressing ^{Cn}*crt2* (*C. necator*) or ^{Yl}*ECH* (*Y. lipolytica*) as enoyl-CoA hydratases resulted in octanoic acid as the main product. Then, we integrated the octanoic (^{Cn}*crt2* or ^{Yl}*ECH*) and the hexanoic acid (^{Ca}*crt*)-producing variants in the genome of the platform strain and we achieved titers of ≈75 mg/L (hexanoic acid) and ≈ 60 mg/L (octanoic acid) when growing these strains in a complex, highly buffered medium. These are the highest titers of octanoic and hexanoic acid obtained in *S. cerevisiae* with the rBOX. Additionally, we deleted *TES1* and *FAA2* to prevent competition for butyryl-CoA and degradation of the produced fatty acids, respectively. However, these deletions did not improve MCFA titers. In addition, we tested two dual acyl-CoA reductase/alcohol dehydrogenases (ACR/ADH), ^{Ca}*adhE2* from *C. acetobutylicum* and the putative ACR/ADH ^{Ec}*eutE* from *Escherichia coli*, in an octanoyl-CoA-producing strain to

produce MCFOH. As a result, we produced 1-hexanol and 1-octanol for the first time in *S. cerevisiae* with these two enzymes. Nonetheless, the titres were low (<10 mg/L and <2 mg/L, respectively), and four-carbon 1-butanol was the main product in both cases (>80 mg/L). This showed the preference of these two enzymes for butyryl-CoA.

In the second part of this work, we expressed the rBOX in the mitochondria of *S. cerevisiae* to benefit from the high levels of acetyl-CoA and the reducing environment in that organelle. First, in an *adh*-deficient strain, we mutated *MTH1*, a transcription factor regulating the expression of hexose transporters, and deleted *GPD2*. This resulted in a strain with a reduced Crabtree effect and, therefore, an increased carbon flux to the mitochondria. We partially validated the increased flux to the mitochondria by expressing the ethanol-acetyltransferase *EAT1* from *Kluyveromyces marxianus* in this organelle. This resulted in a higher isoamyl acetate production in the *MTH1*-mutant strain. Isoamyl acetate is synthesised by Eat1 from acetyl-CoA and isoamyl alcohol, a product of the metabolism of amino acids in the mitochondria. Then, we targeted different butyryl-CoA-producing rBOX variants to the mitochondria, and we used the production of 1-butanol and butyric acid as a proof-of-concept. The strong expression of all the enzymes was toxic for the cell, and the highest butyric acid titres (≈ 50 mg/L) in the mitochondria from the rBOX were obtained from the weak expression of the pathway. The highest 1-butanol titers (≈ 5 mg/L) were obtained with the downregulation of the mitochondrial NADH-oxidase *NDI1*. However, this downregulation led to a non-desirable *petite* phenotype.

In summary, we produced hexanoic and octanoic acid for the first time in *S. cerevisiae* using the rBOX and achieved the highest reported titers of hexanoic and octanoic acid so far using this pathway in *S. cerevisiae*. In addition, we successfully compartmentalised the rBOX in the mitochondria. However, competing reactions, some of them essential for the viability of the cell, limit the use of this organelle for the rBOX.

2 Introduction

2.1 Biotechnology: Impact in society

Biotechnology harnesses living organisms or their components to create or modify specific products and processes beneficial to humans. These products and processes span different sectors like food, pharmaceutical or chemical industries. Microbes are the most widely distributed and diverse living organisms on Earth (Kumar, Kumar et al. 2022), with a vast range of metabolic adaptations and metabolites that make them the preferred organisms in biotechnology.

Until the mid-20th century, microorganisms were used to produce solvents like acetone and butanol with *Clostridium acetobutylicum* (Lee, Park et al. 2008) or in the food industry for the production of, i.e. alcoholic beverages by yeast (Bokulich and Bamforth 2013), fermented dairy products by lactic acid bacteria or citric acid by the fungus *Aspergillus niger* (Ginsberg and Society 2008, Behera 2020). Then, during World War II, Pfizer used stirred-tank fermentation for the first time to produce an antibiotic, Penicillin from *Penicillium sp.* (Ginsberg and Society 2008), opening the door to the medical application of biotechnology. Until the 1970s, the biotechnological applications used unmodified microorganisms found in nature, limiting the range of products to those the microorganisms could provide. This situation changed with the development of recombinant DNA technology, which allowed the precise manipulation of genetic material, enabling the generation of non-native metabolic traits in desired organisms (Khan, Ullah et al. 2016). This technology expanded the use of microorganisms for medical applications beyond antibiotics. For instance, the recombinant human Insulin used today to treat diabetes is produced in the bacteria *Escherichia coli* (Baeshen, Baeshen et al. 2014), and the antigens used in vaccines against Hepatitis B virus and papillomavirus are synthesised in the yeast *Saccharomyces cerevisiae* (Zhao, Zhou et al. 2020, Srivastava, Nand et al. 2023). However, there are also more mundane microbe-derived biotechnology products in our daily lives. The detergent solution used to wash clothes contains microbial recombinant proteases (Vojcic, Pitzler et al. 2015). The lactase pill used by lactose-intolerants to digest foods that have this sugar contains β-galactosidase produced by yeast and fungi (Mahoney 1997, Leis, de Castro et al. 2020). Most of the vanillin in the vanillin extract used for baking comes from a fungal bioconversion (Gallage and Møller 2015). The poly-lactic acid (PLA) used in 3D printers for biomedical purposes derives from lactic acid, which is produced by yeast at large scale (Wehrs, Tanjore et al. 2019).

Microorganisms are widespread in the industrial production of high-value products like the ones mentioned above. However, they can also be a more sustainable platform for manufacturing lower value products like bulk chemicals and small molecules (Lynd, Laser et

al. 2008). The petrochemical industry typically produces these chemicals via chemical synthesis or by extraction processes that are harmful to the environment (Yan and Pfleger 2020). The complete transition to microbial production of bulk chemicals is currently hampered by low production yields and overall production costs, which need to be competitive (Van Dien 2013, Reboredo, Lidon et al. 2017, Nielsen, Tillegreen et al. 2022). Nevertheless, there are examples of successful bioproduction of bulk chemicals at an industrial scale, like 1,3-butanediol and 1,3-propanediol in *E. coli* (Nakamura and Whited 2003, Burgard, Burk et al. 2016), or ethanol and farnesene in *S. cerevisiae* (Meadows, Hawkins et al. 2016, Sarris and Papanikolaou 2016), among many others.

The growing awareness of our negative impact on the environment has resulted in increased regulation of the products and by-products of industrial processes (Wu, Huang et al. 2022, Kiessling, Hinzmann et al. 2023). However, the chemical industry continues to be the largest industrial energy consumer and the third-largest emitter of carbon dioxide (Levi and Cullen 2018). Therefore, it is essential to develop biotechnological processes to manufacture chemical industry products, particularly for those chemicals whose extraction is highly unsustainable, like medium-chain fatty acids (MCFAs) and alcohols (MCFOHs).

2.1.1 Medium-chain fatty acids and alcohols

Medium-chain fatty acids (MCFAs) and alcohols (MCFOHs) are six to ten hydrocarbon chain long carboxylic acids and alcohols, respectively, with applications in various sectors. In the food industry, MCFA-derived products like methyl hexanoate and ethyl hexanoate, both responsible for the characteristic fragrance of pineapples, are derived from hexanoic acid (Wei, Liu et al. 2011, Zheng, Sun et al. 2012). In polymers and material science, octanoic acid can be used to synthesize polyhydroxy octanoate (PHO), a polymer with rubber-like properties of industrial interest (Elbahloul and Steinbuchel 2009, Sofinska 2018), or in functional fibres to enhance properties like thermal storage and antibacterial capacity. In the transportation sector, increasing the fraction of certain MCFOH like 1-octanol and 1-decanol in biodiesel helps reduce fuel consumption and smoke emissions in diesel engines (Ashok, Nanthagopal et al. 2019, Vinodkumar and Karthikeyan 2022). In the cosmetic industry, MCFOHs are used as fragrance precursors (Akyalçın and Altıokka 2012), while in analytical chemistry, they are used as precursors for anionic surfactants like sodium octyl sulfate (Almgren and Rangelov 2004, Yazdabadi, Farrokhpour et al. 2021).

Today, MCFOHs are synthesized at an industrial scale via the catalytic hydrogenation of MCFAs (Fillet, Gibert et al. 2015). MCFAs are either produced chemically via the non-sustainable oligomerization of ethylene (Nanthagopal, Kishna et al. 2020) or extracted directly from palm or coconut tree seeds, where they represent up to 5 and 10 % of the fatty acid

content, respectively (Yan and Pfleger 2020, P.G Roosphashree 2022, Watanabe and Tsujino 2022). However, the extraction of these molecules and the growing demand for vegetable oils come at the price of increasing the extension of monoculture crops, which contributes to deforestation and severe loss in biodiversity (Meijaard, Abrams et al. 2020, Meijaard, Brooks et al. 2020, Zhu, Hu et al. 2020).

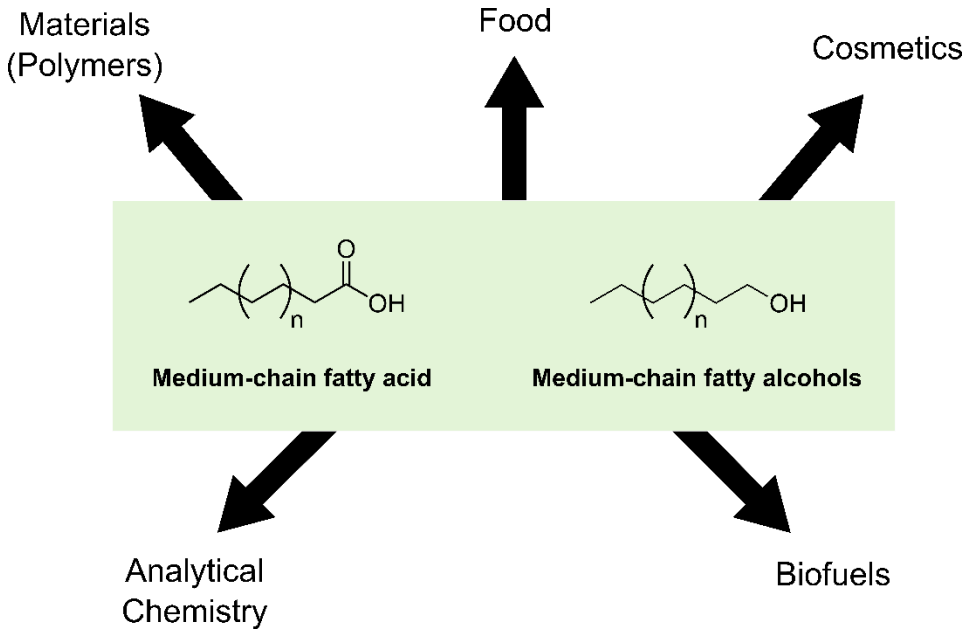

Figure 1. General chemical structures of saturated medium-chain fatty acids and alcohols and their industrial applications.

2.2 *S. cerevisiae* as platform organism in biotechnology

The baker's yeast *S. cerevisiae* is a 'generally recognised as safe' (GRAS) microorganism and one of the best-established microbes in biotechnology. Humans have used this yeast since before modern biotechnology, when it was mainly used for brewing and baking. Today, as mentioned above, *S. cerevisiae* is used at an industrial scale to produce high-value products like vaccines, drugs or antibacterial peptides and low-value products like ethanol.

S. cerevisiae ferments sugars to ethanol and carbon dioxide, a process known as alcoholic fermentation. In fact, the origin of its scientific name is related to this process: '*saccharo*' (sugar in Latin), '*myces*' (fungi in Latin) '*cerevisiae*' ('of beer' in Latin). Using isolated cultures of *S. cerevisiae* for beer brewing started during the second half of the 19th century (Frey 1930). Thus, the study of *S. cerevisiae* in fermentation tanks and the development of fermentation processes for this yeast have been going on for almost two centuries.

Furthermore, our long affair with this yeast has resulted in extensive research on its genetics and metabolism, making it one of the best-studied organisms in microbiology. Its complete genome sequence was released in 1996 (Goffeau, Barrell et al. 1996), making it the first fully

sequenced eukaryotic genome. Since then, well-annotated databases specific to this organism, like the Saccharomyces Genome Database (SGD) (Cherry, Hong et al. 2012) or the Yeast Deletion Collection (YDC), a gene knock-out collection with reported phenotypes (Winzeler, Shoemaker et al. 1999) have been developed. The fully disclosed genome sequence, the vast data available on many metabolic reactions and the relatively recent integration of omics data have resulted in accurate genome-scale metabolic models (GSMM) of this organism, which help understand its metabolism and predict *in silico* its behaviour under different conditions (Bideaux, Alfenore et al. 2006, Salvy and Hatzimanikatis 2021). In addition, years of genetic engineering of this organism have resulted in a plethora of protocols and genetic engineering tools (i.e., CRISPR-Cas9) for its manipulation (Generoso, Gottardi et al. 2016).

Saccharomyces cerevisiae is an excellent host for the large-scale production of bulk chemicals due to its robustness at large scale and the history of successful production of toxic compounds like organic acids, alcohols, aromatic compounds, and volatile esters (Guo, Zhang et al. 2011, Kruis, Levisson et al. 2017, Nandy and Srivastava 2018, Hitschler and Boles 2019). Its genetic accessibility and well-known behaviour at large scale make it the preferred choice over other organisms that produce bulk chemicals like *E. coli, Aspergillus sp.*, or *Clostridia sp*. In the case of *E. coli*, although this bacteria is also widely used in biotechnology, it is less robust, less resistant to phages (Schadeweg and Boles 2016a, Nandy and Srivastava 2018), and less tolerant to bulk chemicals like organic acids when compared to yeast (Royce, Liu et al. 2013, Yang, Zhang et al. 2021).

2.3 MCFAs and MCFOHs in microbial biotechnology

In biotechnology, MCFAs and MCFOHs are produced mainly in *S. cerevisiae*, *E. coli*, and oleaginous yeasts using as precursors the acyl-CoAs generated by fatty acid biosynthesis (FAB) or the rBOX (see **section 2.4** below). The termination enzyme is the determining factor that defines the final product (Kim, Clomburg et al. 2015). For the formation of fatty acids, thioesterases break the thioester bond in the acyl-ACP or acyl-CoAs, releasing fatty acids of different lengths depending on their specificity (Cantu, Chen et al. 2010, Kruis, Levisson et al. 2017). Fatty alcohols, on the other hand, are synthesised from acyl-CoAs by acyl-CoA reductases (ACRs) (Runguphan and Keasling 2014, Kim, Clomburg et al. 2015) or from the ATP-consuming reduction of fatty acids by carboxylic acid reductases (CARs) (Akhtar, Turner et al. 2013, Henritzi, Fischer et al. 2018). The formation of fatty alcohols from CARs or ACRs requires two reduction steps: (1) a reduction of the acyl-CoA to fatty aldehyde, catalysed by ACRs, or a reduction of fatty acids to fatty aldehydes, catalysed by CARs, and (2) a reduction of the fatty aldehyde to MCFOH catalysed by alcohol dehydrogenases. In the case of ACRs,

these two reactions can be catalysed by two separate enzymes (ACR + ADH) or by single, bi-functional ACRs with dual activity (Steen, Kang et al. 2010, Krishnan, McNeil et al. 2020).

Saccharomyces cerevisiae is the preferred yeast host for the large-scale production of bulk chemicals and organic acids due to its genetic accessibility and the history of successful production of toxic compounds like organic acids, alcohols, aromatic compounds, and volatile esters (Guo, Zhang et al. 2011, Kruis, Levisson et al. 2017, Nandy and Srivastava 2018, Hitschler and Boles 2019). So far, the most successful attempts to produce MCFAs and MCFOHs by *S. cerevisiae* have resulted from directly engineering fatty acid synthases (FASs). Expressing a mutant *FAS1* (*FAS1*^{R1834K}) resulted in up to 70 mg/L of hexanoic acid and 245 mg/L of octanoic acid (Gajewski, Pavlovic et al. 2017, Zhu, Zhou et al. 2017). Increasing the tolerance to MCFA via adaptive laboratory evolution (ALE) and engineering of the MCFA transporters in a *FAS*-mutant strain resulted in titres of up to 300 mg/L hexanoic acid, 500 mg/L octanoic acid, and 1.7 g/L decanoic acid (Zhu, Hu et al. 2020). Regarding MCFOH, expressing the CAR from *Mycobacterium marinum* (^{Mm}*CAR*) and the aldehyde dehydrogenase *ahr* from *E. coli* in the *FAS1*^{R1834K} mutant from Gajewski *et al.* (2017) resulted in up to 50 mg/L of 1-octanol (Henritzi, Fischer et al. 2018). Testing a ^{Mm}*CAR* mutant library on a *FAS*-mutant, MCFA-producing *S. cerevisiae* strain with increased tolerance to MCFA led to 171 mg/L of 1-hexanol, 40 mg/L of 1-octanol, and 10 mg/L of 1-decanol (Hu, Zhu et al. 2020).

In *E. coli*, the short- and medium-chain fatty acids, butyric acid (up to 6 g/L), hexanoic acid (up to 3 g/L) (Clomburg, Contreras et al. 2017, Kim, Jang et al. 2018, Vogeli, Schulz et al. 2022) or decanoic acid (up to 277 mg/L) (Kim and Gonzalez 2018) have been produced in engineered strains via the combination of enzymes from the rBOX with specific thioesterases. Regarding the MCFOH production in *E. coli*, using bi-functional enzymes proved to be beneficial when expressing the rBOX: expression of the bi-functional, fatty acyl-CoA reductase *Maqu2507* from *Marinobacter aquaeolei* in a decanoyl-CoA producing strain resulted in 1.4 g/L of decanol in shake flask (Chen and Gonzalez 2023), and expressing the clostridial, bi-functional ^{Ca}*adhE2* led to 40 mg/L of 1-hexanol and 1-octanol (Kim, Clomburg et al. 2015). There are no known CARs with bi-functional reductase and dehydrogenase activities. Therefore, MCFOH synthesis requires the co-expression or overexpression of an aldehyde/alcohol dehydrogenase for the second reduction reaction (Krishnan, McNeil et al. 2020). The expression of ^{Mm}*CAR* and the overexpression of endogenous aldehyde dehydrogenase *ahr* in *E. coli* led to 62 mg/L of 1-octanol (Akhtar, Dandapani et al. 2015). In that experiment, *E. coli* was not overexpressing any acyl-CoA-producing pathway.

Oleaginous yeasts are a promising platform for MCFA and MCFOH production. However, metabolic engineering strategies in *Rhodosporidium toruloides* and *Yarrowia lipolytica* strategies have mainly resulted in C_{14}-C_{18} products. For instance, expressing the ACR

Maqu_2220 from *Marinobacter aquaeolei* in *Rhodosporidium toruloides* resulted in up to 2 g/L of secreted fatty alcohols (C_{14}-C_{18}) (Fillet, Gibert et al. 2015), and deleting the elongase *ELO1* in a *POX1*-mutant *Y. lipolytica* increased the accumulation of MCFA (C_{14}-C_{18}) in the total lipid content to 45% (Rigouin, Croux et al. 2018).

2.4 The reverse β-oxidation pathway: a carbon elongation alternative

Carbon elongation processes exist in all forms of life. Two classic examples of carbon extension pathways present in eukaryotes and prokaryotes are the *de novo* fatty acid biosynthesis (FAB) by FASs (Hu, Zhu et al. 2019), and the synthesis of polyketides by polyketide synthases (PKSs) (Khosla 2009, Klaus and Grininger 2018). In FAB, the synthesised fatty acids are used to create phospholipids for membranes, energy storage molecules like triacylglycerols, and signalling molecules (Tehlivets, Scheuringer et al. 2007, Carman and Han 2011, Klug and Daum 2014). Polyketides, a complex group of molecules present in bacteria, plants and fungal species, are used for signalling and defence purposes (Flores-Sanchez and Verpoorte 2009, Khosla 2009).

The bacterial reverse β-oxidation pathway (rBOX) is another carbon elongation mechanisms with biotechnological interest. The rBOX is a more energy-efficient pathway compared to FAB or polyketide synthesis. Unlike FAB and polyketide synthesis, where acetyl-CoA is first converted to the elongation unit malonyl-CoA at the cost of one ATP, the rBOX directly uses acetyl-CoA as the elongation unit (Tehlivets, Scheuringer et al. 2007, Dellomonaco, Clomburg et al. 2011, Maloney, Gerwick et al. 2016, Schadeweg and Boles 2016a, Hitschler and Boles 2019).

The rBOX is a cyclical set of four reactions that results in the elongation of an acyl-CoA molecule by two carbon units with each round of the cycle (Dellomonaco, Clomburg et al. 2011) (**Figure 2**). It begins with a non-decarboxylative Claisen condensation reaction catalyzed by a thiolase, where acetyl-CoA acts as the donor of two carbon units to an acyl-CoA molecule, generating a β-ketoacyl-CoA. This is later reduced to a 3-hydroxyacyl-CoA by a β-hydroxyacyl-CoA dehydrogenase in a NADH-consuming reaction. The 3-hydroxyacyl-CoA is then dehydrated to a *trans*-Δ^2-enoyl-CoA by an enoyl-CoA hydratase. Finally, the double bond at the α-carbon of the *trans*-Δ^2-enoyl-CoA is reduced at the expense of one NADH molecule by a *trans*-enoyl-CoA reductase, generating an acyl-CoA molecule. This acyl-CoA molecule is available for a new elongation cycle or can be used by a termination enzyme or a different pathway to produce a wide variety of products like alcohols, acids, polyketides, or volatile esters among others (Tarasava, Lee et al. 2022).

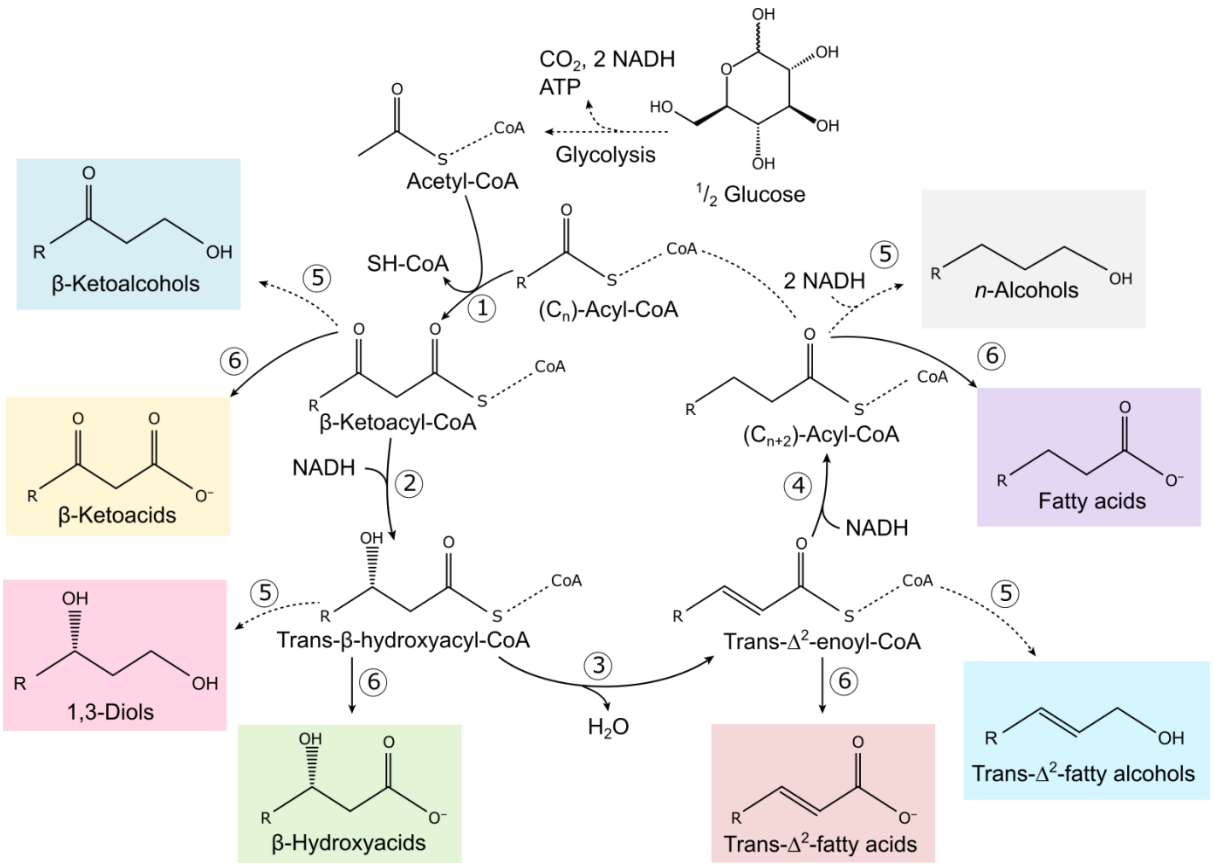

Figure 2. Overview of the reverse β-oxidation pathway and potential products from the pathway. The glucose consumed by the cell is converted into acetyl-CoA, the starting molecule in the rBOX. The rBOX is a cyclical pathway with four core reactions: (1) thiolase, (2) β-hydroxyacyl-CoA dehydrogenase, (3) enoyl-CoA hydratase, and (4) *trans*-enoyl-CoA reductase. The different intermediates in the rBOX are converted into different products depending on the termination enzymes used. For instance, while the joint action of aldehyde reductases and alcohol dehydrogenases (5) produce different alcohols, thioesterases activity (6) results in different fatty acids. Multiple step reactions are depicted by dashed arrows. This figure was adapted from Dellomonaco *et al.* (2011).

In nature, the rBOX pathway is long known in some *Clostridia spp*. like *C. acetobutylicum*, where this pathway is used for the production of butanol (Lee, Park et al. 2008, Yoo, Bestel-Corre et al. 2015), or *C. kluyveri*, where it is used to produce butyric acid and the MCFA hexanoic acid from ethanol and acetate (Barker, Kamen et al. 1945, San-Valero, Fernandez-Naveira et al. 2019). Recently, rBOX has also been confirmed in *Megasphaera spp.* growing on lactic acid, where it produces hexanoic acid (Jeon, Choi et al. 2016, Kang, Kim et al. 2022). In addition, some reactions and intermediates of the rBOX are also present in other pathways like the polyhydroxyalkanoates (PHA) biosynthesis pathway and the ethylmalonyl-CoA pathway, where thiolase and β-hydroxyacyl-CoA dehydrogenase reactions are key steps (Peyraud, Kiefer et al. 2009, Zhang, Kurita et al. 2019). Another example is the fatty acid biosynthesis, which shares the same elongation cycle reactions (condensation, reduction, dehydration, and reduction) with the rBOX (White, Zheng et al. 2005). Interestingly, despite the FAB being associated with ACP-substrates, it has been shown that enzymes from the bacterial type II FAB pathway can also use coenzyme A-bound substrates and run a functional rBOX (Clomburg, Contreras et al. 2017).

2.4.1 The reverse β-oxidation in biotechnology

The clostridial 1-butanol production pathway is the first known rBOX variant expressed in a non-native organism (Atsumi, Cann et al. 2008). In that experiment, they produced up to 552 mg/L of 1-butanol in an engineered *E. coli*. However, in 2011, Dellomonaco *et al.* engineered the native β-oxidation pathway in *E. coli* and reported the first functional, non-clostridial rBOX, producing linear and branched alcohols. Since then, researchers have tested different enzymes for rBOX and termination enzymes in bacterial systems. In *E. coli*, these combinations resulted, for example, in the production of 100 mg/L of the linear carboxylic acid decanoic acid (Kim and Gonzalez 2018), 240 mg/L of the methyl ketone 2-pentanone (Lan, Dekishima et al. 2013), 27 mg/L of the alcohol 1,3- butanediol (Gulevich, Skorokhodova et al. 2016) and 80 mg/L of the polyketide olivetolic acid (Tan, Clomburg et al. 2018). In addition, the termination enzymes are key to determining the products generated in the pathway. For instance, for an identical core of rBOX enzymes and strain background, using a thioesterase or an acyl-CoA reductase as a termination enzyme will result in MCFA or MCFOH, respectively (Kim, Clomburg et al. 2015). Furthermore, the thioesterase used determines the main length of the MCFA product. For instance, in that same experiment, overexpressing the thioesterase *fadM* resulted in a higher fraction of decanoic acid, while the thioesterase *tesA* led to a larger hexanoic and octanoic acid fraction instead. This specificity of FadM for decanoyl-CoA was also observed by Kim and Gonzalez (2018).

In *S. cerevisiae*, the rBOX pathway was first used to produce the four-carbon compound 1-butanol, although at very low titers (2.5 mg/L) (Steen, Chan et al. 2008). Later, the titers of 1-butanol were significantly improved by using a trans-enoyl-CoA reductase from *Treponema denticola* that catalyzes the reduction of enoyl-CoA in an irreversible reaction and by optimizing the NADH and coenzyme A availability, reaching more than 0.85 g/L of 1-butanol (Schadeweg and Boles 2016a, Schadeweg and Boles 2016b). Recently, a new variant of the rBOX expressing the thiolase, *bktB*, and the β-hydroxyacyl-CoA dehydrogenase, *paaH1*, from *Cupriavidus necator* proved to be functional in *S. cerevisiae* to produce hexanoyl-CoA (Krink-Koutsoubelis, Loechner et al. 2018), which was used later in this organism as a precursor to synthesize cannabinoids (Luo, Reiter et al. 2019). All in all, the biotechnological application of the rBOX pathway works in *S. cerevisiae* but seems limited to two cycles, producing only up to C_6-intermediates and products. Extending the length of the products from this pathway in an organism so commonly used in industry like *S. cerevisiae* would accelerate the implementation of sustainable production processes for a previously inaccessible range of products at an industrial scale.

2.5 Yeast carbon metabolism: overview of glucose catabolism

In a complete combustion process, organic matter is fully oxidised to carbon dioxide and water, releasing energy in the form of heat and light. The metabolism of living organisms also works as a slow combustion process. In this process, nutrients (organic matter) can be fully oxidised (loss of electrons) to carbon dioxide and water via respiration, generating energy in the form of ATP or partially oxidised to smaller and more oxidised molecules via fermentation (**Figure 3**). In both processes, the starting substrates are broken down stepwise into smaller and more oxidised ones, in what is known as catabolism. The energy and reducing power generated during the catabolism of nutrients is then used to synthesise nucleic acids, proteins, polysaccharides, and lipids for the growth and maintenance of the cell, in what is known as anabolism (Judge and Dodd 2020).

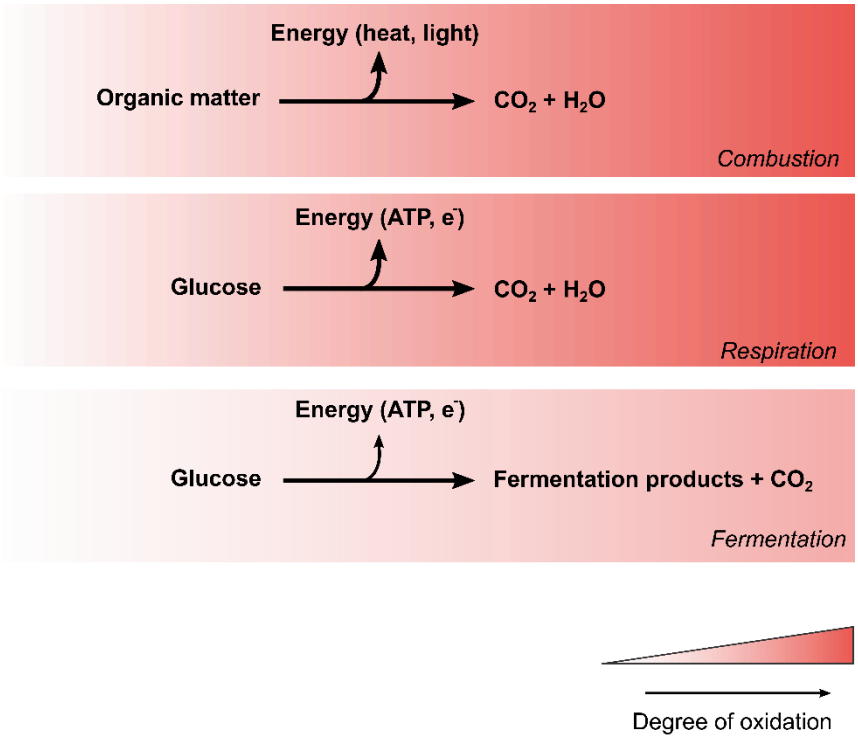

Figure 3. Energy generation and substrate oxidation parallelisms between combustion, respiration and fermentation. In the combustion of organic matter, energy is generated as light and energy, and organic matter is oxidised to carbon dioxide and water. Respiration follows a similar pattern in terms of final products, with glucose being fully oxidised to carbon dioxide and water. However, the energy generated is in the form of ATP and electrons, which are used in metabolism. Fermentation, on the other hand, results in less oxidised products and less energy generation (ATP and electrons).

NAD^+ is the preferred acceptor of the electrons during the oxidation of nutrients. For example, in the catabolism of glucose (**Figure 4**), this carbohydrate is oxidised during glycolysis and broken down into two pyruvate molecules, releasing two electrons and generating 2 mol ATP / 1 mol glucose. This first part of the glucose catabolism takes place in the cytosol, and the electrons released during the oxidation are transferred to NAD^+, which is now reduced to NADH. From pyruvate, the catabolism of glucose can follow two routes: (1) complete oxidation

via tricarboxylic acid cycle (TCA) and respiration in the mitochondria under aerobic conditions or (2) fermentation in the cytosol to regenerate NAD^+ under aerobic or anaerobic conditions.

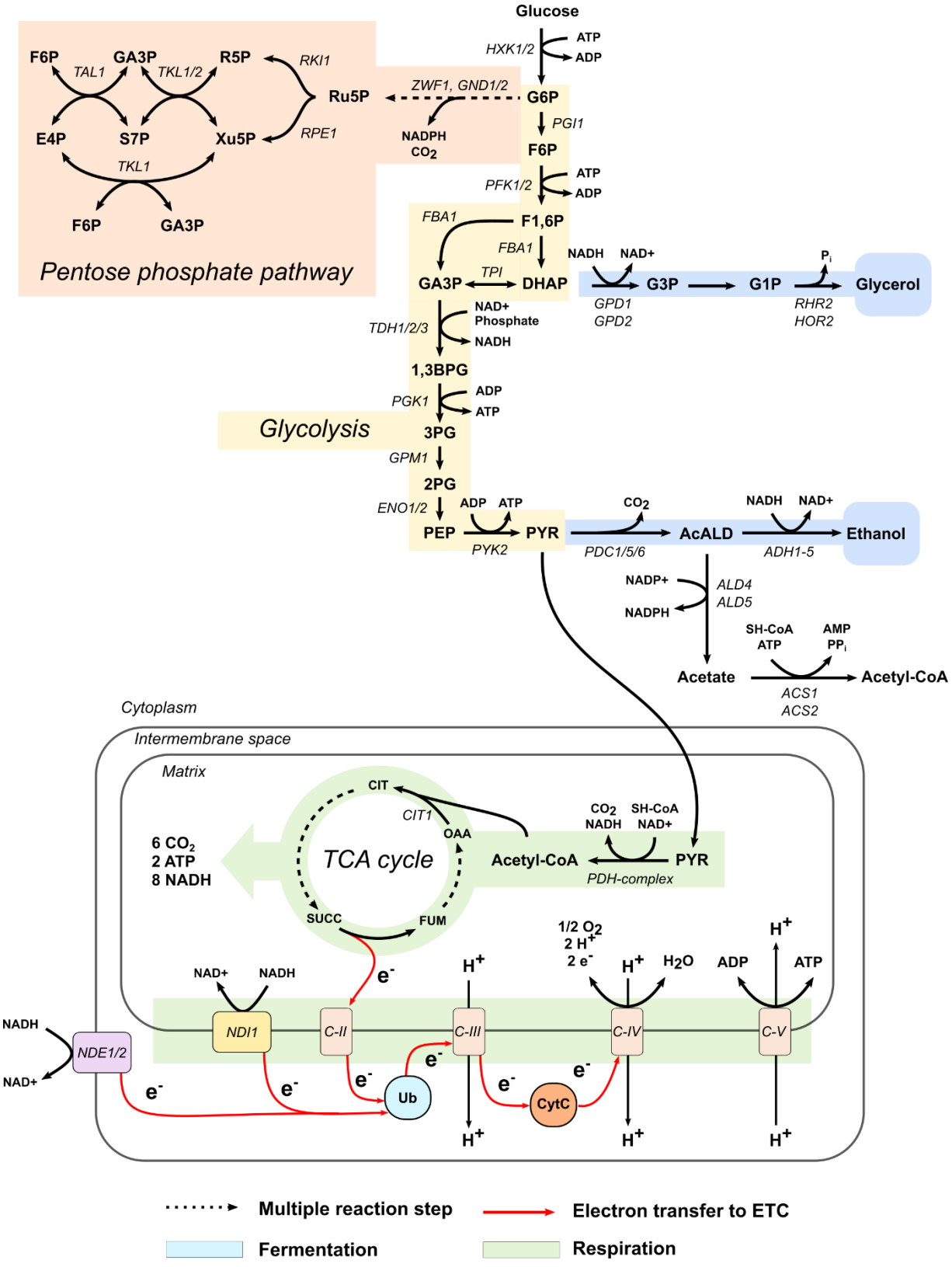

Figure 4. Overview of the central metabolism in the yeast *S. cerevisiae*. Glucose is metabolised in the central carbon metabolism via the pentose phosphate pathway (PPP) and via glycolysis. Glycolysis (in *yellow*) is used to further oxidise glucose, generating NADH and energy. *S. cerevisiae* produces glycerol and ethanol via fermentation

(in *blue*) to regenerate NAD^+ from glycolysis. Under aerobic, glucose limited conditions, *S. cerevisiae* oxidises pyruvate (PYR), the main glycolysis product, via TCA cycle and respiration (both in *green*) in the mitochondria, regenerating NADH and generating energy. The flux of electrons to the electron transport chain is indicated by *red arrows*. Glucose is also oxidised in the PPP (in *orange*) to generate NADPH and precursors for nucleotides and aminoacids. **Pentose phosphate pathway products and intermediates:** Ru5P, ribulose-5-phosphate; R5P, ribose-5-phosphate; Xu5P, xylulose-5-phosphate; GA3P, glyceraldehyde-3-phosphate; S7P, sedoheptulose-7-phosphate; F6P, fructose-6-phosphate; E4P, erythrose-4-phosphate. **Glycolysis products and intermediates**: G6P, glucose-6-phosphate; F6P, fructose-6-phosphate; F1,6P, fructose-1,6-biphosphate; DHAP, dihydroxy-acetone-phosphate; 1,3BPG, 1,3-biphosphoglycerate; 3PG, 3-phosphoglycerate; 2PG, 2-phosphoglycerate; PEP, phosphoenolpyruvate; PYR, pyruvate. **Fermentation products and intermediates**: G3P, glycerol-3-phosphate; G1P, glycerol-1-phosphate; AcALD, acetaldehyde. **TCA cycle intermediates**: CIT, citrate; SUCC, succinate; FUM, fumarate; OAA, oxaloacetate. **Electron transport chain products and intermediates**: Ub, ubiquinone/ubiquinol; CytC, cytochrome C.

In the complete oxidation route in yeast, the two pyruvates enter the mitochondria and are first converted to acetyl-CoA via the Pyruvate dehydrogenase (PDH) complex. Then, they are fully oxidised in the TCA cycle, releasing six molecules of carbon dioxide and reducing eight molecules of NAD^+ to NADH and two ubiquinones to ubiquinol. The reducing equivalents generated during the TCA (NADH and ubiquinol) transfer electrons and protons to the electron transport chain (ETC) in the inner membrane of the mitochondria (IM), regenerating NAD^+ for further reactions (**Figure 4**). In most eukaryotes, the ETC consist of five complexes (I, II, III, IV, and V) and the transfer of electrons in complexes I, III and IV is accompanied by the pumping of protons to the intermembrane space in the mitochondria (IMM), generating a proton gradient that will generate ATP via the H^+-ATP synthase (complex V). However, *S. cerevisiae* lacks complex I and instead, it has an inner membrane (Ndi1) and two outer membrane (Nde1/2) NADH-ubiquinone reductases (Luttik, Overkamp et al. 1998, Melo, Bandeiras et al. 2004). These NADH-ubiquinone reductases do not pump protons to the IMM space but participate in the transfer of electrons in the ETC that will result in the final reduction of oxygen to water (Iwata, Lee et al. 2012). Since the synthesis of ATP via H^+-ATP synthase depends on the pumping of protons, the complete oxidation of glucose in *S. cerevisiae* results in a lower maximum yield of ATP/glucose (16 ATP / 1 glucose) compared to other eukaryotes with complex I (32 ATP/ 1 glucose).

In the fermentation route, pyruvate is not fully oxidised to carbon dioxide but is used as the acceptor of electrons from NADH to regenerate the NAD^+ reduced during glycolysis (Bakker, Overkamp et al. 2001). First, pyruvate is decarboxylated to acetaldehyde by pyruvate decarboxylases (Pdc1/5/6) and then reduced to ethanol via alcohol dehydrogenases (ADHs). Ethanol is the principal fermentation product in *S. cerevisiae* (Sarris and Papanikolaou 2016). However, glycerol production is also a common mechanism to regenerate NAD^+ in this yeast (Papapetridis, Goudriaan et al. 2018, Yang, Jiang et al. 2022).

In the glucose fermentation to ethanol, the only ATP generated comes from substrate-level phosphorylation during glycolysis at the phosphoglycerate kinase (Pgk1) and the pyruvate kinase (Pyk2) reactions. However, two molecules of ATP are consumed prior to these

reactions, one by the hexokinase (Hxk2) to activate the glucose molecule upon uptake via phosphorylation and another by phosphofructokinase (Pfk1/2) to generate fructose-1,6-biphosphate, previous to the branching into dihydroxyacetone-phosphate and glyceraldehyde-3-phosphate (**Figure 4**). Therefore, in *S. cerevisiae*, the energetic yield of producing ethanol is 2 mol ATP/1 mol glucose, far from the 16 mol ATP/1 mol glucose obtained from respiration. This higher energetic yield of respiration over fermentation is present in all aerobes and facultative anaerobes, who only turn to fermentation under anaerobic or semi-anaerobic conditions (Partridge, Sanguinetti et al. 2007, André, Debande et al. 2021). However, some organisms, like *S. cerevisiae*, prefer fermentation over respiration, even in aerobic conditions. This behaviour, known as the Crabtree effect, is explained below in **section 2.5.3**.

2.5.1 Yeast NADH/NAD^+ metabolism

The nicotinamide adenine dinucleotides (abbreviated as NAD^+/$NADP^+$ and NADH/NADPH in their oxidised and reduced form, respectively) are co-factors directly involved in the exchange of electrons and protons in many biological reactions, which is crucial to produce energy and to grow (Aguilera-Méndez, Fernández-Lainez et al. 2012, Croft, Venkatakrishnan et al. 2020, Duncan, Setati et al. 2023) (**Figure 5**).

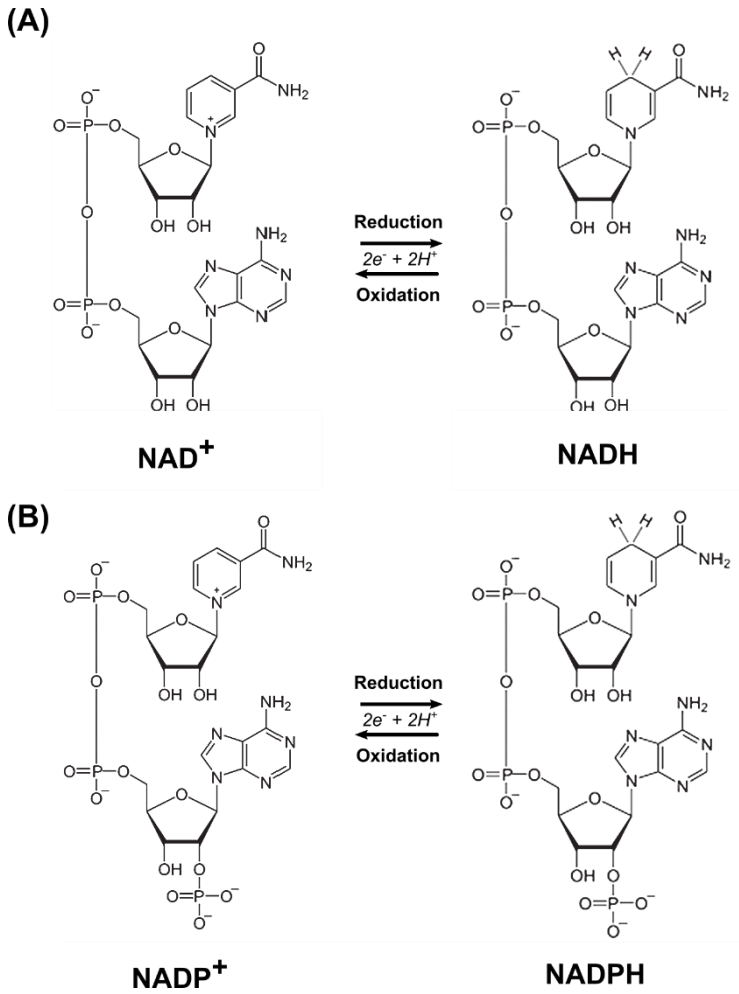

Figure 5. Chemical structures of the redox pairs NAD^+/NADH (A) and $NADP^+$/NADPH (B). NAD^+ and $NADP^+$ act as electron acceptors in oxidation reactions, resulting in the reduced forms NADH and NADPH, respectively, that act as electron donors in reduction reactions. The key element in these reactions is the nicotinamide ring, which acts as an electron sink. In oxidation reactions, a hydride is transferred from an organic molecule to $NAD(P)^+$, with electrons flowing to the positively charged nitrogen in the nicotinamide. In reduction reactions, the hydride in NAD(P)H is removed and the electrons transferred to an organic molecule. At a structural level, the presence of a phosphate group on the 2' position of the ribose ring connected to the adenine moiety is the main difference between NAD(H) and NADP(H) species. This figure was adapted from Aguilera-Méndez et al. (2012).

In general, while the NAD^+/NADH redox pair plays a dominant role in catabolism, where electrons are captured from substrates, the NADPH/$NADP^+$ redox pair is preferred in anabolic reactions for the reductive biosynthesis of molecules instead (Croft, Venkatakrishnan et al. 2020). The source of the reduced forms (NADH and NADPH) also differs for both redox pairs. In glucose-fed *S. cerevisiae*, NADH is generated during glycolysis by glyceraldehyde 3-phosphate dehydrogenases (Tdh1/2/3). NADPH, on the other hand, is mainly generated by synthesising acetate from acetaldehyde by acetaldehyde dehydrogenase Ald6 (Grabowska and Chelstowska 2003) and, in the pentose phosphate pathway (PPP), by the glucose 6-phosphate dehydrogenase (Zwf1) and the decarboxylating 6-phosphogluconate dehydrogenase (Gcn1/2) reactions (Nogae and Johnston 1990, Bro, Regenberg et al. 2004) (**Figure 4**).

NAD^+ regeneration is common in all known life forms. However, life on Earth takes very different forms and is present in many ecosystems, natural or man-made. This diversity results in different metabolic pathways and reactions for NAD^+ regeneration, using different electron acceptors, and leading to various final products with potential interest. For instance, in *S. cerevisiae,* regenerating NAD^+ via fermentation results mainly in ethanol and glycerol. Similarly, NAD^+ regeneration via fermentation in *Clostridium acetobutylicum* produces 1-butanol (Lee, Park et al. 2008), succinic acid in *Mannheimia succiniciproducens* (Ahn, Seo et al. 2020), and 2,3-butanediol in *Bacillus polymixa* (Celińska and Grajek 2009).

The ubiquity of NAD^+/NADH in pathways from different organisms allows metabolic engineers to integrate reactions from a pathway in a new host organism to produce a product of interest (POI). However, there are important factors to consider regarding the metabolic engineering of NADH-utilizing pathways. First, native reactions are competing for NADH in the host organisms and removing this competition can benefit the POI production titers. For instance, lactic acid is produced from the oxidation of pyruvate, a NADH-consuming reaction catalysed by lactate dehydrogenase (LDH). In a ∆*pdc1 S. cerevisiae* strain expressing a bovine *LDH*, deleting the endogenous, NADH-consuming *ADH1* gene increased lactic acid yield ($g/g_{glucose}$) by 53% (Tokuhiro, Ishida et al. 2009). Another example is the production of 2,3-butanediol in *S. cerevisiae*, where deleting *ADH1-5*, *GPD1*, and *GPD2* increased the 2,3-butanediol yield ($g/g_{glucose}$) by 80% (Kim and Hahn 2015). Second, in eukaryotes, metabolic reactions are compartmentalised in distinct organelles, and each of these compartments has reactions that use NADH as an electron donor. However, NAD^+/NADH cannot traverse membranes (Croft, Venkatakrishnan et al. 2020). Therefore, eukaryotes use shuttle reactions to transfer electrons between organelles. In *S. cerevisiae*, some examples of electron shuttle reactions include the ethanol-acetaldehyde shuttle between mitochondria and cytosol catalysed by ADHs (Bakker, Bro et al. 2000) or the malate-oxalacetate shuttle between cytosol and peroxisomes catalysed by malate dehydrogenases (Al-Saryi, Al-Hejjaj et al. 2017). Therefore, the metabolic engineering of NADH-consuming pathways should consider the location of endogenous metabolites required for that pathway. Third, the redox pairs are generally tightly regulated, not interchangeable, and their ratios are condition-dependent in *S. cerevisiae* (Bakker, Overkamp et al. 2001). For example, the cytosolic [NAD^+ / NADH] ratio is higher than 100 under aerobic, glucose-limiting conditions (Canelas, van Gulik et al. 2008) and decreases to 0.5-1.1 under anaerobic conditions (Bekers, Heijnen et al. 2015). On the other hand, the [$NADP^+$ / NADPH] ratio is usually lower than 0.07 and remains relatively constant under different conditions (Zhang, Pierick et al. 2015, Duncan, Setati et al. 2023). However, *S. cerevisiae* lacks transhydrogenases to transfer electrons between NADH and $NADP^+$ or NADPH and NAD^+ (Fiaux, Cakar et al. 2003). Expressing bacterial transhydrogenases has so far resulted in a

bias towards oxidation of NADPH and reduction of NAD^+, leading to accumulation of 2-oxoglutarate, glycerol and reduced growth (Nissen, Anderlund et al. 2001).

Overall, continuous re-generation cycles and shuttle reactions keep co-factor balance and redox homeostasis.

2.5.2 Yeast acetyl-CoA metabolism

Acetyl-CoA is essential in metabolism, acting as a metabolic intermediate and acetyl group donor. It consists of an acetate molecule bound to a coenzyme A cofactor via a thioester bond (**Figure 6**). In *S. cerevisiae*, acetyl-CoA plays a key role in the catabolism of sugars and lipids, fatty acids and isoprenoids biosynthesis, and gene regulation.

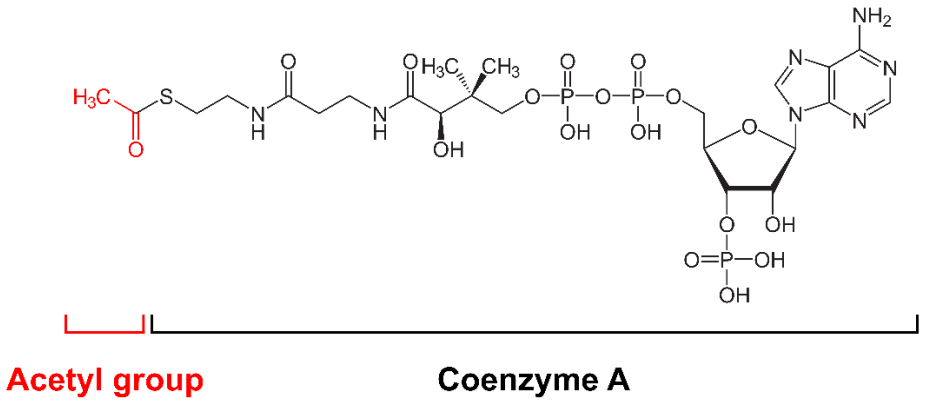

Figure 6. Chemical structure of acetyl-CoA. Acetyl-CoA consists of an acetyl group (in ***red***) bound via a thioester bond to coenzyme A (in ***black***).

In sugar catabolism, acetyl-CoA is the link between glycolysis and the TCA cycle, where it generates precursors for amino acids and nucleotides (Ljungdahl and Daignan-Fornier 2012), and under aerobic conditions, also energy via complete oxidation in the ETC. In fatty acid metabolism, acetyl-CoA is a central element in FAB in the cytosol and fatty acid degradation in the peroxisomes via β-oxidation. During FAB, the fatty acid synthase (Fas1) uses acetyl-CoA as the priming molecule and as the precursor to malonyl-CoA, the elongation unit (Tehlivets, Scheuringer et al. 2007, Hu, Zhu et al. 2019). On the other hand, acetyl-CoA is the main product of β-oxidation, where each iteration results in acetyl-CoA and a shortened acyl-CoA (Hiltunen, Mursula et al. 2003). Acetyl-CoA is also the starting molecule in the mevalonate pathway (MEP). This pathway is essential to synthesise isoprenoids like ergosterol, an integral component of the fungal cell membrane (Jordá and Puig 2020). In addition, acetyl-CoA is required for the acetylation of proteins like histones. In eukaryotes, histone acetylation leads to chromatin unfolding, which activates gene expression (Grunstein 1997, Chou, Lee et al. 2023).

In *S. cerevisiae* grown under aerobic, glucose-limited conditions, acetyl-CoA is generated in the mitochondria via the oxidative decarboxylation of pyruvate by the PDH complex (**Figure 4**). This process results in the release of carbon dioxide and the reduction of one NAD^+ to NADH per acetyl-CoA generated (Krivoruchko, Zhang et al. 2015). Acetyl-CoA is also required in the cytosol for metabolic processes like FAB or the mevalonate pathway. However, the acetyl-CoA synthesised via PDH does not diffuse freely to the cytoplasm (van Rossum, Kozak et al. 2016c). Therefore, *S. cerevisiae* synthesises acetyl-CoA in the cytosol via the *PDH bypass* to fill the requirements for a cytosolic pool of acetyl-CoA. In the *PDH bypass*, aldehyde dehydrogenases (mainly Ald6) oxidise the acetaldehyde previously generated by PDCs into acetate, which is then bound to coenzyme A in an ATP-consuming reaction catalysed by the acetyl-CoA synthase (Acs1/2) (van Rossum, Kozak et al. 2016c) (**Figure 4**).

Acetyl-CoA diffuses freely between cytosol and nucleus. However, it cannot pass freely through peroxisomal and mitochondrial membranes (Yocum, Bassett et al. 2022). *S. cerevisiae* uses a carnitine shuttle to export acetyl-CoA from the peroxisomes to the cytosol and to import acetyl-CoA to the mitochondria (van Rossum, Kozak et al. 2016a). In this process, the peroxisomal carnitine acetyl-CoA transferase (Cat2) first transfers the acetyl group from acetyl-CoA to carnitine, resulting in an acetyl-carnitine molecule. Then, acetyl-carnitine diffuses to the cytosol, where the cytosolic carnitine acetyltransferase Yat2 exchanges carnitine for coenzyme A, regenerating acetyl-CoA (Swiegers, Dippenaar et al. 2001). In addition, the acetyl-carnitine from the peroxisome can also diffuse through the mitochondrial membrane and be converted to acetyl-CoA by the mitochondrial Cat2, which is a product of the same *CAT2* gene coding for the peroxisomal Cat2 (Elgersma, van Roermund et al. 1995). Overexpressing elements of the carnitine shuttle in *PDH*-deficient strains partially recover the acetyl-CoA pool in the mitochondria, suggesting that this is an effective approach to increase the acetyl-CoA flux to organelles of interest (van Rossum, Kozak et al. 2016b). In addition, overexpressing a *CAT2* fused to the peroxisomal membrane increased almost 4-fold the cytosolic acetyl-CoA (Yocum, Bassett et al. 2022). However, *S. cerevisiae* cannot synthesise carnitine and instead imports it from the medium using the Hnm1 transporter (Aouida, Rubio-Texeira et al. 2013, van Rossum, Kozak et al. 2016a). Therefore, carnitine must be added to the medium, which makes this approach unsuitable for large-scale fermentation.

Acetyl-CoA is an essential metabolite to produce valuable biotechnological products in *S. cerevisiae*. These include mevalonate pathway-derived products like farnesene and the antimalarial drug precursor artemisin (Ro, Paradise et al. 2006, Leavell, McPhee et al. 2016), polyketides like m-cresol (Hitschler and Boles 2019), cannabinoid precursors like olivetolic acid (Luo, Reiter et al. 2019) or solvents like 1-butanol (Schadeweg and Boles 2016b). However, in eukaryotes, the acetyl-CoA metabolism is compartmentalised and tightly regulated, which

could result in limited acetyl-CoA availability for production. Therefore, increasing acetyl-CoA synthesis and availability is a common metabolic engineering target to boost the productivity of different fermentation-based processes (Krivoruchko, Zhang et al. 2015, Wiltschi, Cernava et al. 2020).

The endogenous, cytosolic *PDH-bypass* is an ATP-consuming reaction. Thus, three strategies to increase cytosolic acetyl-CoA in a more energy-efficient way have been to (1) express bacterial PDHs, (2) express acetylating acetaldehyde dehydrogenases (AADs), and (3) express pyruvate-formate lyases (PFLs). Expressing a NAD^+-dependent *PDH* complex from *Enterococcus faecalis* in an ∆*acs1*∆*acs2* strain successfully replaced the *PDH-bypass* in *S. cerevisiae* (Kozak, van Rossum et al. 2014). However, the resulting strain exhibited a lipoic acid auxotrophy, which is not desired at industrial scale. Expressing a $NADP^+$-producing *PDH* complex from *E. coli* in a ∆*pda1*∆*mpc2 S. cerevisiae* strain improved the polyketide triacetic acid lactone production titres by 3-fold (Cardenas and Da Silva 2016). No lipoic acid auxotrophy is reported in that study. However, all fermentations were run in rich YPD medium, where lipoic acid auxotrophy would not be detected. AADs, on the other hand, convert acetaldehyde directly into acetyl-CoA. Expressing AADs in *S. cerevisiae* not only replaced the *PDH-bypass* in *ACS*-deficient strains (Kozak, van Rossum et al. 2016) but also increased the observed production titres of farnesene by providing a more ATP-efficient provision of cytosolic acetyl-CoA (Meadows, Hawkins et al. 2016). In addition, in our group, a mutation in the AAD $AdhE^{A267T/E568K}$ from *E. coli* increased the 1-butanol titres by more than 10% when expressed in an engineered *S. cerevisiae* strain (Schadeweg and Boles 2016b). PFLs convert pyruvate and coenzyme A into formate and acetyl-CoA (van Rossum, Kozak et al. 2016c). The generated formate can be detoxified via endogenous NAD+-dependent formate dehydrogenases, Fdh1 and Fdh2, which oxidise formate into carbon dioxide while generating NADH (Zhang, Dai et al. 2015). Expressing a pyruvate-formate lyase from *E. coli* in a ∆*acs1*∆*acs2* S. *cerevisiae* strain partially restored the growth under anaerobic conditions (Kozak, van Rossum et al. 2014). However, this approach led to increased titers of acetate and formate at the end of the fermentation and significantly reduced the yield on biomass, which is not desirable for large-scale processes. In addition, PFLs are deactivated by oxygen and not suitable for semiaerobic or fully aerobic fermentation processes (Waks and Silver 2009, Andorfer, Backman et al. 2021).

Other interesting strategies include the combined expression of phosphoketolases (PKs) and phosphotransacetylases (PTAs) or the expression of ATP-citrate lyases (ACLs). These two strategies do not result in NADH formation and have a lower energy yield from glucose than those mentioned above (PDH, AAD, PFL) (van Rossum, Kozak et al. 2016c). However, they have been successfully implemented in *S. cerevisiae*. PKs convert intermediates of the PPP,

like fructose-6-phosphate, erythrose-4-phosphate, or xylulose-5-phosphate, into acetyl-phosphate molecules. Then, PTAs convert the generated acetyl-phosphate into acetyl-CoA (Bergman, Siewers et al. 2016). This strategy improved the octanoic acid production titres in a *S. cerevisiae* strain with an increased NADPH pool and expressing a mutant *FAS1* (Wernig, Baumann et al. 2021). In addition, the expression of PKs and PTAs also improved the production of the MEP-derived farnesene (Meadows, Hawkins et al. 2016). ATP-citrate lyases convert citrate into acetyl-CoA at the expense of one ATP. Expressing an ACL from *Aspergillus nidulans* in *S. cerevisiae* significantly increased the titres of squalene, a product of the MEP (Rodriguez, Denby et al. 2016). All the validated strategies mentioned above to increase cytosolic acetyl-CoA levels and additional strategies not yet validated in yeast are reviewed in detail by van Rossum *et al.* (2016c).

Another strategy is increasing the synthesis of the precursor coenzyme A (**Figure 7**). In *S. cerevisiae*, high acetyl-CoA levels inhibit coenzyme A synthesis at the pantothenate kinase reaction (Cab1) (Olzhausen, Schubbe et al. 2009). Engineering the acetyl-CoA binding domain in Cab1 to reduce glucose suppression (Olzhausen, Grigat et al. 2021) or expressing *coaA*, a bacterial pantothenate kinase insensitive to acetyl-CoA inhibition (Schadeweg and Boles 2016a), resulted in increased acetyl-CoA levels and improved 1-butanol production titres, respectively.

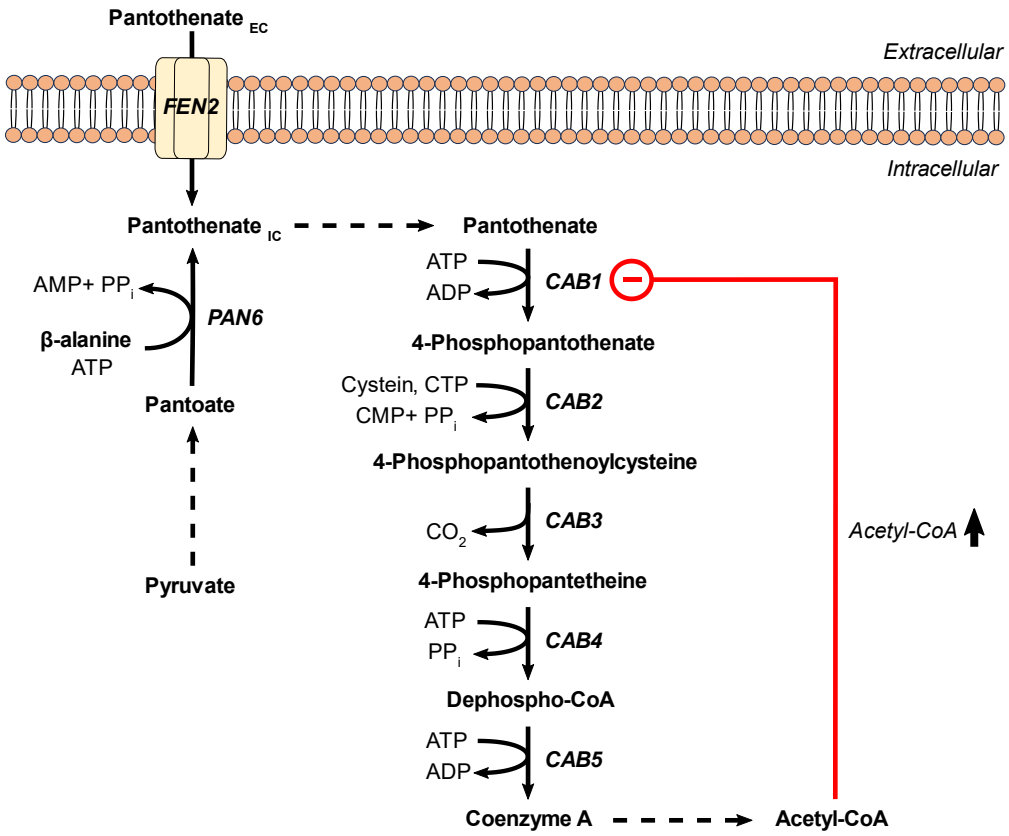

Figure 7. Overview of the coenzyme A biosynthetic pathway. The co-factor coenzyme A is synthesised from pantothenate via four energy-consuming reactions (Cab1, Cab2, Cab4, Cab5) and one decarboxylation (Cab3). Pantothenate is imported via the Fen2 transporter from the fermentation medium or synthesised by the cell from pantoate and β-alanine. Coenzyme A is used to synthesise acetyl-CoA (see **Figure 4**), and high levels of acetyl-CoA inhibit the first reaction of the coenzyme A synthesis, catalysed by Cab1. A *red* arrow represents inhibitory regulation. *Dashed* lines represent multiple reaction steps.

2.5.3 Crabtree effect in yeast

"To be fast, or to be efficient, that is the question". Hamlet's big dilemma would read like this had he been a yeast. As described in **section 2.5**, glucose can be partially oxidised to fermentation by-products via fermentation or, in aerobic conditions, fully oxidised to carbon dioxide and water via respiration. From an energy efficiency standpoint, respiration provides a higher [mol ATP/mol glucose] ratio than fermentation and is the preferred route to oxidise glucose for many yeasts. However, in conditions where glucose is abundant, some yeasts ferment glucose even in aerobic conditions, where more energy-efficient respiration would be possible (Hagman, Säll et al. 2014, Dai, Huang et al. 2018, Malina, Yu et al. 2021). This phenomenon is known as the *Crabtree effect* (Crabtree 1929), and the yeasts exhibiting this behaviour are known as 'Crabtree-positive'. 'Crabtree-negative' yeasts, on the other hand, oxidise glucose completely via respiration in aerobic, glucose-abundant conditions.

In yeasts, the most accepted theory suggests that the Crabtree effect is a trade-off between maximising the [mol ATP/mol glucose] (via respiration) or maximising ATP synthesis rates (via

fermentation) (Malina, Yu et al. 2021, Zhang, Su et al. 2022). Recently, GSMM-based studies have expanded this theory and included proteome allocation in the equation (Malina, Yu et al. 2021, Salvy and Hatzimanikatis 2021, Xia, Sánchez et al. 2022). This expanded model assumes that microorganisms are systems optimised for growth, but the total protein content and synthetic machinery are limited. Respiration requires the synthesis and transport to the mitochondria of a larger number of proteins (TCA proteins + ETC proteins) than fermentation. Therefore, Crabtree-positive yeast prefer fermentation over respiration in aerobic conditions because it reduces the costs associated with protein synthesis and allocation. Malina *et al.* (2021) compared the proteome allocation trends between Crabtree positive and negative yeasts. Their study reported a higher fraction of total protein in mitochondrial pathways of Crabtree-negative yeasts and glycolysis in Crabtree-positive yeasts.

From an evolutionary perspective, and despite resulting in a lower energy yield, the Crabtree effect has been selected because it confers an advantage when competing for carbon resources. For instance, in nature, the Crabtree-positive *S. cerevisiae* quickly oxidises sugars to ethanol. This (1) eliminates competitors to which ethanol is toxic, and (2) reduces the availability of sugars for more ethanol-resistant competitors, as only those harbouring ADHs (like *S. cerevisiae*) can feed on ethanol (Pfeiffer and Morley 2014). From a metabolism perspective, on the other hand, the Crabtree effect is a complex interplay between sugar transport, metabolic adaptations and regulation.

Crabtree-positive yeasts exhibit a higher glucose uptake rate at a transport level than Crabtree-negative yeasts (Hagman, Säll et al. 2014) and a higher abundance of transporters in the protein fraction (Malina, Yu et al. 2021). This increased glucose uptake rate correlates with a higher glycolytic flux than Crabtree-negative yeasts (Sakihama, Hidese et al. 2019), resulting in a higher pyruvate flux. Pyruvate is a key metabolite in the breakpoint between fermentation (via Pdc) and respiration (via PDH-complex) (**Figure 4**). Otterstedt *et al.* (2004) proposed that the Crabtree effect partly results from the PDH-complex's inability to oxidise the pyruvate from glycolysis fast enough. They exchanged the main sugar transporters (HXTs) for a less active chimera in *S. cerevisiae* to reduce the glycolytic flux, which abolished the Crabtree effect in this yeast (Otterstedt, Larsson et al. 2004). However, this strategy significantly reduced the growth rate, which indicates that other elements besides the sugar uptake rate are involved in the Crabtree effect.

Metabolic regulation is one of those elements. In *S. cerevisiae*, the detection of high levels of glucose triggers an expression and repression cascade known as glucose or catabolite repression (Gancedo 2008, Kayikci and Nielsen 2015). This cascade results in the increased expression of *HXTs* transporters and the glycolytic-flux regulator *HXK2*, but also in repressing the expression of transcription factors involved in respiration like *HAP4*, mitochondrial genes

and genes involved in the use of alternative carbon sources (Ulery, Jang et al. 1994, Bourgarel, Nguyen et al. 1999, van Maris, Bakker et al. 2001, Wu, Zhang et al. 2004, Kümmel, Ewald et al. 2010). Two critical elements in the catabolite repression cascade are Rgt1 and Mig1. Rgt1 represses the expression of *HXTs* and *HXK2*, among other genes (Gancedo 2008, Oud, Flores et al. 2012). Mig1, on the other hand, represses the expression of genes involved in gluconeogenesis and respiration (Kayikci and Nielsen 2015). The repressing effect of Rgt1 and Mig1 is released upon phosphorylation. Rgt1 has two paralog co-repressors, Mth1 and Std1, that prevent it from being phosphorylated in glucose-limited conditions (Roy, Jouandot et al. 2014). Under glucose-limited conditions, Mig1 is phosphorylated by Snf1, which results in the re-location of Mig1 to the cytoplasm and the de-repression of respiration genes (Lin 2021). When glucose levels are high, Mth1 and Std1 are ubiquitinated and degraded in proteasomes, resulting in the phosphorylation of Rgt1 and the release of its de-repressing effect. *HXK2*, one of the targets of Rgt1, is now expressed and prevents the phosphorylation of Mig1 by Snf1 (Ahuatzi, Riera et al. 2007, Vega, Riera et al. 2016). This results in the translocation of Mig1 to the nucleus and the repression of respiration and mitochondrial genes.

In large-scale production processes with *S. cerevisiae*, the Crabtree effect could result in lower production yields. Therefore, large-scale production processes run in fed-batch mode under glucose limitation (Hahn-Hägerdal, Karhumaa et al. 2005, Deparis, Claes et al. 2017). However, releasing the Crabtree effect by metabolic engineering can be beneficial in improving the productivity of cytosol-targeted pathways. For instance, Dai *et al.* (2018) generated a Crabtree-negative *S. cerevisiae* strain by engineering the PDH-bypass of a Pdc-deficient strain. They expressed a heterologous pyruvate oxidase and a transacetylase to generate acetyl-CoA in the cytosol and improved the growth of the strain by ALE. The production titres of 2,3-butanediol, *p*-coumaric acid, lactate, farnesene and lycopene were higher in this strain compared to the wild-type, Crabtree-positive CEN.PK113-11c strain (Yao, Guo et al. 2023). In addition, the Crabtree effect reduces the carbon flux to the mitochondria. Mitochondria are interesting targets for production pathways due to this organelle's physiological conditions and metabolome (Hammer and Avalos 2017, Duran, López et al. 2020). Expressing a mitochondria-targeted 3-hydroxypropionic-producing pathway in the same Crabtree-negative strain from Dai *et al.* (2018) significantly improved the production of the 3-hydroxypropionic acid (Zhang, Su et al. 2022).

2.6 The mitochondria of *S. cerevisiae* as a production platform

Unlike prokaryotic cells, eukaryotes have membrane-bound organelles inside the cell (Cooper 2000). One of these organelles is the mitochondria, whose presence is one of the most defining traits of the eukaryotic cell. The most accepted theory for the origin of mitochondria as an organelle is the ‘endosymbiont hypothesis’. This theory, first proposed by Margulis in the early

70s, states that the presence of mitochondria in eukaryotes is a product of one or a series of endosymbiotic events that took place more than 1.45 billion years ago when a facultative anaerobic or strict aerobic α-proteobacteria was taken up by a prokaryotic, strict anaerobic host (Margulis 1970, Koonin 2010, Martin and Mentel 2010).

The mitochondria are home to the TCA cycle and the ETC in eukaryotes. Therefore, mitochondria are essential to generate metabolic energy and are usually described as the 'powerhouse' of the eukaryotic cell. However, while almost a thousand proteins are confirmed to be mitochondrial (Vögtle, Burkhart et al. 2017), only 15% of the mitochondrial proteome is related to energy metabolism (Schmidt, Pfanner et al. 2010). For instance, the partial biosynthesis of essential molecules like heme groups and iron-sulfur clusters and the full biosynthesis of isoleucine and valine occur in the mitochondria (Mühlenhoff and Lill 2000, Swenson, Moore et al. 2020). The presence of other essential pathways besides ATP-synthesis in the mitochondria reflects the role of this organelle as more than just a 'powerhouse'.

Mitochondria contain their own genetic material (mtDNA) (Margulis 1970, Miyakawa 2017, Anderson, Jackson et al. 2019). The size of the genome and the number of proteins encoded can vary depending on the eukaryotic species. These proteins include those involved in the respiratory chain and extend to RNA polymerases, ribosomal proteins, and protein transport proteins, which are essential for cell maintenance and are ubiquitously present not only in eukaryotes but also in all non-eukaryotic organisms (Gray 2012). These features are the primary foundation of the endosymbiotic theory (Margulis 1970, Gray 2012). The rest (and most) of the genes encoding for mitochondrial proteins are in the nucleus, from where they are expressed and the proteins transferred to the mitochondria (Malina, Larsson et al. 2018). For instance, the mtDNA of *S. cerevisiae* is 75-85 kb and contains seven genes coding for proteins in the respiratory complexes III (COB), IV (*COX1*, *COX2*, *COX3*), V (*ATP6*, *ATP8*, *ATP9*) one ribosomal protein (*VAR1*), two ribosomal RNAs (21S and 15S) of the mitochondrial ribosome, 24 tRNAs, and the RNA subunit of RNase P (Turk, Das et al. 2013). However, genes from the TCA cycle, protein transporters (TOM and TIM complexes), and other exclusively mitochondrial pathways like heme biosynthesis are expressed from the nuclear genome (Hase, Müller et al. 1984, Rapaport and Neupert 1999, Swenson, Moore et al. 2020).

Mitochondria have an inner (IM) and outer membrane (OM) that define two major sub-compartments: the intermembrane space (IMS) and the matrix (Ehrenworth, Haines et al. 2017). In *S. cerevisiae*, the matrix contains the TCA cycle, and the IM contains complexes II, III, IV and V of the ETC. Ndi1, the non-proton pumping yeast equivalent to complex I in humans, is also located in the IM (Iwata, Lee et al. 2012). Ndi1 has two *copycats* in the OM, Nde1 and

Nde2 (Bakker, Overkamp et al. 2001). These enzymes transfer electrons from cytosolic NADH to the ETC, which is crucial to regenerating the NAD^+ reduced during glycolysis.

The controlled flux of metabolites in and out of the mitochondria and the specialised set of reactions happening in this organelle give rise to specific physiological conditions: The mitochondrial matrix has a higher pH than the cytosol (Orij, Postmus et al. 2009) and a more reducing environment due to a lower NAD^+/NADH ratio (Bekers, Heijnen et al. 2015). The IMS, on the other hand, has a similar pH to the cytosol but a more oxidising environment (Orij, Postmus et al. 2009, Duran, López et al. 2020), probably due to the electron transfer processes and accumulation of protons occurring in this sub-compartment. Furthermore, in *S. cerevisiae*, some compounds, like fatty acids or steroids, are at higher concentrations in the mitochondria than in the cytosol (Pan, Lindau et al. 2018). In addition, essential metabolites like acetyl-CoA, which are synthesised at a lower energetic cost in this organelle (via PDH complex), are at concentrations 20-30 higher in the mitochondria of *S. cerevisiae* than in the cytosol or the nucleus (Galdieri, Zhang et al. 2014, Weinert, Iesmantavicius et al. 2014).

The especial conditions and metabolite pool in the mitochondria have been exploited by researchers to increase production titres. Some examples are the production of branched-chain alcohols, terpenoids and small chemicals.

Branched-chained amino acids biosynthesis begins in the mitochondria (Duran, López et al. 2020). However, the degradation of branched-chain amino acids, known as the Ehrlich pathway, takes place in the cytosol and results in products like isobutanol and isopentanol (Yuan, Chen et al. 2017, Wess, Brinek et al. 2019). Targeting the Ehrlich pathway enzymes (KDCs and ADHs) in the mitochondria, and overexpressing the native mitochondrial biosynthetic pathway (*ILV2*, *ILV3*, *ILV5*) led to 635 mg/L of isobutanol, a 260% improvement over expressing the Ehrlich pathway in the cytosol (Avalos, Fink et al. 2013). In addition, expressing keto-acyl elongation genes (*LEU1*, *LEU2*, *LEU4*) in the mitochondria of this isobutanol-producing strain and knocking out *BAT1* resulted in isopentanol titers of 1.25 g/L (Hammer, Zhang et al. 2020). Terpenoids, or isoprenoids, are a large and diverse group of natural organic compounds (Holstein and Hohl 2004). Terpenoids are synthesised in the MEP, a cytosolic pathway that requires acetyl-CoA. In *S. cerevisiae*, Yuan *et al.* (2016) expressed the MEP and an amorphadiene synthase (*ADS*) in the mitochondria and produced 427 mg/L of amorphadiene, an antimalarial drug precursor. These production titers represented a 15% increase compared to the overexpression of the MEP genes and *ADS* in the cytosol. This strategy of compartmentalising in the mitochondria the MEP pathway and the key enzymes for conversion to the final product has been successful with other terpenoids, like isoprene and geraniol (Lv, Wang et al. 2016, Yee, DeNicola et al. 2019). The principal hypotheses for the benefit of expressing the MEP in the mitochondria are (1) the higher concentration of acetyl-

CoA in the mitochondria and (2) a reduced competition from the cytosolic reactions that consume MEP intermediates, like the ergosterol and squalene biosynthetic pathways (Zhang, Jennings et al. 1993, Bhattacharya, Esquivel et al. 2018, Paramasivan and Mutturi 2022).

The 3-hydroxypropionate production in engineered *S. cerevisiae* cells is another example of exploiting the higher acetyl-CoA availability and reducing conditions in the mitochondrial matrix. Expressing a 3-hydroxypropionate-producing pathway in the mitochondria and engineering the metabolism in this organelle to accumulate more NADPH by overexpressing *POS5* and *IDP1* resulted in 6.16 g/L of 3-hydroxypropionate (Zhang, Su et al. 2023).

Overall, compartmentalising pathways in the mitochondria is an interesting approach to increase titres. Compartmentalisation can increase the yield on carbon substrate by reducing the byproduct formation by competing pathways, loss of secreted intermediates, and eliminating the need to transport intermediates across multiple membranes.

2.6.1 Transport of proteins to the mitochondria

Most mitochondrial proteins are encoded by genes in the nucleus and produced in the cytosol before being transported to different compartments within the mitochondria (Chacinska, Koehler et al. 2009, Rout, Oeljeklaus et al. 2021). These nuclear-encoded proteins have mitochondrial targeting sequences (MTS) that direct them to their destination (Mossmann, Meisinger et al. 2012).

There are four main pathways to import proteins into the mitochondria: the presequence pathway, importing proteins to the IMS and matrix; the carrier protein pathway, importing proteins to the IM; and the β-barrel, importing proteins to the OM (Chacinska, Koehler et al. 2009). In this section, we focus on the presequence mechanism of importing proteins, as it is the predominant system to import proteins to the matrix (**Figure 8**). This subcompartment harbours favorable conditions for the heterologous expression of acetyl-CoA and NADH-consuming metabolic pathways. A detailed description of the other mitochondrial, protein import mechanisms can be found in Chacinska *et al.* (2009) and Sayyed *et al.* (2022).

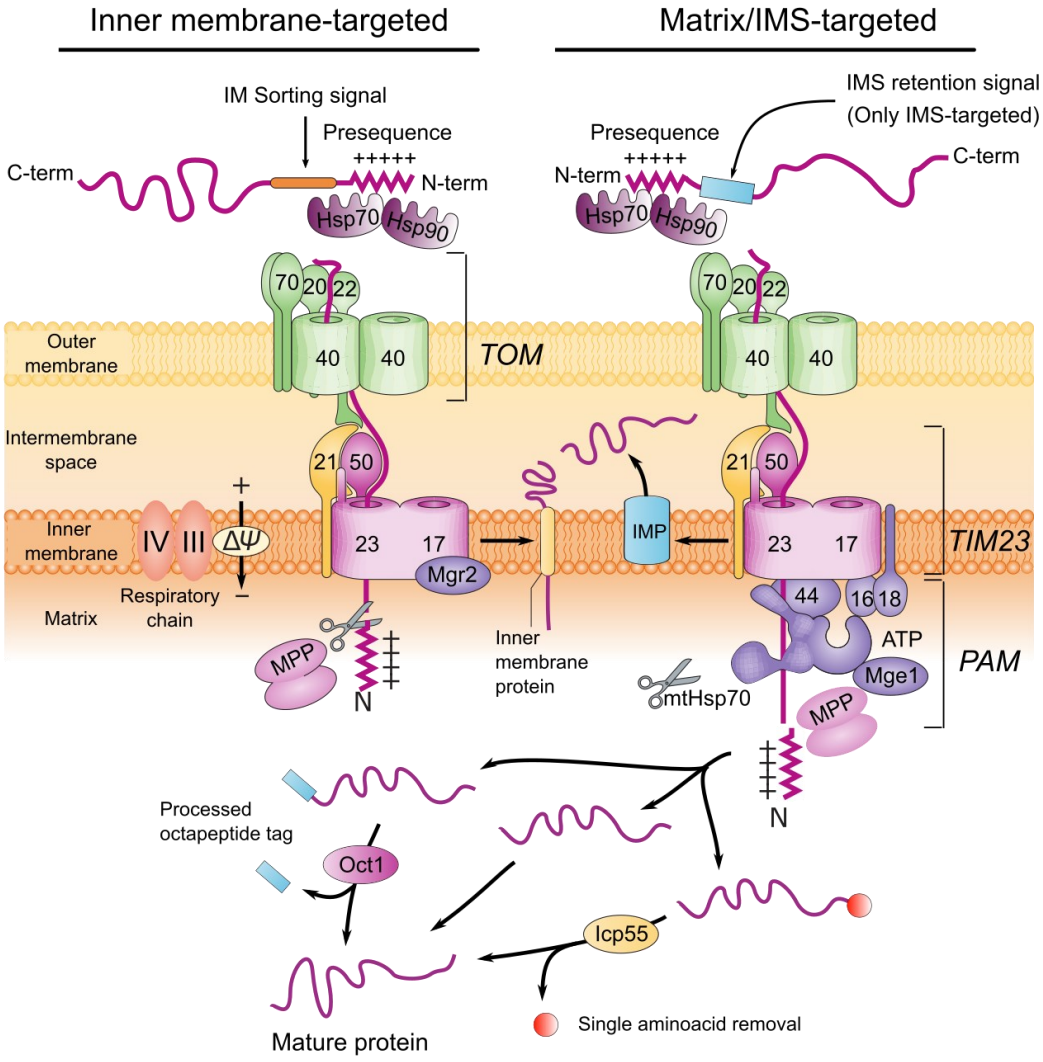

Figure 8. Schematic overview of mitochondrial import mechanisms for presequence-containing proteins. Presequence-containing proteins contain a positively charged targeting signal in the N-terminal region. This sequence is detected by cytosolic chaperones (Hsp70 and 90) and imported via the TOM complex in the outer membrane. IM and IMS-targeted proteins contain additional retention tags. IMS-targeted proteins are processed by the intermembrane peptidase complex (IMP) and retained in the IMS. Matrix and IM-targeted proteins are transferred to the TIM23 complex. Here, IM-targeted proteins are laterally transferred to the inner membrane in a process mediated by Mgr2. IM-targeted proteins can contain matrix-exposed domains. Matrix targeted proteins, on the other hand, are pulled to the mitochondrial matrix via the PAM complex, in an ATP consuming reaction. The respiration chain generates a proton gradient that supports the transfer of proteins through the TIM23 complex. On the matrix side, the peptidase Mpp removes the MTS in matrix-targeted proteins and in the matrix-exposed domains of IM-targeted proteins. In addition, matrix-targeted proteins might require additional processing on the matrix side to become fully functional. Additional matrix peptidases like Oct1 and Icp55 catalyse some of this further processing. This figure was adapted from Schmidt *et al.* (2010) and Sayyed *et al.* (2022).

In yeast, the MTS for the presequence import mechanism consists of a 15-100 amino acid sequence (presequence) in the N-terminal region before the actual protein. This presequence is typically enriched with positively charged amino acids and forms amphipathic α-helices (Malina, Larsson et al. 2018). During the translation by cytosolic ribosomes, chaperones Hsp70 and Hsp90 detect the MTS and bind to the nascent polypeptide, preventing it from aggregation

and transferring it to the translocase of the outer mitochondrial membrane (TOM) complex in the OM (Mossmann, Meisinger et al. 2012). In the TOM complex, Tom20 and Tom22 recognize the hydrophobic side of the presequence and transfer the peptide to the Tom40 channel, where it is translocated first in the IMS. If the polypeptide has an *IMS retention tag* in the presequence, the inner membrane peptidase (IMP) system will cleave the presequence, and the protein will remain in the IMS (Gomes, Palma et al. 2017, Habich, Salscheider et al. 2019). If the protein targets the IM or the matrix instead of the IMS, TOM interacts with the translocase of the mitochondrial inner membrane (TIM23) complex via Tom22, Tim50 and Tim21, resulting in the transfer of the polypeptide into the Tim23 channel (Yamamoto, Esaki et al. 2002, Chacinska, Koehler et al. 2009). Here, matrix-targeted proteins are translocated via a complex interaction between TIM23, the ETC, and the presequence translocase-associated motor (PAM) (Eaglesfield and Tokatlidis 2021). The proton pumping activity of the ETC generates a membrane potential (Δψ) that serves as a driving force to translocate proteins via their positively charged presequences across the Tim23 channel. On the matrix side, the mitochondrial Hsp70, a key component of the PAM, pulls the incoming polypeptide into the matrix in an ATP-consuming process (Malina, Larsson et al. 2018). On the other hand, IM-targeted proteins contain *stop transfer* signals and hydrophobic regions that result in the lateral release of these proteins from the TIM23 channel to the IM. This process is mediated by Mgr2 (Eaglesfield and Tokatlidis 2021). The IM-inserted protein might contain IM or matrix-exposed domains susceptible to further processing (Sayyed and Mahalakshmi 2022). On the matrix side, once the transfer of the matrix-targeted or the IM with matrix domain is complete, the matrix polypeptide peptidase Mpp cleaves the pre-sequence of the polypeptide at a specific site. After Mpp cleavage in the matrix, the polypeptides are mature and ready or can be further processed by additional matrix peptidases like Oct1 and Icp55 (Mossmann, Meisinger et al. 2012). Once polypeptides are fully processed, the cleaved pre-sequences are degraded by proteases Cym1 and Prd1 to prevent disturbing the membrane integrity due to the positively charged residues (Mossmann, Meisinger et al. 2012).

The heterologous expression of a specific reaction or complete pathways in the mitochondria requires MTSs to target the protein of interest in this organelle. Even though the mitochondrial protein import mechanisms are well described in *S. cerevisiae*, the expression of enzymes and pathways in the mitochondria for biotechnological applications is still limited, and only a few MTS are used (Duran, López et al. 2020). For instance, the MTS from Cox4 is the most used to target heterologous proteins in the mitochondria of *S. cerevisiae* and was also used to target multiple proteins for the same pathway (Avalos, Fink et al. 2013, Lv, Wang et al. 2016, Yee, DeNicola et al. 2019, Hammer, Zhang et al. 2020). However, it is preferable to use different MTSs when targeting entire pathways to the mitochondria, as it reduces the risk of undesired homologous recombination events or saturation of the import machinery (den Brave, Gupta et

al. 2021, Dong, Shi et al. 2021). These MTS can also come from other organisms: For instance, the MTS from the Atp9 subunit in *Neurospora crassa* targets heterologous proteins efficiently in the mitochondria of *S. cerevisiae* (Westermann and Neupert 2000). Expanding the number of MTSs available would increase our knowledge of the relation between MTS and protein sequences and its impact on targeting efficiency.

2.7 Aim of the thesis

The global use of chemical compounds keeps increasing. However, the need and demand for more sustainable production processes are also rising. Fatty acyl-CoAs are molecules common in all biological systems and are precursors to many products with industrial interest, of which many are produced today in unsustainable processes (see **section 2.4**). The rBOX is a more energy-efficient pathway to synthesise fatty acyl-CoA than other chain-elongation pathways (Dellomonaco, Clomburg et al. 2011). However, the application of this pathway in the yeast *S. cerevisiae* is so far limited to two cycles and low production titres. *S. cerevisiae* is a robust organism commonly used in industry to produce foods, chemicals, and pharmaceuticals (Wehrs, Tanjore et al. 2019, Parapouli, Vasileiadis et al. 2020). In this study, we aimed to (1) increase the number of cycles when expressing the rBOX pathway in the baker's yeast *S. cerevisiae* and (2) increase the production titres from this pathway in this yeast.

To increase the number of cycles in the pathway, we tested different variants of the rBOX in *S. cerevisiae* and engineered the metabolism to prevent competing reactions. To validate any increase in the number of carbon elongation cycles, we used the production of SCFAs, MCFAs, SCFOHs and MCFOHs.

To improve final production titres, we engineered the metabolism of *S. cerevisiae* to reduce the competition for redox co-factors and other acyl-CoA-targeting reactions. In addition, we engineered the metabolism of this yeast to increase the carbon flux to the mitochondria and expressed a one-cycle version of the rBOX in this organelle.

3 Materials and Methods

3.1 Devices, kits, enzymes, and chemicals

Table 1. Equipment and devices used in this work.

Device	Manufacturer
Agarose gel-electrophoresis chambers	Neolab
Gene Pulser cell-electroporator	Bio-Rad
Spectrophotometer (CLARIOstar Plus)	BMG Labtech
Incubator (Multitron Standard)	Infors HT
Nanodrop 1000 spectrophotometer	Thermo Fisher Scientific
PCR thermocycler (Labcylcler triple block)	SensoQuest
PCR thermocycler (Piko thermal cycler)	Finnzymes
pH-meter (765 Calimatic)	Knick
Pipette, 0.1-2.5 µL	Eppendorf
Pipette, 0.5-10 µL	Eppendorf
Pipette, 10-100 µL	Eppendorf
Pipette, 100-1000 µL	Eppendorf
Shaking incubator	Infors HT
Spectrophotometer (Ultrospec 2100 PRO)	Amersham Bioscience
Thermomixer comfort incubator	eppendorf
Vibrax VXR basic	IKA
Agarose gel-electrophoresis chambers	Neolab
Gel-documentation and visualization device	Vilber Lourmat Vilber Lourmat
HPLC system	
Dionex UltiMate 3000 system	
▪ Autosampler (WPS300SL)	Thermo Scientific
▪ Column oven (TCC-300SD)	Thermo Scientific
▪ Pump system (ISO-3100SD)	Thermo Scientific
▪ Degasser (Ultimate3000)	Thermo Scientific
Column (Coregel 87H3)	Agilent
RI-detector (RI-101)	Shodex
Software (Chromeleon™)	Thermo Scientific
GC systems	
GC-FID	
Instrument (Clarus 400)	Perkin Elmer
Column (Elite 5MS capillary column, 30x0.25x1)	Perkin Elmer
Flame ionization detector	Perkin Elmer
Autosampler	Perkin Elmer
Software (TotalChrom)	Perkin Elmer
GC-MS	
Instrument (7890 A)	Agilent
Column (HP 5MS capillary column, 30x0.25x0.25)	Agilent
Mass detector (MS 5975C Inert MSD)	Agilent
Autosampler (CombiPAL)	PAL systems
Software (Chemstation)	Agilent
Fluorescence microscopy	
Microscope (LSM 780)	Zeiss
Objective (plan-apochromat 63×1.40 Oil DIC M27)	Zeiss

Software (ZEN)	Zeiss

Table 2. Chemicals, enzymes and kits for molecular biology used in this study.

Reagent(s)	Supplier
the chemicals mentioned in this work that are not listed in this table were purchased from Carl Roth	
Bacterial trypton	Difco
Carbenicillin	Carl Roth
Chloramphenicol	Carl Roth
ClonNAT (Nourseothricin)	Werner BioAgents
DNA loading dye	NEB
dNTPs	NEB or ThermoScientific
DreamTaq, incl. buffer	NEB
Hygromycin B	Carl Roth
G418-sulfate, Geneticin	Calbiochem
Geneticin (G418)	Merck
Glass beads (45 µm)	Carl Roth
Glucose-6-phosphate	Carl Roth
Kanamycin sulfate	Carl Roth
Mitotracker Red CMXRos	Invitrogen
PEG-4000	Carl Roth
PEG-8000	Carl Roth
Peptone (bacteriological)	Oxoid
Phusion DNA polymerase, incl. buffer	NEB
Q5 DNA polymerase, incl. buffer	NEB
Restriction enzymes, incl. buffer	NEB
Sheared salmon sperm DNA	Ambion
Synthetic oligonucleotides	biomers, NEB
T4 DNA ligase incl. buffer	NEB
T7 DNA ligase	NEB
Tris-HCl	Difco
Yeast extract	Carl Roth
Yeast Nitrogen base (YNB) without aminoacids	Sigma
Yeast Nitrogen base (YNB) without aminoacids and without ammonium sulfate	Difco
Molecular biology kits	
GeneJET Plasmid Miniprep kit	Thermo Scientific
NucleoSpin Gel and PCR clean up	Macherey-Nagel

3.2 Synthetic DNA

All the oligonucleotides and primers used in this study are listed in **Table 3**. Oligonucleotides and primers created for this study were synthesized by Biomers.net LLC (Germany) or by Microsynth SeqLab GmbH (Switzerland). All the synthetic genes used in this work were ordered from Twist Biosciences after previous codon optimization (see section 3.6.1).

Table 3. Oligonucleotides used and created during this study.

Primers	Sequence	Comments	Reference
ACBseq01	ATCCGCGCTCAAACCAG GCT	Amplification of tVMA16 /sequencing	*This study (Alice Born)*
GDP100	CATGAGCGGATACATATT TGAATTGACGTCGGTCCT TTTCATCACGTGCTAT	Fw CEN/ARS (pAmp//HRRB)	*This study*
GDP101	ATGGCTGAGGCGTTAGA GTAATCTGACGTCGGACG GATCGCTTGCCTGTAAC	Rv CEN/ARS (pAmp//HRRB)	*This study*
GDP130	TAGATACAATTCTATTACC CCCATCCATACTCTAGAA TGTTTAGATCCGTTTGCC GCATTTC	Fw *ter_mtACP* ov pMET25	*This study*
GDP131	GCCTTTAGACATACCAGC ACCAGCGGCCGCCTCGA GTTAAATTCTGTCGAATC TTTCAACTTC	Rv *ter_mtACP* ov L-envy	*This study*
GDP132	TAGATACAATTCTATTACC CCCATCCATACTCTAGAA TGTTGTCAAGAGTAGCTA AAC	Fw *crt_mtMDH* pMET25	*This study*
GDP133	GCCTTTAGACATACCAGC ACCAGCGGCCGCCTCGA GTTATCTGTTCTTGAAAC CTTCAATC	Rv *crt_mtMDH* ov L-envy	*This study*
GDP134	TAGATACAATTCTATTACC CCCATCCATACTCTAGAA TGTTAAGAATCAGATCAC TCCTAAATAATAAG	Fw *adhE2_mtLPD* pMET25	*This study*
GDP135	GCCTTTAGACATACCAGC ACCAGCGGCCGCCTCGA GTTAGAAAGACTTAATGT AGATATCCTTCAATTC	Rv *adhE2_mtLPD* L-envy	*This study*
GDP138	TAGATACAATTCTATTACC CCCATCCATACTCTAGAA TGGCCTCCACTCGTGTC	Fw *ERG10* ov pMET25	*This study*
GDP139	GCCTTTAGACATACCAGC ACCAGCGGCCGCCTCGA GTTAAATCTTTTCAATGAC AATAGAGGAAGC	Rv *ERG10* ov L-GFPenvy	*This study*
GDP150	CTCCAAGTATTTTTTAACG TATATTGAAAG	*MTH1*(169-393)ko check Fw	*This study*
GDP151	TCTTCCTCAATTCCTTGG GAATTTGG	*MTH1*(169-393)ko check Rv	*This study*
GDP200	CTTGGGCGGATTGACCG TTAAGATCATTTATCTTTC ACTGCGGAG	gRNA for *GPD2* deletion Rv	*This study*
GDP201	CTTAACGGTCAATCCGCC CAAGTTTTAGAGCTAGAA ATAGCAAGTTAAAATAAG G	gRNA for *GPD2* deletion Fw	*This study*
GDP341	CAATTCTATTACCCCCAT CCATACTCATGCTTTCAC TACGTCAATC	Fw *mteutE* ov pMET25	*This study*
GDP342	CAATTCCTCGCCTTTAGA ACCAGCACCAGCGGCCG CAACAATTCTGAAAGCAT CGACC	Rv *mteutE* ov *GFPenvy*	*This study*
GDP343	CAATTCTATTACCCCCAT CCATACTCATGGCCTCCA CTCGTGTC	Fw *NC-hbd* ov pMET25	*This study*
GDP344	CAATTCCTCGCCTTTAGA ACCAGCACCAGCGGCCG CCTTAGAGTAATCGTAGA AACCC	Rv *NC-hbd* ov *GFPenvy*	*This study*

GDP418	GATCGGAAGTACGGGATCGTGAGT	Fw gRNA2 for *TES1* deletion	*This study*
GDP419	AAACACTCACGATCCCGTACTTCC	Rv gRNA2 for *TES1* deletion	*This study*
GDP420	CCACCATGAGCAAGACAAGATAAGACAAGATTGCATAAAAGGACAATTCCCTCCCACGTATAAACACATACATATATATTC	Fw donor DNA for *TES1*-ko	*This study (Fabian Haitz)*
GDP421	GAATATATATGTATGTGTTTATACGTGGGAGGGAATTGTCCTTTTATGCAATCTTGTCTTATCTTGTCTTGCTCATGGTGG	Rv donor DNA for *TES1*-ko	*This study (Fabian Haitz)*
GDP438	CTATCCACCAGCCAAAACCAC	*TES1*-KO check Fw	*This study*
GDP439	GCTTGATGAGAATGTGCAGGC	*TES1*-KO check Rv	*This study*
GDP445	GCCTTTAGAACCAGCACCAGCGGCCGCGTAGTCGTAGAAACCCTTACC	Rv MTS *HADyl* ov *L-GFPenvy*	*This study*
GDP456	GATACAATTCTATTACCCCCATCCATACTCATGACTGTTCACCACAGAACTG	Fw *ylECH* ov pMET25	*This study (F. Haitz)*
GDP457	CCTCGCCTTTAGAACCAGCACCAGCGGCCGCTTCGTTCTTGAAGTTTGGTTCTCTC	Rv *ylECH* ov *L-GFPenvy*	*This study (F. Haitz)*
GDP482	CTATAAATCGTAAAGACATAAGAGATCCGCTGTGTATTACGATATAGTTAATAGTT	Rv pAdh2	*This study*
GDP483	TATCAACTATTAACTATATCGTAATACACAGCGGATCTCTTATGTCTTTACGATT	Fw tAdh2	*This study*
GDP484	AGGGCGTGAATGTAAGCGTGACATAATTAATCTCTAGCACTTTTGAGAGATTCAG	Rv for all *kmEAT1* tCYC1	*This study*
GDP485	CAAAAACAAAAAGTTTTTTTAATTTTAATCAAAAAATGCTTCTCGCTTACACCGTCAG	Fw *kmEAT1* ov pHXT7	*This study*
GDP487	CAAAAACAAAAAGTTTTTTTAATTTTAATCAAAAAATGAAAGGGCTTTTGCCATTGC	Fw *kmEAT1*KO 1-30 ov pHXT7	*This study*
GDP488	CTCGCCTTTAGAACCAGCACCAGCGGCCGCATCTCTAGCACTTTTGAGAGATTCAG	Rv for all *kmEAT1* ov *L-Envy*	*This study*
GDP489	GATACAATTCTATTACCCCCATCCATACTCATGCTTCTCGCTTACACCGTCAG	Fw *kmEAT1* ov pMET25	*This study*
GDP490	GATACAATTCTATTACCCCCATCCATACTCATGTACTCTGCTACTGCCAGAGCCTTC	Fw *kmEAT1* KO1-19 ov pMET25	*This study*
GDP491	GATACAATTCTATTACCCCCATCCATACTCATGAAAGGGCTTTTGCCATTGC	Fw *kmEAT1* KO1-30 ov pMET25	*This study*
GDP492	GATACAATTCTATTACCCCCATCCATACTCATGTTCAGATTGACTACTGCTAGAATC	Fw MTS *HADyl* ov pMET25	*This study*
GDP86	CAGATCGCTTCATACAGGGAAAGTTCGGCATGGATC	Rv tAMP (HRRA//AmpR)	*This study*

	CTTTCTACGGGGTCTGAC GCTCAGTG		
GDP87	GCTTAAATGCGTGACGTC AATTCAAATATGTATCCG CTCATGAGAC	Fw pAMP (Amp R//2µ)	*This study*
GDP90	ATGGCCCACTACGTGAAC CATCACCAACGGTAGATC AAAGGATCTTCTTGAGAT CC	Rv ColE1 (HRRB//URA3)	*This study*
GDP91	CAGATTACTCTAACGCCT CAGCCATCATCGCGCGTT GCTGGCGTTTTTCCATAG	Fw ColE1 (HRRB//URA3)	*This study*
GDP92	CTCAAGAAGATCCTTTGA TCTACCGTTGGTGATGGT TCACGTAGTGGGCCATC G	Rv tURA3 (HRRC//ColE1)	*This study*
GDP93	GGCGCGCCTAGACACGG GCATCGTCCTCTCGAAAG GTGAGCTTTTCAATTCAA TTCATCATTTTTTTTTTATT C	Fw pURA3 (HRRC//ColE1)	*This study*
GDP94	CACCTTTCGAGAGGACGA TGCCCGTGTCTAGGCGC GCCGATGCAAGGGTTCG AATCCCTTAG	Fw pMET25 (HRRC//GFP)	*This study*
GDP95	CTCGAGGAGTATGGATG GGGGTAATAGAATTG	Rv pMET25 (HRRC//GFP)	*This study*
GDP96	ATTCTATTACCCCCATCC ATACTCCTCGAGATGTCT AAAGGCGAGGAATTGTTT ACAG	Fw *GFPenvy* (pMET25//tCyc)	*This study*
GDP97	GAATGTAAGCGTGACATA ACTAATTAAGCTTTTATTT GTACAATTCGTCCATTCC TAATG	Rv *GFPenvy* (pMET25//tCyc)	*This study*
GDP98	AAGCTTAATTAGTTATGTC ACGCTTACATTCAC	Fw tCyc (pMET25//HRRA)	*This study*
GDP99	GCCGAACTTTCCCTGTAT GAAGCGATCTGGGCGAA TTGGGTACCGGCCGCAA ATTAAAGC	Rv tCyc (pMET25//HRRA)	*This study*
JWP043	GCAGTATGCATTCAGCGA GCGTTTTAGAGCTAGAAA TAGCAAGTTAAAATAAGG	gRNA for *MTH1*	*Johannes Wess*
JWP044	CGCTCGCTGAATGCATAC TGCGATCATTTATCTTTCA CTGCGGAG	gRNA for *MTH1*	*Johannes Wess*
JWP045	CAGTGATAATGCTTCTTTT CAAAGTTTGCCACTATCA ATGTTTTCTGCCCCCTCT ACTGTGCACACGCAACTA ACTAATG	Fw donor DNA for *MTH1*(169-393)ko	*Johannes Wess*
JWP046	CATTAGTTAGTTGCGTGT GCACAGTAGAGGGGGCA GAAAACATTGATAGTGGC AAACTTTGAAAAGAAGCA TTATCACTG	Rv donor DNA for *MTH1*(169-393)ko	*Johannes Wess*
JWP061	CTCTTTCCCTTTCCTTTTC CTTCGCTCCCCTTCCTTA TCAACACTCTCCCCCCCC CTCCCCCTCTGATCTTTC CTGTTGC	Fw donor DNA for *GPD2*-ko	*Johannes Wess*
JWP062	GCAACAGGAAAGATCAGA GGGGGAGGGGGGGGGA GAGTGTTGATAAGGAAGG GGAGCGAAGGAAAAGGA AAGGGAAAGAG	Rv donor DNA for *GPD2*-ko	*Johannes Wess*

RPP266	GAAGTCCCGGTGTCCCT GACGTTATTGTAG	Fw donor DNA for *FAA2* KO & confirmation	*Renata Pavlovic*
RPP267	GTGACCCATGTACTCCGC TAGATTGACCAG	Rv donor DNA for *FAA2* KO & confirmation	*Renata Pavlovic*
vsp195	GGGTACAACTCACAGGC GAGGG	Rv tAdh2	*Virginia Schadeweg*
vsp196	GGCAGAGGAGAGCATAG AAATGGGG	Fw pAdh2	*Virginia Schadeweg*
VSP269	GGAACATCCGAGCACCC GCGCC	*GPD2*-KO check Fw	*Virginia Schadeweg*
VSP270	GGCGGCATCGAAATCTTC TTCTTGCCC	*GPD2*-KO check Rv	*Virginia Schadeweg*

3.3 Strains and plasmids

The yeast strains used as starting point to develop this work (VSY0) or as a source of DNA are listed and described in **Table 4**. The yeast strains created and developed in this work are listed in **Table 5**. All the plasmids used and created in this work are listed in **Table 6**, including a detailed description of their genetic elements.

Table 4. Yeast strains used in this work.

Strain	genotype	Reference
***Kluyveromyces marxianus* CBS6556**	-	EUROSCARF
***Saccharomyces cerevisiae* CEN.PK2-1C**	*MATa; ura3-52; trp1-289; leu2-3_112; his3 Δ1; MAL2-8C; SUC2*	EUROSCARF
SHY34	*MATa; ura3-52; trp1-289; leu2-3_112; his3 Δ1; MAL2-8C; SUC2, Δfas1, Δfas2, Δfaa2*	(Wernig, Born et al. 2020)
VSY0	*MATa; ura3-52; trp1-289; leu2-3_112; his3 Δ1; MAL2-8C; SUC2 adh1::loxP adh2Δ::LEU2 adh3::loxP adh4Δ::loxP adh5::loxP*	Schadeweg and Boles (2016)

Table 5. Yeast strains created in this work.

Strain	genotype
GDY1	VSY0, *mth1*$\Delta_{169\text{-}393}$
GDY2	GDY1 Δ*gpd2*
GDY2.1	GDY2 Δ*LEU2*
GDY3	GDY1 *ura3*Δ::pPSAC6-*NCmts_ERG10*-tSSA1, pRNR2-*NCmts_*^{Ca}*hbd*-tHIS5, pPSP2-*MDHmts_*^{Ca}*crt*-tPGK1, pRAD27-*ACPmts_*^{Td}*ter*-tADH1, pREV1-*CoxIVmts_*^{Ec}*eutE*-tCYC1, pPOP6-*LPDmts_*^{Ca}*adhE2*-tTDH1, *KanMX*
GDY4	GDY2 ΔpNDI1::pYEN1
GDY8	GDY2 *ura3*Δ::pPSAC6- *NCmts_ERG10*-tSSA1, pRNR2- *NCmts_*^{Ca}*hbd* -tHIS5, pPSP2-*MDHmts_*^{Ca}*crt*-tPGK1, pRAD27-*ACPmts_*^{Td}*ter*-tADH1, pREV1- *CoxIVmts_*^{Ec}*eutE* -tCYC1, pPOP6- *LPDmts_*^{Ca}*adhE2*-tTDH1, *KanMX*
GDY9	GDY4 *ura3*Δ::pPGK1- *NCmts_ERG10*-tVMA16, pRNR2- *NCmts_*^{Ca}*hbd* -tHIS5, pPSP2-*MDHmts_*^{Ca}*crt* -tPGK1, pTDH3- *ACPmts_*^{Td}*ter* -tADH1, pPOP6- *LPDmts_*^{Ca}*adhE2*-tTDH1, *KanMX*
GDY11	GDY4 *ura3*Δ::pPSAC6- *NCmts_ERG10*-tSSA1, pRNR2- *NCmts_*^{Ca}*hbd* -tHIS5, pPSP2-*MDHmts_*^{Ca}*crt* -tPGK1, pRAD27- *ACPmts_*^{Td}*ter* -tADH1, pREV1- *CoxIVmts_*^{Ec}*eutE* -tCYC1, pPOP6- *LPDmts_*^{Ca}*adhE2*-tTDH1, *KanMX*
GDY15	VSY0 Δ*gpd2*
GDY15.1	GDY15 Δ*LEU2*
GDY16	GDY15 Δ*tes1*

GDY19	GDY15 Δ*faa2*
GDY20	GDY4 Δ*ura3*:: pPGK1- *NCmts_ERG10*-tSSA1, pRNR2-^{Yl}*had*-tIDP1, pPSP2-^{Yl}*ECH*-tPGK1, pTDH3- *ACPmts_*^{Td}*ter* -tADH1, pTEF1- *LPDmts_*^{Ca}*adhE2(**)*-tTDH1, *KanMX*
GDY25	GDY4 Δ*ura3*:: pSAC6- *NCmts_ERG10*-tSSA1, pRNR2-^{Yl}*HAD*-tIDP1, pPSP2-^{Yl}*ECH*-tPGK1, pRAD27- *ACPmts_*^{Td}*ter* -tADH1, pPOP6- *LPDmts_*^{Ca}*adhE2*-tTDH1, *KanMX*
GDY27	GDY15: Δ*ura3*::pHHF2-^{Cn}*bktB*-tENO2, pCCW12-^{Cn}*paaH1*-tIDP1, pENO2-^{Ca}*crt*-tPGK1, pTDH3-^{Td}*ter*-tADH1, *KanMX*
GDY28	GDY15 Δ*ura3*:: pHHF2- ^{Cn}*bktB*-tENO2, pCCW12- ^{Cn}*paaH1*-tIDP1, pENO2-^{Cn}*crt2*-tPGK1, pTDH3- ^{Td}*ter* -tADH1, *KanMX*
GDY29	GDY15 Δ*ura3*:: pHHF2- ^{Cn}*bktB* -tENO2, pCCW12- ^{Cn}*paaH1*-tIDP1, pENO2- ^{Yl}*ECH* -tPGK1, pTDH3- ^{Td}*ter* -tADH1, *KanMX*

Table 6. Plasmids used and created in this study.

Plasmid	Characteristics	Reference
ACBV007	*URA3*, CEN6ARS4, *Kanamycin R*, ColE1, pHHF2- ^{cn}*bktB* -tENO2, pCCW12- ^{Ca}*hbd* -tIDP1, pENO2-^{Ca}*crt*-tPGK1, pTDH3- ^{Td}*ter* -tADH1	*This study (A. Born)*
GDV001.2	*URA3*, CEN6ARS4, ColE1, *Ampicillin R*, pMET25-*GFPenvy*-tCYC1 (AscI/PacI)	*This study*
GDV004	*URA3*, CENARS, ColE1, *Ampicillin R*, pMET25- *MDHmts_*^{Ca}*crt* *_GFPenvy*-tCYC1	*This study*
GDV005	*URA3*, CENARS, ColE1, *Ampicillin R*, pMET25- *LPDmts_*^{Ca}*adhE2_GFPenvy*-tCYC1	*This study*
GDV006	*URA3*, CENARS, ColE1, *Ampicillin R*, pMET25- *NCmts_ERG10_GFPenvy*-tCYC1	*This study*
GDV007	*URA3*, CENARS, ColE1, *Ampicillin R*, pMET25- *ACP1mts_*^{Td}*ter_GFPenvy*-tCYC1	*This study*
GDV020	*URA3*, CENARS, ColE1, *Ampicillin R*, pMET25- *NCmts_*^{Ca}*hbd_GFPenvy*-tCYC1	*This study*
GDV060	ColE1, *KanR*, pPGK1- *NCmts_ERG10*-tSSA1, pCCW12- *NCmts_*^{Ca}*hbd*-tHIS5, pENO2- *MDHmts_*^{Ca}*crt* -tPGK1, pTDH3- *ACPmts_*^{Td}*ter*-tADH1, pRPL3-*CoxIVmts_*^{Ec}*eutE*-tCYC1, pTEF1- *LPDmts_*^{Ca}*adhE2*-tTDH1, *KanMX*, URA3 5'- URA3 3' for Homologous recombination	*This study*
GDV061	ColE1, *KanR*, pPSAC6-*NCmts_ERG10*-tSSA1, pRNR2- *NCmts_*^{Ca}*hbd* -tHIS5, pPSP2- *MDHmts_*^{Ca}*crt*-tPGK1, pRAD27- *ACPmts_*^{Td}*ter* -tADH1, pREV1- *CoxIVmts_*^{Ec}*eutE* -tCYC1, pPOP6- *LPDmts_*^{Ca}*adhE2*-tTDH1, *KanMX*, URA3 5'- URA3 3' for Homologous recombination	*This study*
GDV098	*URA3*, CEN6ARS4, *Kanamycin R*, ColE1, pPGK1-*ERG10*-tENO2, pCCW12- ^{Ca}*hbd* -tIDP1, pENO2- ^{Ca}*crt* -tPGK1, pTDH3- ^{Td}*ter* -tADH1	*This study*
GDV105	ColE1, *KanR*, pPGK1- *NCmts_ERG10*-tSSA1, pRNR2- *NCmts_*^{Ca}*hbd* -tHIS5, pPSP2- *MDHmts_*^{Ca}*crt* -tPGK1, pTDH3- *ACPmts_*^{Td}*ter* -tADH1, pPOP6- *LPDmts_*^{Ca}*adhE2*-tTDH1, *KanMX*, URA3 5'- URA3 3' for Homologous recombination	*This study*
GDV116	*URA3*, CEN6ARS4, *Kanamycin R*, ColE1, pHHF2- ^{cn}*bktB* -tENO2, pCCW12- ^{Cn}*paaH1*-tIDP1, pENO2- ^{Cn}*crt2*-tPGK1, pTDH3- ^{Eg}*ter* -tADH1	*This study*
GDV124	*HIS3*, CEN6ARS4, *Kanamycin R*, ColE1, pHHF2- ^{cn}*bktB* -tENO2, pCCW12- ^{Cn}*paaH1*-tIDP1, pENO2- ^{Cn}*crt2*-tPGK1, pTDH3- ^{Td}*ter* -tADH1	*This study*
GDV143	*Kanamycin R*, ColE1, URA3 5' UTR, pHHF2- ^{cn}*bktB* -tENO2, pCCW12- ^{Cn}*paaH1*-tIDP1, pENO2- ^{Cn}*crt2*-tPGK1, pTDH3- ^{Td}*ter* -tADH1, *KanMX*, URA3 3' UTR	*This study*
GDV144	*URA3*, CEN6ARS4, *Kanamycin R*, ColE1, pHHF2- ^{cn}*bktB* -tENO2, pCCW12- ^{Cn}*paaH1*-tIDP1, pENO2- ^{Yl}*ECH* -tPGK1, pTDH3- ^{Td}*ter* -tADH1	*This study*
GDV146	ColE1, *KanR*, pPSAC6-*NCmts_ERG10*-tSSA1, pRNR2-^{Yl}*HAD*-tHIS5, pPSP2-^{Yl}*ECH*-tPGK1, pRAD27-*ACPmts_*^{Td}*ter*-tADH1, pREV1- *CoxIVmts_*^{Ec}*eutE*-tCYC1, pPOP6- *LPDmts_*^{Ca}*adhE2*-tTDH1, *KanMX*, URA3 5'- URA3 3' for Homologous recombination	*This study*
GDV148	ColE1, *KanR*, pPGK1-*NCmts_ERG10*-tSSA1, pRNR2-^{Yl}*HAD*-tHIS5, pPSP2-^{Yl}*ECH*-tPGK1, pTDH3-*ACPmts_*^{Td}*ter*-tADH1, pREV1-*CoxIVmts_*^{Ec}*eutE*-tCYC1, pTEF1- *LPDmts_*^{Ca}*adhE2*-tTDH1, *KanMX*, URA3 5'- URA3 3' for Homologous recombination	*This study*

GDV149	*Kanamycin R*, ColE1, URA3 5' UTR, pHHF2-*^{cn}bktB* -tENO2, pCCW12-*^{Cn}paaH1*-tIDP1, pENO2-*^{Ca}crt*-tPGK1, pTDH3-*^{Td}ter* -tADH1, *KanMX*, URA3 3' UTR	*This study*
GDV150	*Kanamycin R*, ColE1, URA3 5' UTR, pHHF2-*^{cn}bktB* -tENO2, pCCW12-*^{Cn}paaH1*-tIDP1, pENO2-*^{Yl}ECH*-tPGK1, pTDH3-*^{Td}ter* -tADH1, *KanMX*, URA3 3' UTR	*This study*
GDV151	*URA3*, CEN6ARS4, *Kanamycin R*, ColE1, pHHF2-*^{cn}bktB* -tENO2, pCCW12-*^{Yl}HAD*-tIDP1, pENO2-*^{Ca}crt*-tPGK1, pTDH3-*^{Td}ter* -tADH1	*This study*
GDV152	*URA3*, CEN6ARS4, ColE1, *Ampicillin R*, pMET25-*^{Yl}HAD_GFPenvy*-tCYC1	*This study*
GDV153	*URA3*, CENARS, ColE1, *Ampicillin R*, pMET25-*^{Km}EAT1_GFPenvy*-tCYC1	*This study*
GDV154	*URA3*, CENARS, ColE1, *Ampicillin R*, pMET25-*^{Km}EAT1* $_{(\Delta 1\text{-}19)}$_GFPenvy-tCYC1	*This study*
GDV155	*URA3*, CENARS, ColE1, *Ampicillin R*, pMET25-*^{Km}EAT1* $_{(\Delta 1\text{-}30)}$_GFPenvy-tCYC1	*This study*
GDV156	*URA3*, CENARS, ColE1, *Ampicillin R*, pHXT7-*EAT1* (*K.marxianus*)-tCYC1	*This study*
GDV157	*URA3*, CENARS, ColE1, *Ampicillin R*, pHXT7-*EAT1* (km, Δ1-30) -tCYC1	*This study*
GDV163	*HygR*, CEN6ARS4, *Kanamycin R*, ColE1, pTDH3-*^{Ca}adhE2*-tPGK1	*This study*
GDV164	*HygR*, CEN6ARS4, *Kanamycin R*, ColE1, pTDH3-*^{Ec}eutE*-tPGK1	*This study*
GDV169	*URA3*, CENARS, ColE1, *Ampicillin R*, pMET25-*CoxIVmts*_*^{Ec}eutE*_GFPenvy-tCYC1	*This study*
OTV011	*HygR*, CEN6ARS4, *Kanamycin R*, ColE1	*Okbai Tesfamichael*
LBGV022	*LEU2*, CEN6ARS4, *Kanamycin R*, ColE1	*Leonardo Beltran*
LBGV024	*HIS3*, CEN6ARS4, *Kanamycin R*, ColE1	*Leonardo Beltran*
FHV018	*URA3*, CEN6ARS4, *Kanamycin R*, ColE1, pHHF2-*^{cn}bktB* -tENO2, pCCW12-*^{Cn}paaH1*-tIDP1, pENO2-*^{Cn}crt2*-tPGK1, pTDH3-*^{Td}ter* -tADH1	*This study (F. Haitz)*
FHV022	*URA3*, CEN6ARS4, *Kanamycin R*, ColE1, pHHF2-*^{cn}bktB* -tENO2, pCCW12-*^{Cn}paaH1*-tIDP1, pENO2-*^{Ca}crt*-tPGK1, pTDH3-*^{Td}ter* -tADH1	*This study (F. Haitz)*
FHV025	*URA3*, CENARS, ColE1, *Ampicillin R*, pMET25-*^{Yl}ECH*_GFPenvy-tCYC1	*This study (F. Haitz)*
pRCCK_MR02	*KanMX*, 2µ, *Ampicillin R*, ColE1, *Cas9*, gRNA for *URA3* deletion	*Mara Reifenrath*
pRCCK_GD01	*KanMX*, 2µ, *Ampicillin R*, ColE1, *Cas9*, gRNA for *GPD2* deletion	*This study*
FHV016	*KanMX*, 2µ, *Ampicillin R*, ColE1, *Cas9*, gRNA for *TES1* deletion	*This study (F. Haitz)*
pRCCK_SH06	*CloNat*, 2µ, *Ampicillin R*, ColE1, *Cas9*, gRNA for *FAA2* deletion	*Sandra Born*
pRCCK_MTH1	*CloNat*, 2µ, *Ampicillin R*, ColE1, *Cas9*, gRNA for *MTH1* deletion	*Johannes Wess*
BBV001	*CloNat*, 2µ, *Ampicillin R*, ColE1, *Cas9*, gRNA for *LEU2* deletion	*Bernadett Bodnar*
pUCP_pHXT7	*URA3*, CEN6ARS4, *AmpicillinR*, ColE1, pHXT7-tCYC1	*This study*
pVS1	*Ampicillin R*, ColE1, GPD2 5' pHXT7-*ERG10*-tVMA16, pPGK1-*^{Ca}hbd*-tEFM1, pTPI1-*^{Ca}crt*-tYHI9, loxP, *KanMX*, loxP, pPYK1-*^{Eg}ter* -tIDP1, pADH1-*^{Ca}adhE2*-tRPL3, GPD2 3'	*Virginia Schadeweg*
pVS6	*Ampicillin R*, ColE1, GPD2 5' pHXT7-*ERG10*-tVMA16, pPGK1-*^{Ca}hbd* -tEFM1, pTPI1-*^{Ca}crt* -tYHI9, pPYK1-*^{Td}ter* -tIDP1, pADH1-*^{Ca}adhE2*-tRPL3, pTDH3-*^{Ec}eutE*-tRPL41B, *KanMX*, GPD2 3'	*Virginia Schadeweg*

(**) Mutated gene. Two adenine nucleotides missing compared to the consensus sequence.

3.4 Cell Cultivation and Fermentation

3.4.1 Cultivation media

This section describes the composition of the cultivation media used in this work. The carbon source (glucose or galactose) was autoclaved separately from the rest of elements of the media and added once it reached room temperature. The antibiotics were added when the final cultivation medium composition temperature was below 55ºC. For solid media used in plating, agar-agar was added to the medium at a final concentration of 19 g/L.

3.4.1.1 Yeast extract Peptone Dextrose (YPD)

YPD was used for cultivation when no auxotrophic selection was required, or selection was based on dominant markers. YPD contained 10 g/L Yeast extract, 20 g/L peptone and 20 g/L glucose. In some cases, YPD was supplemented with 100 mM potassium phosphate buffer. If the strain selection was based on the resistance to one or more antibiotics, the antibiotics were added according to section 3.4.1.5.

3.4.1.2 Synthetic complete medium (SCD)

Synthetic complete medium with dextrose was used for cultivation of *S. cerevisiae* on solid plates when auxotrophic selection was required. SC contained 1.7 g/L yeast nitrogen base without amino acids, 5 g/L of ammonium sulfate, 50 mL/L of the 20x Amino acid supplement (**Table 7**) and 20 g/L of glucose. The pH of the solution was set to 6.3 by adding KOH. Auxotrophic markers were added according to **Table 8**. The appropriate selection markers were omitted from the final medium composition when auxotrophic selection was required.

Table 7. Composition of the 20x amino acid Mix. 'Concentration in the stock solution is the concentration of the 20x Aminoacid Mix bottle containing the amino acids. 'Final concentration in the media' is the concentration after adding 50 mL/L of the 20x Amino acid Mix.

Compound	Concentration in the stock solution (mg/L)	Concentration in the stock solution (mM)	Final concentration in the media (mM)
Adenine	224	1.66	0.083
Arginine	768	4.41	0.221
Methionine	768	5.15	0.258
Tyrosine	288	1.59	0.08
Isoleucine	1152	8.78	0.439
Lysine	1152	7.88	0.394
Phenylalanine	960	5.81	0.291
Valine	1152	9.83	0.492
Threonine	1152	9.67	0.484

Table 8. Auxotrophic markers used in this study.

Auxotrophic marker	Concentration in the stock solution (g/L)	Concentration in the stock solution (mM)	Final concentration in the media (mM)
Uracil	1.2	10.71	0.171
Histidine	2.4	15.47	0.124
Tryptophan	2.4	11.57	0.093
Leucin	3.6	27.44	0.439

3.4.1.3 Synthetic medium with dextrose (SMD)

Synthetic complete medium with dextrose (SMD) was used in fermentation of *S. cerevisiae* to produce medium-chain fatty acids, medium-chain fatty alcohols or 1-butanol. SMD contained 1.7 g/L yeast nitrogen base without amino acids, 5 g/L of ammonium sulfate, 20 mM of potassium phosphate buffer and 20 g/L of glucose. The pH of the solution was set to 6.3 prior to autoclaving by adding potassium hydroxyde. Auxotrophic markers were added according to **Table 8**. The appropriate selection markers were omitted from the final medium composition when auxotrophic selection was required.

3.4.1.4 Lisogeny broth (LB)

LB media was used for cultivation of *E. coli* and contained 5 g/L NaCl, 10 g/L Tryptone and 5 g/L yeast extract. To select *E. coli* DH10β transformants based on the resistance to one or more antibiotics, the antibiotics were added according to section 3.4.1.5.

3.4.1.5 Antibiotic supplementation

Table 9. List of antibiotics used in this work for bacterial and yeast selection.

Antibiotic	Stock solution (mg/mL)	Final concentration (µg/mL)	Storage
Carbenicillin	100	100	-20°C
Kanamycin sulphate	50	50	-20°C
Chloramphenicol	34 (in 70% ethanol)	34	-20°C
CloNAT (Nourseothricin)	100	100	-20°C
Hygromycin B	200	200	-20°C
Geneticin (G418)	200	200	-20°C

3.4.2 Fermentations to produce medium-chain fatty acids and alcohols

Pre culture. 300 mL Erlenmeyer flasks containing 40 mL of SM with the required auxotrophies were inoculated with their respective strain and grown to exponential phase at 30ºC and 180 rpm.

Fermentation. Once reached the exponential phase, the pre-cultures were washed with de-ionized water and used to inoculate new 100 mL Erlenmeyer flasks containing 40 mL of SM with the required auxotrophies at an initial OD_{600nm} of 0.3. The semi-anaerobic fermentations were performed during 75h at 30ºC and 180 rpm. Samples were collected at time (h) 0, 4, 25, 50, 75 to measure growth (OD_{600nm}) and to measure glucose consumption, ethanol, glycerol, acetate and butyric acid in the HPLC. The production of hexanoic acid, octanoic acid, decanoic acid, 1-butanol, 1-hexanol, 1-octanol and 1-decanol was analysed by GC.

3.4.3 Fermentation to assess mitochondrial metabolism

The fermentations to compare the production and growth behaviour of GDY1, GDY2, GDY15, VSY0, CEN.PK2-1C in YPD (4.2.1.1) were run as follows:

Pre culture. 300 mL Erlenmeyer flasks containing 50 mL of YPD were inoculated with their respective strain and grown to exponential phase at 30ºC and 180 rpm.

Fermentation. Once reached the exponential phase, the pre-cultures were washed twice with de-ionized water and used to inoculate new 300 mL Erlenmeyer flasks containing 50 mL of YPD at an initial OD_{600nm} of 0.3. The semi-anaerobic fermentations were performed during 100h at 30ºC and 180 rpm. Samples were collected at time (h) 0, 4, 25, 50, 75, 100 to measure growth (OD_{600nm}) and to measure glucose consumption, ethanol, acetate, and glycerol in the HPLC.

The fermentations to compare the production pattern of GDY2.1, GDY15.1 and CEN.PK2-1C expressing a mitochondrial or a cytosolic variant of Eat1 (4.2.1.2) were run as follows:

Pre culture. 300 mL Erlenmeyer flasks containing 50 mL of SMD_{URA-} were inoculated with their respective strain and grown to exponential phase at 30ºC and 180 rpm.

Fermentation for expression of EAT1. Once reached the exponential phase, the pre-cultures were washed twice with de-ionized water and used to inoculate new 300 mL Erlenmeyer flasks containing 40 mL of SMD_{URA-} at an initial OD_{600nm} of 0.3. The semi-anaerobic fermentations were performed during 75h at 30ºC and 180 rpm. Samples were collected at time (h) 0, 4, 25, 50, 75h to measure growth (OD_{600nm}) and to measure glucose consumption, ethanol, acetate, and glycerol in the HPLC. Samples at 50h and 75h were also used to screen for volatile compounds and to measure isoamyl alcohol, isoamyl acetate and ethyl acetate in the GC-MS.

3.4.4 Fermentation to produce 1-butanol in the mitochondria

Pre culture. A 300 mL Erlenmeyer flask containing 50 mL of SM was inoculated with the respective strain and grown to exponential phase at 30ºC and 180 rpm.

Fermentation. Once reached the exponential phase, the pre-cultures were washed in de-ionized water and used to inoculate new 300 mL Erlenmeyer flasks containing 50 mL of SM at an initial OD_{600nm} of 0.3. The semi-anaerobic fermentations were performed during 100h at 30ºC and 180 rpm. Samples were collected at time (h) 0, 4, 25, 50, 75, 100 to measure growth (OD_{600nm}) and to measure glucose concentration, ethanol, glycerol and butyric acid in the HPLC. The production of 1-butanol was analysed by GC.

3.5 DNA methods

3.5.1 Genomic DNA isolation from *Saccharomyces cerevisiae* and *Kluyveromyces marxianus*

This was the preferred method to extract DNA for checking genomic insertions and deletions in the generated yeast strains and to be used as the template for amplifying genomic regions of interest for further molecular cloning experiments.

First, the cells were grown for two days (30°C, 180 rpm) in 10 mL of appropriate medium. Then, the cells were centrifuged (3000 xg, 5 min, RT), and the supernatant discarded. The cell pellet was resuspended in 1 mL of sterile water, transferred to a 2 mL tube, and centrifuged (3000 xg, 1 min, RT). We repeated this washing step was repeated, and at the end, discarded the supernatant. Then, we resuspended the washed cell pellet in 400 µL of a 10 mM EDTA, 25 mM Tris-HCl (pH 8) solution containing 100 µg/mL of RNAse A, added 400 µL of a 200 mM NaOH, 1% SDS solution and a volume of approximately 700 µL of glass beads (0,45 mm diameter). We disrupted the cells by bead beating in a VXR Vibrax system (IKA) during 8 min at a shaking speed of 2000 rpm. Then, we centrifuged the disrupted cells (15000 xg, 10 min, 4°C), transferred 650 µL of the supernatant to a 1,5 mL tube, added 325 µL of a 3 M Potassium acetate (pH 5,5) solution, mixed gently and incubated 10 min at 4°C. Next, we centrifuged (15000 xg, 15 min, 4°C), transferred 700 µL of the supernatant to a new 1,5 mL tube, added 700 µL of isopropanol, mixed by vortexing and incubated 10 min at room temperature. Then, we centrifuged (15 000 xg, 15 min, RT) and discarded the supernatant. The pellet was washed twice in 500 µL of a cold (-20°C) 70% Ethanol solution by vortexing and centrifugation (15000 g, 5 min, 4°C). Next, the supernatant was removed and the tubes containing the DNA pellet left to dry during 10 min at 45°C in a heatblock. Finally, the dry cell pellet was resuspended in 30 µL of sterile water.

3.5.2 Plasmid DNA isolation

3.5.2.1 From *Escherichia coli*

Small-scale isolation and purification of plasmid DNA from *E. coli* cultures were performed using the GeneJET Plasmid Miniprep Kit (ThermoFisher Scientific) and according to the manufacturer's instructions.

3.5.2.2 From *Saccharomyces cerevisiae*

S. cerevisiae was used to assemble the plasmid GDV001.2 and the plasmid isolation from this organism was needed for further cloning purposes. Isolating plasmid DNA from *S. cerevisiae* was comparable to isolating genomic DNA from the same strain (3.5.1). However, instead of precipitating the DNA in the 700 µL supernatant with isopropanol, we continued the DNA isolation in a GeneJET Plasmid Miniprep Kit (ThermoFisher Scientific) column as per the manufacturer's instructions. After elution, the obtained DNA was transformed in E. coli DH10β cells for plasmid propagation, isolation, and verification (3.5.3).

3.5.3 Plasmid and sequence verification: Sanger sequencing

The sequence of purified plasmids and, when required, purified PCR products was confirmed by Sanger sequencing. To sequence PCR products, we sent 18 ng DNA for every 100 bp of amplicon in each sample, in a total volume of 15 µL mixed with 2 µM primers. For plasmid DNA, in each sample, we sent 500-800 ng of DNA in a total volume of 15 µL mixed with 2 µM primers. The samples were sent in 1.5 mL Eppendorf tubes labelled accordingly. Sequencing reactions were outsourced to Microsynth Seqlab. The sequencing data was analysed with the Clone Manager software (Sci Ed software).

3.5.4 DNA fragment amplification via polymerase chain reaction (PCR)

We used PCR to amplify DNA from different sources and used different polymerases depending on the purpose of the amplification. To generate fragments for fusion PCR (3.5.4.1) and to amplify genomic regions for further cloning or sequencing (3.5.3), we used proofreading polymerases Q5 (NEB) or Phusion (NEB). To verify genomic insertions and deletions, we used the non-proofreading DreamTaq polymerase (Thermo Fisher Scientific). The reaction conditions and reagents used in the reactions for each polymerase are described in **Tables 10-15**. All PCR reactions were run at a final volume of 50 µL. When DNA from genomic DNA extraction (3.5.1) was used as a template, the concentration of DNA was unknown.

Table 10. Reaction components used to run a PCR with Q5 polymerase.

Component	Concentration in stock solution	Concentration in thereaction solution	µL of stock solution used
Q5 reaction buffer	5x	1x	10
dNTP mix	2 mM each	200 µM	5
Primer (Fw)	10 µM	0.5 µM	2.5
Primer (Rv)	10 µM	0.5 µM	2.5
Q5 polymerase	2000 U/mL	1 U	0.5
DNA template	5-15 ng/µL (plasmids)	0.1-0.25 ng/µL (plasmids)	1
ddH_2O	-	-	To 50 µL

Table 11. PCR program used to run a PCR reaction with Q5 polymerase.

Step	Temperature	Duration	Number of cycles
DNA denaturation	98ºC	3 min	1
Denaturation	98ºC	30 s	30
Primer annealing	50-68ºC	45 s	
DNA extension	72ºC	1-3 min	
Final extension	72ºC	3 min	1
Hold	10ºC	∞ (hold)	1

Table 12. Reaction components used to run a PCR with Phusion polymerase.

Component	Concentration in stock solution	Concentration in the reaction solution	µL of stock solution used
Phusion HF buffer	5x	1x	10
dNTP mix	2 mM each	200 µM	5
Primer (Fw)	10 µM	0.5 µM	2.5
Primer (Rv)	10 µM	0.5 µM	2.5
Phusion polymerase	2000 U/mL	1 U	0.5
DNA template	5-15 ng/µL (plasmids)	0.1-0.25 ng/µL (plasmids)	1
ddH_2O	-	-	To 50 µL

Table 13. PCR program used to run a PCR reaction with Phusion polymerase.

Step	Temperature	Duration	Number of cycles
DNA denaturation	98ºC	3 min	1
Denaturation	98ºC	30 s	30

Primer annealing	50-68ºC	45 s	
DNA extension	72ºC	1-3 min	
Final extension	72ºC	3 min	1
Hold	10ºC	∞ (hold)	1

Table 14. Reaction components used to run a PCR with DreamTaq polymerase.

Component	Concentration in stock solution	Concentration in the reaction solution	µL of stock solution used
10X DreamTaq Green buffer	10x	1x	5
dNTP mix	2 mM each	200 µM	5
Primer (Fw)	10 µM	0.5 µM	2.5
Primer (Rv)	10 µM	0.5 µM	2.5
Phusion polymerase	5 U/µL	2.5 U	0.5
DNA template	variable	variable	1
ddH_2O	-	-	To 50 µL

Table 15. PCR program used to run a PCR reaction with DreamTaq polymerase.

Step	Temperature	Duration	Number of cycles
DNA denaturation	95ºC	3 min	1
Denaturation	95ºC	30 s	
Primer annealing	45-65ºC	45 s	30
DNA extension	72ºC	1-3 min	
Final extension	72ºC	2 min	1
Hold	10ºC	∞ (hold)	1

3.5.4.1 Fusion PCR

The construction of long DNA fragments using concatenated PCR reactions was based on (Shevchuk, Bryksin et al. 2004). Fusion PCR was used to create the donor DNA fragment used to knock out the *LEU2* cassette in the *adh2*-ko locus of strains GDY2 and GDY15 (3.5.10.3), creating strains GDY2.1 and GDY15.1. The Fusion PCR schematic process is depicted in **Figure 9**.

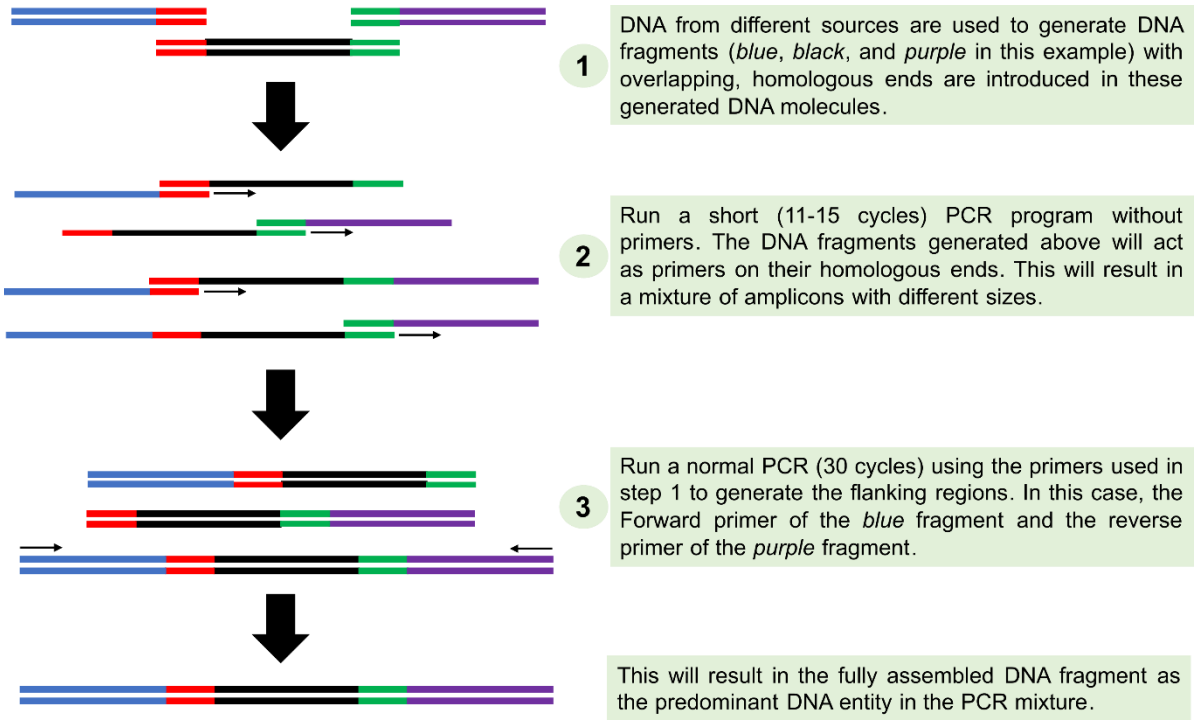

Figure 9. Fusion PCR workflow. In the first step, the fragments to assemble are generated via PCR amplification and homologous, overlapping ends are added to them. In the second step, the fragments to anneal (generated in step 1) are mixed and assembled in a short PCR without additional primers. In this short PCR, the fragments generated in the first step are used as primers, with the homologous ends acting as the priming regions. This results in assembled DNA fragments with different sizes. Then, in the third step, primers are added to the PCR products from step 2 and the desired product is amplified.

For this, we first amplified the promoter and the terminator regions of *ADH2* with primer pairs GDP482 / VSP196 and GDP483 / VSP195, respectively. After purifying these PCR products, we created the donor DNA in a two-step fashion: In the first step (A), the PCR products were annealed in a short PCR run with Q5 polymerase (**Table 16**). In the second step (B), 3 µL of an unpurified product from step (A) was used as a DNA template and further amplified with primers VSP195 and VSP196 in standard PCR conditions with Q5 polymerase (**Table 11**). The product of this Fusion PCR was confirmed by gel electrophoresis.

Table 16. The PCR program used in the first step (A) of fusion PCR.

Step	ºC, time	cycles
Initial denaturation	98ºC, 2 min	1
Denaturation	98ºC, 20 sec	10
Oligo annealing	69ºC, 30 sec	
Extension	72ºC, 40 sec	
storage	10ºC, ∞ (hold)	-

3.5.5 DNA extraction and purification from PCR fragments

The PCR reaction was run in a 1% Agarose gel at 125 V for 30 min. Then, the band of interest was excised from the gel with a stainless-steel scalpel and transferred to a previously weighed 1.5 mL Eppendorf tube. Finally, the PCR product contained in the gel-excised fragments was purified using the NucleoSpin Gel and PCR Clean-Up kit (Macherey-Nagel) according to the manufacturer's instructions.

3.5.6 Measurement of DNA concentration

The concentration and quality of DNA from plasmid DNA isolation procedures, PCR amplified fragments, or genomic DNA isolation procedures was measured in a NanoDrop 1000 Spectrophotometer (Thermo Fisher Scientific).

3.5.7 DNA restriction digestion via restriction endonucleases

The restriction digestion of plasmid DNA at specific sites was used for checking the correct assembly of the fragments during Golden Gate Assembly cloning or Gibson Assembly cloning and for linearising DNA fragments for their genomic integration. For this, restriction enzymes from New England Biolabs (NEB) were used with the provided buffers and following the manufacturer's instructions.

All reactions were incubated for 12 h at the optimal temperature of the restriction enzymes used and consisted of a total reaction volume of 50 µL containing 2-5 units of restriction enzyme per µg of DNA. To assess whether the plasmids generated with Golden Gate Assembly or Gibson Assembly were correct, 600 ng of assembled plasmid DNA were digested with the appropriate restriction enzymes. To linearise DNA fragments for genomic integration, 1000-1500 ng of plasmid DNA were digested with the appropriate restriction digestion enzyme.

3.5.8 Oligo annealing

Used to generate double-stranded, 80 bp long DNA fragments as donor DNA for CRISPR-cas9-based gene deletions of *GPD2* and *TES1*, as well as for removing the regulatory region of MTH1. Also used to generate the double-stranded, 24-27 bp long DNA fragments used to insert the crRNAs of *TES1* gene and the *NDI1* promoter in the CRISPR-cas9 backbone plasmid SiHV138.

For an oligo annealing reaction, 10 µL of each DNA oligo (ordered as 100 mM single-stranded DNA) is mixed with 10 µL of 10X Oligo annealing buffer and 80 µL of water in a 1.5 mL Eppendorf tube (**Table 17**). Then, the mixture is incubated for 5 min at 95ºC and let to cool down overnight at RT. After this step, the newly formed double-stranded DNA fragment is ready for further procedures.

Table 17. Primer annealing reaction components.

Component	Volume (µL)
Oligo DNA(s) (100 mM)	10 (each oligo)
10X Oligo annealing buffer (100 mM TRIS, 500 mM NaCl, 10 mM EDTA)	10
De-ionized water	80

3.5.9 Plasmid assembly

In biotechnology, specifically in metabolic engineering, plasmids are invaluable tools to genetically modify organisms and introduce novel traits. Plasmids, which are circular, closed, extra-chromosomal DNA molecules, harbour the genetic components to manipulate microbes and evaluate diverse characteristics.

Therefore, plasmids play a crucial role in molecular biology, and different methods have been developed over time to generate them. This study employs three plasmid assembly techniques: yeast-mediated homologous recombination, Gibson Isothermal assembly, and Golden Gate assembly.

3.5.9.1 Yeast-mediated homologous recombination

Homologous recombination is the most prominent DNA-repair mechanism in *S. cerevisiae,* and it allows the introduction of targeted genomic modifications used to modify strains. In this work, homologous recombination was also used to create the plasmid GDV001.2, which served as the template plasmid for the GFP-fusion experiments (4.1.2.1, 4.1.2.2 and 4.2.2.1).

To create the plasmid GDV001.2, we amplified the DNA fragments (**Table 18**) by PCR using primers with 20-40 bp homologous overhang ends. Then, *S. cerevisiae* CEN.PK2-1C was transformed with 500 ng of DNA containing the different fragments in equimolar amounts. We plated the transformants in solid SM without uracil and incubated them for two days at 30ºC. Then, we collected the cells from the plate, isolated the plasmid DNA (3.5.2.2), transformed it in *E. coli* DH10β and plated it in LB-Carbenicillin. Next, we isolated the plasmids from two *E. coli* colonies from the plate and verified them by sequencing (3.5.3). After verification by sequencing, one *E. coli* transformant containing the correct GDV001.2 plasmid was prepared as a glycerol stock and stored at -80°C.

Table 18. DNA fragments used for the construction of GDV001.2.

Part	DNA Fragment	Homology with	Primers used
P1	Ampicillin Resistance marker	P2, P7	GDP086/GDP087
P2	Yeast origin of replication (*CEN/ARS*)	P1, P3	GDP100/GDP101
P3	Bacterial origin of replication (ColE1)	P2, P4	GDP090/GDP091
P4	*URA3* yeast selection marker	P3, P5	GDP092/GDP093

P5	*MET25* promoter	P4, P6	GDP094/GDP095
P6	GFPenvy	P5, P7	GDP096/GDP097
P7	*CYC1* Terminator	P6, P1	GDP098/GDP099

3.5.9.2 Gibson isothermal assembly

The Gibson isothermal assembly cloning technique enables the assembly of DNA molecules with overlapping ends in a single reaction (Gibson, Young et al. 2009). In this method, a 5'-exonuclease generates DNA molecules with single-stranded homologous ends, which are then annealed and assembled by the joint action of a DNA polymerase and a ligase, as shown in **Figure 10**. The order of the fragments is determined by the homologous ends in each of the fragments to be assembled. We used Gibson isothermal assembly to generate the GFP fusion plasmids, the plasmids containing the truncated versions of *EAT1* and the CRISPR-Cas9 plasmid pRCCK_GD02 used to knock out *GPD2* from the genome (3.5.10.1).

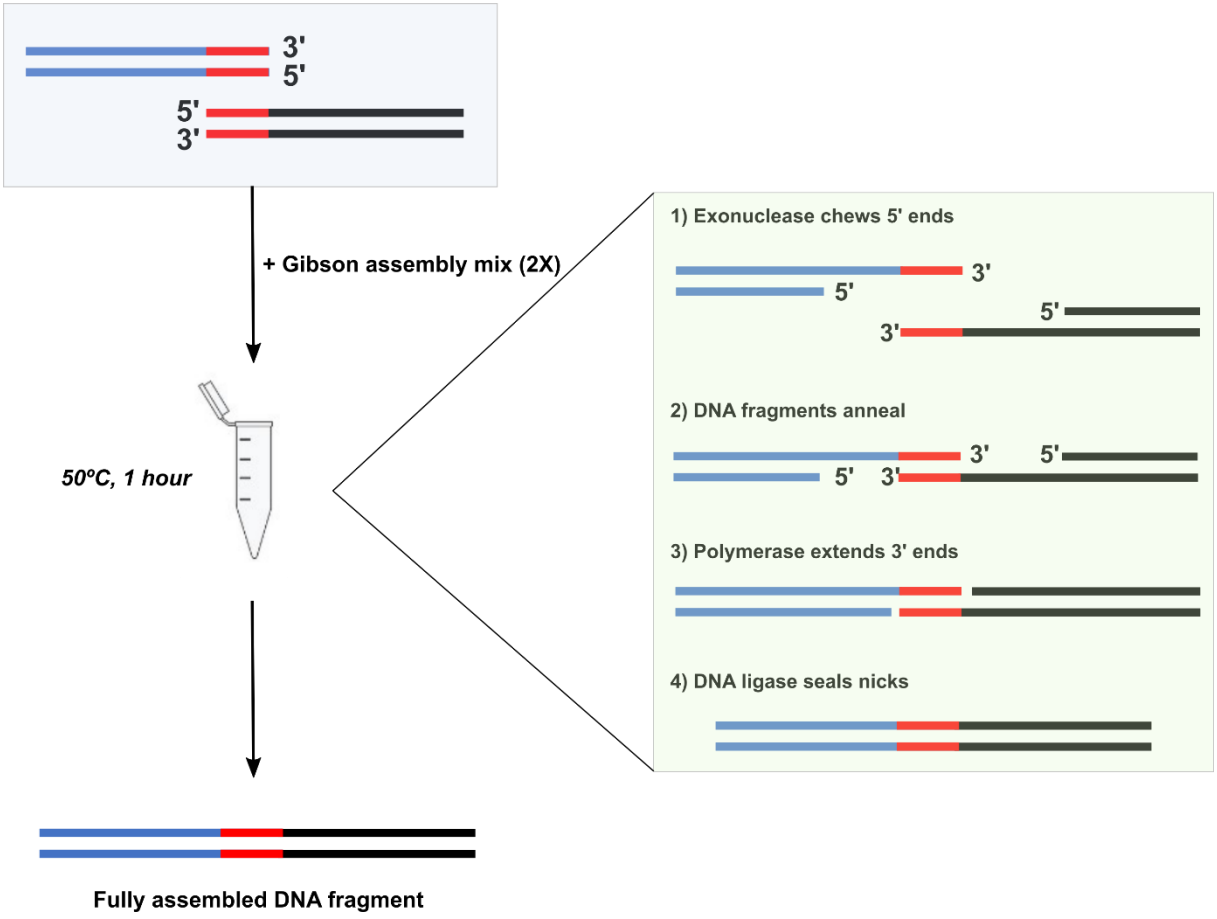

Figure 10. Schematic representation of the Gibson assembly isothermal reaction.

For plasmid assembly, 50 ng of a backbone DNA fragment (the largest fragment in number of bp) was mixed with up to 5 DNA fragments more, in a molar ratio of 1:3 and to a maximum volume of 10 µL. Then, the 2x Gibson assembly master mix was added to the DNA, together with the amount of ddH2O needed. The composition of the assembly master mix is described

in **Table 19**. The reaction mix was incubated (50°C, 1h), transformed into electrocompetent *E. coli* DH10β, and plated on solid LB medium with the appropriate selection agents. The next day, six individual *E. coli* transformants from the plate were isolated for plasmid isolation (3.5.2.1) and sequencing (3.5.3) for confirmation.

Table 19. Composition of the Gibson Assembly master mix.

Reagent	Concentration
5X Isothermal reaction buffer (see **Table 20**)	1X
T5 exonuclease	10 U/μL
Taq DNA ligase	40 U/μL
Phusion DNA polymerase	2 U/μL

Table 20. Composition of the 5X Isothermal reaction buffer. This buffer is a key element in the Gibson Assembly master mix (Table above) and was prepared as stock in the lab and was stored at -20ºC.

Reagent	Concentration
PEG 8000	25%
Tris-HCl, pH 7.5	500 mM
Magnesium chloride	50 mM
DTT	50 mM
dNTPs	1 mM
NAD^+	5 mM

3.5.9.2.1 Cloning of GFP-envy fusion proteins

To construct the plasmids GDV004 (^{MDH1mts}Ca*crt_GFPenvy*), GDV005 (^{LPD1mts}*adhE2_GFPenvy*), GDV006 (^{NCmts}*ERG10_GFPenvy*), GDV007 (^{ACP1mts}Td*ter_GFPenvy*), GDV020 (^{NCmts}Ca*hbd_GFPenvy*), GDV152 (YI*HAD_GFPenvy*), GDV153 (^{km}*Eat1_GFPenvy*), GDV154 (^{Km}*EAT1*$_{\Delta 1\text{-}19}$*_GFPenvy*), GDV155 (^{Km}*EAT1*$_{\Delta 1\text{-}30}$*_GFPenvy*), GDV169 (^{CoxIVmts}*eutE_GFPenvy*) and FHV025 (YI*ECH_GFPenvy*), we first amplified the different constructs using the primer pairs described in **Table 21**. In parallel, we also amplified a GFP-containing backbone fragment from plasmid GDV001.2 with primers pairs GDV152/GDV153. After a PCR clean-up step, we used Gibson assembly cloning to assemble each of the amplicons from the different enzymes with the GFP-containing backbone. The correct sequence of the constructed plasmids was confirmed by Sanger sequencing (3.5.3).

Table 21. PCR amplifications to construct GFPenvy-fusion constructs. The plasmid constructed (*plasmid*) is shown with the primer pairs used to amplify the proteins to be fused to GFPenvy, as well as the DNA source used for the amplification (*DNA template*).

Plasmid	Primer pair used	DNA template
GDV004 (^{MDH1mts}C*acrt_GFPenvy*)	GDP132/GDP133	GDV003
GDV005 (^{LPD1mts}*adhE2_GFPenvy*)	GDP134/GDP135	GDV003
GDV006 (^{NCmts}*ERG10_GFPenvy*)	GDP138/GDP139	GDV003
GDV007 (^{ACP1mts}Td*ter_GFPenvy*)	GDP130/GDP131	GDV003
GDV020 (^{NCmts}C*ahbd_GFPenvy*)	GDP343/GDP344	GDV003
GDV152 (YI*HAD_GFPenvy*)	GDP492/GDP445	GDV142
GDV153 (*EAT1_GFPenvy*)	GDP489/GDP488	*K. marxianus* genomic DNA
GDV154 (*EAT1*$_{\Delta 1\text{-}19}$*_GFPenvy*)	GDP490/GDP488	*K. marxianus* genomic DNA
GDV155 (*EAT1*$_{\Delta 1\text{-}30}$*_GFPenvy*)	GDP491/GDP488	*K. marxianus* genomic DNA
GDV169 (^{CoxIVmts}*eutE_GFPenvy*)	GDP341/GDP342	GDV050
FHV025 (YI*ECH_GFPenvy*)	GDP456/GDP457	GDV111

3.5.9.2.2 Cloning of *EAT1* and *EAT1*-truncated from *Kluyveromyces marxianus*

To construct the plasmids GDV156 (*EAT1*) and GDV157 (*EAT1*$_{\Delta 1\text{-}30}$), we first amplified the two constructs using the primer pairs described in **Table 22**. In parallel, we digested the plasmid pUCP_pHXT7 with SpeI and HindIII. Then, after a PCR clean up step, we assembled the amplified *EAT1* and *EAT1*$_{\Delta 1\text{-}30}$ amplicons in the digested pUCP_pHXT7 plasmid by Gibson assembly. Since *HIS3* was the required auxotrophy for this experiment and pUCP_pHXT7-based plasmids contain a *URA3* marker, we amplified the *HIS3* gene from plasmid LBGV024, and amplified the marker region in pUCP_*EAT1* and pUCP_ *EAT1*$_{\Delta 1\text{-}30}$ to exchange the selection markers. Finally, the amplified HIS3 and the marker-less amplicons of pUCP_*EAT1* and pUCP_ *EAT1*$_{\Delta 1\text{-}30}$ were assembled into GDV156 and GDV157 by Gibson assembly. The correct sequence of the constructed plasmids was confirmed by Sanger sequencing (3.5.3).

Table 22. Primer pairs used during the GDV156 and GDV157 plasmid construction workflow.

Plasmid	Primer pair used	DNA template
pUCP_*EAT1/EAT1*$_{\Delta 1\text{-}30}$	GDP484/GDP485	*K. marxianus* genomic DNA
pUCP_ *EAT1/EAT1*$_{\Delta 1\text{-}30}$	GDP484/GDP487	*K. marxianus* genomic DNA
GDV156 (*EAT1*) and GDV157(*EAT1*$_{\Delta 1\text{-}30}$)	GDP454/GDP455	LBGV024
GDV156 (*EAT1*) and GDV157(*EAT1*$_{\Delta 1\text{-}30}$)	ACBseq01/MGP076	pUCP_ *EAT1*/ *EAT1*$_{\Delta 1\text{-}30}$

3.5.9.3 Golden Gate Assembly

The GoldenGate assembly cloning (Engler, Kandzia et al. 2008) was used to generate CRISPR-Cas9 plasmids FHV016 and the different rBOX variants tested in this study. This method uses the ability of type IIS restriction enzymes to cut outside of their recognition site and generate sticky ends (overhangs) that can be ligated with DNA ligases. The overhangs in each DNA fragment are defined by design, and they determine the order in which the fragments are ligated. Therefore, the DNA fragment of different genetic elements (i.e. promoter, gene of interest, terminators, selection markers) can be assembled in the desired order in the final DNA molecule. In addition, once ligated, the fragments lose the recognition site, which allows for the iterative use of type IIS restriction enzymes without the risk of undoing the obtained assembly. In our study, the hierarchical cloning workflow (**Figure 11**) and the overhangs used for the different genetic elements are those from the Yeast toolkit (Lee, DeLoache et al. 2015).

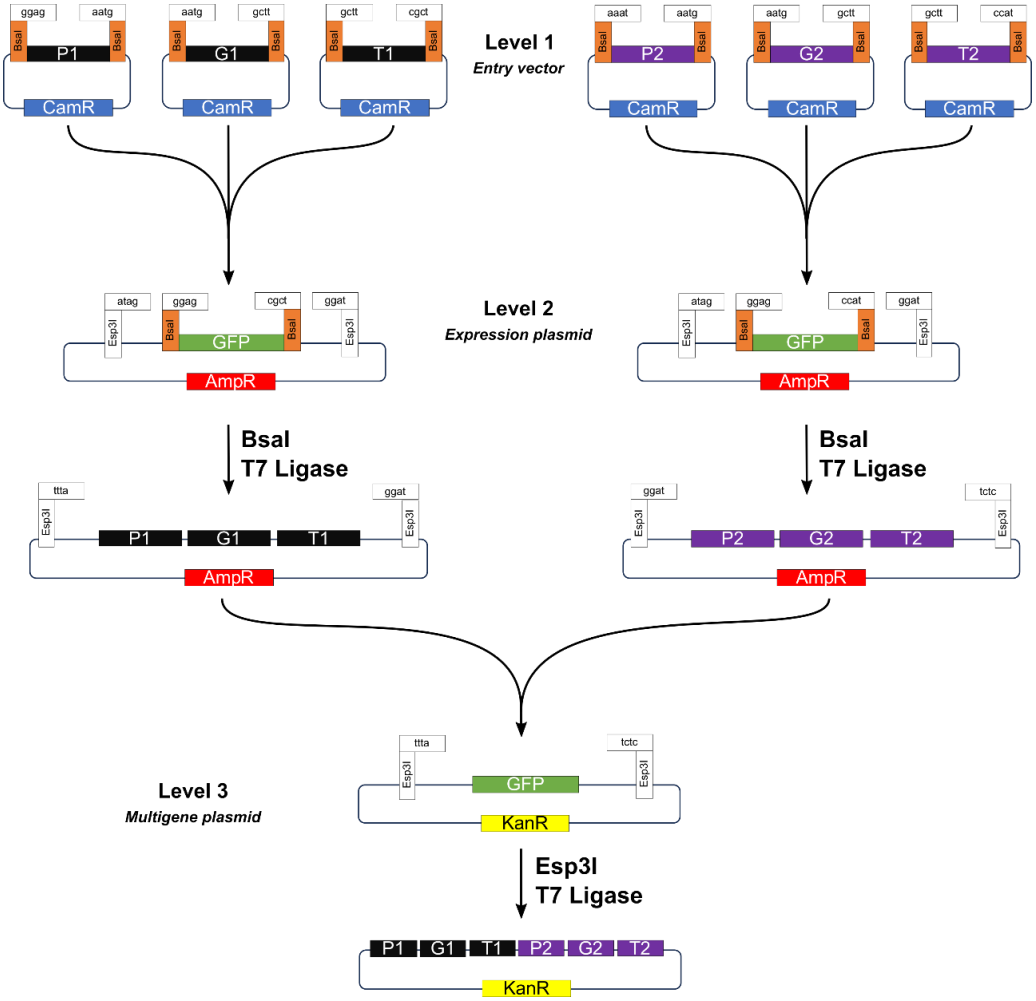

Figure 11. Simplified GoldenGate assembly cloning workflow with the Yeast toolkit. In the first level, the different elements (here promoter (P), gene (G) and terminator (T) are inserted in a Chloramphenicol R (CamR) based plasmid. Then, these elements are assembled into an expression backbone in the second level, generating an expression plasmid selected by resistance to Ampicillicin or Carbenicillin (AmpR). In the third level, the assemblies from multiple expression plasmids can be assembled into a multigene plasmid selected by resistance to kanamycin (KanR).

The DNA fragments were assembled in a 10 µL reaction mix containing 0.5 µL of type IIS restriction enzyme (BsaI or Esp3I), 0.5 µL of T7 Ligase and 1 µL of 10X Ligase buffer and up to 8 µL of DNA containing the different DNA fragments. All the fragments used for GoldenGate Assembly were set to a concentration of 25 ng/ µL, and 25 ng of DNA was used from each fragment during the assembly. Once the reaction mix was prepared, it was transferred to a thermocycler, where the GoldenGate assembly program was run (**Table 23**). If up to 4 fragments were to be assembled, the assembly step was run for 15 cycles. If the number of fragments to assemble was 5 or more, the assembly step was run for 25 cycles.

Table 23. GoldenGate assembly Program. Program used in the thermocycler to generate circular DNA from different fragments using GoldenGate assembly.

Step	Temperature	Duration	Number of cycles
Initial digestion	37ºC	3 min	1
Digestion	37ºC	1.5 min	15 / 25
Ligation	16ºC	3 min	
Final Digestion	37ºC	1-3 min	1
RE and Ligase inactivation	80ºC	10 min	1
Hold	10ºC	∞ (hold)	1

3.5.10 Gene deletions using CRISPR-Cas9

Scarless, direct genomic engineering manipulations were performed using the CRISPR-Cas9 system as described in (Generoso, Gottardi et al. 2016). We used plasmids expressing a codon-optimized Cas9 from *Streptococcus pyrogenes* and the respective sgRNA for each gene target (**Table 24**). To create the CRISPR-plasmids with the required gRNA, we 1) designed the crRNAs needed for recognition by the Cas9 endonucleases using the gRNA designer online tool from ATUM (https://www.atum.bio/catalog/vectors/grna-design). The crRNAs consisted of a 20-nt sequence, with an NNG PAM sequence upstream 2) We PCR amplified the backbone of the backbone plasmid pRCCK_MR02 in two amplicons that contained homologous end, one of them with the crRNAs sequence 3) used Gibson Assembly (3.5.9.2) or GoldenGate cloning (3.5.9.3) to build the final plasmids 4) checked the correct assembly and sgRNA by Sanger sequencing.

Then, we co-transformed the plasmid with a donor DNA in the target *S. cerevisiae* strain and plated the cells in the appropriate antibiotic selection marker needed for the CRISPR-plasmid after 4h of incubation in YPD. The clones selected for validation were first cured from the CRISPR-Plasmid by overnight incubation without the antibiotic marker. The genetic modifications were validated by colony PCR.

Table 24. List of plasmids used for CRISPR-Cas9-based deletion.

Deletion target	Plasmid	sgRNA
GPD2	pRCCK_GD01	TTAACGGTCAATCCGCCCAA**G**
TES1	FHV016	GGAAGTACGGGATCGTGAGT**G**
FAA2	pRCCN_SH06	GAAGATTTTGAAACCTTACG**G**
MTH1	pRCCK_MTH1	GCAGTATGCATTCAGCGAGC**G**
LEU2	BBV001	AGGCTTCCAGCGCCTCATC**G**

3.5.10.1 Gene knock-out of *GPD2*, *TES1* and *FAA2*

To create the plasmid pRCCK_GD01 used to delete *GPD2*, we PCR amplified the backbone plasmid pRCCK_MR02 in two amplicons with primer pairs GDP200 / WGP234 and GDP201 / WGP235. Then, we assembled the final pRCCK_GD01 by Gibson Assembly reaction of both amplicons. To create the FHV016 plasmid used to delete *TES1*, we first generated a short dsDNA from oligo annealing of primers GDP418 and GDP419. Then, we assembled the final FHV016 plasmid by a GoldenGate assembly reaction of plasmid SiHV138 and the annealed GDP418/419 oligo.

The donor DNA to knock out *GPD2* was obtained from annealing 80 bp long oligo primers JWP061 and JWP062. The donor DNA to knock out *TES1* was obtained from annealing 80 bp long oligo primers GDP420 and GDP421. In both cases, these annealed products consisted of two merged 40 bp regions homologous to the downstream and the upstream regions of the target gene.

To knock out *GPD2*, we co-transformed pRCCK_GD01 with the annealed JWP061/JWP062 oligo in VSY0 *and* in GDY1. Clones with the successful deletion of *GPD2* were confirmed by colony PCR using primers VSP269 and VSP270. To knock out *TES1*, we co-transformed FHV016 with the annealed GDP420/GDP421 oligo in GDY15. Clones with the successful deletion of *TES1* were confirmed by colony PCR using primers GDP438 and GDP439. To knock out *FAA2*, we used the plasmid pRCCN_SH06 (Henritzi, Fischer et al. 2018) and a PCR-amplified *FAA2* region of a ∆*faa2*-ko strain (SHY34), which was used as donor DNA. The primers used to amplify the *FAA2*-ko region were RPP266 and RPP267. Both plasmid and donor DNA were transformed in GDY15. Clones with the successful deletion of *FAA2* were confirmed by colony PCR using primers RPP266 and RPP267.

3.5.10.2 Deletion of the regulatory region of Mth1

To remove the regulatory region from Mth1 (Oud, Flores et al. 2012) we used the plasmid pRCCK_MTH1. The donor DNA used to create the mutation was obtained from annealing 80 bp long oligo primers JWP045 and JWP046. Both plasmid and donor DNA were transformed

in VSY0. Clones with a successful deletion in the regulatory region were confirmed by colony PCR using primers GDP150 and GDP151.

3.5.10.3 Removal of *LEU2* cassette

We used plasmid BBV001 to remove the *LEU2* cassette from strains GDY2 and GDY15. The donor DNA used for the deletion was obtained through Fusion PCR, and its creation is described in 3.5.4.1. Both the plasmid and donor DNA were transformed in GDY2 and GDY15. Clones with a successful *LEU2* deletion were first confirmed by their inability to grow on medium without leucine, and then validated by colony PCR with primers VSP195 and VSP196.

3.5.11 Electrocompetent cells preparation and transformation of *Escherichia coli*

To prepare *E. coli* electrocompetent cells, a 5 mL preculture of LB-medium was inoculated with a single colony of E. coli DH10β from a plate and incubated overnight (37 °C, 180 rpm). The next day, a 30 °C pre-warmed 1 L baffled shake flask containing 400 mL LB medium was inoculated with the preculture and incubated (30 °C, 180 rpm) until an OD600nm of 0.6-0.7 was reached. Then, the culture was transferred to eight previously cooled 50 mL tubes on ice, and the culture was left to cool down for 30 min. After 30 min, the cells were centrifuged (4000 xg, 15 min, 4ºC). Next, the cells were washed by resuspending them in 25 mL of ice-cold ddH_2O, pooled into 50 mL suspensions, and pelleted (4000 xg, 15 min, 4 °C). This washing step was repeated until the culture could be condensed in a single 50 mL tube. The pellet from this 50 mL culture of pooled cells was washed in 4 mL 10 % (w/v) ice-cold sterile glycerol and centrifuged (4000 xg, 15 min, 4 °C). The supernatant was discarded, the pelleted cells were resuspended again in 4 mL 10 % (w/v) ice-cold sterile glycerol and aliquoted in 50 µL each and frozen at -80 °C directly.

To transform *E. coli*, the frozen electrocompetent cells were first taken out of the -80ºC and left on ice. Then, 1 µl of DNA or 20 ng of DNA was transferred to the tube containing the frozen electrocompetent cells, and the solution was left to thaw. Next, the cell-DNA mixture was mixed (avoiding the formation of bubbles) by pipetting up and down and transferred to a previously cooled, sterile electroporation cuvette. The cuvette was transferred to the Gene Pulser electroporation chamber (BioRad), and an electric pulse of 2.5 kV was applied (Resistance 200 Ω, capacity 25 µF). 900 µL of LB medium were immediately transferred to the cuvette, mixed by pipetting, and the content was transferred to a 1.5 mL Eppendorf tube. Here, the electroporated cells were recovered at 37 °C for 1 hour. After recovery, the culture was centrifuged (3000 g, 7 min, RT), and the supernatant was removed except for 50 µl. The pellet was resuspended in the remaining 50 µl and plated in solid LB with appropriate antibiotics.

3.5.12 Preparation of competent cells of *Saccharomyces cerevisiae* and transformation

To prepare chemically competent *S. cerevisiae* cells, an overnight pre-culture was started by transferring a single colony or a swap from a plate to 5 mL of YPD medium and incubating at 30ºC and 200 rpm. The next day, a 50 mL shake flask culture was started from the overnight pre-culture at a starting OD600nm of 0.05-0.1 and incubated (30ºC, 200 rpm) until an OD600nm between 1-1.5. Then, the cells were harvested by centrifugation (3000 xg, 3 min, RT) and washed twice with 50 ml ddH_2O. The supernatant of the second wash was discarded, and the pellet resuspended in Frozen Competent cells (FCC) solution (glycerol 5% (v/v) and DMSO 10% (v/v)) at 0.01 x culture volumes per OD600nm at the time of harvesting. This re-suspension was then aliquoted by 50 µL in 1.5 mL tubes and used directly for transformation or stored at -80ºC for up to 6 months.

To transform *S. cerevisiae* competent cells, the freshly prepared or thawed aliquots were first pelleted by centrifugation (3000 xg, 1 min, RT). The supernatant was discarded, 306 µl of cold yeast transformation mix (**Table 25**) were added to the pelleted cells and mixed by pipetting. Then, 54 µl of DNA solution was added. This DNA solution contained up to 500 ng of plasmid DNA or up to 2000 ng of DNA for gene insertion or deletion. After the DNA solution was added, the DNA-cells mixture was carefully mixed until homogeneity and incubated at 42°C for 40-60 min. Then, if a dominant marker was used for selection, the solution was transferred to 5 ml YPD medium, and the cells recovered for up to 4h at 30°C. After the recovery phase, the transformations were harvested by centrifugation (3000 xg, 2 min, RT). Then, the supernatant was discarded, the cells were resuspended in 100 µL of sterile ddH_2O and plated on solid medium containing the appropriate selection marker. If an auxotrophic selection marker was used instead, recovery was not necessary, and the cells were directly harvested, resuspended in 100 µL of sterile ddH_2O and plated in the appropriate solid medium.

Table 25. Composition of the yeast transformation mix used to transform *S. cerevisiae* cells.

Compound	Concentration in stock	Volume added (µL)	Final concentration
PEG 4000	50 % (w/v)	260	36 % (w/v)
Lithium acetate	1 M	36	100 mM
Salmon sperm DNA	2 mg/mL	10	56 µg/mL
	Total volume added	306	

3.6 Bioinformatic methods

3.6.1 Codon optimization of synthetic genes

In this study, all the genes of interest that are not native to *S. cerevisiae* are codon optimized to improve their expression and translation in this yeast. To obtain the codon optimized DNA sequences, we used the algorithm from the online tool Jcat (http://www.jcat.de/) (Grote, Hiller et al. 2005) to back translate the amino acid sequence into the *S. cerevisiae* codon optimized DNA sequence.

3.6.2 PROSITE and UniProtKB analysis

PROSITE is a database that provides information on protein domains, families, functional sites, and patterns. Therefore, an analysis in PROSITE was run to identify alternative enoyl-CoA hydratases to ^{Cn}Crt2 with the ability to hydrate the double bond in 3-hydroxyacyl-CoAs longer than 8-carbon (4.1.2.2). First, the complete amino acid sequence of ^{Cn}Crt2 was analysed in ScanProsite to find the protein signature in this enzyme. For this search, we excluded the analysis of motifs with a high probability of occurrence. This was done to avoid getting hits belonging to possible common post-translational modification patterns present in the sequence. Then, a list of all the UniProtKB entries matching the obtained protein signature (PS00166 - Enoyl-CoA hydratase/Isomerase) was retrieved, and the hits were filtered by taxonomy to *Cryptococcus curvatus*, *Lipomyces lipofer*, *Rhodosporidium toruloides*, *Rhodotorula glutinis*, *S. cerevisiae* and *Y. lipolytica*.

3.6.3 Analysis of mitochondrial targeting sequences

In this study, the presence and amino acid sequence of mitochondrial targeting signals (MTS) were assessed with the online software MitoProt II (https://ihg.helmholtz-muenchen.de/ihg/mitoprot.html) (Claros and Vincens 1996), MitoFates (Fukasawa, Tsuji et al. 2015) (https://mitf.cbrc.pj.aist.go.jp/MitoFates/cgi-bin/top.cgi) and TargetP (Emanuelsson, Brunak et al. 2007) (https://services.healthtech.dtu.dk/services/TargetP-2.0/). MitoProtII was used to scan for MTS in the putative enoyl-CoA hydratase Ech and 3-hydroxyacyl-CoA dehydrogenase Had from *Y. lipolytica* and in Eat1 from *K. marxianus*. MitoFates and TargetP were used to assess the targetability in the mitochondria of different rBOX enzymes and MTS combinations before cloning and analysis by fluorescence microscopy (4.1.2.1, 4.1.2.2 and 4.2.1.2). MitoFates and TargetP were used when the MitoProtII server stopped functioning. Regardless of the online software used, the complete amino acid sequence of the protein was used as input in all the analyses.

3.7 Analytical methods

3.7.1 OD_{600nm} measurements

The cell growth in liquid cell cultures was quantified by absorption at $OD600_{nm}$ in an Ultrospec 2100 PRO spectrophotometer (Amersham Bioscience). The cell culture of interest was measured directly or diluted with a blank diluent. For this, the sample was transferred to a polystyrene cuvette, and the Blank and the sample were analysed. The cell suspension aimed to obtain $OD600_{nm}$ value between 0.05-0.6. If the values were out of this range, the dilution was adjusted accordingly and re-measured.

3.7.2 HPLC measurements

HPLC was the preferred method to analyse glucose, galactose, raffinose, glycerol, ethanol, butyric acid and crotonic acid.

1 mL of sample was centrifuged (10 min, RT, 15000 xg), the pellet discarded and the supernatant filtered with a 0.22 µm nylon-membrane filter and transferred to a new 1.5 mL tube. 450 µL of the filtered supernatant were then mixed with 50 µL of 50 % (w/v) 5-sulfosalicylic acid in a 1.5 mL HPLC glass vial (VWR) with a screw cap.

The samples were analysed in a Dionex UltiMate 3000 (ThermoScientific) system equipped with a Coregel 87H3 (Agilent) column and a refractive index (RI) detector (Thermo Shodex RI-101). The HPLC was operated at 40ºC with 5 mM sulfuric acid and a constant flow rate of 0.4 mL/min. Glucose, glycerol, acetic acid, ethanol, and butyric acid were identified and quantified by comparison to standard samples ranging from 0.1 to 20 g/L for glucose, glycerol and ethanol, and by comparison to standard samples ranging from 0.01 to 5 g/L for acetic acid and butyric acid.

3.7.3 GC measurements

Gas chromatography was the selected method to analyse hexanoic acid, octanoic acid, decanoic acid, 1-butanol, 1-hexanol, 1-octanol and 1-decanol.

3.7.3.1 Medium-chain fatty acid extraction and derivatisation

To extract the free fatty acids (FFA) produced in the fermentation, 13 mL of each culture were centrifuged (3000 xg, 10 min, RT), and the pelleted cell fraction was discarded. Then, 200 µg of heptanoic acid was added as an internal standard to 10 mL of each supernatant and mixed with 1 mL of 1 M HCl and 2.5 mL of a methanol/chloroform solution (1:1). The solution was vigorously shaken for 5 min and then centrifuged (3000 xg, 10 min, RT). The chloroform fraction was transferred to a 1.5 mL Eppendorf tube and evaporated overnight.

For fatty acid methylation, both the samples from the FFA extraction and standard samples containing 5, 25, 50, 100 and 200 mg/L of hexanoic, octanoic and decanoic acid (Sigma Aldrich) were dissolved in 200 µL of toluene, mixed with 1.5 mL of methanol and 300 µL of an 8.0% (w/v) HCl solution, vortexed vigorously and incubated at 100 °C for three h to generate fatty acid methyl ester (FAME). Then, samples were cooled at 4ºC for 15 min, and 1 mL of water and 1 mL of hexane were added. The mixture was briefly shaken in a vortex, and after a clear separation of the organic and aqueous phases, the organic phase was transferred to a GC vial.

3.7.3.2 Medium-chain fatty alcohols extraction

To extract the MCFOH produced in the fermentation, we took 1.5 mL of each culture and pelleted the cells by centrifugation (8000 xg, 10 min, RT). Then, 500 µL of the supernatant was mixed with 400 µL of ethyl acetate containing 50 mg/L of heptanol as an internal standard. Next, the mixture was shaken vigorously in a VXR Vibrax system (IKA) (2000 rpm, 4 min) and centrifuged to separate the aqueous and the organic phases (5000 rcf, 2 min, RT). Finally, 250 µL of the organic phase was transferred to a GC vial for analysis.

3.7.3.3 FAMEs and MCFOH analysis in GC-FID

GC analyses for detection and quantification of FAMEs and MCFOH were carried out on a Perkin Elmer Clarus 400 instrument (Perkin Elmer, Germany) equipped with an Elite 5MS capillary column (30 m × 0.25 mm, film thickness 1.00 µm, Perkin Elmer, Germany) and a flame ionisation detector (Perkin Elmer, Germany). 1 µL of the sample was analysed after split injection (1:10), and helium was used as carrier gas (90 kPa).

For the quantification of FAMEs, the injector and detector temperatures were 250 and 300 °C, respectively. The following temperature program was used: 50 °C for 5 min; increase of 10 °C/min to 120 °C and hold for 5 min; increase of 15 °C/min to 220 °C and hold for 10 min; increase of 20 °C/min to 300 °C and hold for 5 min. Medium-chain FAMEs were identified and quantified by comparison to FAMEs in standard samples.

For the quantification of MCFOH, the temperatures of both the injector and detector were 250 °C. First, an initial temperature of 50 °C was maintained for 5 min. Next, we increased the temperature to 210ºC at a rate of 20 °C/min and kept it constant for 5 min. As final steps, we further increased the temperature to 230ºC at a 20ºC/min rate and kept it constant for 6 min. Fatty alcohols were identified and quantified by comparison against known MCFOH standards.

3.7.4 GC-MS for identification of volatile compounds

GC-MS analyses for detection and quantification of ethyl acetate, 1-butanol, isoamyl alcohol and isoamyl acetate were carried out on a 7890 A instrument (Agilent) equipped with a HP-

5MS capillary column (30 m × 0.25 mm, film thickness 0.25 µm, Agilent) and connected to a CombiPAL automated sampler with heating capacity (PAL systems) and to a MS 5975C Inert MSD (Agilent) operating at 70 eV.

The samples were pre-heated (65ºC, 500 rpm, 15 min), then 1 µL of samples was injected at a 1:5 split ratio. Helium was used as carrier and operated at a constant flow rate of 1.2 mL/min throughout the run with a head pressure of 9.0901 psi. After injection, the oven temperature was kept at 40ºC for 2 min, then, it was increased to 120ºC at a 4°C/min rate. Once 120ºC were reached, the temperature was increased to 300ºC at a rate of 50ºC/min and was kept at 300ºC for 2 min. The temperature for the injection syringe, and the interface were 65ºC and 250ºC, respectively. The MS was operated in EI. The detector was operated with a delay of 1.8 min and set to scan from 30 to 300 amu. GC-MS data files were visually analysed using Chemstation.

Ethyl acetate, isoamyl alcohol and isoamyl acetate detection was validated and quantified by comparison against known standards. 1-butanol was used as internal standard for normalization.

3.7.5 Fluorescence microscopy

Fluorescence microscopy was used to study the cellular localisation in *S. cerevisiae* of different enzymes used in this work: Eat1 and Eat1-truncation variants, Had and Ech from *Y. lipolytica* and rBOX enzymes expressed with different mitochondrial targeting sequences. All these proteins were fused at the C-terminal to GFPenvy.

3.7.5.1 Sample preparation

Yeast cells harbouring expressing the GFP-fusion protein were pre-cultured in low fluorescence SC medium with galactose (2%) and without uracil (SCG_{-URA}). This medium contained a low-fluorescence Yeast nitrogen base instead of the one described in section 3.4.1.2. The cells were grown for 16h at a volume of 50 mL in a 300 mL flask at 30ºC and 180 rpm. The next day, the cell culture was diluted to an OD600nm of 0.8 in SCG_{-URA}, and the cells were grown for 4h at 30ºC and 180 rpm. Then, Mitotracker Red CMXRos (Invitrogen) was added to the samples to a final concentration of 250 nM, and the samples were incubated 20 min more at 30ºC and 180 rpm. Then, the cells were pelleted (3000 xg, 2 min, RT), washed three times in sterile de-ionized water and resuspended again in SCG_{-URA}. Right before analysis in the confocal microscope, we transferred 5 µL of the culture to an object plate and sealed it with a cover slide.

3.7.5.2 Image analysis and processing

We used the confocal laser scanning microscope Zeiss LSM 780 to analyse the image. The cells were detected using the plan-apochromat 63×1.40 Oil DIC M27 objective. The excitation wavelengths for GFPenvy and Mitotracker Red CMXRos were 488 nm and 561 nm, respectively. The emission wavelengths were measured in bandwidth between 493nm and 598nm for GFPenvy and between 573nm and 678nm for Mitotracker Red CMXRos. Image processing and analysis and processing were done using the Fiji ImageJ software.

4 Results

4.1 Optimization of the reverse β-oxidation pathway to produce selected medium-chain fatty acids and alcohols in *S. cerevisiae*

The rBOX pathway is a cyclical set of reactions that could be used as a metabolically cheaper alternative to elongate hydrocarbon chains. However, the biotechnological expression of this pathway in *S. cerevisiae* seems limited to two cycles, producing only up to C6-intermediates and products. In this chapter, we extended the chain length of the products from the rBOX. For this, we first created a *S. cerevisiae* platform strain suitable for the expression in the cytosol of NADH-consuming pathways. Then, we tested different variants of the rBOX, validated the production of longer chain products based on the titers of different MCFA, and attempted to improve the pathway yield through further modifications at the fermentation and genomic level. We used MCFA as a proof of concept, due to the natural ability of endogenous *S. cerevisiae*'s thioesterases to hydrolyse medium-chain fatty acyl-CoAs to MCFA. The results achieved on the production of MCFA have been published as Garces Daza *et al.* (2023). Finally, we tested one of these pathway variants on the production of MCFOH. An overview of the metabolic engineering strategies tested in this chapter is shown in **Figure 12**.

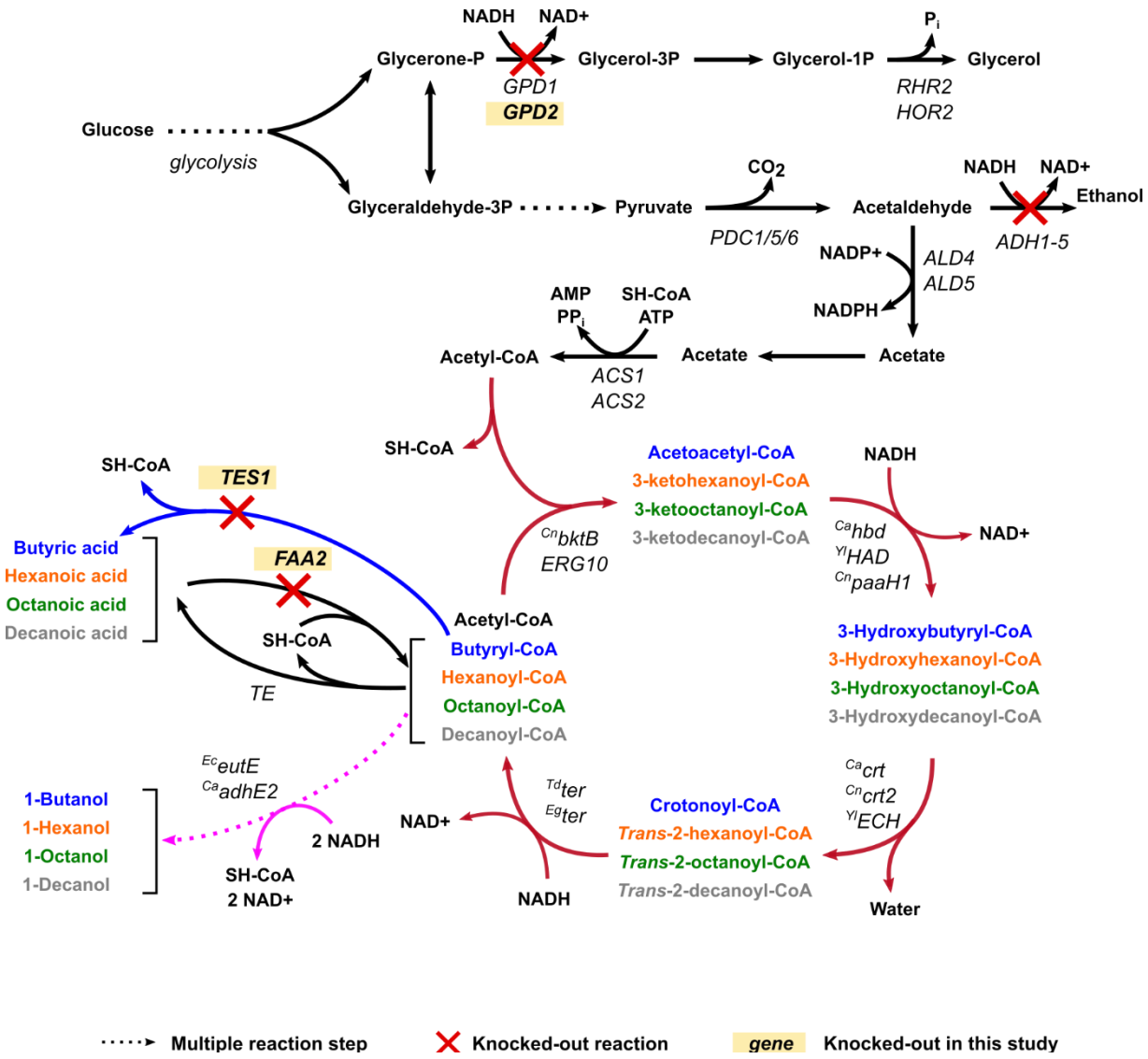

Figure 12. Overview of the reverse β-oxidation pathway and the *S. cerevisiae*'s metabolic modifications used in this study to produce medium-chain fatty acids and alcohols. The rBOX pathway reactions (red arrows) are depicted with the isoenzymes tested in each reaction during this study. The intermediates and products after one cycle (in *blue*), two cycles (in *orange*), three cycles (in *green*), and four cycles (in *grey*) run of the rBOX pathway are shown. The reactions knocked out in the different strains used in this study are displayed with a red cross. The knocked-out reactions generated during this study (*GPD2*, *TES1*, *FAA2*) are highlighted in bold. The reaction of Tes1 is shown in blue. The reaction of alcohol dehydrogenases ^{Ec}EutE and ^{Ca}AdhE2 is shown in *magenta*.

4.1.1 Generating a minimal strain for screening reverse β-oxidation variants

S. cerevisiae is a Crabtree-positive yeast. Therefore, it metabolizes glucose preferentially via fermentation in the cytosol over respiration in the mitochondria. This way, it re-oxidizes the NADH generated in glycolysis and obtains energy via substrate-level phosphorylation (see section 2.5). In this organism, glucose fermentation results mainly in ethanol production (Malina, Yu et al. 2021). Since the rBOX pathway requires NADH to function, fermentation constitutes a major competing pathway for carbon and reducing equivalents.

In this study, we tested different modified rBOX pathway variants. To assess the impact of these variants more accurately, we developed a platform strain with reduced fermentation capacity while retaining good growth and transformation phenotypes.

4.1.1.1 Thiolase BktB is essential for medium-chain fatty acid production

We constructed a rBOX pathway expressing ^{Ca}*hbd* and ^{Ca}*crt* from *C. acetobutylicum* as a 3-hydroxyacyl-CoA dehydrogenase and a crotonase, respectively, and ^{Td}*ter* from *T. denticola* as a trans-2-enoyl-CoA reductase. As a thiolase, we expressed ^{Cn}*bktB* from *C. necator* or the native *ERG10* from *S. cerevisiae* to compare their effect on producing MCFA. It should be noted, though, that *ERG10* is a vital gene for *S. cerevisiae*. Therefore, in our study, all the strains contain an additional, native copy of thiolase *ERG10* in the genome besides the thiolase expressed from the rBOX. ^{Cn}BktB has been used previously to produce medium-chain coenzyme A bound pathway intermediates (Luo, Reiter et al. 2019), and the combined expression of ^{Cn}*bktB* with ^{Ca}*hbd*, ^{Ca}*crt* and ^{Td}*ter* in the yeast *K. marxianus* led to more than 100 mg/L of hexanoic acid (Cheon, Kim et al. 2014). On the other hand, the expression of *ERG10* with ^{Ca}*hbd*, ^{Ca}*crt* and ^{Td}*ter* in a highly engineered *S. cerevisiae* strain produced up to 860 mg/L of the 1-round rBOX product n-butanol (Schadeweg and Boles 2016b). However, the production of MCFA with *ERG10* was not assessed in that study. As mentioned above, NADH is a required co-factor for the proper function of the rBOX pathway. Therefore, we compared the two thiolases in *S. cerevisiae* VSY0, a strain lacking the principal alcohol dehydrogenase enzymes (Δ*adh1-5*), to minimise competition for NADH and carbon.

Butyric acid, the product of a single cycle of the rBOX pathway, was produced when expressing either the *ERG10* pathway variant (GDV098: ***ERG10***, ^{Ca}*hbd*, ^{Ca}*crt*, ^{Td}*ter*) or the ^{Cn}*bktB* pathway variant (ACBV007: ^{Cn}***bktB***, ^{Ca}*hbd*, ^{Ca}*crt*, ^{Td}*ter*) (**Figure 13**). This indicates that the enzymes selected for the rBOX pathway variants were catalytically active. The *ERG10*-containing pathway (GDV098) supported the production of 58 ± 11.9 mg/L of butyric acid, 47% more than when ^{Cn}*bktB* (ACBV007) was the preferred thiolase (39,23 ± 0.71 mg/L) (**Fig 13A**). The expression of ^{Cn}*bktB*, on the other hand, slightly increased the production of hexanoic acid (1.07± 0.12 mg/L), while the overexpression of *ERG10* did not (**Fig 13B**). Octanoic and decanoic acid were produced in meagre amounts, even without a rBOX pathway, probably by fatty acid synthases in the cytosol and mitochondria (Gajewski, Pavlovic et al. 2017). Regarding decanoic acid, we observed an apparent increase in production with both Erg10 and ^{Cn}BktB, with 0.559 ± 0.090 mg/L and 0.555 ± 0.052 mg/L, respectively. In addition, we observed that the deletion of alcohol dehydrogenases 1-5 in VSY0 resulted in a glycerol-producing phenotype (**Fig 13C**), with titers at the end of fermentation of 6.74 ± 0.18 g/L, 7.46

± 1.16 g/L and 7.07 ± 0.2 g/L when carrying an empty vector EV, GDV098 and ACBV007, respectively.

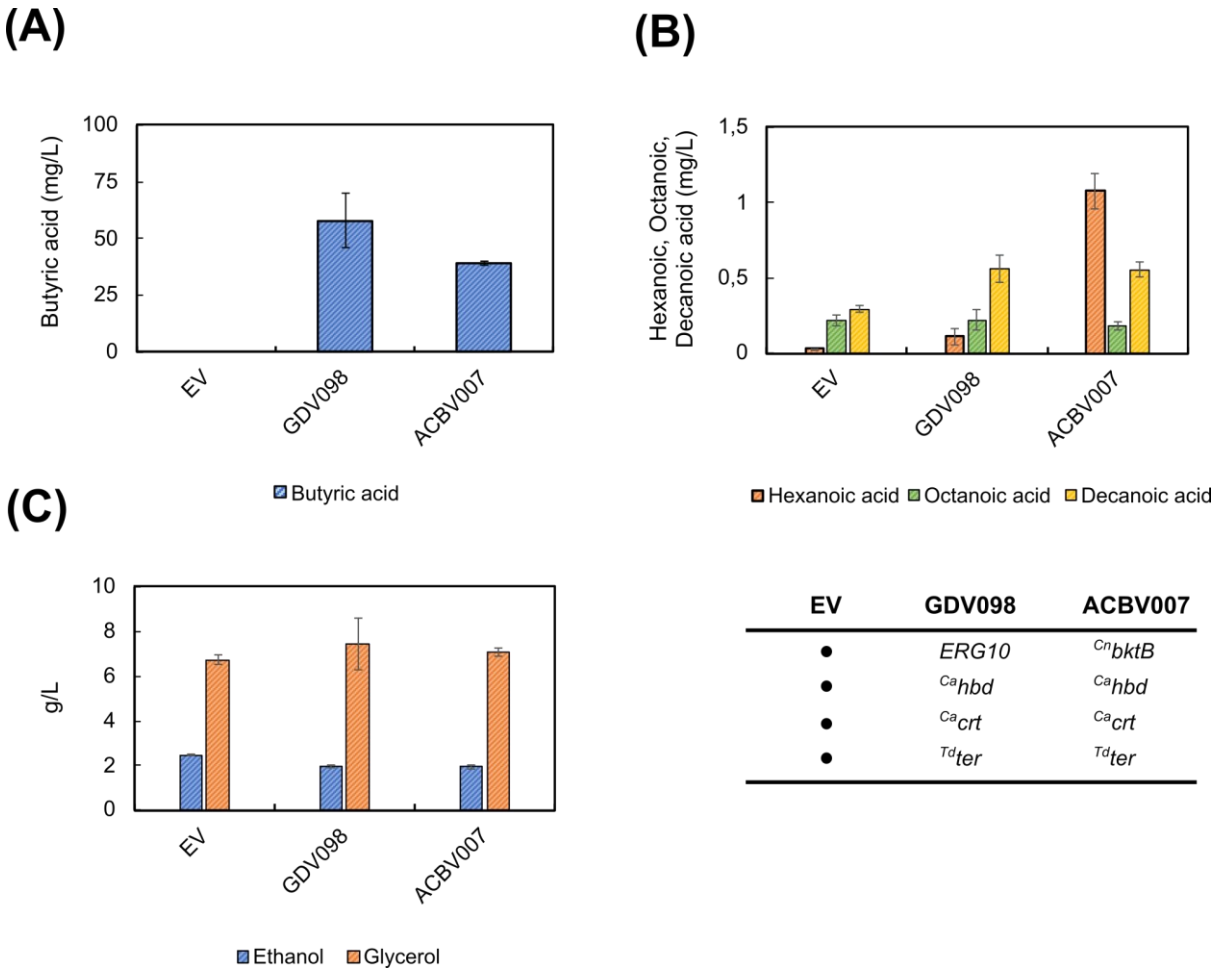

Figure 13. I Effect of two different thiolases (Erg10 or BktB) on the production of medium-chain fatty acid in the *adh*-deficient *S. cerevisiae* VSY0 strain. A) Production of butyric acid (in *blue*) by VSY0 expressing a rBOX pathway with either overexpressed *ERG10* as thiolase (**GDV098**: ***ERG10***, *Cahbd*, *Cacrt*, *Tdter*) or *bktB* as thiolase (**ACBV007**: ***Cnbktb***, *Cahbd*, *Cacrt*, *Tdter*), or with the empty vector (EV) after 75 h of fermentation in buffered synthetic medium (SM) without uracil. **B)** Production of hexanoic (in *orange*), octanoic (in *green*) and decanoic acid (in *yellow*) by VSY0 expressing a rBOX pathway with either overexpressed *ERG10* as thiolase (GDV098) or *bktB* as thiolase (ACBV007) or with the empty vector (EV) after 75 h of fermentation in buffered synthetic medium (SM) without uracil. C) Production of ethanol (in *blue*) and glycerol (in *orange*) at the end of fermentation (75h) by VSY0 expressing a rBOX pathway with either overexpressed *ERG10* as thiolase (GDV098), or *bktB* as thiolase (ACBV007) or with the empty vector (EV). Error bars represent the standard deviation between three independent replicates.

Altogether, the rBOX pathway was functional in *S. cerevisiae* VSY0, but the overall production of MCFAs was deficient (<2 mg/L), independently of the thiolase used. Nonetheless, we decided to continue with CnBktB as the thiolase in further MCFA-production experiments as it produced the highest hexanoic acid titers in this experiment and due to the reported ability of this enzyme to synthesise medium-chain fatty acyl-CoAs (Clomburg, Contreras et al. 2017, Krink-Koutsoubelis, Loechner et al. 2018).

Alice Born (Bachelor student) built the plasmid ACBV007 and conducted the cultivation and probing of the samples under the author's supervision.

4.1.1.2 The provision of more NADH increases the reverse β-oxidation pathway's activity

The synthesis of MCFA via the rBOX may require a higher availability of NADH due to the number of cycles necessary. Therefore, we needed a strain with a higher cytosolic NADH pool to properly assess the different rBOX variants tested for MCFA production. As mentioned in 4.1.1.1, the titres of glycerol when expressing the rBOX in VSY0 (Δ*adh1-5*) were high (**Fig 13C**). Therefore, we deleted *GPD2*, encoding the primary glycerol 3-phosphate dehydrogenase to reduce the competition for NADH, generating strain GDY15 (Δ*adh1-5*, Δ*gpd2*).

We compared GDY15 with VSY0, both transformed with an empty vector or ACBV007 (^{Cn}*bktB*, ^{Ca}*hbd*, ^{Ca}*crt*, ^{Td}*ter*) and investigated whether a potential higher availability of NADH in GDY15 could improve the MCFA production by the rBOX pathway (**Figure 14**). On average, the deletion of *GPD2* (strain GDY15) reduced 5-fold the production of glycerol (**Fig 14A**) and significantly improved the growth phenotype compared to the VSY0 strain (**Fig 14B**).

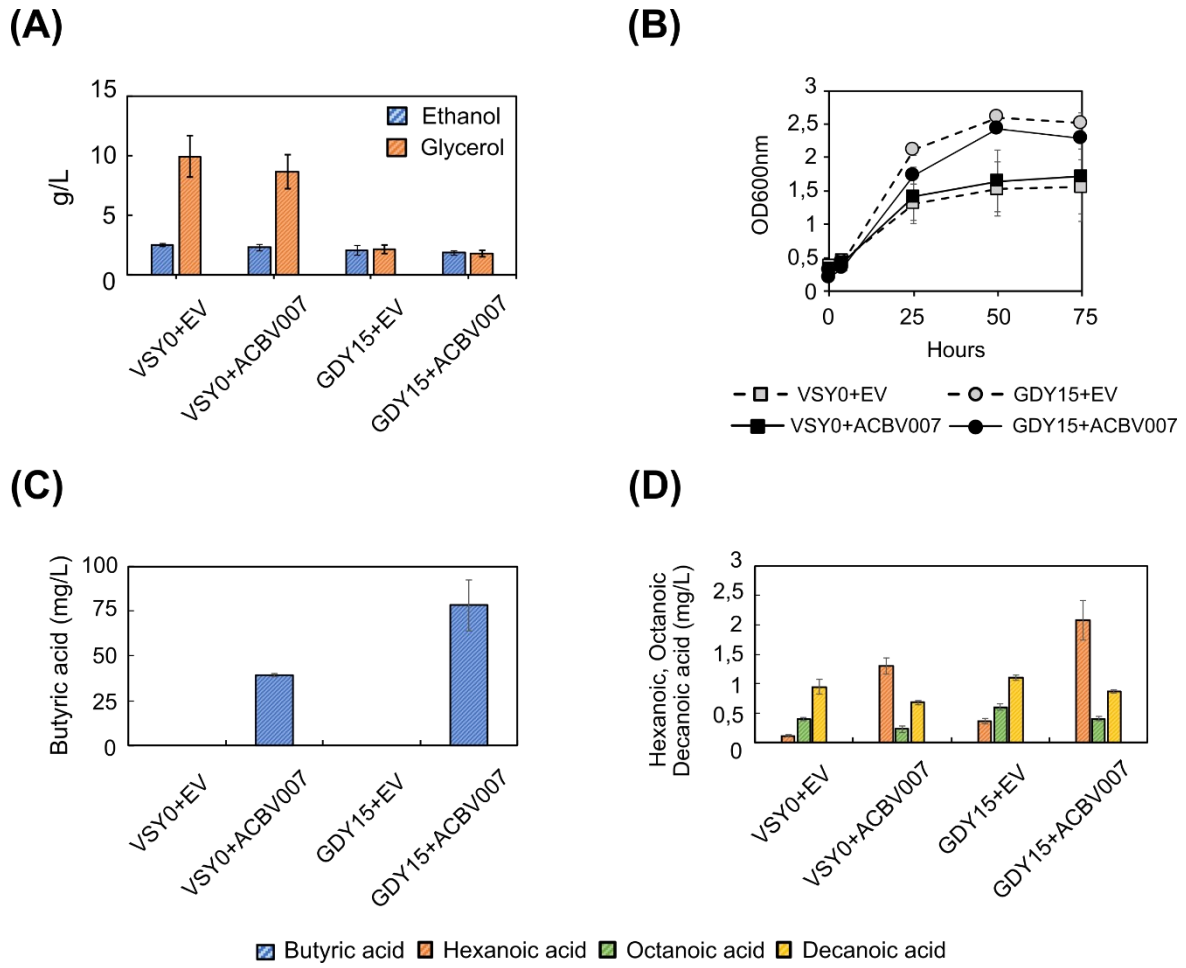

Figure 14. C4-C10 fatty acid production in a *GPD2*-ko strain. A) Ethanol (*blue*) and glycerol (*orange*) production (g/L) in VSY0 or GDY15 strains with **ACBV007** (^{Cn}***bktB***, ^{Ca}*hbd*, ^{Ca}*crt*, ^{Td}*ter*) or an empty vector (EV). Growth (OD600nm) of VSY0 or GDY15 with ACBV007 or EV. C) Production of butyric acid by VSY0 and GDY15 expressing the rBOX pathway (ACBV007) or with (EV) after 75h of fermentation. D) Production of hexanoic (*orange*), octanoic (*green*) and decanoic acid (*yellow*) by VSY0 and GDY15 expressing the rBOX pathway (pACB007) or with the

empty vector (EV) after 75h of fermentation. Fermentation was run in buffered synthetic medium (SM) without uracil for 75h. Error bars represent the standard deviation between four independent replicates.

In addition, it doubled butyric acid production to 78.2 ± 14.18 mg/L (**Fig 14C**), and hexanoic acid production increased by 59%, reaching 2.07 ± 0.34 mg/L (**Fig 14D**), indicating a higher flux within the rBOX pathway. However, the octanoic and decanoic acid titers remained very low in all the strains.

Overall, butyric acid was the main product of the pathway. This indicates that NADH availability, although pushing the pathway's activity, is not the only factor limiting the production of longer MCFAs.

4.1.2 Testing different reverse β-oxidation variants

In section 4.1, we created a *S. cerevisiae* strain with an improved cytosolic NADH pool. In this strain, we produced hexanoic acid only with the combined expression of thiolase ^{Cn}*bktB* with ^{Ca}*hbd*, ^{Ca}*crt* and ^{Td}*ter*. However, the titres of butyric acid were almost 40-fold higher, and the production of octanoic and decanoic acid was not improved. This could indicate that the reactions following ^{Cn}BktB might be limiting the production of MCFA. Therefore, we tested alternative NADH-dependent 3-hydroxyacyl-CoA dehydrogenases, enoyl-CoA hydratases, and *trans*-enoyl-CoA reductases to improve MCFA production.

4.1.2.1 The selection of 3-hydroxyacyl-CoA dehydrogenase is crucial for generating MCFAs with reverse β-oxidation

We first tested two additional NADH-dependent 3-hydroxyacyl-CoA dehydrogenases: PaaH1 from *C. necator* and the putative YALI0C08811 from *Yarrowia lipolytica*, which we will refer to as ^{Yl}Had throughout this study, and compared them against ^{Ca}Hbd. An analysis in MitoProt II suggests that ^{Yl}Had is a mitochondrial protein in *Y. lipolytica* (**Table 26**).

Table 26. Analysis in MitoProt II of three different 3-hydroxyacyl-CoA dehydrogenases. The sequence of ^{Cn}PaaH1, ^{Ca}Hbd and ^{Yl}Had and their probability of mitochondrial import based on the MitoProt II prediction tool ($P_{MITOPROTII}$). The putative MTS is underlined in the sequence.

Enzyme	Amino acid sequence	$P_{MITOPROTII}$
^{Cn}PaaH1	MSIRTVGIVGAGTMGNGIAQACAVVGLNVVMVDISD AAVQKGVATVASSLDRLIKKEKLTEADKASALARIKG STSYDDLKATDIVIEAATENYDLKVKILKQIDGIVGENV IIASNTSSISITKLAAVTSRADRFIGMHFFNPVPVMALV ELIRGLQTSDTTHAAVEALSKQLGKYPITVKNSPGFV VNRILCPMINEAFCVLGEGLASPEEIDEGMKLGCNHP IGPLALADMIGLDTMLAVMEVLYTEFADPKYRPAMLM REMVAAGYLGRKTGRGVYVYSK*	0.004

^{Ca}Hbd	MKKVCVIGAGTMGSGIAQAFAAKGFEVVLRDIKDEFV DRGLDFINKNLSKLVKKGKIEEATKVEILTRISGTVDLN MAADCDLVIEAAVERMDIKKQIFADLDNICKPETILASN TSSLSITEVASATKRPDKVIGMHFFNPAPVMKLVEVIR GIATSQETFDAVKETSIAIGKDPVEVAEAPGFVVNRILIP MINEAVGILAEGIASVEDIDKAMKLGANHPMGPLELGD FIGLDICLAIMDVLYSETGDSKYRPHTLLKKYVRAGWL GRKSGKGFYDYSK*	0.006
^{Yl}Had	MFRLTTARIASVRGFSTSASLSKKVDSLSVIGAGQMGL GIALVAANKAGLQVNLIDANQGALDKGLKFMDKLLEKD VGKGRLTSDEAQAVRGRVTGHTNLQSAVADVDMIIEA VPEIPKLKFDIFRDLNEWTQKDTILATNTSSISITKIAAAA GAGAPRVISAHFMNPVPVQKGVEIITGLQTSPETLATTL EVVKRMGKIPSISKDSPGFLANRILMPYINEAIITLETGV GEKEDIDNILKNGCAMPMGPLALADFIGLDTCLAIMRVL YEDTGDSKYRPSVLLNKYVDAGWLGKKSGKGFYDY*	0.891

Since we were expressing the rBOX in the cytosol, we first validated the cellular localisation of ^{Yl}Had when expressed in *S. cerevisiae.* We confirmed that it also localises in the mitochondria of this organism (**Figure 15**). Therefore, we removed the putative mitochondrial targeting sequence (MTS) from ^{Yl}Had and used this cytosolic version in the rBOX constructs used for MCFA production.

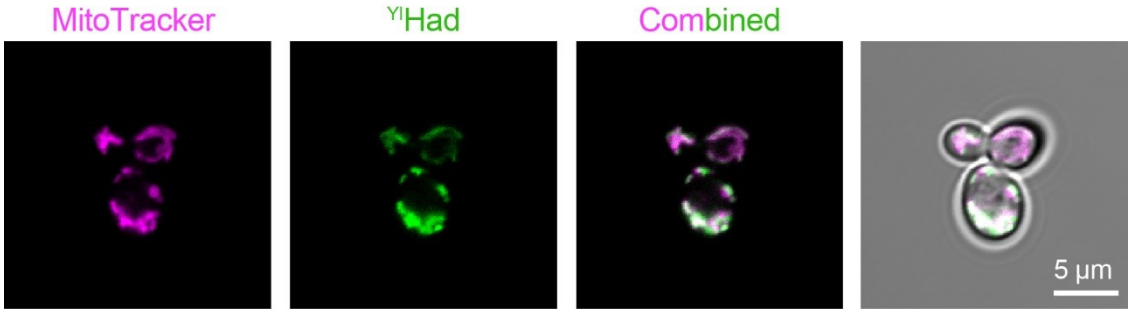

Figure 15. The localisation of the full ^{Yl}Had protein in *S. cerevisiae*. The full ^{Yl}Had protein was fused to GFP and expressed from a CENARS-based plasmid (GDV152) in *S. cerevisiae* CEN.PK2-1C. The localisation of the fusion protein (in green) was analysed by fluorescence microscopy. Mitochondria were dyed with Mitotracker Red CMXRos and are here represented in magenta.

We transformed *S. cerevisiae* GDY15 with the plasmids ACBV007 (^{Cn}*bktB*, ^{Ca}***hbd***, ^{Ca}*crt*, ^{Td}*ter*), FHV022 (^{Cn}*bktB*, ^{Cn}***paaH1***, ^{Ca}*crt*, ^{Td}*ter*), GDV151 (^{Cn}*bktB*, ^{Yl}***HAD***, ^{Ca}*crt*, ^{Td}*ter*) and compared the impact of each 3-hydroxyacyl-CoA dehydrogenase on the production of butyric acid and MCFA (**Figure 16**). The variants expressing ^{Ca}*hbd* (ACBV007) or ^{Yl}*HAD* (GDV151) produced mainly butyric acid (89.25 ± 4.03 and 99.2 ± 7.85 mg/L, respectively). Also, while ACBV007 (^{Ca}*hbd*) produced 1.57 ± 0.13 mg/L of hexanoic acid, GDV151 (^{Yl}*HAD*) did not produce significant amounts of any MCFA. On the other hand, the variant expressing ^{Cn}*paaH1* (FHV022) produced hexanoic acid as the main product in considerable amounts (32.88 ± 1.09 mg/L) (**Figure 16B**). In this variant, not only the titer of butyric acid (10.35 ± 2.10 mg/L) is decreased compared to ^{Ca}*hbd* (ACBV007) and ^{Yl}*HAD* (GDV151), but also the octanoic acid titer (2.68 ± 0.04 mg/L) is higher than in those variants (p-value < 0.0001), none of which reached a titer of 1 mg/L.

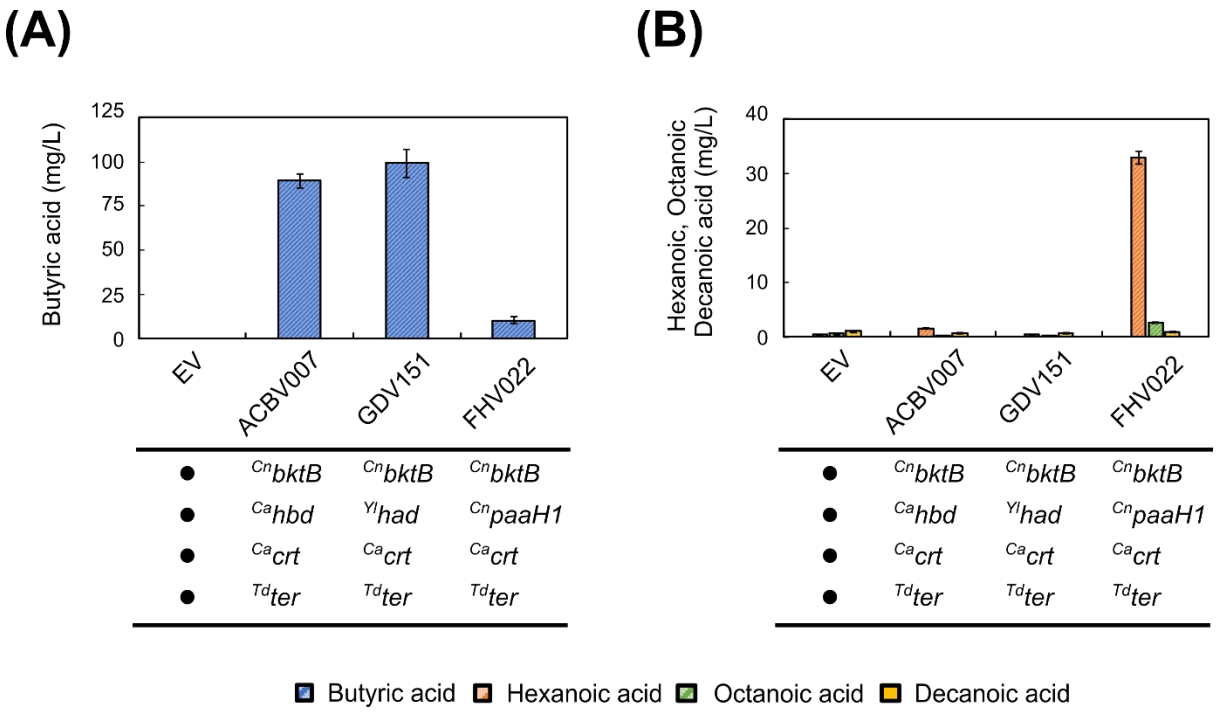

Figure 16. Impact of the selected β-hydroxyacyl-CoA dehydrogenase on the production of MCFA. A) Production of butyric acid by GDY15 expressing the rBOX pathway variants (**ACBV007**: ^{Cn}*bktB*, ***^{Ca}hbd***, ^{Ca}*crt*, ^{Td}*ter*, **GDV151**: ^{Cn}*bktB*, ***^{Yl}HAD***, ^{Ca}*crt*, ^{Td}*ter*, **FHV022**: ^{Cn}*bktB*, ***^{Cn}paaH1***, ^{Ca}*crt*, ^{Td}*ter*) or with the empty vector (EV) after 75 h of fermentation in buffered synthetic medium (SM) without uracil. B) Production of hexanoic (*orange*), octanoic (*green*) and decanoic acid (yellow) by GDY15 expressing the rBOX pathway variants (ACBV007, GDV151, FHV022) or with the empty vector (EV) after 75 h of fermentation in buffered synthetic medium (SM) without uracil. Error bars represent the standard deviation between four independent replicates.

4.1.2.2 The enoyl-CoA hydratase reaction also controls the fatty acid chain length

The expression of ^{Cn}*paaH1* as the 3-hydroxyacyl-CoA dehydrogenase of the pathway increased the overall MCFA production up to 20-fold (4.1.2.1). However, the chain length seemed to be limited to hexanoic acid. Therefore, we wanted to test whether the choice of enoyl-CoA hydratase could also have an impact on the chain length of the MCFA. To assess this, we initially tested one additional enoyl-CoA hydratase, *crt2* from *C. necator*, first described by Segawa *et al.* 2019 (Segawa, Wen et al. 2019).

We transformed GDY15 with the plasmids FHV018 (^{Cn}*bktB*, ^{Cn}*paaH1*, ***^{Cn}crt2***, ^{Td}*ter*), FHV022 (^{Cn}*bktB*, ^{Cn}*paaH1*, ***^{Ca}crt***, ^{Td}*ter*) or an empty vector (EV) and compared the impact of each enoyl-CoA hydratase on the production of butyric acid and MCFA. The expression of ^{Cn}*crt2* (FHV018) as enoyl-CoA hydratase did not change the production of butyric acid, but it almost doubled the overall production of MCFA compared to ^{Ca}*crt* (FHV022) (**Table 28**). As observed in **Fig 17A**, octanoic acid production increased 15-fold (40.26 ± 1.05 mg/L) with ^{Cn}*crt2* (FHV018). On the other hand, hexanoic acid titers still reached 21.88 ± 0.78 mg/L with FHV018 (^{Cn}*crt2*) and remained lower compared to FHV022 (^{Ca}*crt*) (32.88 ± 1.09 mg/L). Although still at low titers,

decanoic acid increased 2-fold with the expression of ^{Cn}*crt2* (1.97 ± 0.05 mg/L) compared to ^{Ca}*crt* (0.96 ± 0.06 mg/L).

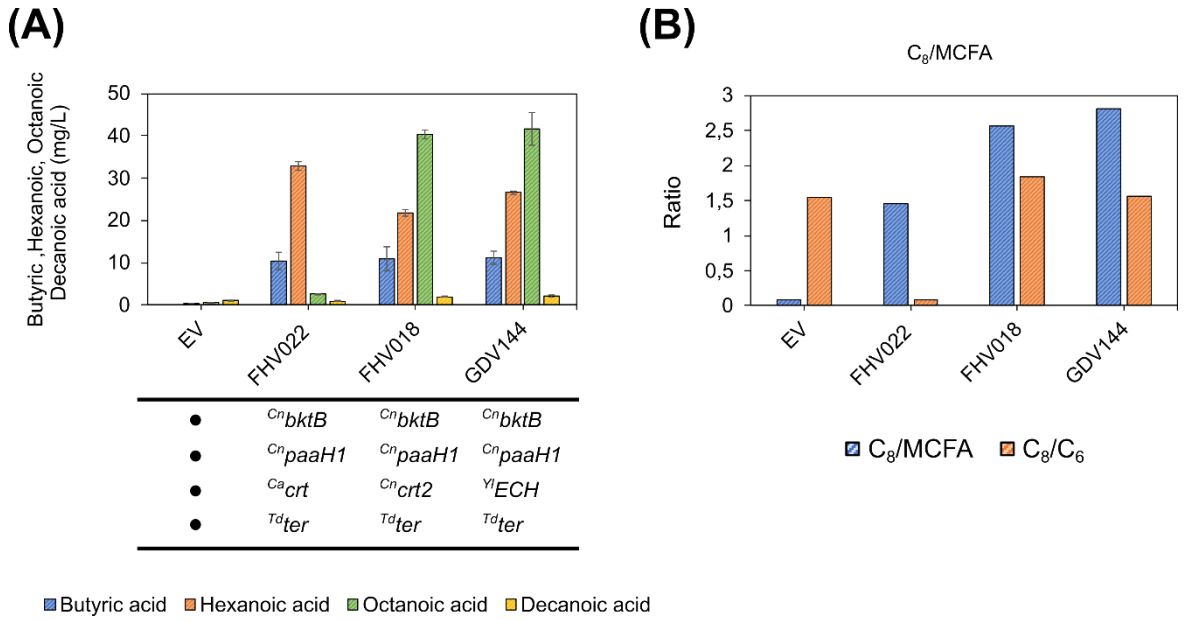

Figure 17. Growth and MCFA production with different enoyl-CoA reductases. A) Production of butyric (*blue*), hexanoic (*orange*), octanoic (*green*) and decanoic acid (*yellow*) by GDY15 expressing the rBOX pathway variants (**FHV022**: ^{Cn}*bktB*, ^{Cn}*paaH1*, ^{Ca}***crt***, ^{Td}*ter*), (**FHV018**: ^{Cn}*bktB*, ^{Cn}*paaH1*, ^{Cn}***crt2***, ^{Td}*ter*), (**GDV144**: ^{Cn}*bktB*, ^{Cn}*paaH1*, ^{Yl}***ECH***, ^{Td}*ter*) or with the empty vector (EV) after 75h in buffered synthetic medium (SM) without uracil. B) Ratio of octanoic acid to total MCFA (*blue*) and to hexanoic acid (*orange*) in GDY15 expressing EV, FHV022, FHV018 or GDV144. Error bars represent the standard deviation between three independent replicates.

We produced significant titers of octanoic acid for the first time using ^{Cn}Crt2 as enoyl-CoA hydratase. To increase the octanoic to hexanoic acid ratio as well as the titers of decanoic acid, we investigated ^{Cn}Crt2 homologs in yeast. We analysed ^{Cn}Crt2 in PROSITE and identified an amino acid signature (PS00166) typically found in the enoyl-CoA hydratase/isomerase family (de Castro, Sigrist et al. 2006). We screened for enzymes with this motif in *S. cerevisiae* and the known oleaginous yeasts *Cryptococcus curvatus*, *Lipomyces lipofer*, *Rhodosporidium toruloides*, *Rhodotorula glutinis* and *Yarrowia lipolytica* (Lamers, van Biezen et al. 2016) (**Table 27**). We selected oleaginous yeast due to their ability to accumulate fatty acids and triglycerides (Shaigani, Awad et al. 2021, Duman-Özdamar, Martins Dos Santos et al. 2022), and due to the convergent set of reactions between FAB and the rBOX. From this analysis, only Ehd3 (*S. cerevisiae*) and two putative enzymes from *Y. lipolytica* (YALI0B10406 and YALI0F22121) were distinguished as interesting enzymes. Then, we performed a protein BLAST of these three candidates against ^{Cn}Crt2. As a result, YALI0B10406, a putative enoyl-CoA hydratase from *Y. lipolytica*, which will be referred to as ^{Yl}Ech throughout this study, resulted as the most promising yeast enoyl-CoA hydratase candidate.

Fabian Haitz (Master student) built the plasmid FHV018 and FHV022 and conducted conducted the cultivation and probing of the samples under the author's supervision.

Table 27. PROSITE search of ^{Cn}CRT2 homologs, BLAST and MitoProt II analysis. Search for enzymes with PS00166 signature motifs in different yeast. The amino acid sequence (AA sequence) and the putative mitochondrial targeting sequence ($MTS_{MitoProtII}$) from all enzymes is also shown. The hits' identity percentage against ^{Cn}Crt2 after a protein BLAST query is also shown (% identity).

UniProtKB (PS00166)	Name	Organism	AA sequence (<u>$MTS_{MitoProtII}$</u>)	% identity	Comments
non-identified	NA	*Cryptococcus curvatus*	NA	NA	
non-identified	NA	*Lipomyces lipofer*	NA	NA	
non-identified	NA	*Rhodosporidium toruloides*	NA	NA	
non-identified	NA	*Rhodotorula glutinis*	NA	NA	
N1P4J6	Ehd3	*Saccharomyces cerevisiae*	<u>MLKYTLKCAQSSSKYGFRTTTRTFMSTRVQL</u>NASSTPPVLFTA QDTARVITLSRPNKLNALNTEMSESMFKTLNEYAKSGTTNLIILK SSNGPRSFCAGGDVATVATHNIKQEFNKSIEFFTAEYSLNFQIA TYLKPIVTFMDGITMGGGVGLSIHTPFRIATENTKWAMPEMDIG FFPDVGSTFALPRIVTVANSNSQMALYLCLTGEIVTGADAYML GLASHYISSENLDALQKRLGEISPPFNNDAQSAYFFGMVNESID EFVSPFPKDYVFKYSNEKLNVIEACFNLSKSGTIEDIMNNLSQY EGSSEGKAFAQEIKTKLLTKSPSSLQIALRLVQENSRDHIESVIK RDLYTAANMCINQDSLVEFTEATKYKLLDKQKVPYPWTKKEQL FVSQLTSITSPKPSLPISLLRNTANVTWTQYPYHSKYQLPTEREI AAYIEKRTNDNAGAKITEGEVIDHFANVVPSRRGKLGIQSLCKIV CERKCEEVNGGLKWK*	27.84	
Q6CF43	YALI0B10406 (^{Yl}Ech)	*Yarrowia lipolytica*	<u>MRSLYINVPGLFPSTSLARETVHHRTEMLRTIRSSSRLGVRAM STAATRRAAQIGFHTRVPTVVTKAPTLRM</u>QTTPFSSSAPAQTF GDKKYEHILTSTPVPKVALVTLNRPKALNALCTPLIKELNEALQA ADADPTIGAIVLTGSEKSFAAGADIKEMKDKTVTSVLNENFIEE WGNMANIKKPIIAAVNGFALGGGCELAMMADIIYAGAKAKFGQ PEIKLGVIPGAGGTQRLTRAIGLYRANHYILTGEMFTAQQAAD WGLAAKVYEPAQLVDESVKAAAQIASYGQLAVQAAKASVHQS AEVGLRAGLEFERVRFHGLFGTHDQKEGMAAFAEKREPNFKN E*	52.34	Putative function. Tested in *Zhao et al.* (2015)
Q6C0S5	YALI0F22121	*Yarrowia lipolytica*	<u>MLRTISRTRTMVPSRHLISYRFFSDVSTTK</u>GETFTLTKHFLDAS NTAHIAVYSLNRPEAMNSISKKLLEEFETYINSLAAEGRHQNVT NTRALILSSELPKVFCAGADLKERKTFTDADTAAFLNKLNGTLD TIQSLHMPTITAIQGFALGGGAEISLATDFRVLSDVAQFGLPETR LAILPGAGGTKRLPKLIGYSRALDLVLTGRRVKADEALHLGIAN RTGENALETALEMAKLICEGGPIAINAAKMAVRGQSKEWEIAAY NKVVNSEDKFEALSAFKEKRKPIFKGR*	30.86	Putative function.

Analysis in MitoProt II suggested that ^{Yl}Ech is a mitochondrial protein in *Y. lipolytica* (**Table 27**). We tagged GFPenvy to the C-terminal end of ^{Yl}Ech, analysed the cellular localization by fluorescence microscopy and confirmed that the full-length ^{Yl}Ech is targeted in the mitochondria (**Figure 18**). Therefore, we removed the putative MTS from ^{Yl}Ech and used this cytosolic version in the rBOX constructs used for MCFA production.

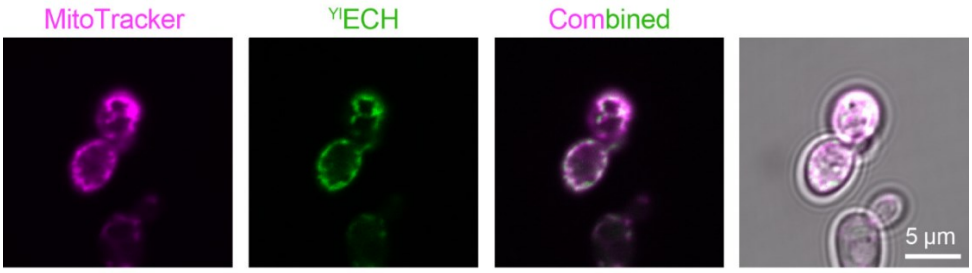

Figure 18. The localisation of the full ^{Yl}Ech protein in *S. cerevisiae*. The full ^{Yl}Ech protein was fused to GFP and expressed from a CENARS-based plasmid (FHV025) in *S. cerevisiae* CEN.PK2-1C. The localisation of the fusion protein (in green) was analysed by fluorescence microscopy. Mitochondria were dyed with Mitotracker Red CMXRos and are here represented in magenta.

We tested the expression of ^{Yl}*ECH* for MCFA production in plasmid GDV144 (^{Cn}*bktB*, ^{Cn}*paaH1*, ^{Yl}***ECH***, ^{Td}*ter*). When expressing this pathway variant, hexanoic acid and octanoic acid titers reached 26.57 ± 0.39 mg/L and 41.66 ± 3.81 mg/L, respectively (**Fig 17A**). Compared to ^{Cn}*crt2* (FHV018), the expression of ^{Yl}*ECH* (GDV144) led to higher yields of MCFA on glucose ($Y_{MCFA/S}$) (**Table 28**), mainly from an increase in hexanoic acid production. The octanoic acid to hexanoic acid ratio did not improve with ^{Yl}*ECH* (GDV144). On the contrary, it decreased by 20% compared to ^{Cn}*crt2* (FHV018) (**Fig 17B**). No significant changes in butyric acid production were observed, and the production of decanoic acid was also not improved.

We also observed that the final OD_{600nm} decreased with hexanoic acid production (FHV022) and decreased further with octanoic as the main product (FHV018 and GDV144), suggesting a growth inhibitory effect proportional to the chain length of the primary MCFA produced (**Figure 19**). In addition, we observed that, in the octanoic acid-producing variants, ^{Yl}*ECH* (GDV144) expression resulted in a slight growth impairment compared to ^{Cn}*crt2* (FHV018).

Fabian Haitz (Master student) build the ^{Yl}*ECH*-GFP fusion plasmid (FHV025) and conducted the analysis of the samples by confocal microscopy under the author's supervision.

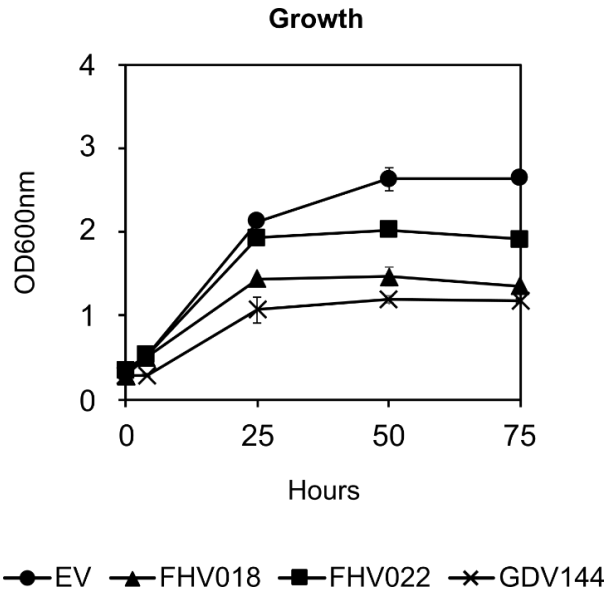

Figure 19. Growth of GDY15 with EV (*filled circle*, ●), FHV018 (*filled triangle*, ▲), FHV022 (*filled square*, ■) or GDY144 (*cross*, ×) over 75h in buffered synthetic medium (SM) without uracil. Error bars represent the standard deviation between three independent replicates.

Table 28. Consumption of glucose (in mg) and yields on glucose (g/g) of glycerol ($Y_{GLY/S}$), ethanol ($Y_{ETOH/S}$), overall medium chain fatty acids ($Y_{MCFA/S}$) and biomass ($Y_{X/S}$), as well as yields on biomass (g/g) of butyric acid ($Y_{BUT/X}$), hexanoic acid ($Y_{HEX/X}$), octanoic acid ($Y_{OCT/X}$), decanoic acid ($Y_{DEC/X}$)and overall medium chain fatty acids ($Y_{MCFA/X}$) after 75h in buffered synthetic medium by GDY15 expressing plasmids ACBV007 (^{Cn}*bktB*, ^{Ca}*hbd*, ^{Ca}*crt*, ^{Td}*ter*, *URA* marker), GDV144 (^{Cn}*bktB*, ^{Cn}*paaH1*, ^{Yl}*ECH*, ^{Td}*ter*, *URA* marker) GDV151 (^{Cn}*bktB*, ^{Yl}*HAD*, ^{Ca}*crt*, ^{Td}*ter*, *URA* marker) FHV018 (^{Cn}*bktB*, ^{Cn}*paaH1*, ^{Cn}*crt2*, ^{Td}*ter*, *URA* marker), FHV022 (^{Cn}*bktB*, ^{Cn}*paaH1*,^{Ca}*crt*, ^{Td}*ter*, *URA* marker) or the empty vector (EV).

Plasmid	Glucose consumed	Total MCFA produced (C6-C10)	$Y_{GLY/S}$	$Y_{ETOH/S}$	$Y_{BUT/S}$	$Y_{MCFA/S}$	$Y_{X/S}$	$Y_{BUT/X}$	$Y_{HEX/X}$	$Y_{OCT/X}$	$Y_{DEC/X}$	$Y_{MCFA/X}$
EV	650.08	0.080206	0.1502	0.1482	-	0.00012	0.089843	-	0.00026	0.0004	0.00072	0.00137
ACBV007	442.53	0.096103	0.2144	0.104	0.008067	0.00022	0.114473	0.070474	0.00124	0.00015	0.00051	0.001897
GDV144	324.01	2.811773	0.14	0.0893	0.001385	0.00867	0.080291	0.017246	0.04085	0.06406	0.00316	0.108083
GDV151	542.79	0.049884	0.2028	0.1164	0.007310	0.00009	0.08676	0.08426	0.00035	0.00013	0.00058	0.001059
FHV018	387	2.564987	0.1163	0.0554	0.001136	0.00663	0.109213	0.010406	0.02919	0.0537	0.00263	0.085515
FHV022	411.06	1.461311	0.1225	0.0651	0.001008	0.00355	0.102819	0.009802	0.03112	0.00254	0.00091	0.034575

Table 29. Consumption of glucose (in mg), total production of MCFA (in mg) and yields on glucose (g/g) of glycerol ($Y_{GLY/S}$), ethanol ($Y_{ETOH/S}$), butyric acid ($Y_{BUT/S}$) overall medium chain fatty acids ($Y_{MCFA/S}$) and biomass ($Y_{X/S}$), as well as yields on biomass (g/g) of butyric acid ($Y_{BUT/X}$), hexanoic acid ($Y_{HEX/X}$), octanoic acid ($Y_{OCT/X}$), decanoic acid ($Y_{DEC/X}$) and overall medium chain fatty acids ($Y_{MCFA/X}$) after 75h in buffered synthetic medium by GDY15 expressing plasmids FHV018 (^{Cn}*bktB,* ^{Cn}*paaH1,* ^{Cn}*crt2,* ^{Td}*ter, URA* marker), GDV116 (^{Cn}*bktB,* ^{Cn}*paaH1,* ^{Cn}*crt2,* ^{Eg}*ter*, *URA* marker) or the empty vector (EV).

Plasmid	Glucose consumed	Total MCFA produced (C6-C10)	$Y_{GLY/S}$	$Y_{ETOH/S}$	$Y_{BUT/S}$	$Y_{MCFA/S}$	$Y_{X/S}$	$Y_{BUT/X}$	$Y_{HEX/X}$	$Y_{OCT/X}$	$Y_{DEC/X}$	$Y_{MCFA/X}$
EV	482.88	0.08507	0.1544	0.1442	-	0.00018	0.08984	-	0.00026	0.00049	0.00087	0.00162
FHV018	400.25	2.19552	0.1152	0.0831	0.00124	0.00549	0.08043	0.01545	0.03113	0.04433	0.00335	0.07881
GDV116	380.60	1.82314	0.1591	0.0775	0.00095	0.00479	0.10281	0.01118	0.02195	0.03249	0.00218	0.05662

4.1.2.3 The selection of an appropriate *trans*-enoyl-CoA reductase determines the product titres

The *trans*-enoyl-CoA reductase reaction was a bottleneck in the rBOX pathway when producing *n*-butanol (Schadeweg and Boles 2016b). Therefore, we tested one additional *trans*-enoyl-CoA reductase from the microalgae *Euglena gracilis*, which will be referred to as ^{Eg}Ter. This enzyme was first described by *Inui et al.* (1984) (Inui, Miyatake et al. 1984) as part of a mitochondrial form of anaerobic fatty acid synthesis in *E. gracilis*, and later characterized by *Hoffmeister et al.* (2005) (Hoffmeister, Piotrowski et al. 2005). ^{Eg}Ter has a reported higher specificity for *trans*-2-hexenoyl-CoA and *trans*-2-octenoyl-CoA than for crotonoyl-CoA (Inui, Miyatake et al. 1984), which made it a suitable candidate to improve the MCFA production. ^{Eg}Ter was used previously in our group to produce 1-butanol (Schadeweg and Boles 2016a). In that study, the MTS was removed from the sequence, and this cytosolic ^{Eg}Ter variant is the one we use in our experiments.

We transformed GDY15 with the plasmid GDV116 (^{Cn}*bktB*, ^{Cn}*paaH1*, ^{Cn}*crt2*, ^{Eg}***ter***) and compared the production of butyric acid and MCFA against FHV018 (^{Cn}*bktB*, ^{Cn}*paaH1*, ^{Cn}*crt2*, ^{Td}***ter***) and an empty vector control after 75h of fermentation in SM medium. The production pattern did not change, with octanoic acid as the main MCFA with both *trans*-enoyl-CoA reductases, followed by hexanoic acid (**Fig 20A**). However, the expression of ^{Eg}*ter* (GDV116) significantly decreased the overall production of MCFA (45.57 ± 1.59 mg/L) compared to ^{Td}*ter* (FHV018) (54.89 ± 1.89 mg/L). Butyric acid production did not significantly differ between *trans*-enoyl-CoA reductases, although we also saw a trend of lower titers with ^{Eg}*ter* (GDV116) expression.

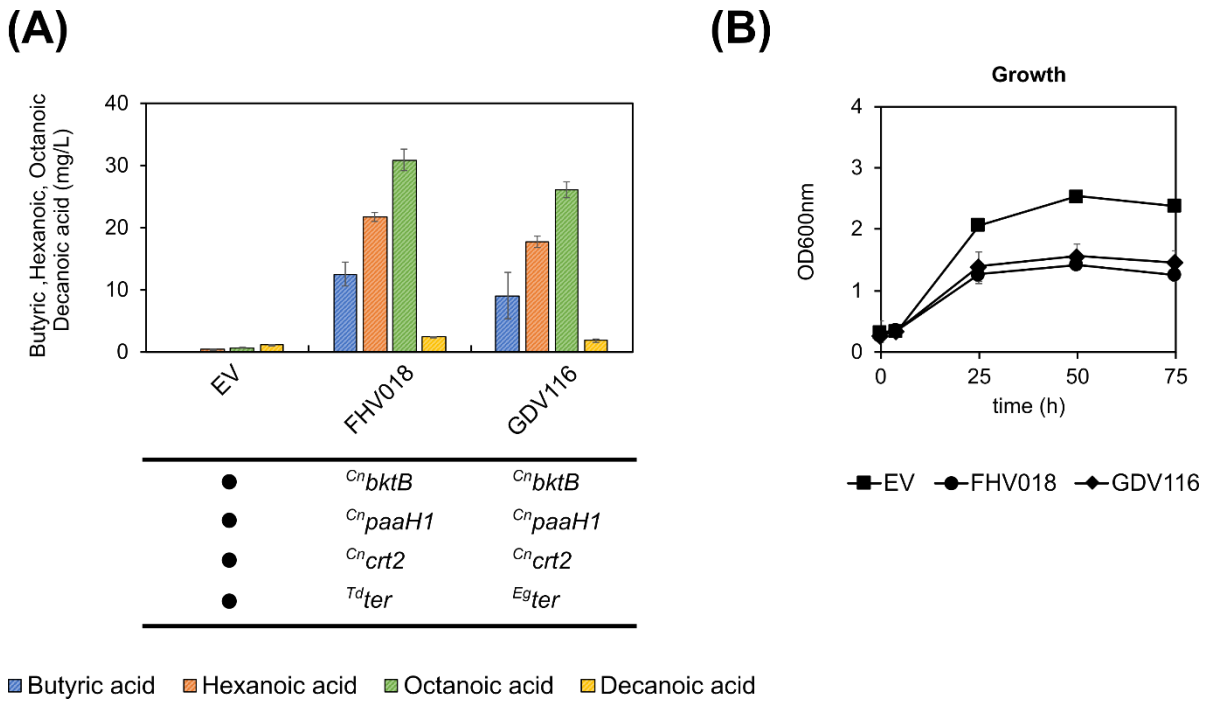

Figure 20. Growth and MCFA production with different *trans*-enoyl-CoA reductases. A) Production of butyric (*blue*), hexanoic (*orange*), octanoic (*green*) and decanoic acid (*yellow*) by GDY15 expressing the reverse β-oxidation pathway variants (**FHV018**: ^{Cn}*bktB*, ^{Cn}*paaH1*, ^{Cn}*crt2*, ^{Td}***ter***, **GDV116**: ^{Cn}*bktB*, ^{Cn}*paaH1*, ^{Cn}*crt2*, ^{Eg}***ter***) or with the empty vector (EV) B) Growth of GDY15 with EV (*filled square*, ■), FHV018 (*filled circle*, ●), or GDV116 (*filled diamond*, ♦) over 75h in synthetic medium (SM) without uracil. Error bars represent the standard deviation between three independent replicates.

The production of significant titers of MCFA resulted, again, in impaired growth compared to the empty vector control (**Fig 20B**). However, the growth with both plasmids FHV018 (^{Td}*ter*) and GDV116 (^{Eg}*ter*) is similar, suggesting that the higher MCFA production with ^{Td}Ter is not growth-related but that ^{Td}Ter is a better enzyme for this reaction. When we compare the MCFA yield on biomass ($Y_{MCFA/X}$) and the yield on glucose ($Y_{MCFA/S}$) (**Table 29**) of each clone, we observed that GDY15 expressing ^{Td}*ter* as *trans*-2-enoyl-CoA reductase had a 40% and 54% higher yield on biomass and glucose, respectively, compared to ^{Eg}*ter*.

Finally, the yield of glycerol on biomass ($Y_{GLY/X}$) and on glucose ($Y_{GLY/S}$) was higher expressing ^{Eg}*ter* ,13% and 40% respectively, than ^{Td}*ter*. This might indicate that NADH re-oxidation via the ^{Eg}Ter-containing pathway variant was insufficient, leading to increased glycerol production through the remaining Gpd1.

4.1.3 Improving pathway yield

In section **4.1.2**, we established a combination of enzymes leading to octanoic acid using the reverse β-oxidation pathway. To increase the production titres and to increase the ratio of octanoic acid to hexanoic acid (C_8/C_6), we tested increasing the production of upstream short/medium-chain fatty acyl CoAs, removed potentially competing pathways and studied the effect of changing the composition of the fermentation medium.

4.1.3.1 Increasing butyryl-CoA availability boosts hexanoic acid production

Butyryl-CoA is the product of a single cycle of the reverse β-oxidation pathway. It is key to producing hexanoyl-CoA, a precursor of hexanoic acid that can be further elongated to octanoyl-CoA, precursor of octanoic acid. Therefore, we tested whether increasing the first round of the rBOX pathway could further improve MCFA production. In GDY15 we combined GDV124 (***^{Cn}bktB***, *^{Cn}paaH1, ^{Cn}crt2, ^{Td}ter*), containing the best combination of enzymes to produce MCFA, with the butyryl-CoA producing GDV098 (***ERG10***, *^{Ca}hbd, ^{Ca}crt, ^{Td}ter*) or an empty vector (EV) control.

The addition of a butyryl-CoA producing pathway increased butyric acid titers almost 3-fold (GDV098+GDV124) (37.79 ± 0.61 mg/L) compared to when the MCFA producing pathway operates alone (EV_{URA}+ GDV124) (13.09 ± 0.93 mg/L) (**Fig 21A**). Hexanoic acid production also increased 23% with GDV098 (31.04 ± 0.96 mg/L), probably due to higher availability of butyryl-CoA. However, neither octanoic nor decanoic acid titers changed significantly with the additional expression of the butyryl-CoA producing pathway variant. As a result, the octanoic to hexanoic acid ratio decreased by 10.7% with this strategy (**Fig 21B**). No significant butyric acid or MCFA were detected in the absence of any rBOX pathway variant.

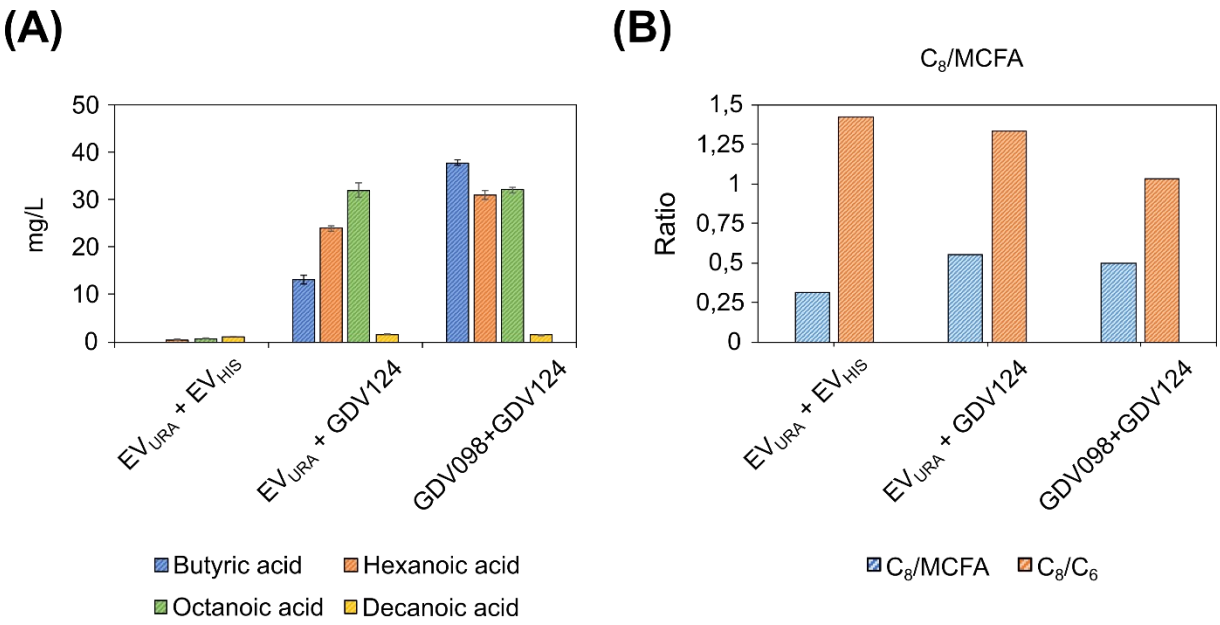

GDV098	GDV124
ERG10	*[Cn]bktB*
[Ca]hbd	*[Cn]paaH1*
[Ca]crt	*[Cn]crt2*
[Td]ter	*[Td]ter*

Figure 21. Effect of increasing butyryl-CoA availability on MCFA production. A) Production of butyric (*blue*), hexanoic (*hexanoic*), octanoic (*green*) and decanoic acid (*yellow*) in GDY15 expressing the MCFA producing pathway alone (**GDV124**: ***[Cn]bktB***, *[Cn]paaH1, [Cn]crt2, [Td]ter*), in combination with GDV098 (***ERG10***, *[Ca]hbd, [Ca]crt, [Td]ter*) or with empty vector (EV_{URA} + EV_{HIS}) controls after 75h in synthetic medium (SM) without uracil or histidine. B) ratio of octanoic acid to total MCFA (*blue*) and to hexanoic acid (*orange*) in GDY15 expressing EV_{URA} + EV_{HIS}, EV_{URA} + GDV124 or GDV098 + GDV124. Error bars represent the standard deviation between three independent replicates.

As observed in previous experiments, the growth of the MCFAs-producing strains was impaired compared to that of the non-producing strains (**Figure 22**). Interestingly, the higher butyric acid production in the strain expressing both GDV098 and GDV124 did not compromise the growth compared to the strain only expressing the MCFA-producing pathway.

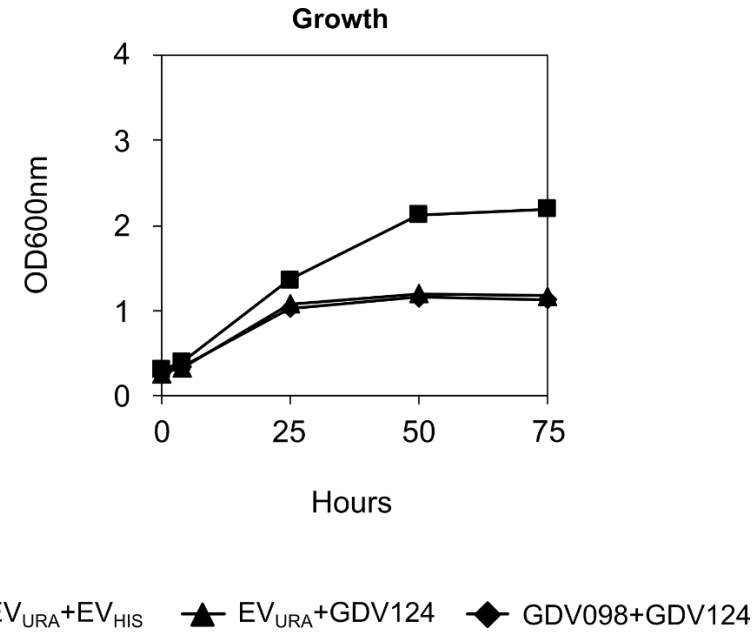

Figure 22. Growth of GDY15 with EV (filled square, ■), EV$_{URA}$ + GDV124 (filled triangle, ▲) or GDV098 + GDV124 (filled diamond, ♦) over 75h in synthetic medium (SM) without uracil or histidine. Error bars represent the standard deviation between three independent replicates.

4.1.3.2 The deletions of *FAA2* and *TES1* do not improve MCFA production

Competing reactions could still hinder the production of MCFAs. The activity of the short-chain acyl-CoA thioesterases *TES1*, known to target butyryl-CoA in *S. cerevisiae* (Maeda, Delessert et al. 2006), could lead to butyric acid production and therefore compromise the chain elongation capacity of the pathway. Furthermore, once released, medium-chain free fatty acids can be degraded in the peroxisomes upon their activation by Faa2, a medium-chain fatty acyl-CoA synthetase (Leber, Choi et al. 2016) (**Figure 12**). To increase the production of free MCFA, we deleted *TES1* or *FAA2* in strain GDY15, generating strains GDY16 (Δ*adh1-5*, Δ*gpd2*, Δ*tes1*) and GDY19 (Δ*adh1-5*, Δ*gpd2*, Δ*faa2*). We compared the expression of the octanoic acid-producing pathway (FHV018) in these strains against their parental GDY15 and VSY0 (**Figure 23**). Deleting *TES1* or *FAA2* did not significantly increase MCFA titers (**Fig 23A**), improve the octanoic acid to decanoic acid ratio (**Fig 23B**) nor reduce butyric acid titers compared to their parental GDY15 strain.

Fabian Haitz (Master student) built the *TES1*-knockout plasmid (FHV016) and conducted the deletion of *TES1* in GDY15 under the author's supervision.

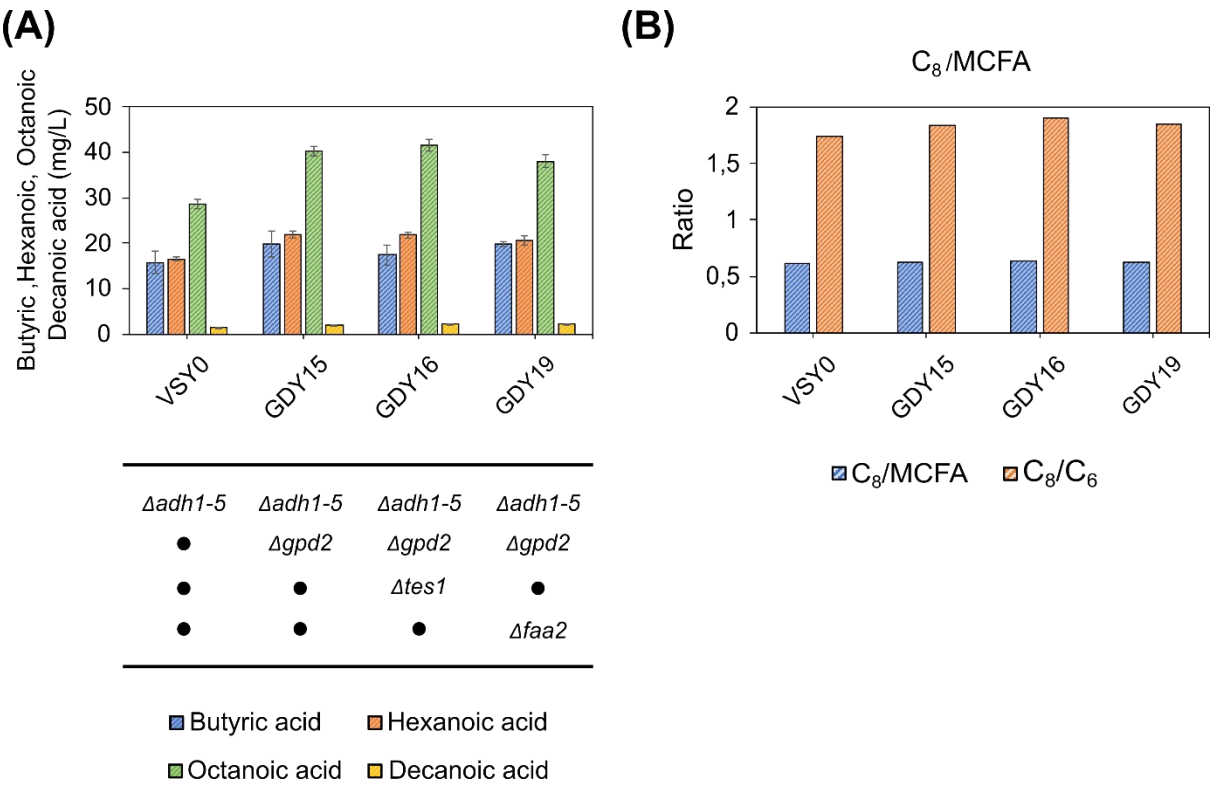

Figure 23. Effect of deleting potential competing reactions on the production of MCFA. (A) Production of butyric (*blue*), hexanoic (*orange*), octanoic (*green*) and decanoic acid (*yellow*) in VSY0, GDY15, GDY16 (Δ*tes1*) and GDY19 (Δ*faa2*) expressing the rBOX pathway from plasmid **FHV018** (*[Cn]bktB, [Cn]paaH1, [Cn]crt2, [Td]ter*) after 75h in synthetic medium (SM) without uracil. (B) Ratio of octanoic acid to total MCFA (blue) and to hexanoic acid (orange) in VSY0, GDY15, GDY16 or GDY19 expressing FHV018. Error bars represent the standard deviation between three independent replicates.

4.1.3.3 Fermentation medium and expression of the reverse β-oxidation pathway from the genome

As observed above, an increased chain length in MCFAs decreased growth. In addition, strategies to increase the chain length improved hexanoic acid production, but not those of octanoic or decanoic acid (sections 4.1.3.1 and 4.1.3.2). Therefore, we compared growth and MCFA production in buffered synthetic medium (SM) against an equally buffered (20 mM phosphate) YPD medium to test whether these limitations arise from the medium composition used during fermentation. In addition, we also tested if an increased buffering capacity could improve MCFA production. For that, we also tested YPD with 100 mM phosphate concentration (YPD-100 mM).

The leucine, uracil, tryptophan and histidin auxotrophies used in previous sections cannot be used in YPD. Therefore, and to avoid using antibiotic resistance-based expression plasmids, we genomically integrated the hexanoic acid (with [Ca]*crt*) and the octanoic acid (with [Cn]*crt2* or [Yl]*ECH*) producing pathway cassettes in strain GDY15, generating strains GDY27 ([Ca]*crt*), GDY28 ([Cn]*crt2*) and GDY29 ([Yl]*ECH*). We fermented GDY15 and the producing strains in different media up to 75h and compared MCFA and butyric acid production after 50h and 75h.

Overall, the production titres of butyric acid, hexanoic acid and octanoic acid peaked at 50h in the three different fermentation media tested (**Figure 24**). Also, production titres were higher in YPD-based medium than in SM and increased further with increased buffering. Interestingly, the $Y_{HEX/S}$ for GDY27 were the highest ($Y_{HEX/S}$=0.004) in SM, where hexanoic acid represented up to 60% of the products from the rBOX, and the lowest in YPD-20 mM (**Table 30**). On the other hand, the $Y_{OCT/S}$ for the octanoic acid producers were the highest in YPD-100 mM, yet similarly to GDY27, the lowest $Y_{OCT/S}$ were in YPD-20 mM. Octanoic acid represented on average 37% of the products from the rBOX in GDY28 and GDY29, regardless of the condition. This pattern of MCFA production described above was exclusive of GDY27, GDY28 and GDY29. The control strain GDY15 did not produce butyric acid and all MCFA were produced at titers below 2 mg/L (**Fig 24A** and **Table 30**).

After 50h in YPD-20 mM, the butyric acid, hexanoic acid and octanoic acid production titers in GDY27 (**Fig 24B**) reached 46.97 ± 3.71 mg/L, 62.17 ± 0.6 mg/L and 4.27 ± 0.04 mg/L, respectively, representing a 75%, 35% and 45% increase compared to titers in SM. Butyric and hexanoic acid titers were further increased in YPD-100 mM, reaching 64.74 ± 3.57 mg/L and 74.58 ± 0.39 mg/L, respectively. In the case of hexanoic acid and to our knowledge, these are the highest titers produced in *S. cerevisiae* using the rBOX pathway. In this strain, octanoic acid titers were slightly reduced (3.29 ± 0.21 mg/L) in YPD-100 mM.

In the octanoic acid producing strains, GDY28 and GDY29, octanoic acid production increased by 36% in GDY28 (43.04 ± 0.28 mg/L) and by 50% in GDY29 (47.98 ± 0.15 mg/L) in YPD-20 mM compared to SM (**Fig 24C, D**). In these two strains, butyric acid and hexanoic acid increased in YPD-20 mM by 30%, on average, compared to fermentation in SM, with butyric acid and hexanoic acid reaching 26.31 ± 4.31 mg/L and 42.53 ± 0.93 mg/L in GDY28, respectively, and 31.03 ± 3.38 mg/L (butyric acid) and 42.92 ± 3.23 mg/L (hexanoic acid) in GDY29. As in the case of GDY27, the titers of butyric, hexanoic and octanoic acid increased in both strains when cultivated in the more buffered YPD-100 mM medium. Here, butyric acid and hexanoic acid titers reached 38.75 ± 2.22 mg/L and 60.23 ± 0.78 mg/L in GDY28, respectively, and 38.46 ± 2.65 mg/L and 61.67± 1.71 mg/L in GDY29. Regarding the production of octanoic acid by these two strains in YPD-100 mM, we produced 56.88 ± 0.41 mg/L in GDY28 and 58.31 ± 1.06 mg/L in GDY29, a 30% and a 20% improvement to the octanoic acid titers observed in YPD-20 mM and, to our knowledge, the highest titers of octanoic acid produced in yeast via the rBOX pathway so far.

After 75h of fermentation, we observed a slight decrease in the final titers of butyric acid, hexanoic acid and octanoic acid in all strains. Interestingly, the only exception was GDY27, where hexanoic acid was almost completely consumed after 75h in YPD-100 mM (7.51 ± 2.23 mg/L) (**Fig 24B**).

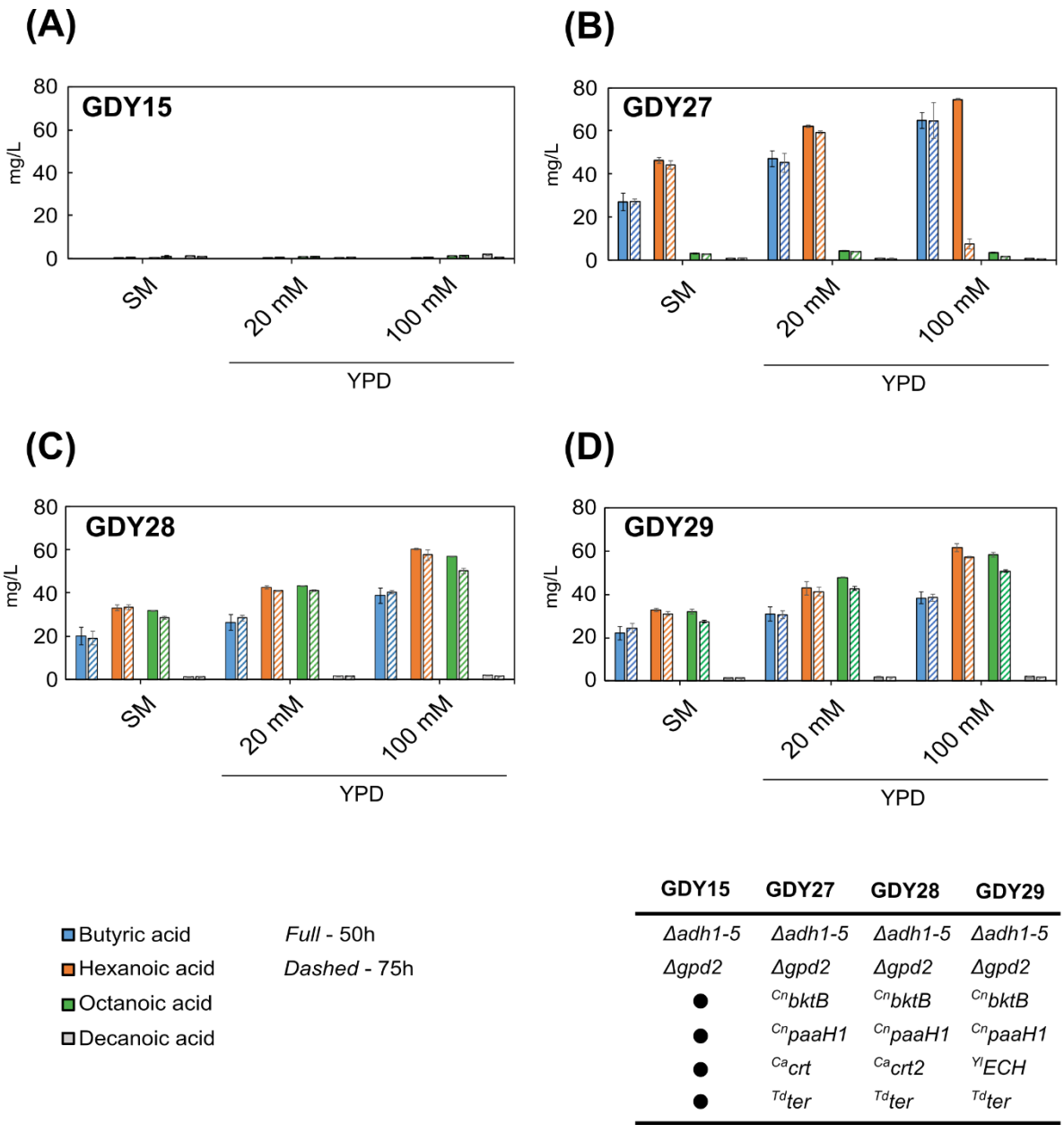

GDY15	GDY27	GDY28	GDY29
Δadh1-5	*Δadh1-5*	*Δadh1-5*	*Δadh1-5*
Δgpd2	*Δgpd2*	*Δgpd2*	*Δgpd2*
●	*^{Cn}bktB*	*^{Cn}bktB*	*^{Cn}bktB*
●	*^{Cn}paaH1*	*^{Cn}paaH1*	*^{Cn}paaH1*
●	*^{Ca}crt*	*^{Ca}crt2*	*^{Yl}ECH*
●	*^{Td}ter*	*^{Td}ter*	*^{Td}ter*

Figure 24. MCFA production in strains with integrated reverse β-oxidation pathway variants in different cultivation media. Production of butyric (*blue*), hexanoic (*orange*), octanoic (*green*) and decanoic acid (*grey*) by strains GDY15 (A), GDY27 (B), GDY28 (C) and GDY29 (D) after 50h (*Full*) or 75h (*Dashed*) of fermentation in synthetic medium (SM), YPD with 20 mM phosphate buffer or YPD with 100 mM phosphate buffer. Error bars represent the standard deviation between three independent replicates.

The composition of the fermentation medium and the phosphate buffer concentration also significantly influenced the growth of the different strains, their metabolite consumption and production pattern (**Figure 25** and **Table 30**). While in SM glucose was never completely consumed in any of the strains, switching to YPD-20 mM increased the overall glucose consumption of the strain by 60% and led to glucose being depleted from the fermentation medium in GDY15 and GDY27 already after 50 hours, and in GDY28 and GDY29 after 75h (**Fig 25A**). Fermentation in YPD-20 mM also more than doubled (2.4-fold) the final OD_{600nm} of the control strain GDY15, increased it by 80% for GDY27 and by 46% and both octanoic acid

producers compared to fermentation in SM (**Fig 25B**). In addition, we observed that changing the medium to YPD-20 mM increased the production of acetic acid almost 3-fold in the three producing strains (GDY27, GDY28 and GDY29) after 75h, reaching the highest acetic acid concentrations among all the fermentations in GDY27 (3.35 ± 0.08 g/L), GDY28 (3.37 ± 0.07 g/L) and GDY29 (3.25 ± 0.05 g/L) (**Fig 25C**). However, this did not occur in GDY15 where, on the contrary to what we had observed in SM, the acetic acid produced in earlier stages of the fermentation was almost completely consumed after 50h.

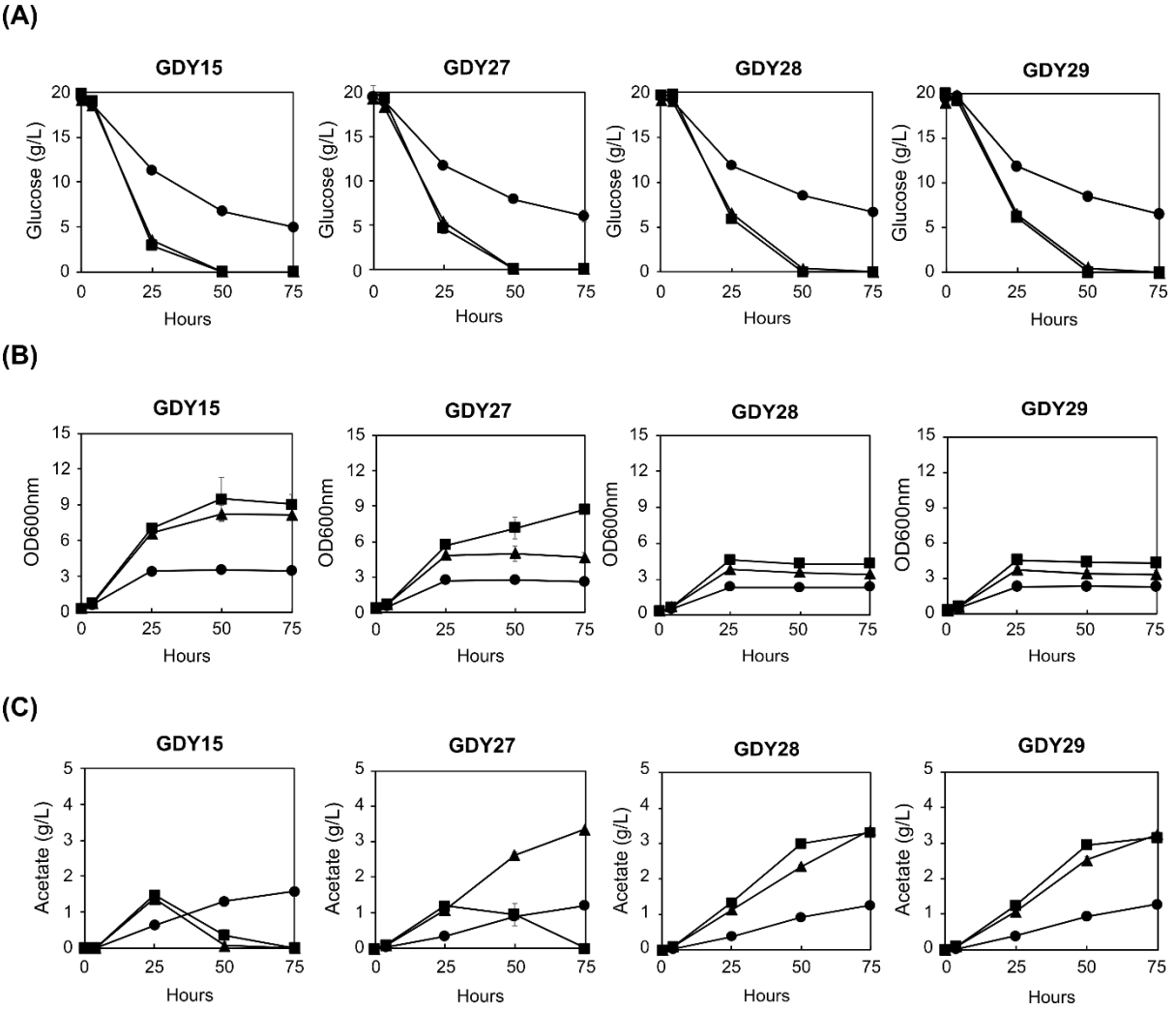

Figure 25. Growth ($OD600_{nm}$), glucose consumption and acetic acid production by *S. cerevisiae* strains with integrated reverse β-oxidation pathway variants in different cultivation media. (A) glucose consumption (in g/L), (B) $OD600_{nm}$, and (C) acetic acid production (in g/L) by strains GDY15, GDY27 GDY28 and GDY29 in synthetic medium (SM) (filled circle, ●), YPD with 20 mM phosphate buffer (filled triangle, ▲) or YPD with 100 mM phosphate buffer (filled square, ■) over 75h. Error bars represent the standard deviation from three independent replicates.

Table 30. Consumption of glucose (in mg), production of MCFA (in mg) and yields on glucose (g/g) of glycerol ($Y_{GLY/S}$), ethanol ($Y_{ETOH/S}$), biomass ($Y_{X/S}$), butyric acid ($Y_{BUT/S}$), hexanoic acid ($Y_{HEX/S}$), octanoic acid ($Y_{OCT/S}$), decanoic acid ($Y_{DEC/S}$) and overall medium chain fatty acids ($Y_{MCFA/S}$), as well as yields on biomass (g/g) of medium chain fatty acids ($Y_{MCFA/X}$) after 50h and 75h (in parenthesis) of fermentation in either buffered synthetic medium (SM), YPD with 20 mM phosphate buffer or YPD with 100 mM phosphate buffer. The strain tested are the hexanoic acid producing strain GDY27, the octanoic acid producing strains GDY28 and GDY29 and the control strain, GDY15, which lacked any reverse β-oxidation pathway variant.

Strain	Glucose consumed	MCFA (C6-C10)	$Y_{GLY/S}$	$Y_{ETOH/S}$	$Y_{X/S}$	$Y_{BUT/S}$	$Y_{HEX/S}$	$Y_{OCT/S}$	$Y_{DEC/S}$	$Y_{MCFA/S}$	$Y_{MCFA/X}$
SM – 20 mM Phosphate											
GDY15	498.72	0.073	0.1127	0.1213	0.1581	-	<0.0001	<0.0001	<0.0001	0.0001	0.0009
	(570.87)	(0.084)	(0.1036)	(0.1124)	(0.1342)	-	(<0.0001)	(<0.0001)	(<0.0001)	(0.0001)	(0.0011)
GDY27	460.89	1.997	0.0851	0.0664	0.1311	0.0023	0.0040	0.0003	0.0001	0.0043	0.0330
	(535.87)	(1.903)	(0.0779)	(0.0581)	(0.1069)	(0.0020)	(0.0033)	(0.0002)	(0.0001)	(0.0036)	(0.0332)
GDY28	438.78	2.654	0.0667	0.0638	0.1164	0.0018	0.0030	0.0029	0.0001	0.0060	0.0520
	(511.6)	(2.527)	(0.0616)	(0.0561)	(0.1008)	(0.0015)	(0.0026)	(0.0022)	(0.0001)	(0.0049)	(0.049)
GDY29	437.06	2.648	0.0663	0.0697	0.1187	0.0020	0.0030	0.0029	0.0001	0.0061	0.0510
	(516.83)	(2.395)	(0.0605)	(0.0615)	(0.0985)	(0.0019)	(0.0024)	(0.0021)	(0.0001)	(0.0046)	(0.0470)
YPD – 20 mM Phosphate											
GDY15	765.25	0.053	0.1636	0.2238	0.238	-	<0.0001	<0.0001	<0.0001	<0.0001	0.0003
	(765.24)	(0.062)	(0.1609)	(0.2150)	(0.236)	-	(<0.0001)	(<0.0001)	(<0.0001)	(<0.0001)	(0.0004)
GDY27	768.72	2.686	0.0807	0.1506	0.1432	0.0024	0.0032	0.0002	<0.0001	0.0035	0.0244
	(768.72)	(2.558)	(0.0829)	(0.1497)	(0.1336)	(0.0023)	(0.0031)	(0.0002)	(<0.0001)	0.0033	0.0249
GDY28	749.23	3.507	0.0598	0.1242	0.1054	0.0014	0.0023	0.0023	0.0001	0.0047	0.0444
	(763.73)	(3.348)	(0.0605)	(0.1264)	(0.099)	(0.0015)	(0.0021)	(0.0022)	(0.0001)	(0.0044)	(0.0443)
GDY29	740.39	3.712	0.0666	0.1306	0.1025	0.0017	0.0023	0.0026	0.0001	0.0050	0.0489
	(758.76)	(3.432)	(0.0671)	(0.1315)	(0.0985)	(0.0016)	(0.0022)	(0.0023)	(0.0001)	(0.0045)	(0.0459)
YPD – 100 mM Phosphate											
GDY15	794.98	0.068	0.216	0.2052	0.2638	-	<0.0001	<0.0001	<0.0001	0.0001	0.0003
	(794.98)	(0.079)	(0211)	(0.1971)	(0.2514)	-	(<0.0001)	(<0.0001)	(<0.0001)	(<0.0001)	(0.0004)
GDY27	802.57	3.136	0.1376	0.1778	0.1969	0.0032	0.0037	0.0002	<0.0001	0.0039	0.0198
	(802.57)	(0.378)	(0.1143)	(0.1596)	(0.2395)	(0.0032)	(0.0004)	(<0.0001)	(<0.0001)	(0.0005)	(0.0020)
GDY28	784.9	4.764	0.1290	0.1643	0.1204	0.0020	0.0031	0.0030	0.0001	0.0061	0.0504
	(784.9)	(4.382)	(0.1365)	(0.1572)	(0.1207)	(0.0021)	(0.0029)	(0.0026)	(<0.0001)	(0.0056)	(0.0462)
GDY29	795.63	4.880	0.1215	0.1683	0.1234	0.0019	0.0031	0.0029	0.0001	0.0061	0.0497
	(795.63)	(4.394)	(0.1236)	(0.1622)	(0.1206)	(0.0019)	(0.0029)	(0.0026)	(<0.0001)	(0.0055)	(0.0458)

Further increasing the buffering capacity of the medium (YPD-100 mM) resulted in the total consumption of glucose after 50h of fermentation in all the strains. Fermentation in YPD-100 mM also boosted the growth of all strains (except for GDY15), which was particularly noticeable in strain GDY27, where the final OD_{600nm} increased by 87% compared to when grown in YPD-20 mM. In the case of the octanoic acid producing strains GDY28 and GDY29, final OD_{600nm} increased by 25% and 28%, respectively, compared to those in YPD-20 mM. Acetic acid titres were also altered in YPD-100 mM, where we observed that the acetate produced during the fermentation was completely consumed after 75h by GDY15 and GDY27, but not by the octanoic acid producers (**Fig 25C**).

4.1.4 Production of medium-chain fatty alcohols from the reverse β-oxidation pathway

The products of the rBOX are determined by the terminal enzymes used on the acyl-CoAs generated. To increase the range of products from our engineered pathway variant, we explored the production of medium-chain fatty alcohols (MCFOH). MCFOH derive from reducing medium-chain fatty acyl-CoAs using aldehyde dehydrogenases and alcohol dehydrogenases. Therefore, we tested and compared as terminal enzymes the alcohol dehydrogenase ^{Ca}AdhE2 and the aldehyde dehydrogenase ^{Ec}EutE (**Figure 26**). The clostridial ^{Ca}AdhE2 is known to produce up to 1-octanol from the rBOX pathway in *E. coli* (Kim, Clomburg et al. 2015). ^{Ec}EutE, on the other hand, is a putative aldehyde dehydrogenase with a high activity towards butyraldehyde (Schadeweg and Boles 2016a), and a potential alcohol dehydrogenase activity. However, neither ^{Ca}AdhE2 nor ^{Ec}EutE has been tested on an octanoyl-CoA-producing yeast strain.

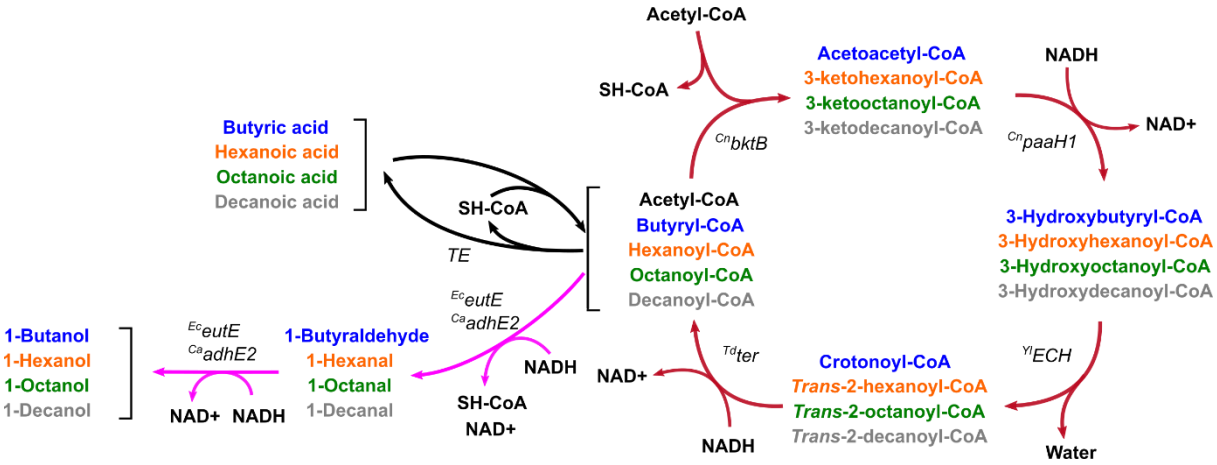

Figure 26. Overview of the reverse β-oxidation variant tested (red arrow) and the genes in termination reactions for MCFA (TE, black arrow) and for MCFOH (^{Ec}*eutE* and ^{Ca}*adhE2*, magenta arrow).

We transformed GDY29 with the hygromycin resistance-based expression plasmids GDV163 (***^{Ca}adhE2***), GDV164 (***^{Ec}eutE***) and an empty vector (EV). We compared the production of 1-

butanol, 1-hexanol, 1-octanol and 1-decanol (**Fig 27A**) and of butyric acid and MCFA (**Fig 27B**) after 75h of fermentation in YPD-100 mM medium with hygromycin.

When expressing ^{Ca}*adhE2* or ^{Ec}*eutE*, 1-butanol was the main alcohol produced, with titers reaching 82.33 ± 14.03 mg/L and 87.12 ± 1.84 mg/L, respectively (**Fig 27A**). Interestingly, the EV control strain also produced 46.32 ± 8.7 mg/L of 1-butanol. Regarding MCFOH, we observed a tendency to slightly higher titers with ^{Ec}*eutE* than with ^{Ca}*adhE2*: the titers of 1-hexanol reached 8.72 ± 0.09 mg/L (^{Ec}*eutE*) and 8.24 ± 1.21 mg/L (^{Ca}*adhE2*), and the titers of 1-octanol reached 1.52 ± 0.12 mg/L (^{Ec}*eutE*) and 0.87 ± 0.09 mg/L (^{Ca}*adhE2*). No MCFOH were produced in the EV control.

The expression of ^{Ec}*eutE* or ^{Ca}*adhE2* changed the production pattern of SCFA and MCFA in strain GDY29 (**Fig 27B**). Butyric acid was the main product, and the titers of hexanoic acid and octanoic acid were significantly lower than in the EV control. Expressing ^{Ec}*eutE* led to 37.47 ± 2.81 mg/L of butyric acid and almost identical titers of hexanoic acid (26.91 ± 1.32 mg/L) and octanoic acid (27.82 ± 0.90 mg/L). In the case of ^{Ca}*adhE2*, its expression resulted in 45.91 ± 2.85 mg/L of butyric acid and hexanoic acid titers (32.68 ± 3.17 mg/L) becoming higher than those of octanoic acid (27.53 ± 1.68 mg/L). In the EV-transformed strain, octanoic acid titers (47.66 ± 1.78 mg/L) were higher than those of hexanoic acid (37.46 ± 0.67 mg/L). However, not significantly higher than those of butyric acid (44.01 ± 7.72 mg/L).

Based on the yields of the alcohol fraction ($Y_{SMCFOH/S}$) and the fatty acid fraction ($Y_{SMCFA/S}$) on glucose, SCFA and MCFA remained as the main product of the rBOX when expressing ^{Ca}*adhE2* or the EV (**Fig 27C**). Only the expression of ^{Ec}*eutE* resulted in slightly higher $Y_{SMCFOH/S}$ than $Y_{SMCFA/S}$, with 1-butanol representing 89% of the total SCFOH and MCFOH fraction. We also observed that ^{Ca}*adhE2* significantly increased the yield of ethanol ($Y_{ETOH/S}$) (0.2411 g_{ETOH}/g_{GLUC}) compared to ^{Ec}*eutE* (0.1909 mg_{ETOH}/mg_{GLUC}) or the EV (0.1734 mg_{ETOH}/mg_{GLUC}).

Overall, expressing ^{Ec}*eutE* or ^{Ca}*adhE2* increased the titers of ethanol, 1-butanol, and indirectly resulted in butyric acid as the principal fatty acid from the pathway. In addition, we confirmed the production of the MCFOH 1-hexanol and 1-octanol with ^{Ca}*adhE2* and, for the first time, with ^{Ec}*eutE*. However, 1-hexanol and 1-octanol titers were 10-fold and >60-fold lower, respectively, than those of 1-butanol.

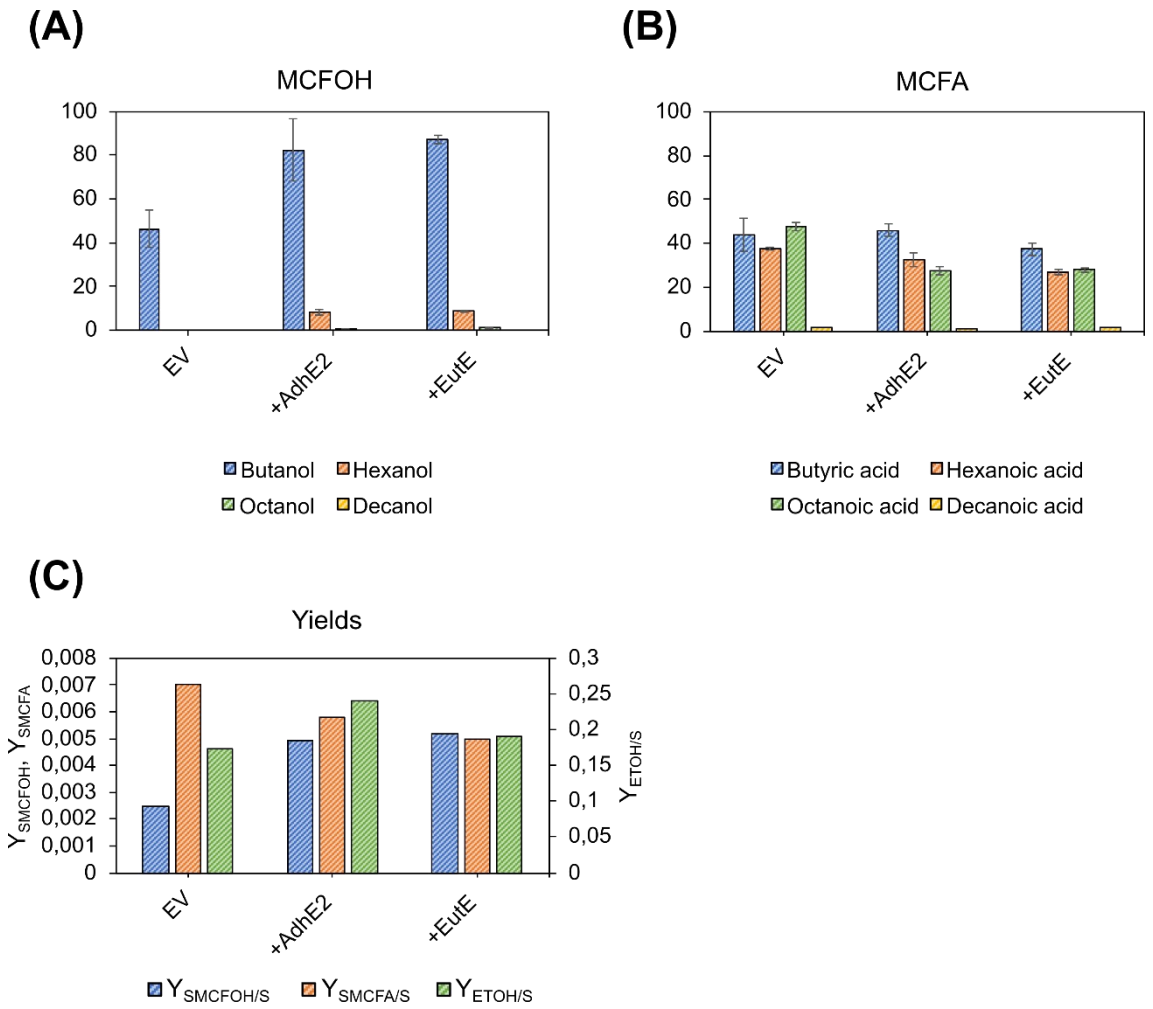

Figure 27. Production of MCFOH and MCFA in the octanoyl-CoA-producing strain GDY29. A) Production of 1-butanol (in blue), 1-hexanol (in orange), 1-octanol (in green) and 1-decanol (in yellow) by GDY29 transformed with GDV163 (^{Ca}*adhE2*), GDV164 (^{Ec}*eutE*) or the empty vector (EV) OTV011. B) Production of butyric (in blue), hexanoic (in orange), octanoic (in green) and decanoic acid (in yellow) by GDY29 transformed with GDV163 (^{Ca}*adhE2*), GDV164 (^{Ec}*eutE*) or the empty vector (EV) OTV011 C) Yield on glucose (mg/mg) of 1-butanol, 1-hexanol, 1-octanol and 1-decanol ($Y_{SMCFOH/S}$), yield on glucose (mg/mg) of butyric acid and MCFA ($Y_{SMCFA/S}$) and yield on glucose (mg/mg) of ethanol ($Y_{ETOH/S}$). All values after 75h of fermentation in YPD-100 mM. Error bars represent the standard deviation from three independent replicates.

4.2 Expression of the reverse β-oxidation in the mitochondria of *S. cerevisiae*

The rBOX pathway is driven mainly by the availability of acetyl-CoA and NADH (Shen, Lan et al. 2011, Schadeweg and Boles 2016b). In *S. cerevisiae*, acetyl-CoA is produced in the cytosol via the Pdh-bypass and at even higher levels in the mitochondria via the Pdh complex (Duran, López et al. 2020). In addition, the mitochondrial matrix provides a reducing environment (Orij, Postmus et al. 2009). This environment could favour reactions that involve the oxidation of NADH, like some of the ones in the rBOX pathway.

In this chapter, we expressed the rBOX in the mitochondria of *S. cerevisiae*. To do this, we created *S. cerevisiae* strains with enhanced carbon flux to the mitochondria, we developed a

method to assess this increased flux and targeted the rBOX into the mitochondria to produce 1-butanol as a proof-of-concept. An overview of all the strain modifications tested in this study is depicted in **Figure 28**.

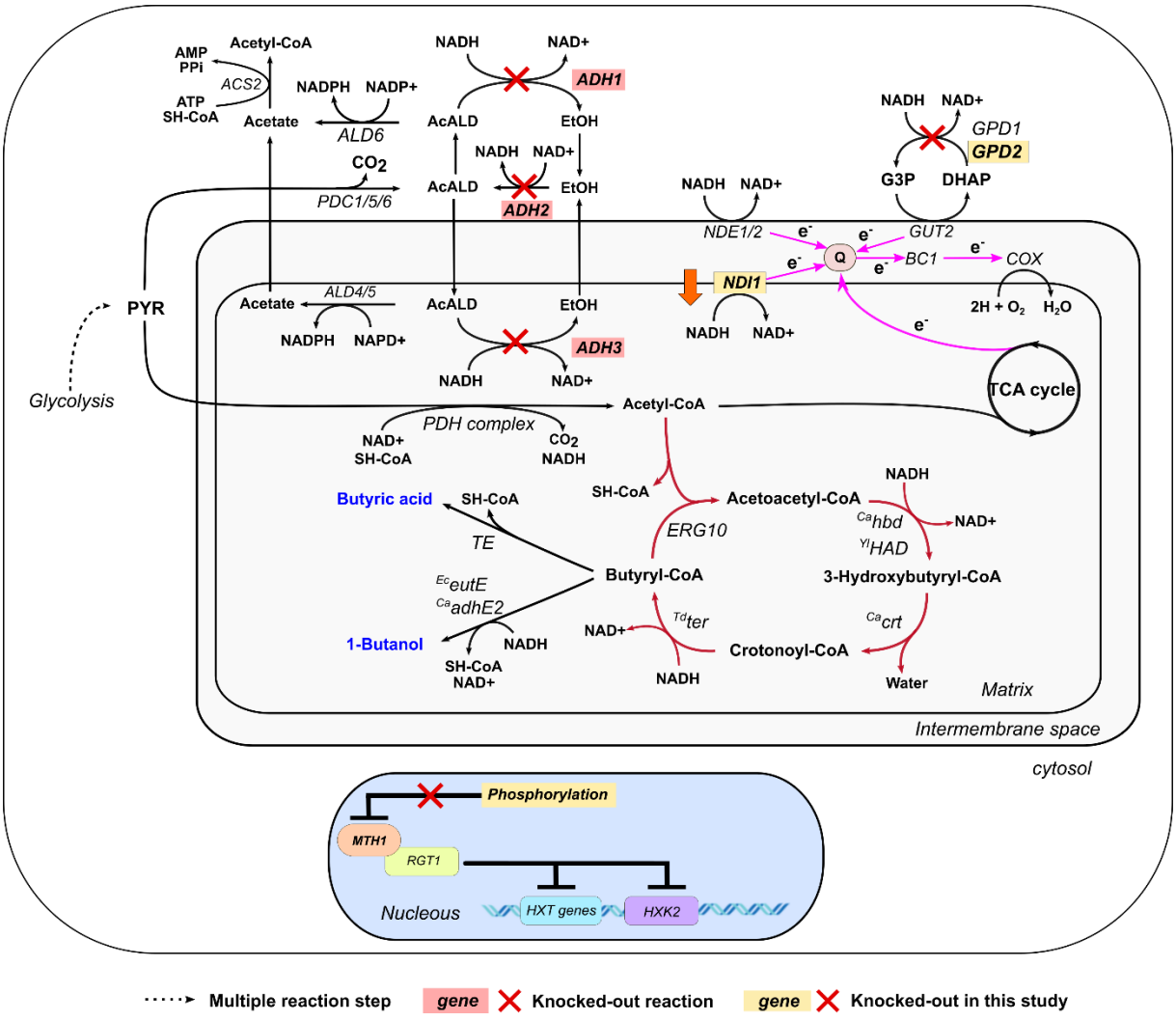

Figure 28. Overview of the strategies used in this chapter to produce 1-butanol in mitochondria of *S. cerevisiae*. The rBOX pathway reactions (*red arrows*) are depicted with the different genes tested in each reaction during this study. The final products, 1-butanol and butyric acid are depicted in *blue*. The reactions knocked out in the different strains used in this study are displayed with a *red cross*. The downregulation of *NDI1* is indicated with an *orange arrow*. The reactions in the electron transport chain are shown in *magenta*. **Abbreviations**: AcALD, acetaldehyde; DHAP, dihydroxy-acetone-phosphate; EtOH, ethanol; G3P, glycerol-3-phosphate; PYR, pyruvate.

4.2.1 Generating a *S. cerevisiae* strain with increased mitochondrial acetyl-CoA

As introduced in 4.1.1, *S. cerevisiae* is a Crabtree-positive yeast that, even when growing aerobically, ferments sugars mainly to ethanol. Ethanol fermentation takes place in the cytosol and regenerates NAD^+ from NADH.

We wanted a *S. cerevisiae* strain with the carbon flux directed to the mitochondria to benefit from the higher acetyl-CoA levels and higher reducing environment in that compartment.

However, the preference of *S. cerevisiae* to direct the carbon flux towards ethanol fermentation is challenging. Therefore, the engineering strategies to obtain such a strain were performed in VSY0, an *adh*-deficient strain with reduced ethanol production capacity.

4.2.1.1 The deletion of *GPD2* and the regulatory region *of MTH1* in an *adh*-deficient strain results in increased carbon flux to the mitochondria

When grown aerobically under glucose limitation, *S. cerevisiae* switches from fermentation (in the cytosol) to respiration (in the mitochondria) (Kolkman, Daran-Lapujade et al. 2006). In this yeast, mutations in the regulatory region of the transcription factor Mth1 resulted in a lower expression of glucose transporters (Oud, Flores et al. 2012), which could mimic the metabolism under glucose limitation and re-direct the carbon flux to the mitochondria. Therefore, we removed the regulatory region of Mth1 in the *adh*-deficient strain VSY0, resulting in strain GDY1. Additionally, as mentioned above, the deletion of *GPD2* present in GDY15 resulted in reduced glycerol production and an increased final OD_{600nm} compared to the parental VSY0 (**Figure 13D**). This growth improvement could also be linked to a reduced Crabtree effect and increased respiratory metabolism in this engineered strain.

To assess the increase in mitochondrial metabolism with these two mutations, we compared the fermentation patterns of GDY1 (Δ*adh1-5*, Δ$mth1_{169-393}$) and GDY15 (Δ*adh1-5*, Δ*gpd2*) against wild-type CEN.PK2-1C and VSY0 (Δ*adh1-5*) when grown in YPD 2% (**Figure 29**).

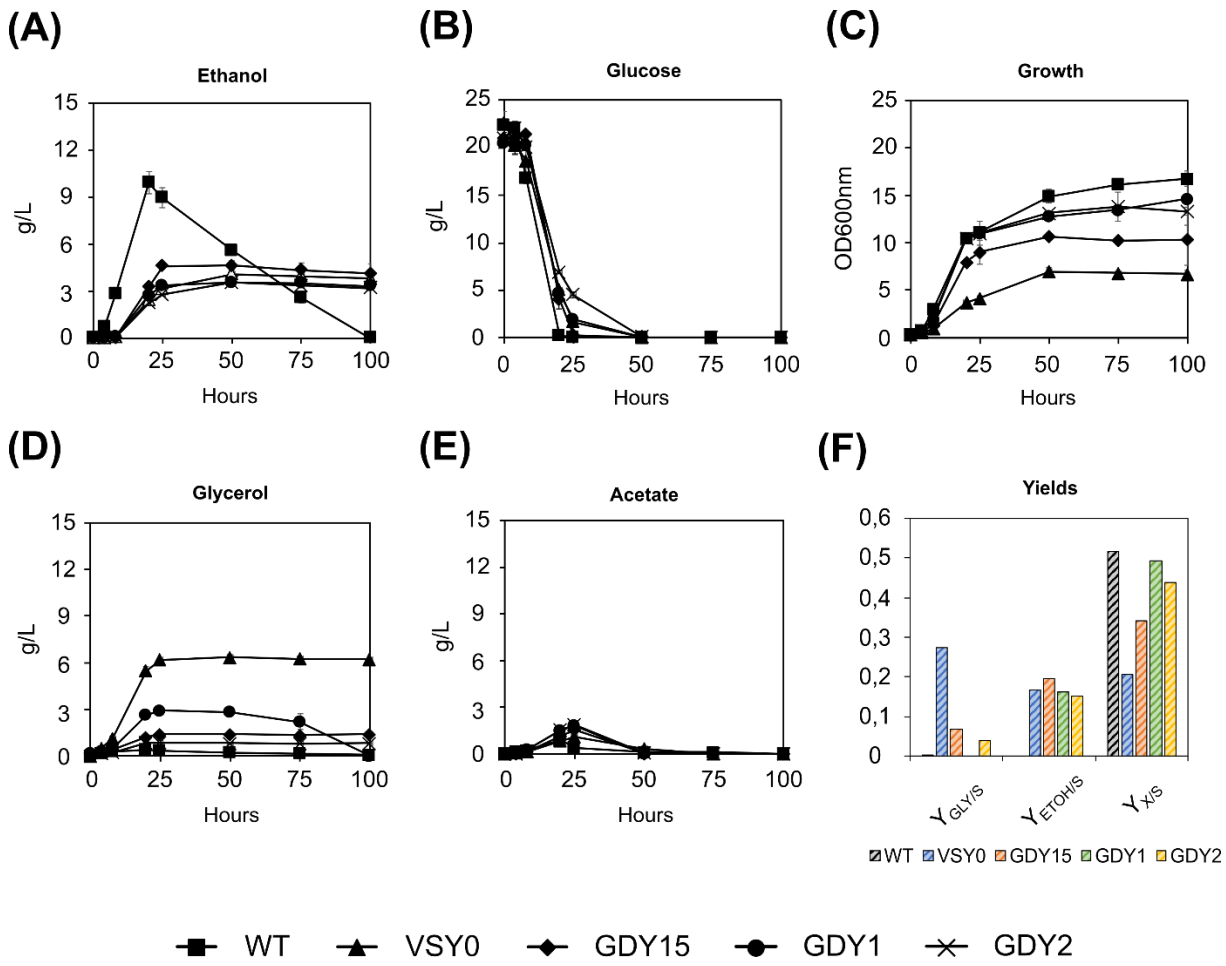

Figure 29. Effect of changing carbon metabolism in *S. cerevisiae*. (A) Ethanol production (B) glucose consumption, (C) growth (D) glycerol and (E) acetate production over 100h of fermentation.(F) the yield of glycerol ($Y_{GLY/S}$), ethanol ($Y_{ETOH/S}$) and biomass (Y_{XS}) on glucose of strains WT (CEN.PK2-1C), VSY0 (Δ*adh1-5*), GDY15 (Δ*adh1-5*, Δ*gpd2*), GDY1 (Δ*adh1-5*, Δ$mth1_{169-393}$) and GDY2 (Δ*adh1-5*, Δ*gpd2,* Δ$mth1_{169-393}$) after 100h of fermentation. Fermentation was performed in in YPD 2%. Error bars represent the standard deviation between duplicates.

Compared to the wild type, the deletion of *ADH1-5* (VSY0) reduced ethanol production during the exponential growth phase and the absence of Adh2 prevented its consumption once glucose was depleted (**Fig 29A, B**). Furthermore, it reduced the final OD_{600nm} of the strain by 60% (**Fig 29C**) and increased 88-fold the final titre of glycerol, reaching 6.21 ± 0.11 g/L (**Fig 29D**).

The additional deletion of *GPD2* (GDY15) did not significantly change the production of ethanol at the end of the fermentation (4.11 ± 0.62 g/L) compared to VSY0 (3.78 ± 0.33 g/L) but resulted in a 4.4-fold lower glycerol production titre (1.39 ± 0.02 g/L). Deleting *GPD2* also improved the growth impairment observed in VSY0, increasing by 54% the final OD_{600nm}. However, the final OD_{600nm} was still reduced by 38% compared to the wild-type CEN.PK2-1C.

Truncating the regulatory region of Mth1 (GDY1) in the *adh*-deficient strain VSY0 did not change the ethanol production titre (3.31 ± 0.01 g/L) compared to that strain or GDY15 (**Fig 29A**). However, it improved growth significantly, reaching a final OD_{600nm} (14.63 ± 0.75) close

to that of the wild-type CEN.PK2-1C (16.76 ± 0.79) (**Fig 29C**). The Y_{XS} in GDY1 ($Y_{XS, GDY1}$=0.492 g/g $_{Glucose}$) is also very close to that in CEN.PK2-1C ($Y_{XS, CEN.PK2-1C}$=0.512 g/$g_{Glucose}$) (**Fig 29E**). In addition, in GDY1, the glycerol production peaked at 2.91 ± 0.07 g/L at 25h of fermentation, probably due to the presence of Gpd2 in this strain. However, it was completely consumed at the end of the fermentation (100h) (**Fig 29D**).

The production of glycerol is the main NADH-consuming reaction in VSY0. The *GPD2* deletion (GDY15) and the *MTH1* deregulation (GDY1) reduced glycerol production and improved growth in this strain. Therefore, we combined both strategies and created strain GDY2 (∆*adh1-5*, ∆*gpd2*, ∆*mth1*$_{169-393}$).

In this strain, glycerol production at the end of the fermentation (0.83 ± 0.01 g/L) decreased by 59% compared to GDY15 and remained lower than in GDY1 and VSY0 during the fermentation. Ethanol production was only slightly reduced (3.18 ± 0.1 g/L) compared to VSY0, GDY1 and GDY15 at the end of the fermentation and compared to GDY15, the additional *MTH1*$\Delta_{169-393}$ mutation in GDY2 improved growth by 28%, reaching a final OD_{600nm} of 13.32 ± 0.39. However, the combined mutations did not improve growth or Y_{XS} significantly compared to GDY1 (**Fig 29C, F**).

Acetate production pattern was identical among all strains **(Figure 29E**), with a peak around 25h but fully consumed between 25h and 75h. If anything, the acetate production peak at 25h was higher in GDY1 (1.81 ± 0.01 g/L), GDY2 (1.86 ± 0.05 g/L) and GDY15 (1.53 ± 0.06 g/L) than in the wild-type strain (0.36 ± 0.02 g/L) and VSY0 (1.10 ± 0.01 g/L).

Overall, deleting *GPD2* and mutating *MTH1* in an *adh*-deficient strain (VSY0) reduces ethanol and glycerol fermentation while increasing the yield of cell biomass formed on the glucose consumed (Y_{XS}).

4.2.1.2 ^{Km}Eat1 as a platform to assess mitochondrial metabolism

We used the mitochondrial ethanol acetyltransferase Eat1 from *K. marxianus* (Kruis, Levisson et al. 2017) to further evaluate the mitochondrial metabolism of the engineered *S. cerevisiae* strains described above (see section 4.2.1.1). This enzyme catalyses mainly the formation of ethyl acetate from ethanol and acetyl-CoA, where acetyl-CoA is the limiting substrate. Hence, we can use ^{Km}Eat1 to assess acetyl-CoA levels in the mitochondria and the cytosol in different strains. In addition, ^{Km}Eat1 can use alcohols different from ethanol, like isoamyl alcohol, to produce other volatile esters (Kruis, Levisson et al. 2017, Kruis, Gallone et al. 2018). Isoamyl alcohol is a product of the degradation of leucine, a process that occurs partially in the yeast mitochondria. Therefore, the formation of isoamyl acetate, a product of the esterification of

isoamyl alcohol and acetyl-CoA, could be used as another indicator of mitochondrial metabolism.

We aimed to express ^{Km}*EAT1* in the cytosol and the mitochondria of different engineered strains and compare their volatile ester production pattern. As the full-length Eat1 targets the mitochondria, we built two truncated versions of ^{Km}Eat1, *Δ1-19* missing the first 19 amino acids and *Δ1-30* missing the first 30 amino acids, to retain this enzyme in the cytosol and compare the production pattern in both compartments (**Table 31**).

Table 31. Analysis of ^{Km}Eat1 and its truncated versions in MitoFates. In this table we list the amino acid sequences of ^{Km}Eat1 (full-length), ^{Km}Eat1 (Δ1-19) and ^{Km}Eat1 (Δ1-30), their probability of mitochondrial import ($P_{MitoFates}$) and their predicted mitochondrial processing sites based on the MitoFates prediction tool. The amino acids from the predicted MTS are underlined in the sequence.

Variant	AA sequence	$P_{MitoFates}$
^{Km}Eat1 (Full-length)	MLLAYTVRPSNWSFTRRAYSATARAFNQQKGLLPLPIK ETVDMAYDLHLPERSVIGKMPYHSPEPIIFYHGLLGSKR NYRHDCKKLATALQTPVYTVDIRNHGSSEHALPFDYNT LVNDLVHFAETHSLGKVNLVGYSLGAKVAMLACLKHPE RFSAACIIDNSPEEQPHIKPLLTALVKSCVKLLDHHNVRA DDKLWRHKASEALKKYIPDAGIRYYLLSNIINNPRVVEYR SPVINYDDGMLHFKNPVRHMMDFVTKEVAAWPTQELEG KQFLGPVNFIKATRSDFINPKSLQAINQYFPYHNIDEINAT HFILNERPQEYLRAVTDFFKVTRYQLEKKREQDLAKIDQL NASESLKSARD*	0.86
^{Km}Eat1$_{(Δ1-19)}$	MYSATARAFNQQKGLLPLPIKETVDMAYDLHLPERSVIGK MPYHSPEPIIFYHGLLGSKRNYRHDCKKLATALQTPVYTV DIRNHGSSEHALPFDYNTLVNDLVHFAETHSLGKVNLVG YSLGAKVAMLACLKHPERFSAACIIDNSPEEQPHIKPLLTA LVKSCVKLLDHHNVRADDKLWRHKASEALKKYIPDAGIRY YLLSNIINNPRVVEYRSPVINYDDGMLHFKNPVRHMMDFV TKEVAAWPTQELEGKQFLGPVNFIKATRSDFINPKSLQAIN QYFPYHNIDEINATHFILNERPQEYLAVTDFFKVTRYQLEK KREQDLAKIDQLNASESLKSARD*	0.159
^{Km}Eat1$_{(Δ1-30)}$	MKGLLPLPIKETVDMAYDLHLPERSVIGKMPYHSPEPIIFYH GLLGSKRNYRHDCKKLATALQTPVYTVDIRNHGSSEHALP FDYNTLVNDLVHFAETHSLGKVNLVGYSLGAKVAMLACLK HPERFSAACIIDNSPEEQPHIKPLLTALVKSCVKLLDHHNV RADDKLWRHKASEALKKYIPDAGIRYYLLSNIINNPRVVEY RSPVINYDDGMLHFKNPVRHMMDFVTKEVAAWPTQELEG KQFLGPVNFIKATRSDFINPKSLQAINQYFPYHNIDEINATHF ILNERPQEYLRAVTDFFKVTRYQLEKKREQDLAKIDQLNAS ESLKSARD*	0.002

Predicted MPP cleavage site
Predicted Icp55 cleavage site
Predicted Oct1 cleavage site
Predicted TOM recognition motif

To assess the subcellular localisation of the truncated constructs, we fused them to GFPenvy and expressed them in *S. cerevisiae* CEN.PK2-1C (**Figure 30**). While the full ^{Km}Eat1 and the truncated ^{Km}Eat1$_{Δ1-19}$ co-localized with the mitochondria (**Fig 30A and 30B**), the truncated

^{Km}Eat1$_{\Delta 1\text{-}30}$ was expressed in the cytosol (**Fig 30C**). These results indicate that deleting 19 to 30 amino acids at the N-terminal is necessary to remove the MTS from Eat1 completely.

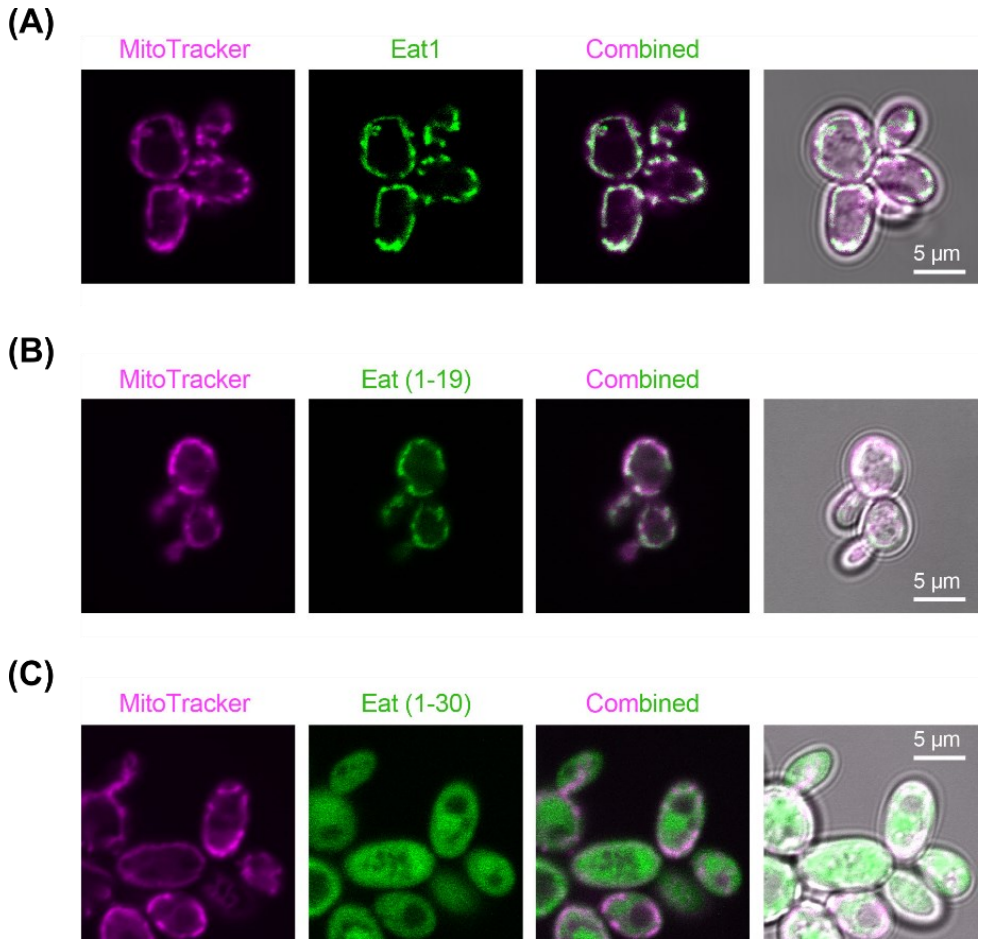

Figure 30. Subcellular localisation in *S. cerevisiae* CEN.PK2-1C of different truncated Eat1 versions from *K. marxianus*. The full Eat1 (A) and two truncated versions missing the first 19 amino acids (Δ1-19) (B) or the first 30 amino acids (Δ1-30) (C) were fused to GFP and expressed from CENARS-based plasmids (GDV153, GDV154 and GDV155, respectively) in *S. cerevisiae* CEN.PK2-1C. The localisation of the fusion proteins (in green) was analysed by fluorescence microscopy. Mitochondria were dyed with Mitotracker Red CMXRos and are here represented in magenta.

To validate the use of ^{Km}Eat1 variants in evaluating mitochondrial metabolism, we aimed to compare the expression of ^{Km}*EAT1* in the cytosol and the mitochondria of *S. cerevisiae* strains CEN.PK2-1C (a wild-type strain), GDY15 and GDY2. To avoid confusions, we shall refer to the cytosolic-targeted ^{Km}Eat1$_{\Delta 1\text{-}30}$ as **^{Km}Eat1$_{CYT}$**, and to the mitochondria-targeted ^{Km}Eat1 as **^{Km}Eat1$_{MIT}$**. We used isoamyl alcohol and isoamyl acetate, both products of the leucine degradation pathway, as indicators of mitochondrial metabolism (**Figure 31**). However, CEN.PK2-1C is a leucine auxotroph, whereas GDY15 and GDY2 are not (see **Table 4** and **Table 5**). Therefore, we removed the *LEU2* cassette from these two strains to prevent a misinterpretation of the results, generating leucine auxotrophic strains GDY15.1 and GDY2.1, and used these strains for the validation.

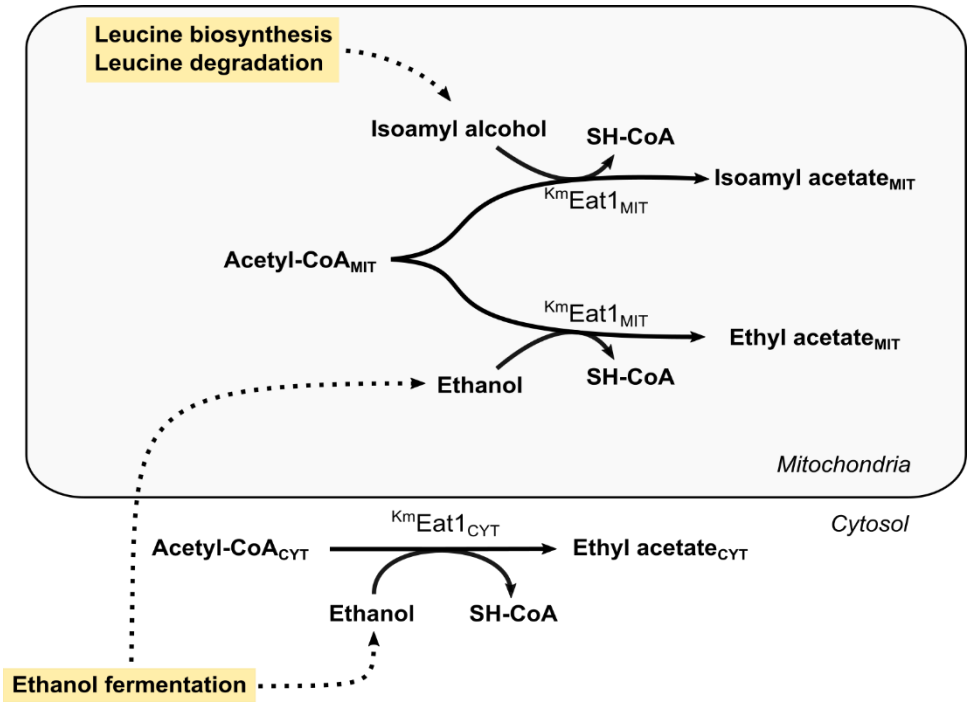

Figure 31. Proposed mechanism of ^{Km}Eat1 as an acetyl-CoA biosensor. ^{Km}Eat1 synthesises ethyl acetate and/or isoamyl acetate in the mitochondria (^{Km}Eat1$_{MIT}$) and the cytosol (^{Km}Eat1$_{CYT}$) using the acetyl-CoA pool in these organelles. Isoamyl acetate is synthesised from isoamyl alcohol, product of the mitochondrial reactions of the leucine metabolism. Ethyl acetate is synthesised from ethanol, product of the ethanol synthesised during alcoholic fermentation.

We transformed each strain with the full-length ^{Km}*EAT1* (GDV156) targeting the mitochondria or the ^{Km}*EAT1*$_{CYT}$ (GDV157) targeting the cytosol. We then compared the production of isoamyl acetate, isoamyl alcohol, ethyl acetate and ethanol after 75h of fermentation in SMD without uracil (**Figure 32** and **Figure 33**).

All the strains produced isoamyl alcohol regardless of the expression of an ^{Km}*EAT1* variant, with CEN.PK2-1C (WT) being the best producer (**Fig 32**). CEN.PK2-1C produced on average 2.5-fold and 2-fold more isoamyl alcohol than GDY15.1 and GDY2, respectively. CEN.PK2-1C produced 8.78 ± 0.81 mg/L of isoamyl alcohol with the EV, 11.54 ± 1.15 mg/L expressing the mitochondrial ^{Km}*EAT1*$_{MIT}$, and 13.52 ± 0.83 mg/L with the cytosolic ^{Km}*EAT1*$_{CYT}$. GDY15.1 produced 4.79 ± 1.06 mg/L (EV), 4.98 ± 1.11 mg/L (^{Km}*EAT1*$_{MIT}$), and 3.07 ± 1.08 mg/L (^{Km}*EAT1*$_{CYT}$) of isoamyl alcohol. GDY2.1 produced 6.67 ± 1.46 mg/L of isoamyl alcohol with the EV, 4.54 ± 0.21 mg/L expressing ^{Km}*EAT1*$_{MIT}$, and 5.17 ± 1.16 mg/L with ^{Km}*EAT1*$_{CYT}$.

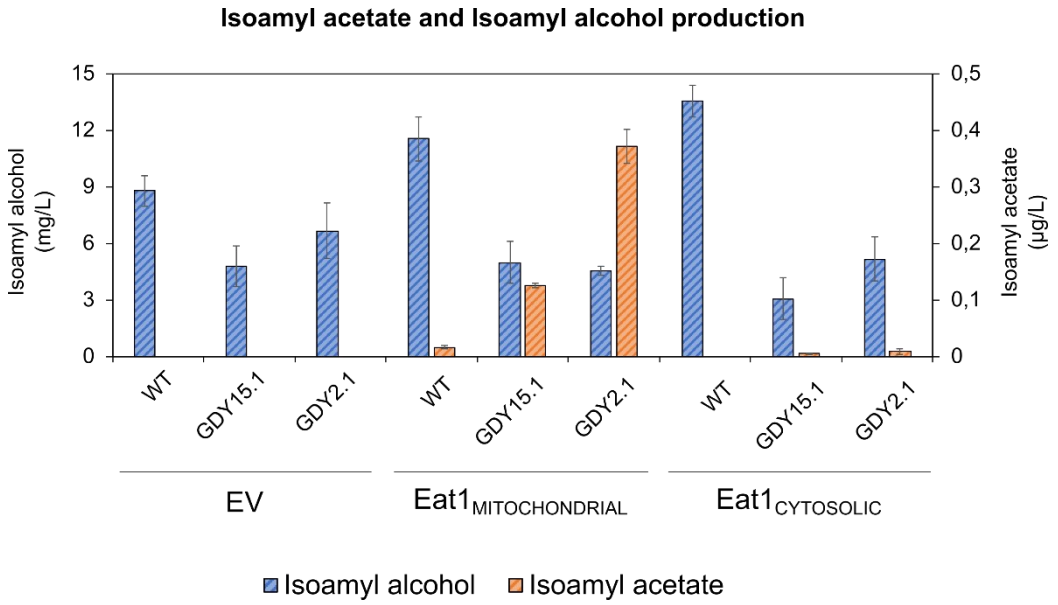

Figure 32. Isoamyl acetate and isoamyl alcohol production from the expression of ^{km}*EAT1* in the cytosol and in the mitochondria. Production of isoamyl alcohol (*blue*) and isoamyl acetate (*orange*) in strains wild-type (CEN.PK2-1C, abbreviated '**WT**'), **GDY15.1** (Δ*adh1-5,* Δ*gpd2*) and **GDY2.1** (Δ*adh1-5,* Δ*gpd2,* Δ*mth1*$_{169-393}$). All the strains expressed *EAT1* in the mitochondria (Eat1$_{MITOCHONDRIAL}$, plasmid GDV156) or the cytosol (Eat1$_{CYTOSOLIC}$, plasmid GDV157). Plasmid LBGV024 was used as empty vector (EV) control. The production values are endpoint measurements after 75h of fermentation in SMD medium without uracil. Error bars represent the standard deviation between two replicates.

Isoamyl acetate was only produced when an ^{Km}*EAT1* variant was expressed, and the highest titres in all strains resulted from expressing the full, mitochondria-targeted version (^{Km}*EAT1*$_{MIT}$) (**Fig 32**). The isoamyl acetate titres from the mitochondria-targeted ^{Km}Eat1$_{MIT}$ varied between strains, with 16.64 ± 2.12 µg/L in CEN.PK2-1C, 125.39 ± 4.52 µg/L in GDY15.1 and 372.16 ± 29.79 µg/L in GDY2.1, the best producer. The isoamyl acetate production in GDY2.1 represented a 3-fold and a 22-fold increase in production compared to GDY15.1 and CEN.PK2-1C, respectively.

Ethyl acetate was the main product of expressing ^{Km}*EAT1* in all strains, and overall, the levels of ethyl acetate production correlated with the levels of ethanol production (**Fig 33**). CEN.PK2-1C (WT) produced the highest titers of ethanol after 75 hours of fermentation, with 7.43 ± 0.06 g/L of ethanol expressing ^{Km}*EAT1*$_{MIT}$ and 7.16 ± 0.73 g/L expressing ^{Km}*EAT1*$_{CYT}$. Surprisingly, the ethyl acetate production titres in this strain with ^{Km}*EAT1*$_{MIT}$ (54.68 ± 6.74 mg/L) were 4-fold higher than with ^{Km}*EAT1*$_{CYT}$ (13.53 ± 0.83 mg/L). Since CEN.PK2-1C (WT) is a clear Crabtree-positive strain (see section 4.2.1.1), we expected more ethyl acetate production from the expression of ^{Km}*EAT1*$_{CYT}$. GDY15.1 produced similar levels of ethanol expressing the cytosolic ^{Km}*EAT1*$_{CYT}$ (0.92 ± 0.08 g/L) and the mitochondrial ^{Km}*EAT1*$_{MIT}$ (0.55 ± 0.01 g/L). However, the ethyl acetate production expressing ^{Km}*EAT1*$_{MIT}$ (31.05 ± 5.24 mg/L) was 8-fold higher than with ^{Km}*EAT1*$_{CYT}$ (3.73 ± 0.55 mg/L). GDY2.1 produced the lowest titres of ethanol and ethyl acetate: 0.049 ± 0.021 g/L of ethanol and 17.23 ± 2.18 mg/L of ethyl acetate expressing ^{Km}*EAT1*$_{MIT}$ and 0.0389 ± 0.0054 g/L of ethanol and 0.22 ± 0.01 mg/L of ethyl acetate expressing ^{Km}*EAT1*$_{CYT}$.

In this strain, the expression of $^{Km}EAT1_{CYT}$ led to 80-fold lower ethyl acetate titres than $^{Km}EAT1_{MIT}$. No Ethyl acetate was produced in the absence of $^{Km}EAT1$ (EV) in any of the strains.

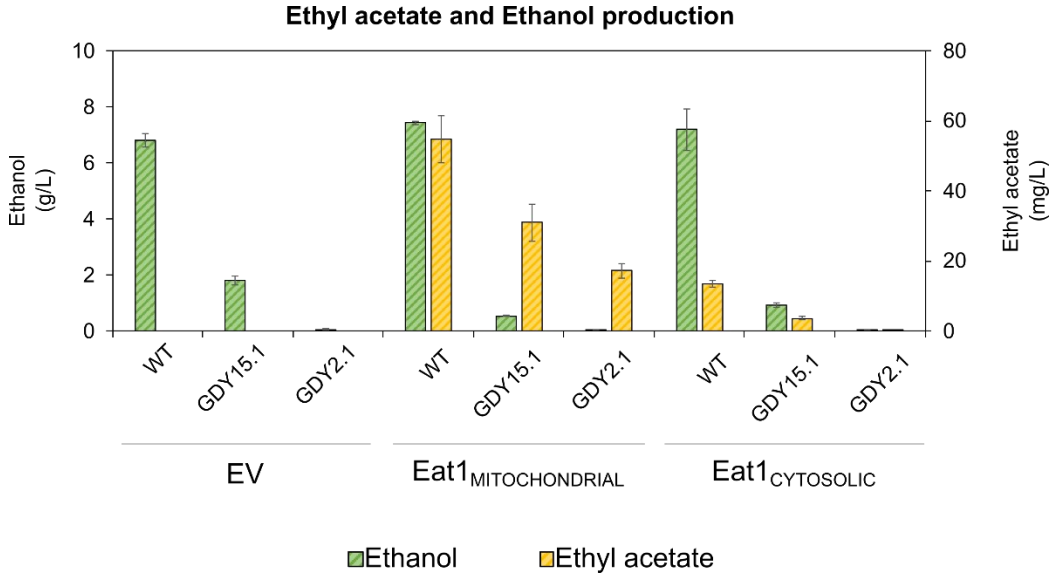

Figure 33. Ethyl acetate and ethanol production from the expression of $^{km}EAT1$ in the cytosol and in the mitochondria. Production of ethanol (*green*) and ethyl acetate (*yellow*) in strains wild-type (CEN.PK2-1C, abbreviated '**WT**'), **GDY15.1** (Δ*adh1-5,* Δ*gpd2*) and **GDY2.1** (Δ*adh1-5,* Δ*gpd2,* Δ*mth1*$_{169-393}$). All the strains expressed *EAT1* in the mitochondria (Eat1$_{MITOCHONDRIAL}$, plasmid GDV156) or the cytosol (Eat1$_{CYTOSOLIC}$, plasmid GDV157). Plasmid LBGV024 was used as empty vector (EV) control. The production values are endpoint measurements after 75h of fermentation in SMD medium without uracil. Error bars represent the standard deviation between two replicates.

Overall, these results show that the application of $^{Km}EAT1$ as an acetyl-CoA biosensor has limitations. On one side, the isoamyl acetate production results match with the expected ranking of the strains based on the carbon flux to the mitochondria. However, the ethyl acetate production results suggest that (1) the higher substrate preference of ^{Km}Eat1 for ethanol over other alcohols limits the comparison between ethanol-producing and not-producing strains and (2) $^{Km}Eat1_{CYT}$ seems to perform worse than the mitochondrial $^{Km}Eat1_{MIT.}$

4.2.2 Generating a mitochondrial reverse β-oxidation pathway and improving the pathway utilisation in *S. cerevisiae*

In the section 4.2.1.1 we generated *S. cerevisiae* strains with a reduced fermentative metabolism and an increased carbon flux to the mitochondria. Here, we tested whether the rBOX pathway could benefit from the presumably higher acetyl-CoA and NADH levels in the mitochondria of these strains. For this, we created different mitochondria-targeted variants of the rBOX pathway and expressed them in these engineered strains. All the tested pathway variants aimed to produce 1-butanol as a proof-of-concept.

4.2.2.1 Targeting different reverse β-oxidation enzymes and alcohol dehydrogenases ^{Ca}*AdhE2* to the mitochondria

In section 4.1, we studied different pathway variants and their impact on the production of MCFA and MCFOH. Here, we are using the production of 1-butanol as a proof of concept. Therefore, the enzymes used in this experiment are Erg10, ^{Ca}Hbd, ^{Ca}Crt and ^{Td}Ter, as this pathway variant led almost exclusively to butyryl-CoA (4.1.1.1). Alcohol dehydrogenases catalyse the final conversion of butyryl-CoA to 1-butanol. Thus, we included both ^{Ec}EutE and ^{Ca}AdhE2. To express the rBOX in the mitochondria, we needed to target the enzymes of this pathway in this organelle. For that, we added different mitochondrial targeting signals (MTS) at the N-terminus of each enzyme (**Table 32**). We selected the different MTS based on previous experience, as in the case of the MTS from the subunit 9 of *Neurospora crassa* ATPase (Westermann and Neupert 2000) and based on literature (Vogtle, Wortelkamp et al. 2009, Avalos, Fink et al. 2013, Yee, DeNicola et al. 2019).

Table 32. Mitochondrial targeting signals used to target the reverse β-oxidation enzymes in the mitochondria.

MTS	Amino acid sequence	Source	Reference
NC_{MTS}	MASTRVLASRLASQMAASAKVARPAVR VAQVSKRTIQTGSPLQTLKRTQMTSIVN ATTRQAFQKRAYSS	ATPase subunit 9 (*N. crassa*)	(Westermann and Neupert 2000)
$Acp1_{MTS}$	MFRSVCRISSRVAPSAYRTIMGRSVMS NTILAQRFY	Acyl carrier protein 1 (*S. cerevisiae*)	(Vogtle, Wortelkamp et al. 2009)
$Pdb1_{MTS}$	MFSRLPTSLARNVARRAPTSFVRPSAA AAALRF	E1-β subunit of the pyruvate dehydrogenase (PDH) complex	(Vogtle, Wortelkamp et al. 2009)
$Mdh1_{MTS}$	MLSRVAKRAFSSTVANP	Malate dehydrogenase 1 (*S. cerevisiae*)	(Vogtle, Wortelkamp et al. 2009)
$Lpd1_{MTS}$	MLRIRSLLNNKRAFSSTVRTL	Lipoamide dehydrogenase (*S. cerevisiae*)	(Vogtle, Wortelkamp et al. 2009)
$CoxIV_{MTS}$	MLSLRQSIRFFKPATRTLCSSRYLL	Cytochrome c oxidase (*S. cerevisiae*)	(Avalos, Fink et al. 2013)

To determine the optimal MTS-protein combinations required to target the rBOX in the mitochondria, we first assessed the probability of import to the mitochondria of each combination using the online tools MitoFates (Fukasawa, Tsuji et al. 2015) and TargetP (Emanuelsson, Brunak et al. 2007) (**Table 33**). Then, we selected some of these MTS-protein combinations to validate their correct localisation in the mitochondria *in vivo*. We attached them to GFPenvy, expressed them in *S. cerevisiae* CEN.PK2-1C, and studied their localisation by fluorescence microscopy. As for the combinations tested, we used the following criteria: (1) if possible, different MTS for each rBOX enzyme to reduce the risk of homologous recombination events and (2) high probability of import based on TargetP and MitoFates.

Table 33. Combinations of reverse β-oxidation enzymes and MTS tested in this study. The probability of mitochondrial import of the different MTS and rBOX enzymes based on TargetP ($P_{TargetP}$) and MitoFates ($P_{MitoFates}$) prediction tools. Result of validating the targeting of these MTS-protein combinations by fluorescence microscopy (Mitochondrial target validation).

Enzyme	MTS	P TargetP	P MitoFates	Mitochondrial targeting validation
Erg10	NC_{MTS}	0.978525	0.995	***Successful***
	$PDB1_{MTS}$	0.999404	0.999	Not successful
^{Ca}Hbd	NC_{MTS}	0.987162	0.998	***Successful***
	$MDH1_{MTS}$	0.995009	0.994	Not successful
	$ACP1_{MTS}$	0.997578	0.996	Not successful
	$LPD1_{MTS}$	0.996964	1	Not successful
^{Ca}Crt	$MDH1_{MTS}$	0.97543	0.845	***Successful***
^{Td}Ter	$ACP1_{MTS}$	0.995703	0.997	***Successful***
^{Ec}EutE	$CoxIV_{MTS}$	0.988222	0.987	***Successful***
	$ACP1_{MTS}$	0.996426	0.996	***Successful***
^{Ca}AdhE2	$LPD1_{MTS}$	0.992799	0.999	***Successful***

We validated by fluorescence microscopy MDH_{MTS}, $ACP1_{MTS}$, $CoxIV_{MTS}$ and $LPD1_{MTS}$ as suitable MTS for ^{Ca}Crt, ^{Td}Ter, ^{Ec}EutE and ^{Ca}AdhE2, respectively (**Table 33** and **Figure 34**). We selected NC_{MTS} for both Erg10 and ^{Ca}Hbd. Erg10 did not target the mitochondria when tested with $PDB1_{MTS}$, and in the case of ^{Ca}Hbd, we only observed mitochondrial targeting with NC_{MTS} and not with any of the other three MTS ($MDH1_{MTS}$, $ACP1_{MTS}$ and $LPD1_{MTS}$) tested on this enzyme. Altogether, these are the MTS-protein combinations used to target the rBOX pathway in the mitochondria in further experiments.

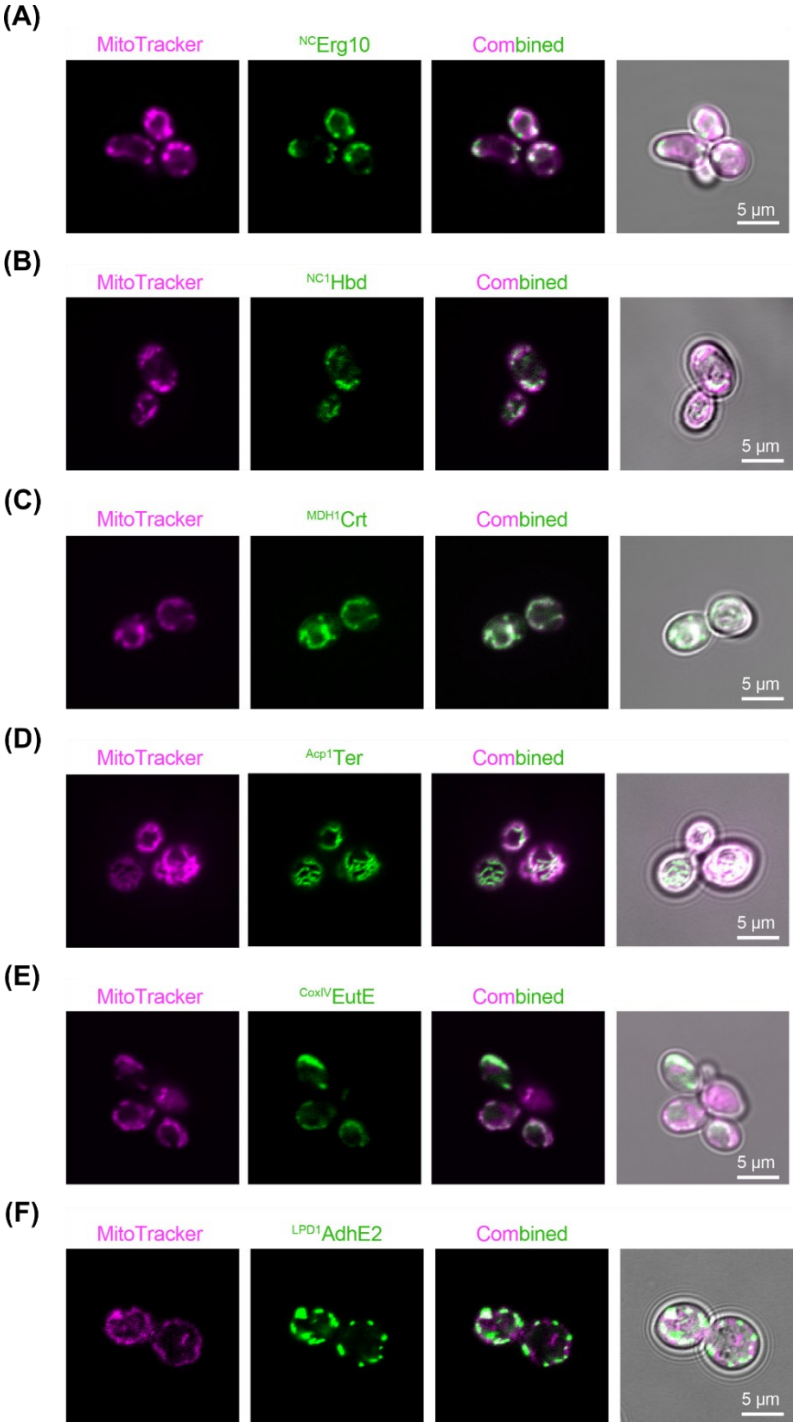

Figure 34. Subcellular localisation in *S. cerevisiae* CEN.PK2-1C of different reverse β-oxidation enzymes and alcohol dehydrogenases ^{Ec}EutE and ^{Ca}AdhE2. NC_{MTS}_Erg10 (A), NC_{MTS}_^{Ca}Hbd (B), $Mdh1_{MTS}$_^{Ca}Crt (C), $Acp1_{MTS}$_^{Td}Ter (D), $CoxIV_{MTS}$_^{Ec}EutE (E) and $Lpd1_{MTS}$_^{Ca}AdhE2 (F) were fused to GFP and expressed from CENARS-based plasmids (GDV006, GDV020, GDV004, GDV007, GDV169 and GDV005, respectively) in *S. cerevisiae* CEN.PK2-1C. The localisation of the fusion proteins (in green) was analysed by fluorescence microscopy. Mitochondria were dyed with Mitotracker Red CMXRos and are here represented in magenta.

4.2.2.2 Expression of the reverse β-oxidation pathway in the mitochondria and effect of downregulating *NDI1* expression

We generated two variants (GDV060 and GDV061) of the rBOX together with 1-butanol-specific alcohol dehydrogenases ^{Ca}*adhE2* and ^{Ec}*eutE*. All the genes expressed in both variants

were targeting the mitochondria (4.2.2.1). In the first variant (GDV060), all the genes were expressed under strong promoters, and in the second variant (GDV061), under weak promoters (**Table 34**).

Table 34. Reverse β-oxidation expression variants transformed in GDY1, GDY2 and GDY4. Plasmid used for the transformation (*Plasmid*), level of expression of each gene in the plasmid based on the promoter selected for its expression (*Level of expression*), the parental strain used in the transformation (GDY1 or GDY2), name of the strain generated (*Strain*) and the result of the transformation based on the apparition or not of surviving cells (*Transformation outcome*).

Strain	Parental strain	Plasmid	Level of expression (high / low)	Transformation outcome
-	GDY1 (Δ*adh1-5*, *mth1*Δ169-393)	GDV060	***pPGK1***-NC_{MTS}_*ERG10-tVMA16* ***pCCW12***-NC_{MTS}_^{Ca}*hbd-tIDP2* ***pENO2***-MDH_{MTS}_^{Ca}*crt-tPGK1* ***pTDH3***-ACP_{MTS}_^{Td}*ter-tADH1* ***pRPL3***-$CoxIV_{MTS}$_*EceutE-tPRM9* ***pTEF1***-LPD_{MTS}_^{Ca}*adhE2-tTDH1*	Unsuccessful
GDY3	GDY1 (Δ*adh1-5*, *MTH1*Δ169-393)	GDV061	*pSAC6-*NC_{MTS}_*ERG10-tSSA1* *pRNR2-*NC_{MTS}_^{Ca}*hbd-tHIS5* *pPSP2-*MDH_{MTS}_^{Ca}*crt-tPGK1* *pRAD27-*ACP_{MTS}_^{Td}*ter-tADH1* *pREV1-*$CoxIV_{MTS}$_^{Ec}*eutE-tCYC1* *pPOP6-*LPD_{MTS}_^{Ca}*adhE2-tTDH1*	**Successful**
-	GDY2 (Δ*adh1-5*, Δ*gpd2*, *MTH1*Δ169-393)	GDV060	***pPGK1***-NC_{MTS}_*ERG10-tVMA16* ***pCCW12***-NC_{MTS}_^{Ca}*hbd-tIDP2* ***pENO2***-MDH_{MTS}_^{Ca}*crt-tPGK1* ***pTDH3***-ACP_{MTS}_^{Td}*ter-tADH1* ***pRPL3***-$CoxIV_{MTS}$_^{Ec}*eutE-tPRM9* ***pTEF1***-LPD_{MTS}_^{Ca}*adhE2-tTDH1*	Unsuccessful
GDY8	GDY2 (Δ*adh1-5*, Δ*gpd2*, *MTH1*Δ169-393)	GDV061	*pSAC6-*NC_{MTS}_*ERG10-tSSA1* *pRNR2-*NC_{MTS}_^{Ca}*hbd-tHIS5* *pPSP2-*MDH_{MTS}_^{Ca}*crt-tPGK1* *pRAD27-*ACP_{MTS}_^{Td}*ter-tADH1* *pREV1-*$CoxIV_{MTS}$_^{Ec}*eutE-tCYC1* *pPOP6-*LPD_{MTS}_^{Ca}*adhE2-tTDH1*	**Successful**
GDY11	GDY4 (Δ*adh1-5*, Δ*gpd2*, *MTH1*Δ169-393, *ΔpNDI1::pYEN1*)	GDV061	*pSAC6-*NC_{MTS}_*ERG10-tSSA1* *pRNR2-*NC_{MTS}_^{Ca}*hbd-tHIS5* *pPSP2-*MDH_{MTS}_^{Ca}*crt-tPGK1* *pRAD27-*ACP_{MTS}_^{Td}*ter-tADH1* *pREV1-*$CoxIV_{MTS}$_^{Ec}*eutE-tCYC1* *pPOP6-*LPD_{MTS}_^{Ca}*adhE2-tTDH1*	**Successful**

We first transformed both pathway variants in strains GDY1 and GDY2. However, we only obtained viable colonies after transforming the weakly expressing variant (GDV061) in GDY1 or GDY2, generating GDY3 and GDY8, respectively.

Expressing the rBOX in the mitochondria of GDY1 resulted in 54.07 ± 0.12 mg/L of butyric acid, but no 1-butanol was detected (**Fig 35A**). The additional deletion of the glycerolphosphate dehydrogenase *GPD2* (GDY8) slightly decreased the butyric acid production from the pathway (48.26 ± 4.81 mg/L) and did not result in 1-butanol production.

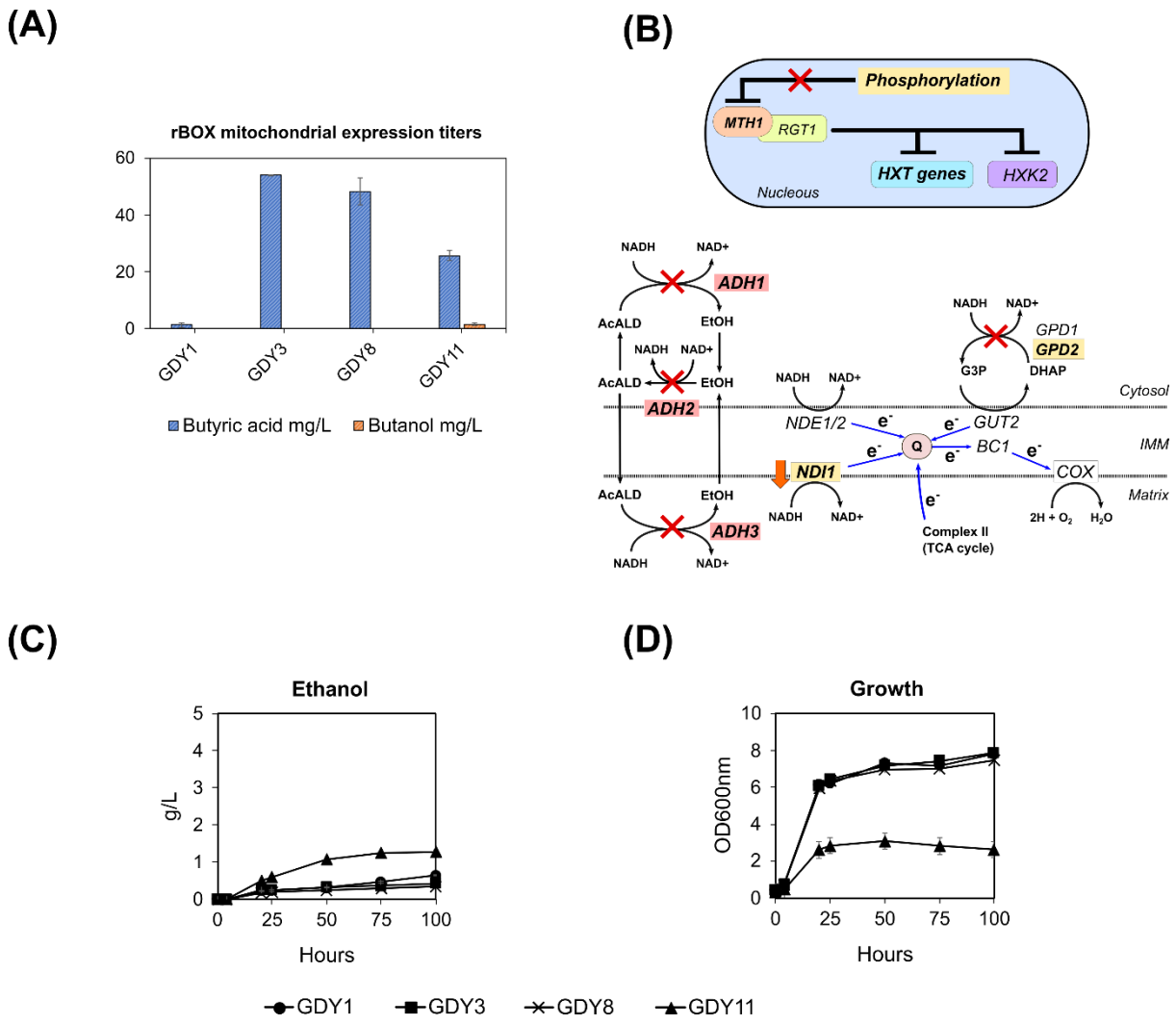

Figure 35. Expression of the reverse β-oxidation in the mitochondria of engineered *S. cerevisiae* strains. (A) Production of butyric acid and butanol from expressing a mitochondrial rBOX variant in GDY1 (GDY3), GDY2 (GDY8) and GDY4 (GDY11). (B) Representation of the genetic modifications used to increase the carbon flux to the mitochondria of *S. cerevisiae*. (C) Ethanol production by GDY1, GDY3, GDY8, and GDY11 over 100h of fermentation (D) Growth of strains GDY1, GDY3, GDY8 and GDY11 over 100h of fermentation. All the fermentations were run for 100h in SMD. Error bars represent the standard deviation between two independent replicates. **Abbreviations**: AcALD, acetaldehyde; EtOH, Ethanol; G3P, glycerol-3-phosphate; DHAP, dihydroxy-acetone-phosphate.

To reduce the competition for NADH in strain GDY2, we replaced the native promoter in *NDI1* with the weak *YEN1* promoter (Hassing, de Groot et al. 2019), creating strain GDY4 (GDY2 Δ*pNDI1::pYEN1*). Ndi1 plays a crucial role in *S. cerevisiae* by catalysing the oxidation of NADH in the mitochondrial matrix (Luttik, Overkamp et al. 1998), which is necessary for the latter stages of oxidative phosphorylation (**Figure 35B**). Additionally, the rBOX pathway variants used here are also located in the mitochondrial matrix. Downregulating the expression of *NDI1* in GDY11 resulted in yeast with a *petite* phenotype (see **Figure 36**) and further reduced the titres of butyric acid (25.63 ± 1.79 mg/L) by 52% and 47% compared to GDY3 and GDY8, respectively. However, contrary to GDY3 and GDY8, GDY11 produced 1.51 ± 0.48 mg/L of 1-butanol after 100 h of fermentation (**Fig 35A**). GDY11 also produced the highest titres of ethanol among the strains tested (1.28 ± 0.04 g/L after 100h) (**Fig 35C**), twice as much as

GDY1, the second-best ethanol producer (0.63 ± 0.01 g/L after 100h). The ethanol titres of GDY3 and GDY8 were below 0.5 g/L at the end of fermentation. Finally, the expression of the rBOX in the mitochondria pathway did not significantly impact the growth of the strains, as observed comparing GDY3 and GDY8 against GDY1. However, the downregulation of *NDI1* significantly reduced the final OD600nm of GDY11 by approximately 65% compared to the rest of the strains (**Fig 35D**).

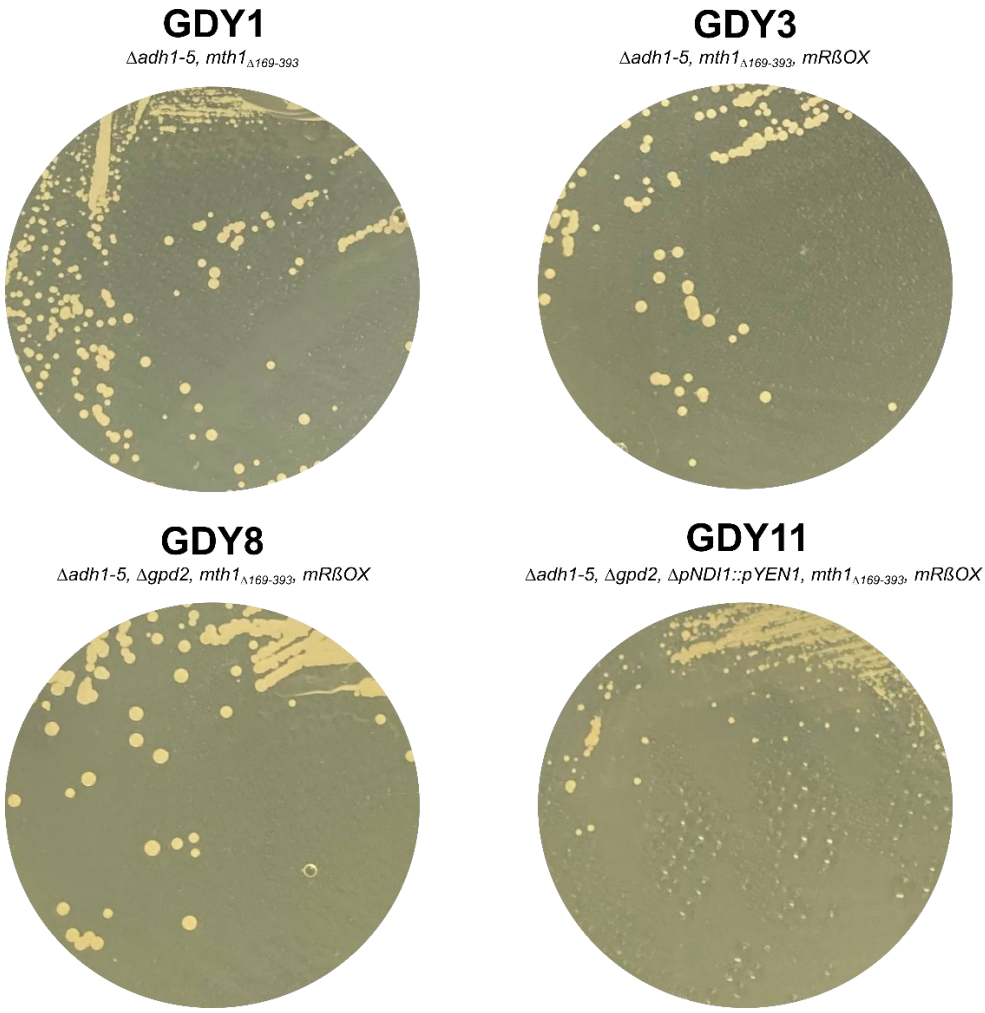

Figure 36. Growth test of strains expressing the reverse β-oxidation in the mitochondria. The phenotype of control strain GDY1 and strains expressing the reverse β-oxidation in the mitochondria (GDY3, GDY8 and GDY11) when grown in YPD-agar plates after 3 days of incubation at 30ºC. GDY11 (Δ*pNDI1::pYEN1*) cells are significantly smaller (*petite* phenotype) compared to the rest.

Altogether, the expression of the rBOX in the mitochondria only worked when the genes were weakly expressed, resulting mainly in butyric acid production. The downregulation of *NDI1*, intended to reduce the competition for NADH, resulted in decreased titres of butyric acid but in the production of 1-butanol, although in very low titres.

4.2.2.3 Testing different variants of the mitochondrial reverse β-oxidation pathway

Production of 1-butanol was only achieved at low titres when weakly expressing the rBOX in the mitochondria of a *S. cerevisiae* strain with downregulated *NDI1* expression (4.2.2.2). The reduction of crotonoyl-CoA to butyryl-CoA is a known limiting step in the rBOX pathway catalysed by trans-2-enoyl-CoA reductases (Schadeweg and Boles 2016b). Therefore, we created the integrative plasmid GDV105, where a mitochondrially targeted ^{Td}*ter* (^{Td}*ter*$_{MT}$) is expressed under the strong *TDH3* promoter. Additionally, to increase the flux through the pathway, we expressed *ERG10*$_{MT}$, the first enzyme of the pathway, under the strong *PGK1* promoter. Finally, as observed in **4.1.4**, both ^{Ec}EutE and ^{Ca}AdhE2 can catalyse the conversion of butyryl-CoA to 1-butanol. Observing that the level of expression in the mitochondria might burden the cells (**Table 34**), in GDV105, we expressed only ^{Ca}*adhE2*$_{MT}$ as alcohol dehydrogenase.

In addition, we know that *Y. lipolytica*'s 3-hydroxyacyl-CoA dehydrogenase ^{Yl}Had and enoyl-CoA hydratase ^{Yl}Ech are targeted in the mitochondria (**Figure 15** and **Figure 18**). Since the mitochondrial matrix is the natural environment of these two enzymes, we used them instead of ^{Ca}Hbd$_{MT}$ and ^{Ca}Crt$_{MT}$, and created plasmid GDV146 for this purpose. This plasmid contains all the mitochondrial rBOX enzymes expressed under weak promoters, and ^{Ec}*eutE*$_{MT}$ and ^{Ca}*adhE2*$_{MT}$ are utilized as alcohol dehydrogenases. Furthermore, and similar to expression strategy in GDV105, we created GDV148. In GDV148, *ERG10*$_{MT}$ and ^{Td}*ter*$_{MT}$ are expressed under strong promoters (*PGK1* and *TDH3* promoter, respectively). In this plasmid, ^{Ca}*adhE2* is the only alcohol dehydrogenase. However, and in contrast to GDV105, it is expressed under the strong *TEF1* promoter.

We created strains GDY9, GDY20 and GDY25 after transforming strain GDY4 with GDV105, GDV148 and GDV146, respectively (**Table 35**). Then, we compared the 1-butanol and butyric acid production of these strains against GDY11 and included GDY4 as the non-producer strain (**Figure 37**). After 100h of fermentation, GDY9 (40.9 ± 0.14 mg/L), GDY20 (40.95 ± 0.07 mg/L) and GDY25 (47.65 ± 1.06 mg/L) had increased by 45%, 45% and 68% the final titres of butyric acid compared to GDY11 (28.2 ± 0.56 mg/L) (**Fig 37A**). Only the strains expressing the mitochondrial rBOX variants produced 1-butanol, although at low titres. GDY9 (5.01 ± 0.42 mg/L) and GDY25 (4.05 ± 0.11 mg/L) more than doubled the titres of 1-butanol produced by GDY11 (2.39 ± 0.20 mg/L). GDY20, on the other hand, produced scarce amounts of 1-butanol (0.85 ± 0.08 mg/L). It should be noted, that when checking the insertion of the rBOX in GDY20, the open reading frame of ^{Ca}*adhE2*$_{MT}$ contained a two-adenosine nucleotide deletion (See **Appendix IV**). In addition, the growth of strain GDY20 was clearly impaired and the ethanol production pattern slightly delayed when compared to strains GDY9, GDY11, GDY25 and the parental GDY4. (**Fig 37B, C**).

Table 35. Reverse β-oxidation expression variants transformed in GDY4. Plasmid used for the transformation (*Plasmid*), level of expression of each gene in the plasmid based on the promoter selected for its expression (*Level of expression*), the *parental strain* used in the transformation (GDY4), name of the strain generated (*Strain*) and the result of the transformation based on the apparition or not of surviving cells (*Transformation outcome*).

Strain	Parental strain	Plasmid	Level of expression (high / low)	Transformation outcome
GDY9	GDY4 (Δ*adh1-5,* Δ*gpd2*, *mth1*Δ169-393, Δ*pNDI1::pYEN1*)	GDV105	***pPGK1***-NC_{MTS}_*ERG10-tVMA16* *pRNR2-*NC_{MTS}_^{Ca}*hbd-tHIS5* *pPSP2-*MDH_{MTS}_^{Ca}*crt-tPGK1* ***pTDH3***-ACP_{MTS}_^{Td}*ter-tADH1* *pPOP6-*LPD_{MTS}_^{Ca}*adhE2-tTDH1*	Successful
GDY11	GDY4 (Δ*adh1-5,* Δ*gpd2*, *mth1*Δ169-393, Δ*pNDI1::pYEN1*)	GDV061	*pSAC6-*NC_{MTS}_*ERG10-tSSA1* *pRNR2-*NC_{MTS}_^{Ca}*hbd-tHIS5* *pPSP2-*MDH_{MTS}_^{Ca}*crt-tPGK1* *pRAD27-*ACP_{MTS}_^{Td}*ter-tADH1* *pREV1-*$CoxIV_{MTS}$_^{Ec}*eutE-tCYC1* *pPOP6-*LPD_{MTS}_^{Ca}*adhE2-tTDH1*	Successful
GDY20	GDY4 (Δ*adh1-5,* Δ*gpd2*, *mth1*Δ169-393, Δ*pNDI1::pYEN1*)	GDV148	***pPGK1***-NC_{MTS}_*ERG10-tVMA16* *pRNR2-*^{Yl}*HAD-tHIS5* *pPSP2-* ^{Yl}*ECH-tPGK1* ***pTDH3***-ACP_{MTS}_^{Td}*ter-tADH1* ***pTEF1***-LPD_{MTS}_^{Ca}*adhE2**-tTDH1*	Successful**
GDY25	GDY4 (Δ*adh1-5,* Δ*gpd2*, *mth1*Δ169-393, Δ*pNDI1::pYEN1*)	GDV146	*pSAC6-*NC_{MTS}_*ERG10-tSSA1* *pRNR2-*^{Yl}*HAD-tHIS5* *pPSP2-* ^{Yl}*ECH-tPGK1* *pRAD27-*ACP_{MTS}_^{Td}*ter-tADH1* *pREV1-*$CoxIV_{MTS}$_^{Ec}*eutE-tCYC1* *pPOP6-*LPD_{MTS}_^{Ca}*adhE2-tTDH1*	Successful

** LPD_{MTS}_^{Ca}AdhE2 contained two Adenine nucleotide deletions

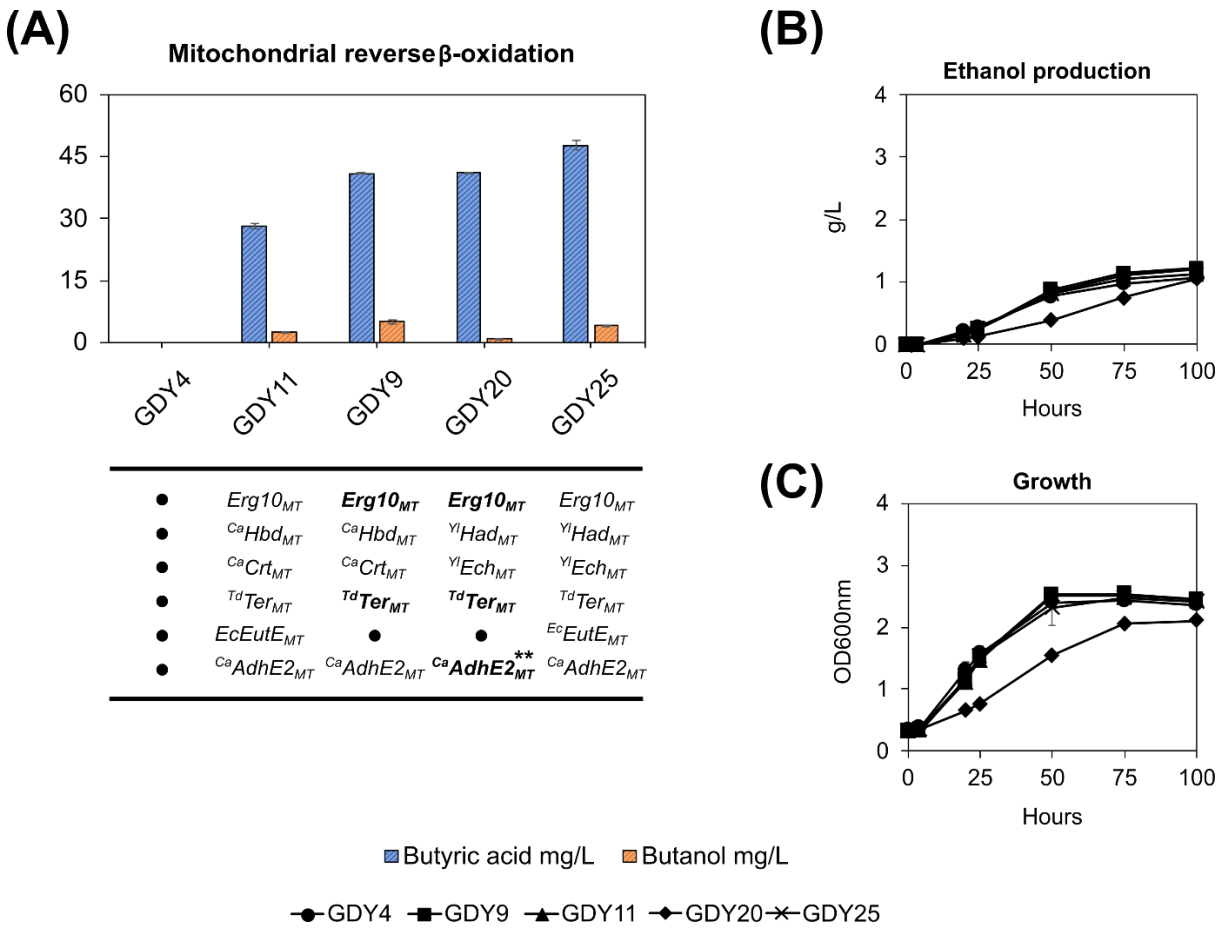

Figure 37. Expression of reverse β-oxidation pathway variants in engineered *S. cerevisiae* strain GDY4. (A) Production of butyric acid and butanol from expressing mitochondrial rBOX variants in GDY4 (*(Δadh1-5, Δgpd2, mth1Δ169-393, ΔpNDI1::pYEN1*). In bold, enzymes expressed under strong promoters in each variant. (B) Ethanol production and (C) growth of strains GDY4, GDY9, GDY11, GDY20 and GDY25 over 100h of fermentation in SMD. Error bars represent the standard deviation between three independent replicates. (**) indicates a mutation in the ORF of this enzyme.

5 Discussion

In this thesis, I explored strategies to improve the output of expressing the rBOX in *S. cerevisiae*. The rBOX is a chain elongation pathway that can produce a diverse range of products like alcohols, acids, polyketides, or volatile esters (Tarasava, Lee et al. 2022). Extending the length of the products and improving the yields from this pathway in the industrial yeast *S. cerevisiae* would accelerate the implementation of sustainable production processes for a previously inaccessible range of products at an industrial scale.

In this chapter, I reflect on the research performed, the results obtained and their impact. I also discuss this study's limitations and suggest future recommendations. For this, the discussion is divided into three parts: (i) the metabolic engineering strategies used to increase NADH in the cytosol and to re-direct the C-flux to the mitochondria, (ii) the strategy used to increase the length and variety of products from this pathway and (iii) the attempts to increase the titres of this pathway by compartmentalising it in the mitochondria.

In this section, the first person, '*I*', is the default voice used whenever the text speaks about my decisions, interpretations, and hypotheses. The first person, '*we*', is used to address the reader regarding a result or observation previously presented in the thesis and when describing processes where other colleagues (i.e. students) were involved. In addition, '*we*' is used when discussing challenges to address as humanity or the research community.

5.1 Strain engineering strategies to improve NADH and acetyl-CoA availability in *S. cerevisiae*

Acetyl-CoA is required for the starting and chain-elongation reactions in the rBOX. Furthermore, in the pathway variants used in this study, the 3-HBD and the TER reactions use NADH as cofactor. Therefore, acetyl-CoA and NADH are two crucial metabolites for the rBOX. In this work, we expressed the pathway in the cytosol and increased the NADH availability in this cellular compartment, resulting in increased MCFA titres (**Figure 23A**). In addition, we engineered strains with increased C-flux to the mitochondria by removing the Crabtree effect (**Figure 29**). Then, we expressed a 1-cycle pathway variant of the rBOX and produced butyric acid in the mitochondria (**Figure 35**).

5.1.1 Creating a platform strain to express the reverse β-oxidation in the cytosol by increasing the NADH pool

To express the pathway in the cytosol, we started with VSY0 (Δ*adh1-5*) as the platform organism. As observed in **Figure 29A**, the NADH generated by wild-type *S. cerevisiae* during

glycolysis is mainly re-oxidised to NAD^+ via ethanol fermentation, leading to high ethanol yields. Since VSY0 has a limited ethanol-producing capacity, I expected a higher availability of NADH for the rBOX. However, this resulted in high glycerol titres by VSY0 (**Figure 13** and **Figure 29**). The $Y_{GLY/S}$ in wild-type *S. cerevisiae* strains is highly strain dependent, but values usually range between 0.01-0.1 when grown semi-aerobically (Bideaux, Alfenore et al. 2006, Hubmann, Guillouet et al. 2011). In the fermentations in YPD, we observe similar values close to that range (0.01-0.1) for the wild-type strain CEN.PK2-1C ($Y_{GLY/S}$ =0.0086). However, the $Y_{GLY/S}$ in VSY0 was almost 40-fold that of CEN.PK2-1C (**Figure 29F**). Increased glycerol production in strains with knocked out ADHs was previously reported in *S. cerevisiae* (de Smidt, du Preez et al. 2012). In *S. cerevisiae*, glycerol production starts with an NADH-consuming reduction of dihydroxyacetone phosphate to glycerol 3-phosphate (Nevoigt and Stahl 1997). The glycerolphosphate dehydrogenase Gpd2 catalyses this reaction to prevent NADH from accumulating under anaerobic conditions (Ansell, Granath et al. 1997, Aslankoohi, Rezaei et al. 2015). Therefore, the higher glycerol production in the *adh*-deficient VSY0 strain is probably a response to regenerating NADH in the absence of primary alcohol dehydrogenases. In addition, VSY0 (and all its derived strains) produces slightly more acetate than CEN.PK2-1C (**Figure 29E**). ADHs are the main consumers of the acetaldehyde generated from the pyruvate decarboxylase reaction (de Smidt, du Preez et al. 2012, Ia-Rosa, García-Ramírez et al. 2021). Therefore, I suggest that this increase in acetate results from a higher flux to acetaldehyde dehydrogenases, given the reduced competition for acetaldehyde from ADHs in VSY0 and derived strains. Interestingly, acetate is consumed in all strains already after 50h (CEN.PK2-1C included).

To reduce the NADH being oxidised for glycerol production, I created GDY15 by knocking out *GPD2*. This increased the production titres of the rBOX (**Figure 14** and **Figure 23A**) and decreased $Y_{GLY/S}$ by 4-fold compared to VSY0 (**Figure 29F**). Blocking competing reactions is a proven strategy in *E. coli* and *S. cerevisiae*. In these organisms, deleting the main NADH-consuming pathways led to increased production of 1-butanol or hexanol from the rBOX (Shen, Lan et al. 2011, Lian, Si et al. 2014, Schadeweg and Boles 2016b). In the specific case of deleting glycerol-3-phosphate dehydrogenases, using this approach in *adh*-deficient strains to prevent competition for NADH resulted in increased titres of iso-butanol and 2,3-butanediol (Kim, Lee et al. 2019, Wess, Brinek et al. 2019). Furthermore, Lian *et al.* (2014) measured acetyl-CoA in a *S. cerevisiae* strain with reduced fermentation (Δ*gpd1*, Δ*gpd2*, Δ*adh1*, Δ*adh4*) and observed a 2-fold increase in acetyl-CoA. Therefore, GDY15 could have both a higher NADH and cytosolic acetyl-CoA pool than CEN.PK2-1C and VSY0.

Interestingly, we also observe that growth was partially recovered in the Δ*adh1-5* Δ*gpd2* strain (GDY15) compared to the Δ*adh1-5* strain (VSY0) (**Figure 14** and **Figure 29**). Glycolysis results

in 2 moles of NADH and 2 moles of ATP from a mole of glucose when run entirely. However, glycerol production occurs upstream of the first ATP-generating reactions in glycolysis (see **Figure 4**). Therefore, I hypothesise that an increased glycerol production from glucose, as in VSY0, might result in a reduced generation of ATP and, thus, decreased growth. I propose that once the main glycerol-3-phosphate dehydrogenase is knocked out in VSY0, the flux of NADH re-oxidised in the mitochondria via the respiratory chain (RC) increases. This increased flux through the RC leads to an increased ATP production downstream via oxidative phosphorylation, which should result in higher growth.

Besides NADH, the rBOX pathway also needs acetyl-CoA. The synthesis of acetyl-CoA in the cytosol requires acetate and coenzyme A (van Rossum, Kozak et al. 2016c). Coenzyme A is synthesised from pantothenate in a 5-step pathway catalysed by PanK, Cab2, Cab3, Cab4 and Cab5 (Leonardi and Jackowski 2007), where pantothenate kinase (PanK) is the limiting reaction (Vadali, Bennett et al. 2004) (for more details, see **Figure 7**). Schadeweg and Boles (2016b) expressed in a highly engineered (Δ*adh1-6*, Δ*sfa1*, and Δ*gpd1-2*) yeast strain a pantothenate kinase from *E. coli* (*coaA*) non-repressed by high acetyl-CoA levels and overexpressed the endogenous amine oxidase *FMS1*. Fms1 is the rate-limiting reaction for the synthesis of β-alanine, a precursor of pantothenate (White, Gunyuzlu et al. 2001). The resulting strain VSY18, highly dependent on NADH-consuming pathways to re-generate NAD^+, produced 0.86 g/L of 1-butanol from the rBOX. However, in the present study, expressing the octanoic acid-producing variant of the BOX in VSY18 resulted in minimal growth and no MCFA production (data not shown). The main differences with the experiments by Schadeweg and Boles (2016) are the expression of the ADHs, ^{Ec}*eutE* and ^{Ca}*adhE2*, and a rBOX variant that can run two cycles further. Therefore, it would be interesting to run a fermentation with VSY18 expressing only the ADHs or the butyric acid-producing rBOX variant tested in this study (GDV098: *ERG10*, ^{Ca}*hbd*, ^{Ca}*crt*, ^{Td}*ter*) to assess the individual impact of these changes better.

Overall, the objective of this experiment was to generate a strain able to produce MCFA and grow well in the fermentation conditions used. Increasing the cytosolic availability of NADH resulted in the desired phenotype. However, the strain should be further improved to reach production titres that suit economically feasible industrial production processes. For that, future strain engineering strategies should focus on (1) increasing the availability of coenzyme A, (2) further reducing the product titres of fermentation products from NADH-consuming pathways, and especially (3) improving the strains' tolerance to MCFAs, as product inhibition seems to be the main issue when producing MCFAs. Some suggestions for the last point are listed in section 5.2.2.

5.1.2 Pushing the carbon flux to the mitochondria: Reducing the Crabtree effect

Acetyl-CoA is the other key metabolite for the rBOX pathway. The synthesis of acetyl-CoA in the cytosol via PDH-bypass implies the consumption of ATP, making its synthesis less energy-efficient than in the mitochondria via PDH (van Rossum, Kozak et al. 2016c). In addition, a current theory suggests that acetyl-CoA levels are higher in the mitochondria than in the cytosol of *S. cerevisiae* (Galdieri, Zhang et al. 2014, Weinert, Iesmantavicius et al. 2014, Duran, López et al. 2020). Therefore, I aimed to express the rBOX in the mitochondria of *S. cerevisiae*. However, *S. cerevisiae* is a well-known Crabtree-positive yeast. This means that most of the C-flux under non-glucose limiting conditions is channelled towards ethanol fermentation in the cytosol. At the same time, C-flux to mitochondria is minimized due to the repression of both TCA cycle and respiration (Fendt and Sauer 2010). A key factor determining a strain's respiration/fermentation behaviour is the glucose uptake rate, which is higher in Crabtree-positive than Crabtree-negative yeast (Hagman, Säll et al. 2014, Malina, Yu et al. 2021). The glucose uptake depends on the abundance of hexose transporters (HXTs) and their kinetics (Reifenberger, Boles et al. 1997, Otterstedt, Larsson et al. 2004). Mutating the regulation domain of Mth1 recovered the growth in high-glucose of a *pdc*-deficient *S. cerevisiae* strain and is believed to do so by blocking the expression of *HXTs* in non-glucose limiting conditions (Oud, Flores et al. 2012). Therefore, to push the C-flux towards the mitochondria, I deleted the regulatory region of Mth1 in VSY0 and in GDY15, resulting in strains GDY1 (Δ*adh1-5*, Δ$mth1_{169\text{-}393}$) and GDY2 (Δ*adh1-5*, Δ*gpd2*, $mth1_{\Delta 169\text{-}393}$), respectively.

In GDY1, the $MTH1_{\Delta 169\text{-}393}$ mutation reduced the glycerol fermentation and increased $Y_{X/S}$ more than 2-fold compared to its predecessor VSY0 (**Figure 29D** and **Figure 29F**). This pattern resembles that of the *GPD2* deletion in GDY15 described above (5.1.1). However, the change in metabolic behaviour is more marked in GDY1, with the final OD_{600nm} in this strain reaching close to that of the wild-type strain and improving substantially compared to GDY15 (**Figure 29C**). Mutating *MTH1* in GDY15 (resulting in GDY2), brought this strain to $Y_{X/S}$ and final OD_{600nm} close to those in GDY1. When comparing GDY1 and GDY2, the only significant difference is the glycerol production pattern (**Figure 29D**). Unlike the *gpd2*-ko strains GDY2 and GDY15, GDY1 shows a peak in glycerol titres at 50h, probably a product of endogenous Gpd2 activity in this strain. The lingering glycerol production in GDY2 and GDY15 may result from the activity of Gpd1, the remaining glycerolphosphate-dehydrogenase in these strains (Ansell, Granath et al. 1997).

The marked recovery in biomass yields and the decreased fermentation yields observed with the $MTH1_{\Delta 169\text{-}393}$ mutation is characteristic of an increased mitochondrial metabolism (Malina, Yu et al. 2021). Mth1 is a negative glycolysis regulator that binds to Rgt1 under glucose-limiting conditions and prevents its phosphorylation (Lakshmanan, Mosley et al. 2003). However, at high-glucose conditions, Mth1 is phosphorylated at its regulation domain and degraded,

resulting in the phosphorylation of Rgt1 and subsequent release from blocking the expression of *HXTs* (Ozcan, Leong et al. 1996). In strains GDY1 and GDY2, Rgt1 is constantly repressing the expression of these glucose transporters, probably resulting in a reduced glucose uptake. In addition, Rgt1 also represses the expression of the hexokinase *HXK2* (Palomino, Herrero et al. 2005). Besides phosphorylating glucose, Hxk2 binds to Mig1 and activates the glucose catabolite repression in *S. cerevisiae* (Vega, Riera et al. 2016). As an example of its pivotal role in the catabolite repression, knocking out *HXK2* in CEN.PK2-1C reduced the Crabtree effect by increasing TCA cycle and respiration (Schuurmans, Rossell et al. 2008, Kümmel, Ewald et al. 2010). Therefore, I propose that removing the regulatory region of Mth1 reduces the Crabtree effect via Rgt1's repression cascade. This results in a combination of (i) reduced glucose import due to lower expression of HXTs, (ii) reduced flux through glycolysis due to a reduced hexokinase activity and (iii) reduced catabolite repression by Hxk2's signalling cascade. Altogether, this results in an increased mitochondrial metabolism. However, it should be taken into consideration that I mutated *MTH1* in *adh*-deficient strains (VSY0 and GDY15). It could be interesting to test the $MTH1_{\Delta 169\text{-}393}$ mutant in the wild-type CEN.PK2-1C. This would help assessing the impact of the Mth1-Rgt1 regulation cascade at high glucose on a strain with full fermentation capabilities.

Regarding the intermediate respiratory metabolism observed in GDY15, I hypothesise that this strain's increase in biomass and reduced fermentation does not result from a de-regulation in glucose metabolism like in GDY1 or GDY2. Instead, the additional *GPD2* deletion in this already *adh*-deficient strain results in better accessibility of the respiratory chain for substrates and co-factors usually consumed via ethanol and glycerol fermentation.

5.1.2.1 ^{Km}Eat1 as a platform to quantify acetyl-CoA levels in engineered strains

To further study the changes in the metabolism of our engineered strains, I aimed to develop a bio-sensing system to study the accumulation of acetyl-CoA using the mitochondrial ethanol acetyltransferase Eat1 from *K. marxianus*. This enzyme catalyses the formation of acetate esters from acetyl-CoA and a broad range of alcohols like ethanol, isoamyl alcohol, iso-butanol or phenyl ethanol (Kruis, Gallone et al. 2018). Ethanol is broadly distributed in the cell and is the preferred alcohol substrate of ^{Km}Eat1. Isoamyl alcohol, on the other hand, is a product of the biosynthesis of leucine but also of leucine degradation, both partially mitochondrial processes (Hirata and Hiroi 1991). Therefore, I assessed the level of acetyl-CoA accumulation based on the production of ethyl acetate (from ethanol) and isoamyl acetate (from isoamyl alcohol). For this, ^{Km}*EAT1* was expressed in the mitochondria and the cytosol of GDY2.1, GDY15.1 and CEN.PK2-1C. GDY2.1 was selected as an example of a strain with a high respiratory (mitochondrial) metabolism. CEN.PK2-1C, on the other hand, was selected as an

example of a strain with a clear fermentative (cytosolic) metabolism with good growth properties. Regarding GDY15.1, it was selected to assess if the growth improvement observed in this strain (Δ*adh1-5*Δ*gpd2*) compared to VSY0 (Δ*adh1-5*) results from an increased carbon flux to the mitochondria. To target ^{Km}Eat1 in the cytosol, I used a truncated version of this enzyme, missing the first 30 amino acids (^{Km}Eat1$_{CYT}$). In *K. marxianus*, removing 19 amino acids was sufficient to target this enzyme in the cytosol (Lobs, Schwartz et al. 2018). However, I showed that expressing an Eat1$_{\Delta 1\text{-}19}$ truncation variant in *S. cerevisiae* still results in mitochondrial targeting (**Figure 30B**). These different results could arise from differences in the MTS cleavage recognition sites between these two yeast species. In *S. cerevisiae*, proteins targeted to the mitochondrial matrix contain an Mpp cleavage site that removes the MTS once the pre-protein reaches the matrix (Chacinska, Koehler et al. 2009). However, additional matrix peptidases like Oct1, Icp55 or Cym1 can further cleave additional amino acids of the immature protein before it reaches its final form (Mossmann, Meisinger et al. 2012). These additional maturation steps can be specific for different yeast species. For instance, when comparing the MTS of Eat1 (*K. marxianus*) against its *Wickerhamomyces anomalus* and *S. cerevisiae* homologs, Kruis *et al.* (2020) observed that the three Eat1 homologs contained a different MTS structure in each organism, probably product of different maturation requirements.

Ethyl acetate production was significantly higher when expressing ^{Km}*EAT1*$_{MIT}$ than ^{Km}*EAT1*$_{CYT}$ in all the strains (**Figure *33***), and ethanol titres were similar when expressing ^{Km}*EAT1*$_{MIT}$ or ^{Km}*EAT1*$_{CYT}$. Since ethanol diffuses easily through cell membranes (Yang and Hinner 2015), I do not expect differences in ethanol concentration between organelles. In addition, acetyl-CoA is the limiting substrate of the ester-forming reaction (Kruis, Levisson et al. 2017). Therefore, these results would suggest higher availability of acetyl-CoA in the mitochondria than in the cytosol. However, the first 30 amino acids were truncated in the cytosol-targeted ^{Km}Eat1$_{CYT}$. Besides preventing its import to the mitochondria, this truncation could negatively affect the activity of the cytosol-targeted version of this enzyme. A less active ^{Km}Eat1$_{CYT}$ compared to the full ^{Km}Eat1$_{MIT}$ would bias the interpretation of the results because lower cytosolic ethyl acetate titers would not come from a lower availability of acetyl-CoA in the cytosol, but from a worse ^{Km}Eat1 enzyme activity in this cellular compartment. Therefore, and given that the MTS can vary between organisms, performing a more extensive analysis on ^{Km}Eat1$_{CYT}$ truncation variants would be very interesting. A similar approach was used in *E. coli* to identify Eat1 truncated variants with high thermal stability and reaction rate (Kruis, Bohnenkamp et al. 2020). Interestingly, the 30-amino acid truncated version of ^{Km}Eat1 was the best variant in that study.

Additionally, I expected strains with an increased mitochondrial acetyl-CoA availability to produce more ethyl acetate and isoamyl acetate with ^{Km}Eat1$_{MIT}$ than with ^{Km}Eat1$_{CYT}$. GDY2.1 produced the highest titres of isoamyl acetate, followed by GDY15.1 and CEN.PK2-1C (WT)

with $^{Km}Eat1_{MIT}$. However, CEN.PK2-1C (WT) produced the highest titres of ethyl acetate in the mitochondria, followed by GDY15.1 and GDY2.1 (**Figure 33**). This does not necessarily suggest a higher mitochondrial accumulation of acetyl-CoA in CEN.PK2-1C than in the other strains, but rather suggests that ^{Km}Eat1 prefers ethanol, abundant in CEN.PK2-1C, over isoamyl alcohol. In fact, a preference of ^{Km}Eat1 towards alcohols longer than ethanol and branched alcohols has been previously described (Patinios, Lanza et al. 2020). Since ethanol is the preferred substrate for ^{Km}Eat1, this enzyme is not the best tool for comparing the acetyl-CoA accumulation in *adh*-deficient strains against high ethanol-producers like CEN.PK2-1C. Instead, I suggest comparing the production of ethyl acetate and isoamyl acetate among strains with similar genetic backgrounds. In this specific case, among *adh*-deficient strains. For instance, GDY2.1 and GDY15.1 are both *adh*-deficient strains. Comparing them, we see that the isoamyl acetate titres in the mitochondria are higher in GDY2.1 than GDY15.1 (**Figure 32**). This is in line with what is previously discussed in section 5.1.2: while mutating Mth1 pushes the C-flux to mitochondria in part by altering the catabolite repression regulation, knocking out the major NADH-consuming reactions (ADHs and Gpd2) increase the availability of NADH and glycolysis end-products for respiration and other mitochondrial processes.To validate this using ^{Km}Eat1, I suggest using the also *adh*-deficient VSY0 as a fermentative (cytosolic)-strain control and GDY1 or GDY2.1 as respiration (mitochondrial)-strain controls.

5.2 Expanding the range of products of the reverse β-oxidation pathway in *S. cerevisiae*

5.2.1 Testing different reverse β-oxidation pathway variants to produce medium-chain fatty acyl-CoAs in *S. cerevisiae*

In this work, we extended the length of the rBOX pathway products to octanoyl-CoA, resulting in the highest titers of octanoic acid reported in *S. cerevisiae* with this pathway (see section 4.1). Previous studies expressing the rBOX in *S. cerevisiae* reported hexanoyl-CoA formation (Krink-Koutsoubelis, Loechner et al. 2018, Luo, Reiter et al. 2019). However, those reporting the production of hexanoic, octanoic, and decanoic acid produced meagre amounts (>8 mg/L) (Lian and Zhao 2015, Teixeira, Siewers et al. 2017), and we cannot discard the endogenous fatty acid β-oxidation as the primary source of the precursor medium-chain fatty acyl-CoAs.

I chose the production of MCFAs to assess the pathway improvement due to economic and technical reasons: (1) the methods to detect medium-chain fatty acids via GC were available in our group (2) MCFAs are cheaper to purchase than medium-chain fatty acyl-CoAs, making it easier to run standard calibration curves for accurate quantification and finally, as mentioned

above, (3) *S. cerevisiae* contains endogenous thioesterases that can efficiently cleave medium-chain acyl-CoAs into Coenzyme A and MCFAs (Saerens, Verstrepen et al. 2006, Gajewski, Pavlovic et al. 2017). This allows for a screening system without testing additional enzymes or reactions. I chose GDY15 as a platform strain due to its increased cytosolic NADH pool and good growth phenotype (see section 4.1.1).

The rBOX consists of four cyclical reactions. We tested different enzymes at each reaction and identified suitable combinations of enzymes optimal for butyric, hexanoic and octanoic acid production. Overall, octanoic acid was the main product when using ^{Cn}BktB as thiolase, ^{Cn}PaaH1 as 3-hydroxyacyl-CoA dehydrogenase, ^{Cn}Crt2 or ^{Yl}Ech as enoyl-CoA hydratases and ^{Eg}Ter or ^{Td}Ter as trans-enoyl-CoA reductases. Using the clostridial ^{Ca}Crt as enoyl-CoA hydratase instead of ^{Cn}Crt2 or ^{Yl}Ech limited the production to hexanoic acid. Finally, selecting Erg10 as thiolase and ^{Ca}Hbd or ^{Yl}Had as 3-hydroxyacyl-CoA dehydrogenase limited the production to butyric acid.

An overview of the enzymes used at each reaction, their substrates and the products obtained is shown in **Figure 38**.

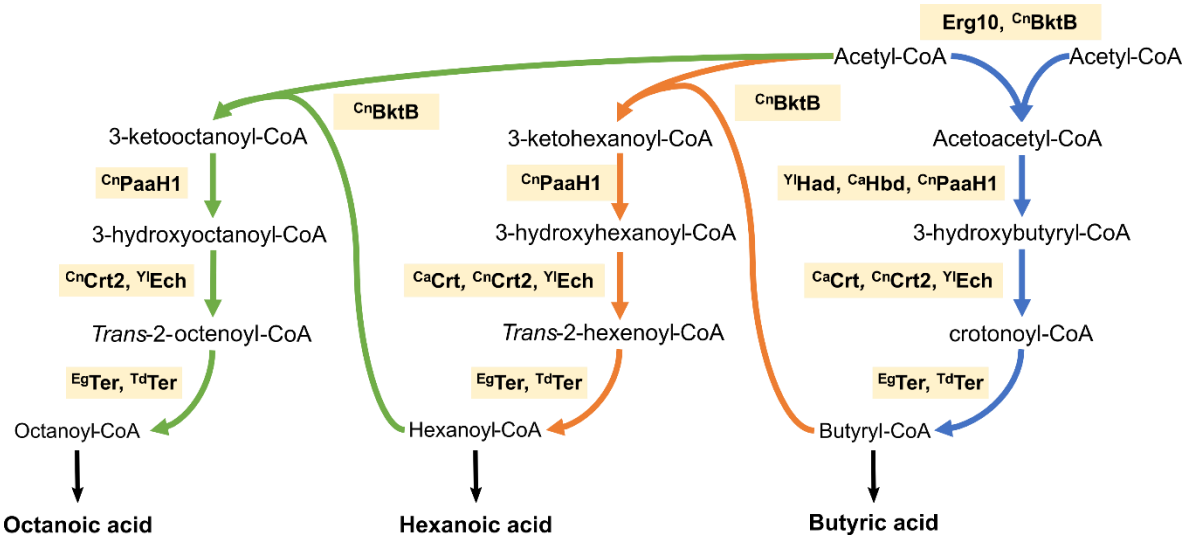

Figure 38. Enzymes used at each reaction of the reverse β-oxidation and the intermediates and products obtained.

Expressing ^{Cn}*bktB* and ^{Cn}*paaH1* was critical to producing hexanoic and octanoic acid. In previous studies, the combined expression of ^{Cn}*bktB* and ^{Cn}*paaH1* in *S. cerevisiae* resulted in hexanoyl-CoA as the longest product (Krink-Koutsoubelis, Loechner et al. 2018, Luo, Reiter et al. 2019). However, ^{Cn}BktB can catalyse the condensation of acetyl-CoA with various acyl-CoAs like propionyl-CoA, butyryl-CoA, pentanoyl-CoA or hexanoyl-CoA in *E. coli* (Slater, Houmiel et al. 1998, Tseng, Martin et al. 2009, Dekishima, Lan et al. 2011). Therefore, this limitation to hexanoyl-CoA in *S. cerevisiae* observed in Krink-Koutsoubelis *et al.* (2018) and

Luo *et al.* (2019) suggested either that the condensation of acetyl-CoA and butyryl-CoA by ^{Cn}BktB is an upper limit in this organism, or that ^{Cn}PaaH1 cannot reduce substrates longer than 3-oxohexanoyl-CoAs. In the present study, we produced octanoic acid and showed for the first time (i) the condensation of acetyl-CoA and hexanoyl-CoA using ^{Cn}BktB in *S. cerevisiae* and (ii) the reduction of 3-oxooctanoyl-CoA by ^{Cn}PaaH1 in *S. cerevisiae*, leading to octanoic acid production. The key difference with Krink-Koutsoubelis *et al.* (2018) and Luo *et al.* (2019) is the choice of enoyl-CoA hydratases. In those studies, they combined ^{Cn}BktB and ^{Cn}PaaH1 with ^{Ca}Crt and ^{Td}Ter. In the present study, this combination limited the pathway to two cycles, producing mainly hexanoyl-CoA as in their experiments (**Figure 17A**). By using ^{Cn}Crt2 or ^{Yl}Ech instead of ^{Ca}Crt, the pathway can run another cycle, as these enoyl-CoA hydratases can utilise 3-hydroxyoctanoyl-CoA as a substrate. In addition, it should be noted that the strains used in this study, as well as in Krink-Koutsoubelis *et al.* (2018) and Luo *et al.* (2019), contained a native copy of the thiolase *ERG10*, which very likely contributed to the butyric acid fraction produced in these experiments and to synthesising part of the butyryl-CoA used by ^{Cn}BktB.

The expression of *ERG10*, ^{Ca}*hbd* or ^{Yl}*HAD*, limited the production to butyric acid. Erg10 is an endogenous *S. cerevisiae*'s thiolase that had been selected as the best to produce 1-butanol in that organism via rBOX (Schadeweg and Boles 2016a). However, no MCFA titres were determined in that study. Here, I showed that its thiolase activity is limited to the condensation of two acetyl-CoA molecules, resulting in the SCFA butyric acid (**Figure 13**). Also, as mentioned above, the native copy of *ERG10* present in the genome contributed to the production of butyric acid also when overexpressing *ERG10* from plasmid GDV098. *ERG10* is an essential gene catalysing the synthesis of acetoacetyl-CoA in the conserved mevalonate pathway. This pathway is critical for the synthesis of ergosterol in yeast and fungi (Hu, He et al. 2017, Jordá and Puig 2020). For instance, mutations in *ERG10* result in ergosterol auxotrophy (Hiser, Basson et al. 1994). Therefore, I hypothesise that the high substrate specificity towards acetyl-CoA has been selected and conserved throughout evolution to ensure viability and survival.

I included in the screening ^{Ca}*hbd,* a clostridial 3-HBD, because (i) it produced hexanoyl-CoA when expressed in *E. coli*, although significantly less than ^{Ca}*paaH1* (Machado, Dekishima et al. 2012) and (ii) when combined with ^{Cn}*bktB*, ^{Ca}*crt* and ^{Td}*ter*, it produced up to 101 mg/mL of hexanoic acid in *K. marxianus* (Cheon, Kim et al. 2014). Nevertheless, in our experiments, expressing ^{Ca}*hbd* in *S. cerevisiae* resulted mainly in butyric acid, with hexanoic acid titers not reaching 2 mg/L (**Figure 14**). Similar to the Erg10 case, I believe that the substrate preference of ^{Ca}Hbd is a product of evolutionary selection. ^{Ca}Hbd is part of the conserved clostridial 1-butanol production pathway (Lee, Park et al. 2008), and therefore, it has a high specificity towards the 4-carbon long acetoacetyl-CoA. However, unlike Erg10, where no products longer than C4 were obtained, I hypothesise that the substrate preference of ^{Ca}Hbd for acetoacetyl-

CoA does not involve a limitation in the catalytic site to accommodate bigger substrates, but rather that it is due to a higher affinity or catalytic rate for acetoacetyl-CoA. Regarding the high titres of hexanoic acid in *K. marxianus* using ^{Ca}Hbd, I can only hypothesise that the conditions in the cytosol of this Crabtree-negative organism could have been better for this reaction than in the cytosol of *S. cerevisiae*.

The third enzyme limiting the production to butyric acid was ^{Yl}Had, a putative mitochondrial 3-hydroxyacyl-CoA dehydrogenase from the oleaginous yeast *Y. lipolytica* (Vorapreeda, Thammarongtham et al. 2012). I confirmed ^{Yl}Had as a mitochondrial enzyme by fluorescence microscopy (**Figure 15**) and by the inability of the pathway to produce any MCFA when ^{Yl}*HAD* was expressed with the MTS (results not shown). The expression of a cytosolic ^{Yl}*HAD* resulted mainly in butyric acid production, and even the hexanoic acid titers were lower than with ^{Ca}*hbd* (**Figure 16B**). When expressed previously in *S. cerevisiae*, a cytosolic ^{Yl}*had* produced up to 8 mg/mL of octanoic acid (Lian and Zhao 2015). In GDV151, none of the other enzymes (^{Cn}BktB, ^{Ca}Crt, ^{Td}Ter) should limit the size of the product to the 4-carbon butyryl-CoA (**Figure 16**). Thus, I hypothesise that the medium-chain specific thioesterase (FatB1 from *Candida parapsilosis*) used by Lian and Zhao (2015) cleaved products from the endogenous, catabolic β-oxidation instead of products generated from anabolic rBOX pathway. All in all, and similarly to ^{Ca}Hbd, the cytosolic ^{Yl}Had can only reduce substrates up to acetoacetyl-CoA under the conditions tested.

I selected ^{Cn}Crt2, ^{Yl}Ech and ^{Ca}Crt as enoyl-CoA hydratases (ECHs). The hydratase activity of ^{Cn}Crt2 on 3-hydroxyhexanoyl-CoA was known as its overexpression in modified *C. necator* and *M. extorquens* increased the production of poly((R)-3-hydroxybutyrate-co-(R)-3-hydroxyhexanoate), a polymer made partially of hexanoyl-CoA (Zhang, Kurita et al. 2019, Orita, Unno et al. 2022). In the case of ^{Yl}Ech, its substrate specificity seemed to be limited to 3-hydroxybutyryl-CoA when used in a modified rBOX pathway in *S. cerevisiae* (Lian and Zhao 2015). In this study, I show for the first time that ^{Yl}Ech can use 3-hydroxyhexanoyl-CoA as substrate and that both ^{Yl}Ech and ^{Cn}Crt2 enzymes can use 3-hydroxyoctanoyl-CoA, leading to octanoic acid. Compared to Lian and Zhao (2015), we expressed ^{Cn}*bktB* and ^{Cn}*paaH1* in the first two steps of the pathway before ^{Yl}*ECH*. This combination proved to be better than overexpressing the cytosolic *FOX3* as thiolase and a cytosolic ^{Yl}*HAD*, which I also showed to be limited to 4-carbon substrates (see section 4.1.2.1).

Regarding the clostridial ^{Ca}Crt enzyme, this ECH has been exploited in *S. cerevisiae* to produce hexanoyl-CoA, an essential precursor for cannabinoid synthesis (Taura, Tanaka et al. 2009, Luo, Reiter et al. 2019, Tahir, Shahbazi et al. 2021) and to produce hexanoic acid and 1-hexanol in *E. coli* (Machado, Dekishima et al. 2012, Vogeli, Schulz et al. 2022). Expression of ^{Ca}*crt* limited the production to hexanoic acid (**Figure 17A**), confirming its previously observed

activity up to 3-hydroxyhexanoyl-CoA. In addition, under the same conditions, the production of octanoic or decanoic acids with ^{Ca}*crt* remained insignificant compared to when expressing ^{Cn}*crt2* or ^{Yl}*ECH*. This suggests that ^{Ca}Crt has no affinity towards 3-hydroxyacyl-CoAs longer than 6-carbons.

Comparing ^{Yl}*ECH* with ^{Cn}*crt2* in the plasmid-based expression experiment, ^{Cn}*crt2* led to a slightly higher Octanoic acid/Hexanoic acid ratio (**Figure 17B**), but overall rBOX activity is higher with ^{Yl}*ECH* expression, based on the $Y_{MCFA/S}$ (**Table 28**). On the other hand, if we compare strains GDY28 (^{Cn}*crt2*) and GDY29 (^{Yl}*ECH*), the $Y_{MCFA/S}$ are almost identical (**Table 30**). However, the Octanoic acid/Hexanoic acid ratio is slightly higher in GDY29. Nonetheless, we cannot discard this difference coming from mutations arising in these strains during fermentation. Overall, no major differences between these two enzymes are observed under the tested conditions.

Despite octanoic acid being the main product with ^{Yl}*ECH* and ^{Cn}*crt2* expression, hexanoic acid and butyric acid were also produced in the fermentation. A possible explanation is a catalytic inefficiency in this cyclic pathway, where 2-carbon, 4-carbon and 6-carbon substrates compete for the same enzymes. This is observed in other rBOX variants expressed in *E. coli* (Clomburg, Contreras et al. 2017, Kim, Jang et al. 2018, Mehrer, Incha et al. 2018) but also in cell-free systems (Vogeli, Schulz et al. 2022). Another explanation for the combined production of different MCFAs is the activity of endogenous thioesterases cleaving butyryl-CoA and hexanoyl-CoA into butyric acid and hexanoic acid. This last point is discussed in section 5.2.2.

In this work, I selected ^{Eg}Ter and ^{Td}Ter as *Trans*-enoyl-CoA reductases. Both TERs are reported to produce MCFAs up to decanoic acid (Kim and Gonzalez 2018, Wu, Wang et al. 2019). ^{Eg}Ter and ^{Td}Ter were previously compared in Schadeweg and Boles (2016a) for 1-butanol production. However, MCFAs were not measured in that study, and therefore, it only gives us a hint about their activity towards crotonoyl-CoA. In addition, Kim and Gonzalez (2018) co-expressed both TERs and showed that expressing ^{Td}*ter* from a plasmid in an *E. coli* with an integrated copy of ^{Eg}*ter* boosts decanoic acid production. However, they did not compare the expression of each TER alone. In the present study, the enzyme variants selected for the reactions preceding the *trans*-enoyl-CoA reductase limited the production up to octanoic acid, as we did not produce relevant titres of decanoic acid. This constrained the comparison between the activities towards longer chain substrates of the *trans*-enoyl-2-CoA reductases. Nonetheless, we observe a 20% increase in total MCFA production with ^{Td}Ter and better yields on glucose (**Table 29**), suggesting a higher catalytic activity with this enzyme under the tested conditions. The MCFA pattern did not change, with octanoic acid as the main product.

Overall, I identified different combinations of enzymes for the rBOX producing short and medium-chain fatty acids ranging from butyric acid up to octanoic acid. However, the

production of decanoic acid remained limited. The combined expression of thiolase *[Cn]bktB* and the *trans*-enoyl-CoA reductases *[Td]ter* and *[Eg]ter* with *fadB* produced nearly 100 mg/L of decanoic acid in *E. coli* (Kim and Gonzalez 2018). Using the same thiolase (*[Cn]bktB*) and TERs (*[Td]ter* and *[Eg]ter*), I did not detect significant titers of decanoic acid (**Figure 20A**). This suggests that the three 3-hydroxyacyl-CoA dehydrogenases and enoyl-CoA hydratases used in this study may have no affinity for 10-carbon long 3-hydroxyacyl-CoAs or 3-oxoacyl-CoAs and that more enzymes should be tested to identify 3-HBDs and ECHs using 10-carbon substrates. *E. coli*'s FadB, a dual 3-hydroxyacyl-CoA dehydrogenase/ enoyl-CoA hydratase mentioned above, is an interesting candidate. Besides producing decanoic acid, FadB was also used to produce 1-decanol in *E. coli* (Mehrer, Incha et al. 2018). Another interesting strategy is using enzymes from the bacterial type II fatty acid biosynthesis. The bacterial type II FAB uses ACP-bound substrates and is closely related to the mitochondrial FAB present in some eukaryotes (Marrakchi, Zhang et al. 2002, Hiltunen, Schonauer et al. 2009). Furthermore, type II FAB has equivalent reactions to the rBOX pathway, like those catalysed by FabB, FabG, FabZ and FabI in *E. coli*, equivalent to the thiolase, 3-HBD, ECH and TER reactions in the rBOX, respectively (Janßen and Steinbüchel 2014). In *E. coli*, combining the overexpression of *[Cn]bktB* with *fabG*, *fabZ* and *fabI* resulted in MCFA production up to decanoic acid, showing that these enzymes could also use CoA-bound and, therefore, be used in the rBOX (Clomburg, Contreras et al. 2017). In addition, type II FAB enzymes are present in different bacteria. Therefore, it would be interesting to screen for 3-HBDs and ECHs in, for example, saturated fatty acid-producing bacteria like *Prevotella*, *Alistipes*, and some *Lactobacillus* species (Zhao, Huang et al. 2018) or in known MCFA producers like *Megasphaera eldensii* (Jeon, Choi et al. 2016).

5.2.2 Strategies to improve the pathway selectivity and titers

Despite producing significant octanoic acid titers for the first time with the rBOX in *S. cerevisiae*, some outcomes from this work were limiting the titres of the pathway and the MCFAs production pattern: (1) The presence of butyric acid and hexanoic acid as by-products in the plasmid-based fermentation (see section 4.1.2). Although expected in a cyclical pathway, by-products hamper the titres of longer-chain MCFAs. (2) Octanoic acid was the longest MCFA produced. Some of the enzymes used in the octanoic acid-producing pathway variants ([Cn]BktB, [Cn]PaaH1, [Yl]ECH or [Cn]Crt2, [Td]Ter) were previously reported to produce decanoic acid. However, in the best case, no more than 2 mg/L of decanoic acid were produced (**Figure 17**). (3) Toxicity limiting the final titers. I observed a growth impairment in the octanoic acid-producing strains (**Figure 19**), probably due to product toxicity. In this section, I discuss the strategies tested in the present work to overcome these issues.

5.2.2.1 Increasing the acyl-CoA pool by boosting butyryl-CoA titers and by deleting *FAA2* and *TES1*

Thiolases catalyse a condensation reaction that is only thermodynamically favourable at high substrate concentrations (Dellomonaco, Clomburg et al. 2011, Beber, Gollub et al. 2021). To discard the possibility of ^{Cn}BktB cleaving octanoyl-CoA or decanoyl-CoA, an octanoic acid-producing pathway variant and a butyryl-CoA-producing pathway were co-expressed (see section 4.1.3.1). With this, I expected to tilt the reaction towards condensation by increasing the concentration of medium-chain acyl-CoAs upstream of octanoyl-CoA. This strategy is based on Le Chatelier's principle. In nature, Le Chatelier's principle is observed in some acyltransferases that can act as thioesterases (cleavage) or as acyltransferases (condensation) depending on the concentration of substrates (Saerens, Delvaux et al. 2010, Kruis, Levisson et al. 2017). Le Chatelier's is also observed in some transaminases, like the alanine-aminotransferase, that catalyses the transamination of pyruvate to alanine or the reverse deamination depending on the alanine concentration (García-Campusano, Anaya et al. 2009).

Increasing the butyryl-CoA availability led to butyric acid becoming the main product and increased the production of hexanoic acid (**Figure 21**). The significant production of butyric acid indicates (i) the presence of specific and efficient thioesterases acting on butyryl-CoA, (ii) a tilt to termination in the pathway's termination/elongation equilibrium due to an imbalance between the high catalytic rate of Erg10 to form butyryl-CoA and the conversion rate of ^{Cn}BktB to generate medium-chain acyl-CoAs. This difference in activity is also observed in **Figure 13A**; the expression of *ERG10* resulted in higher titers of butyric acid than ^{Cn}*bktB* when both were part of a butyric acid-producing rBOX variant (with ^{Ca}*hbd*, ^{Ca}*crt*, and ^{Td}*ter*). Hexanoic acid, the only MCFA with increased titres in this experiment, results from running butyryl-CoA one additional cycle in the rBOX. Therefore, I hypothesise that increasing the hexanoyl-CoA pool could boost octanoic acid production. To do this, instead of co-expressing the octanoic acid and the butyric acid-producing pathway, we should test co-expressing the octanoic acid and the hexanoic acid-producing pathway variants.

I also tackled the by-product formation by deleting the endogenous thioesterase *TES1* and the medium-chain acyl-CoA synthase *FAA2* in GDY15. The short-chain acyl-CoA thioesterases Tes1 is known to target butyryl-CoA in *S. cerevisiae* (Maeda, Delessert et al. 2006). This target-specificity could lead to an increased butyric acid production that would compromise the chain elongation capacity of the pathway. Faa2, on the other hand, is a medium-chain fatty acyl-CoA synthetase that activates medium-chain free fatty acids in the peroxisomes, leading to their degradation via β-oxidation (Leber, Choi et al. 2016).

Neither deletion strategy resulted in a significant change in titres or pattern of MCFA produced (**Figure 23**). Tes1 is located in the peroxisomes of *S. cerevisiae*, while the rBOX enzymes are in the cytosol, making the impact of its deletion harder to assess due to pre-existing limited access of this thioesterase to the acyl-CoA intermediates of the pathway. As a comparison, in *E. coli*, the deletion of *tesB*, a cytosolic thioesterase closely related to *TES1* (Maeda, Delessert et al. 2006, Ishihama, Schmidt et al. 2008), led to a significant increase in the C_6-C_{10} MCFA titers produced by overexpressing the rBOX in the cytosol of this organism (Kim, Clomburg et al. 2015). Deleting *FAA2* is reported to increase MCFA production (Leber, Choi et al. 2016, Baumann, Doughty et al. 2021) and MCFOH production in *S. cerevisiae* (Henritzi, Fischer et al. 2018). Therefore, I did not expect the lack of impact of this deletion on the MCFA titers. Nonetheless, in those studies, the fermentation was performed in YPD medium, while in 4.1.3.2, the fermentation was performed in SM. When testing different medium compositions (see section 4.1.3.3), we observe that GDY15 (a non-MCFA producer) and GDY27 (hexanoic acid-producer) started consuming acetic acid earlier (between 50 and 75h of cultivation) in YPD-100 mM than in SM or any other MCFA-producing strains. In the case of GDY27, the acetic acid consumption was accompanied by the consumption of hexanoic acid, where Faa2 activation would be required (**Figure 24**). Therefore, I propose that the effect of knocking out *FAA2* was not visible in GDY19 (GDY15△*faa2*) after 75h because the switch to an organic acid consumption phase takes longer in SM. Hence, I suggest assessing the impact of deleting *FAA2* in complex YPD-100 mM at different time-points in the fermentation.

In this sub-chapter, I aimed to increase octanoic acid production by (1) increasing the butyryl-CoA pool and (2) avoiding the degradation or cleavage of acyl-CoA intermediates. However, neither strategy resulted in increasing titres of octanoic acid or in improved C_8/MCFA ratios. Therefore, I suggest further investigating the balance between acyl-CoA building and cleaving reactions. Thioesterases catalyse the cleavage of acyl-CoA into fatty acids. The best-known thioesterases acting on medium-chain fatty acyl-CoAs are Eeb1 and Eht1 (Saerens, Verstrepen et al. 2006, Knight, Bull et al. 2014). However, their single deletion resulted mainly in hexanoic acid or in overall reduced titers, and the double deletion (∆*eht1* ∆*eeb1*) led to a growth phenotype (Gajewski, Pavlovic et al. 2017). In addition, thioesterases also act as acyltransferases depending on the abundance and type of acyl-CoAs and alcohols. For example, overexpressing the thioesterase *EHT1* increased the ethyl hexanoate and ethyl decanoate production in *S. cerevisiae* (Chen, Li et al. 2014, Kruis, Gallone et al. 2018). Therefore, it could be interesting to analyse both the MCFA and the volatile esters production pattern during the fermentation and run an RNA-seq analysis in parallel. This could help identify thioesterases/acyltransferases targets for deletion, preventing the early cleavage into SCFA or the loss of MCFAs as medium-chain volatile esters. Finally, it would also be interesting to overexpress some MCFA-specific thioesterases in the MCFA-producing strains generated

in this study. As an example, those with reported MCFA-specificity in bacteria and plants, like *fadM* in *E. coli* (Kim and Gonzalez 2018), *fatB1* in *Candida parapsilosis*, ^{Coco}*fatB1* in coconut tree (Yuan, Chen et al. 2013) or ^{Cp}*fatB1* from *Cuphea palustris* (Südfeld, Kiyani et al. 2022).

5.2.2.2 Genomic expression and optimisation of the fermentation medium

We integrated the hexanoic acid-producing pathway and the two octanoic acid-producing pathway variants in the *URA3*-loci of GDY15 (see section 4.2.2.2). I opted for this to be able to work with complex YPD medium, which is not possible with auxotrophy-based systems, and to boost MCFAs titers since 1-butanol titers increased after genomic integration of the rBOX in *S. cerevisiae* (Schadeweg and Boles 2016a, Schadeweg and Boles 2016b). As observed in **Table 36**, expressing the pathway from the genome improved the butyric and hexanoic acid titers but decreased the octanoic acid production. This comparison is only based on the fermentations performed in SM (SMD_{URA-} for the plasmid expression of the pathway). I chose *CENARS*-based plasmids for plasmid expression to keep the copy number low and minimise variability (Karim, Curran et al. 2013, Lian, Jin et al. 2016). However, even if *CENARS*-based, plasmid-based expression systems exhibit a higher expression variability than genome-based expression in *S. cerevisiae* (Lee, DeLoache et al. 2015). In addition, the improved expression from chromosomal integrations could also be explained by the absence of plasmid burden, especially when using big (>10 kb) plasmids like the ones in this study. Also, the genome-based expression producers have a higher final $OD600_{nm}$ in SM (**Figure 24**) than the plasmid-based expression producers (**Figure 17**), which is in line with the impaired growth in strains with *CENARS* + auxotrophic markers reported by Karim *et al.* (2013). Less growth could result in fewer cells expressing the pathway and lower production titers.

Table 36. Comparison of titers between episomal and chromosomal expressions of the reverse β-oxidation pathway in SMD. The titers from the plasmid-based expression of the hexanoic acid and octanoic acid-producing variants are reported in sections 4.1.2.2. The titers from the chromosomal expression of the pathway are reported in section 4.1.3.3. 'Plasmid'= Expression from plasmid, 'Integration'= Expression from genome integrated pathway.

	Butyric acid	Hexanoic acid	Octanoic acid	Decanoic acid
Expressing hexanoic acid-producing variant				
FHV022$_{Plasmid}$	10.36 ± 2.108	32.88 ± 1.099	2.69 ± 0.046	0.97 ± 0.063
GDY27$_{Integration}$	26.94 ± 4.051	46.18 ± 1.368	2.95 ± 0.104	0.79 ± 0.019
Expressing octanoic acid-producing variant				
FHV018 $_{Plasmid}$	10.99 ± 2.841	21.89 ± 0.783	40.27 ± 1.050	1.97 ± 0.046
GDY28 $_{Integration}$	20.03 ± 5.692	33.14 ± 0.329	31.75 ± 0.051	1.45 ± 0.071
GDV144 $_{Plasmid}$	11.21 ± 1.559	26.57 ± 0.390	41.67 ± 3.811	2.06 ± 0.228
GDY29 $_{Integration}$	22.04 ± 3.278	32.82± 0.605	31.98 ± 1.170	1.40 ± 0.067

Combined with chromosomal integration, the composition of the fermentation medium also played an essential role in the titers obtained. Synthetic-defined medium (SM) is broadly used in *S. cerevisiae* when using expression systems based on auxotrophic selection and in

fermentations where the nutrient composition is tightly controlled (Wu, Zhang et al. 2004, Hahn-Hägerdal, Karhumaa et al. 2005, Xia, Sánchez et al. 2022). However, *S. cerevisiae* grows faster in a complex medium like YPD (Roberts, Kaltenbach et al. 2020). Therefore, I compared growth and production in SM against YPD and tested YPD with two different concentrations of phosphate buffer: (1) YPD-20 mM, equally buffered as SM, was used to compare the impact of complex medium and (2) YPD-100 mM, was used to study the impact of increasing the buffering capacity of the medium. Switching from a buffered, defined medium (SM) to a buffered, complex medium (YPD-20 mM) significantly increased growth, butyric acid, and MCFA production in all the producing strains (**Figure 24** and **Figure 25**). Hahn-Hägerdal *et al.* (2005) reviewed studies where switching to a complex medium improved growth and production in *S. cerevisiae*. As an example, the production of the anticoagulant Hirudin increased by 70% after including yeast extract in the medium composition (Choi, Sohn et al. 1994). After observing the benefits of switching to a complex medium, I increased the phosphate buffer concentration used in YPD. This strategy was previously effective in *S. cerevisiae* strains engineered to produce octanoic acid via a modified FAS enzyme (Gajewski, Pavlovic et al. 2017, Baumann, Doughty et al. 2021). In yeasts, organic acids toxicity is a combination of acidification and perturbation of the membrane structure (Jarboe, Royce et al. 2013). In the cytosol, the produced organic acids dissociate and acidify the intracellular pH (Thomas, Hynes et al. 2002). Yeasts pump protons out via H^+-ATPase to counteract the acidification (Liu, Chernyshov et al. 2013, Martinez-Munoz and Kane 2017). This results in ATP consumption to keep pH homeostasis. In addition, the toxicity of the organic acid increases proportionally to the chain length. We observe this in the plasmid-based expression of the pathway: octanoic acid producers grow less than hexanoic acid producers (**Figure 19**), and hexanoic acid producers grow less than butyric acid producers (results not shown). Liu *et al.* (2013) suggest that octanoic acid is also toxic due to its highly liposoluble behaviour, perturbing the lipid bilayer of the plasma membrane and resulting in a loss of membrane integrity. In this study, increasing the buffering strength significantly increased butyric acid and MCFA production.

Interestingly, and except for the hexanoic acid producer (GDY27), the fermentation in YPD-100 mM had a lower impact on the growth of the strains than switching from defined (SM) to complex medium (YPD-20 mM) (**Figure *25***). This suggests that increasing the buffer concentration increases the tolerance to the MCFA produced. Therefore, I propose that increasing buffering capacity at pH 6.3 prevents the anionic forms of butyric, hexanoic and octanoic acid (pKa's around 4.8 - 4.9) from re-entering the cell through passive diffusion. This way, the cell only has to metabolize the intracellularly produced MCFAs, where a portion of them will not be charged due to a lower cytosolic pH (5.5-5.8) than the medium (Reifenrath and Boles 2018) and could, therefore, exit the cell by passive diffusion. The remaining cytosolic

charged fraction of the MCFAs should be either consumed in the β-oxidation or possibly secreted via Pdr12 and Tpo1, ABC transporters involved in the adaptation to weak acid stress in yeast (Piper, Mahe et al. 1998, Legras, Erny et al. 2010).

Overall, expressing the pathway from the genome and optimizing the fermentation conditions resulted in the highest titers of hexanoic and octanoic acid from the rBOX produced in *S. cerevisiae.* I hypothesize that (1) switching to complex medium improves cell growth, which increases the number of producing cells, and (2) increasing the buffering strength of the medium improves the tolerance to the MCFAs, which improves the toxicity threshold. To further increase the production titers, we should increase the tolerance to MCFA. In this study, I used YPD-100 mM. However, the phosphate buffer concentration should be increased to at least 250 mM. Gajewski *et al.* (2017) used this concentration and reported 245 mg/L of octanoic acid in *S. cerevisiae* with an engineered Fas1 enzyme. In addition, we should further engineer the organic acid detoxification mechanism in the strain. One solution is overexpressing H^+-ATPases to decrease acidification in the cytoplasm. For example, overexpression of the membrane H^+-ATPase *PMA1* increased the tolerance of *S.cerevisiae* to weak acids (Lee, Nasution et al. 2017). Another interesting strategy is overexpressing *PDR12* and *TPO1*, two octanoic and decanoic acid exporters (Borrull, Lopez-Martinez et al. 2015). As an example, engineering the fatty acid exporter Tpo1 and performing ALE in *S. cerevisiae* increased the tolerance to MCFA and resulted in more than 1 g/L of MCFAs (Zhu, Hu et al. 2020). Both H^+-ATPases and MCFA-exporters proposed here for overexpression consume ATP. Therefore, one should tune the expression levels of these elements so as not to negatively impact growth and productivity. Finally, mentioning that the hexanoic acid-producing strain (GDY27) was still growing and consuming acetic acid and hexanoic acid between 50h and 75h in YPD-100 mM (**Figure 24B** and **Figure 25B, C**). Yeast can use organic acids as a carbon source once glucose is depleted (Thomas, Hynes et al. 2002). However, GDY27 did not consume butyric acid for unknown reasons. We should further investigate the mechanisms and dynamics of hexanoic acid consumption at high buffering capacity to prevent the loss of end products.

5.2.3 Production of MCFOH from the reverse β-oxidation pathway

MCFOHs have interesting properties and a broad range of applications. For instance, 1-hexanol is used in the formulation of lubricants or as a solid release agent in agriculture (Yaman, Doğan et al. 2021), and 1-octanol and 1-decanol are gaining interest as fossil fuel replacement or as additives for blending (Henritzi, Fischer et al. 2018). MCFOH are synthesised through a two-step reduction of medium-chain fatty acyl-CoAs. Since in this study strains producing up to octanoyl-CoA were generated (see section 4.1.2), I decided to test the MCFOH production from the rBOX variants created here.

^{Ca}*adhE2* and ^{Ec}*eutE* were expressed in the octanoyl-CoA-producing strain GDY29. I selected strain GDY29 over GDY28, the other octanoyl-CoA-producing strain, because GDY29 showed a higher octanoic to hexanoic acid ratio (1,11 mg_{OCT}/mg_{HEX}) compared to that of GDY28 (1.01 mg_{OCT}/mg_{HEX}) (section 4.1.3.3). ^{Ca}AdhE2 is a dual aldehyde-forming acyl-CoA reductase/alcohol dehydrogenase from *C. acetobutylicum* that catalyses the last two steps in the production of 1-butanol: the reduction to butyraldehyde from butyryl-CoA and (2) the reduction to 1-butanol from butyraldehyde, regenerating 2 NAD^+/butyryl-CoA molecule (Fontaine, Meynial-Salles et al. 2002). I selected ^{Ca}AdhE2 because, when used as a terminal enzyme for the rBOX, it produced 1-hexanol and 1-octanol in *E. coli* (Dekishima, Lan et al. 2011, Kim, Clomburg et al. 2015). In addition, it has been previously used in *S. cerevisiae,* where it produced 1-butanol (Schadeweg and Boles 2016b). ^{Ec}EutE is a putative CoA-dependent aldehyde dehydrogenase involved in ethanolamine degradation (Stojiljkovic, Baumler et al. 1995). I chose ^{Ec}EutE for its interesting features: First, Lian and Zhao (2015) and Schadeweg and Boles (2016a) already expressed ^{Ec}*eutE* to produce 1-butanol from the rBOX. In both studies, ^{Ec}EutE was used to convert butyryl-CoA into butyraldehyde. Then, ^{Ca}BdhB (Lian and Zhao 2015) or ^{Ca}AdhE2 (Schadeweg and Boles 2016a) were used in the final reduction step from butyraldehyde to 1-butanol. Second, ^{Ec}EutE is thought to catalyse the conversion of acetaldehyde to acetyl-CoA in the ethanolamine degradation pathway (Stojiljkovic, Baumler et al. 1995, Kozak, van Rossum et al. 2014). In fact, an ^{Ec}EutE homolog from *Dickeya zeae* could complement growth on glucose in a Δ*acs2* S. cerevisiae strain (Meadows, Hawkins et al. 2016). Since acetyl-CoA is a crucial substrate for the rBOX, the expression of ^{Ec}*eutE* could increase the titres from the pathway. Third, ^{Ec}EutE has a high amino acid sequence similarity with ^{Ec}AdhE, a bi-functional enzyme with aldehyde forming acyl-CoA reductase and alcohol dehydrogenase activity also present in *E. coli* (Membrillo-Hernandez, Echave et al. 2000). Therefore, I hypothesised that it could catalyse both reduction steps from medium-chain acyl-CoA to MCFOH, as is demonstrated by the production of 1-butanol, 1-hexanol and 1-octanol in our experiments (**Figure 27A**).

Expressing ^{Ca}*adhE2* and ^{Ec}*eutE* resulted in the production of 1-butanol and the MCFOHs 1-hexanol and 1-octanol. This is the first time reporting MCFOH production with these enzymes in yeast. However, 1-butanol was the principal fatty alcohol produced. I expected ^{Ca}AdhE2 to have a substrate preference for butyryl-CoA over longer fatty acyl-CoAs since this enzyme is key in the conserved 1-butanol production pathway in *Clostridia* (Yoo, Croux et al. 2016). Nonetheless, these results contradict those from Kim et al. (2015), where expressing ^{Ca}*adhE2* produced more 1-hexanol and 1-octanol than 1-butanol in *E. coli*. These differences could arise from a different accessibility to metabolites in the cytoplasm of these organisms. I*n silico* metabolic models comparing *E. coli* and *S. cerevisiae* for MCFOH production suggest that *E. coli* has a more flexible central metabolism due to less cellular compartmentalization (Matsuda,

Furusawa et al. 2011). This could lead to a better provision of substrates and co-factors in this bacterium. However, these claims have yet to be validated experimentally and are beyond the scope of this thesis. In addition, experimental conditions could also affect the catalysis of ^{Ca}*AdhE2*: *E. coli* and *S. cerevisiae* have optimum growth temperatures of 37ºC and 30ºC, respectively. The optimal growth temperature of *Clostridia* spp., the source of ^{Ca}*AdhE2*, is 37ºC (Biebl 1999, Lee, Park et al. 2008), making its expression more suitable in *E. coli*. While temperature should not affect substrate specificity, it can reduce the reaction rate.

Regarding ^{Ec}EutE, the production of SCFOH and MFCOH with this enzyme partially confirms the putative dual aldehyde/alcohol dehydrogenase activity of ^{Ec}EutE. Nevertheless, as discussed below, we should not discard a contribution from endogenous alcohol dehydrogenases in our experiment. Interestingly, although not statistically significant, expressing ^{Ec}*eutE* resulted in slightly higher SCFOH and MCFOH titers than with ^{Ca}*adhE2*. Most of this was 1-butanol, but it suggests that ^{Ec}EutE has a higher reaction rate than ^{Ca}AdhE2. This aligns with Schadeweg and Boles (2016a), who observed a similar pattern in enzymatic assays using cell extracts. However, in their study, only the butyraldehyde dehydrogenase activity was tested.

As previously observed in the MCFA-producing strains (see section 4.1), ethanol was also a fermentation by-product in this MCFOH production experiment (**Figure 27C**). This means that known and putative alcohol dehydrogenases remain in this *adh*-deficient strain. Furthermore, we observe that GDY29 with an EV produced 1-butanol, too (**Figure 27A**). Given the substrate promiscuity of some ADHs (Reid and Fewson 1994, Pal, Park et al. 2009, Ottone, Bernal et al. 2018), this suggests that one of these enzymes or combinations of aldehyde dehydrogenases and ADHs still present in GDY29 are reducing butyryl-CoA to 1-butanol. This or these enzymes are limited to four-carbon compounds, as no 1-hexanol or longer MCFOH were detected with the EV. It would be interesting to identify the endogenous enzymes responsible for 1-butanol production and knock them out in GDY29. In addition, we also observe this substrate promiscuity of alcohol dehydrogenases in ^{Ca}AdhE2 (**Figure 27C**). Although theoretically specific for four-carbon long compounds, expressing ^{Ca}*adhE2* significantly increased the $Y_{ETOH/S}$.

Interestingly, a higher butyrate production is observed when expressing these dehydrogenases compared to the EV. These titers are higher than in YPD-100 mM producing only MCFA (see section 4.1.3.3). Since both ^{Ca}AdhE2 and ^{Ec}EutE compete with thiolase ^{Cn}BktB for butyryl-CoA, I propose that this competition prevents some of the butyryl-CoA being used for further elongation cycles of the rBOX.

Overall, the selected termination enzymes, ^{Ca}AdhE2 and ^{Ec}EutE, produced 1-butanol over 1-hexanol and 1-octanol in *S. cerevisiae*. Alternative bi-functional enzymes should be tested to

increase the MCFOH to 1-butanol ratio. A reported strategy is using bi-functional fatty acyl-CoA reductases from animals like mFAR from mice (Runguphan and Keasling 2014) and tFAR from barn owls (Feng, Lian et al. 2015). However, both enzymes are NADPH-dependent, and the rBOX pathway variants generated in the present study consume NADH and are used in Δ*adh1-5*Δ*gpd2* yeast strains. Hence, NADH-consuming acyl-CoA reductases are preferred to regenerate NAD^+ and push the flux to MCFOH production. Therefore, I suggest expressing the NADH-consuming acyl-CoA reductase *Maqu2507* from *Marinobacter aquaeolei*. In *E. coli*, expressing *Maqu2507* as a termination enzyme to the rBOX resulted in higher titers of 1-hexanol and 1-octanol than 1-butanol (Kim, Clomburg et al. 2015, Mehrer, Incha et al. 2018). This enzyme was also expressed in the oleaginous yeast *Rhodosporidium toruloides* to produce fatty alcohols (Fillet, Gibert et al. 2015).

Finally, I would highlight that MCFOHs and MCFAs represented 5% and 30% of the rBOX products when expressing ^{Ca}*adhE2* and ^{Ec}*eutE*. These percentages suggest that endogenous thioesterases have better catalysis for the medium-chain fatty acyl-CoA substrates than ^{Ca}AdhE2 and ^{Ec}EutE*,* which clearly prefer butyryl-CoA. In order to increase the MCFOH/MCFA ratio, we should test the expression of carboxylic acid reductases (CAR). CARs are ATP and NADPH-consuming enzymes that reduce fatty acids to aldehydes, which can then be further reduced to fatty alcohols by endogenous or heterologous alcohol dehydrogenases (Zhou, Buijs et al. 2016). For instance, in an octanoic acid-producing *S. cerevisiae* strain, the co-expression of ^{Mm}*Car* from *Mycobacterium marinum* and the aldehyde reductase *Ahr* from *E. coli* resulted in 50 mg/L of 1-octanol and neglectable titres of octanoic acid (Henritzi, Fischer et al. 2018). Furthermore, the rational engineering of ^{Mm}*Car* increased the octanoic acid production to almost 160 mg/L in a MCFA-producing *S. cerevisiae* growing in a minimal medium (Hu, Zhu et al. 2020). Interestingly, they used no heterologous aldehyde reductases in that study and relied on endogenous reductases to convert octanal into 1-octanol. In addition, they observed no toxicity from MCFOHs or MCFAs in minimal medium.

5.3 Compartmentalization of the reverse β-oxidation in the Mitochondria

Yeast mitochondria have higher acetyl-CoA concentrations than the cytosol (Weinert, Iesmantavicius et al. 2014, Duran, López et al. 2020). This higher acetyl-CoA availability in the mitochondria was previously exploited to produce terpenoids (Yuan and Ching 2016, Jia, Chen et al. 2020). Since the two main driving forces for rBOX are acetyl-CoA and NADH availability (Dellomonaco, Clomburg et al. 2011, Shen, Lan et al. 2011), I decided to target different 1-butanol-producing rBOX variants to the mitochondria of engineered *S. cerevisiae* strains and I chose 1-butanol as proof-of-concept because it is relatively non-toxic to the cell compared to MCFOH (4.1.4). In addition, the engineered strains used in these experiments are all *adh*-

deficient strains with a mutation in the regulatory region of Mth1, resulting in reduced fermentation and increased mitochondrial metabolism (**Figure 29F**).

The enzymes in the rBOX contained MTSs targeting the mitochondrial matrix. I aimed at the mitochondrial matrix because it has a reducing environment suitable for NADH-consuming reactions (Orij, Postmus et al. 2009). The correct targeting of the enzymes to the mitochondria was validated by confocal microscopy (**Figure 34** and **Figure 15** for ^{Yl}Had and **Figure 18** for ^{Yl}Ech), and it was shown for the first time that the MTS of Acp1 and Lpd1 can be used to target proteins into the mitochondria. Initially, I aimed for different mitochondrial matrix-targeted MTS for each of the enzymes (Erg10$_{MT}$, ^{Ca}Hbd $_{MT}$, ^{Ca}Crt $_{MT}$, ^{Td}Ter $_{MT}$, ^{Ec}EutE$_{MT}$ and ^{Ca}AdhE2$_{MT}$) to avoid unwanted homologous recombination events. However, as observed in **Table 33**, not all mitochondrial tag-protein combination results in mitochondrial translocation. Therefore, Erg10$_{MT}$ and ^{Ca}Hbd $_{MT}$ both share the same MTS from the ATPase subunit 9 from *N. crassa* (Westermann and Neupert 2000) because it was the only MTS targeting ^{Ca}Hbd to the mitochondria in the fluorescence microscopy experiments (**Figure 34B**). MTS can vary in sequence and length, but generally, they are positively charged, amphipathic α-helical amino acid sequences located at the N-terminal end of a protein (Chacinska, Koehler et al. 2009). These features are critical to be recognized by Tom20 and Tom22, which pass the protein to Tom40 for translocation inside the mitochondria (Mossmann, Meisinger et al. 2012). In addition, prior to recognition by Tom20, the precursor protein is detected by chaperones (mainly Hsp70), that keep it in an unfolded state prior to import (MacKenzie and Payne 2007). Small changes can result in no translocation. For instance, mutating an arginine to a proline in the human pyruvate dehydrogenase E1-alpha gene results in the cytosolic retention of this enzyme and developing a PDH complex deficiency (Takakubo, Cartwright et al. 1995). Therefore, it is possible that in the non-translocated combinations, the sequence preceding the MTS altered key features for the recognition of the secretion tag by the chaperones or by the TOM-complex, resulting in no mitochondrial import of the peptide.

Mitochondria are crucial in carbon, amino acid, and energy metabolism. Hence, protein translocation in the mitochondria is a tightly controlled process (Chacinska, Koehler et al. 2009, den Brave, Gupta et al. 2021). To de-risk saturating the import machinery, two expression variants were created: (i) a low-expression variant with all the genes under weak promoters and (ii) a high-expression variant with strong promoters. The transformation of both variants only yielded viable clones with the low expression variant (**Table 34**).

Expressing the low-expression, mitochondrial rBOX variant in GDY3 (Δ*adh1-5*, Δ*mth1*$_{169\text{-}393}$) and GDY8 (Δ*adh1-5*, Δ*mth1*$_{169\text{-}393}$, Δ*gpd2*) resulted in approximately 50 mg/L of butyric acid (**Figure 35A**), showing for the first time that this pathway is functional in the mitochondria. However, we did not produce 1-butanol. In addition, butyric acid production was lower

compared to the plasmid-based expression of the same enzymes in the cytosol of GDY15 (**Figure 14**). In the mitochondria, the respiratory chain also consumes NADH. This competition for NADH could challenge the run of the mitochondrial rBOX. Therefore, I opted for downregulating the expression of the mitochondrial NADH/ubiquinone oxidoreductase *NDI1* by exchanging the native promoter with the weak, constitutive *YEN1* promoter (Papapetridis, Goudriaan et al. 2018, Hassing, de Groot et al. 2019). Ndi1 is the *S. cerevisiae* equivalent to the human complex I. It oxidises the NADH generated by the TCA cycle in the mitochondrial matrix and transfers the electrons to ubiquinone in the respiratory chain (Marres, de Vries et al. 1991). However, unlike the human Complex I, it does not pump protons in the intermembrane mitochondrial space (Iwata, Lee et al. 2012).

Downregulating Ndi1 (GDY11) decreased butyric acid titres but resulted in 1-butanol production in the mitochondria for the first time (**Figure 35A**). I hypothesise that the downregulation of such an avid NADH-utilizing reaction led to increased accessibility of this co-factor to $^{Ec}EutE_{MT}$ and $CaAdhE2_{MT}$. The downregulation of Ndi1 also boosted the fermentative behaviour of the strain: ethanol production increased, and growth decreased (**Figure 35C, D**). In addition, this weaker expression of *NDI1* resulted in a *petite* phenotype. The *petite* phenotype consists of cells smaller in size than the average and has been previously described in *S. cerevisiae* strains with mutations in the mitochondrial genome or genes involved in the oxidative phosphorylation (Day 2013, Vowinckel, Hartl et al. 2021), as is the case with *NDI1*.

To increase the titres in the GDY4-based (Δ*adh1-5*, Δ$mth1_{169\text{-}393}$, Δ*gpd2,* Δ*pNDI1::pYEN1*) strains:

1. The full-length ^{Yl}Had and ^{Yl}Ech were tested instead of $^{Ca}Hbd_{MT}$ and $^{Ca}Crt_{MT}$ for the 3-HBD and ECH reactions.
2. $^{Ca}Hbd_{MT}$/ $^{Ca}Crt_{MT}$ and ^{Yl}Had/ ^{Yl}Ech-containing variants with $^{Ca}AdhE2_{MT}$ as the only ACR/ADH were created.
3. Some selected enzymes in the pathway were expressed under strong promoters.

I aimed to test ^{Yl}Had and ^{Yl}Ech because these are two native mitochondrial enzymes, and I expected them to perform better than $^{Ca}Hbd_{MT}$ and $^{Ca}Crt_{MT}$ in this organelle. $^{Ec}EutE_{MT}$ was removed from the screening because ^{Ca}AdhE2 is known to catalyse both reactions (see section 4.1.4), and at this point, it was not discarded that the butyraldehyde reduction to 1-butanol was being catalysed by endogenous *S. cerevisiae* ADHs instead of ^{Ec}EutE. Regarding the selected expression of genes with strong promoters, we chose $ERG10_{MT}$ as it catalyses the first reaction of the pathway, $^{Td}ter_{MT}$ as it is a reported reaction bottleneck (Schadeweg and Boles 2016b) and $^{Ca}adhE2_{MT}$ as it is the key enzyme for 1-butanol production.

Overall, the absence of $^{Ec}eutE_{MT}$ and the strong expression of $ERG10_{MT}$ and $^{Td}ter_{MT}$ in the $^{Ca}hbd_{MT}$/ $^{Ca}crt_{MT}$-containing strain GDY9 increased the titres of butyric acid and 1-butanol compared to GDY11. I propose that the overexpression of $ERG10_{MT}$ and $^{Td}ter_{MT}$ increased the competition for acetyl-CoA ($Erg10_{MT}$) and the final conversion to butyryl-CoA ($^{Td}Ter_{MT}$). The slight increase in 1-butanol might be due to the increased availability of butyryl-CoA more than due to absence of $^{Ec}EutE_{MT}$. However, the best butyric acid titers were obtained in GDY25 using a weak-expression pathway (weak $ERG10_{MT}$, $^{Td}ter_{MT}$ and $^{Ca}adhE2_{MT}$ expression) with ^{Yl}had and ^{Yl}ECH (**Figure 37A**). Since both ^{Yl}Had and ^{Yl}Ech are native mitochondrial enzymes (**Figure 15** and **Figure 18**), this observed improvement could result from their native MTS leading to a better import in the mitochondria and a better fit of these enzymes for the conditions in the mitochondrial matrix than $^{Ca}Hbd_{MT}$/ ^{Ca}Crt. In the case of the strong expression of $^{Ca}adhE2_{MT}$, I only obtained a viable clone, strain GDY20, in the cells transformed with the ^{Yl}Had/^{Yl}Ech-containing variant, which contained a frameshift deletion in $^{Ca}adhE2_{MT}$ (see **Appendix IV**) and led to lower titers of butyric acid than GDY25 (**Figure 37A**). In addition, this strain exhibited an impaired growth (**Figure 37C**), which suggests that the mutation in $^{Ca}AdhE2_{MT}$ is a burden for the cells. AdhE2 is an 859 amino acid-long enzyme, and the mutation results in a 450 amino acid-long product. While not affecting viability, I hypothesise that this 450 amino acid-long product results in either problems during import or a burden due to misfolding.

As mentioned above, no transformants were obtained with the high-expression pathway variant (**Table 34**). In GDY9, $^{Ec}eutE_{MT}$ was missing and only $ERG10_{MT}$ and $^{Td}ter_{MT}$ were strongly expressed, resulting in viable cells (**Table 35**). In strain GDY20, the only viable strain with $^{Ca}adhE2_{MT}$ expressed under strong promoters, there is a frameshift deletion in $^{Ca}adhE2_{MT}$. Furthermore, in GDY3, GDY8, GDY11 and GDY25 (low-expression variants) the butyric acid/1-butanol ratio was high. This suggests a malfunction of the ACRs/ADHs used in that experiment (^{Ec}EutE and ^{Ca}AdhE2). Therefore, I propose that the reaction catalysed by bi-functional ACRs/ADHs (particularly $^{Ca}AdhE2_{MT}$) results toxic for the cells when targeted to the mitochondria. We cannot discard an additional toxicity contribution from 3-HBD or ECH. However, these two reactions are critical for the rBOX, and the pathway was functional, as we observe by the production of butyric acid.

Regarding the mechanism of toxicity by ACR/ADHs, I propose that (i) the ACR/ADH reaction interferes with critical reactions in the mitochondria. In that scenario, the strong expression of such enzymes could result in cell death or (ii) the high expression of ACRs/ADHs, and particularly $^{Ca}adhE2_{MT}$, could have clogged the mitochondrial import and triggered the mitochondrial precursor over-accumulation stress response (mPOS) (Wang and Chen 2015). mPOS activation results in decreased translocation of proteins to the mitochondria, increased chaperone activity in the mitochondria, protein degradation in the cytosol, and reduced protein

synthesis (Boos, Krämer et al. 2019). If the source of mPOS persists, it results in cell death (Shakya, Barbeau et al. 2021).

Expression of pathways with strong promoters in the mitochondria of *S. cerevisiae* has previously resulted in the successful production of short, branched-chain alcohols (Avalos, Fink et al. 2013) and terpenes (Yuan and Ching 2016). Neither of those studies reported a negative correlation between strong pathway expression and cell viability. However, the number of proteins translocated to the mitochondria is smaller than in the present study. Only Avalos *et al.* (2013), with the overexpression of *ILV2*, *ILV3*, *ILV5*, an α-KDC and an ADH, imported a similar number of proteins to the mitochondria. Nevertheless, the three ILVs used there are already endogenous mitochondrial enzymes in *S. cerevisiae*, and their translocation might be more efficient than with heterologous proteins. Therefore, while the load to the mitochondrial import machinery is similar, it is possible that importing seven heterologous, natively non-mitochondrial genes, as in our case, results in a higher burden because of increased misfolding or mislocalisation.

Overall, I showed the functional expression of the rBOX in the mitochondria of *S. cerevisiae* by producing butyric acid. However, the competition for resources from endogenous mitochondrial pathways like the TCA cycle (for acetyl-CoA) and the respiratory chain (for NADH) challenges the application of the rBOX pathway in this organelle. These are two critical pathways for the general metabolism of the cell, and interfering with them to increase the flux of metabolites and co-factors to the pathway can result in phenotypes unsuitable for industrial applications. I also expanded the number of experimentally validated MTS and showed two new MTS that can be used to target this organelle. Nevertheless, and as observed in this study, not all enzymes are suitable for mitochondrial expression due to limitations during import, interference with critical mitochondrial processes or production of toxic compounds. For future projects targeting the mitochondria for production, using inducible or glucose-repressed promoters might be an interesting strategy to prevent toxicity. This way higher biomass can be achieved without compromising cell viability during the growth phase, and then we can start production. This approach was used to produce 8-hydroxygeraniol and sabinene (Yee, DeNicola et al. 2019, Jia, Chen et al. 2020).

5.4 Perspective and limitations

The main objective of this study was to extend the length of the products from the rBOX and increase the titres with this pathway in *S. cerevisiae*.

I successfully extended the products of this pathway by one cycle, producing significant titres of octanoic for the first time in this organism via rBOX. However, the highest octanoic acid titres (58.32 ±1.06 mg/L) and MCFOH titers are still low compared to those obtained via modified

Fas1 (Gajewski, Pavlovic et al. 2017, Henritzi, Fischer et al. 2018). I identified pathway variants that resulted in the specific production of butyric acid (>95% of the pathway's products) and hexanoic acid (>60% of the pathway's products). Nevertheless, expressing the octanoic acid-producing variants results in octanoic acid representing 36% or less of the pathway products. Gajewski *et al.* (2017) reached an octanoic acid yield of 85% by mutating Fas1. We should test additional enzyme combinations and reduce competing pathways to (i) increase the percentage of the desired MCFA and (ii) further increase the length of the products. In the case of MCFOH, we should test CARs and aldehyde/alcohol reductases with a substrate affinity for compounds longer than hexanoyl-CoA and a higher catalytic rate for medium-chain fatty acyl-CoAs.

In addition, the MCFA and MCFOH titres from the rBOX reported in *E. coli* are usually higher than in yeast (Kim, Clomburg et al. 2015, Henritzi, Fischer et al. 2018, Tan, Yoon et al. 2018, Chen and Gonzalez 2023). In fact, similarly to octanoic acid, the best titers of 1-octanol in *S. cerevisiae* were obtained via mutating Fas1 (Henritzi, Fischer et al. 2018), an enzyme that is endogenous to this yeast. Thus, it is possible that the enzymes used for the rBOX, usually of bacterial origin, work at suboptimal conditions in *S. cerevisiae*. Besides testing additional enzymes for each reaction, searching for enzymes from fungi that grow optimally at 30ºC would be interesting. For example, a search for 'fatty acid metabolism' in the KEGG database reveals that *Y. lipolytica*'s mitochondria harbour interesting Coenzyme A-utilising reactions similar to those in the rBOX. Two enzymes catalysing these reactions, ^{Yl}Had and ^{Yl}Ech, were used in this study. In the case of ^{Yl}Ech, it was critical to produce octanoic acid.

Deleting *GPD2* in VSY0 increased cytosolic NADH and improved the activity of the rBOX pathway. However, ethanol and glycerol remained a significant fraction of the fermentation products, with $Y_{ETOH/S}$ and $Y_{GLYOH/S}$ being up to 30-fold higher than $Y_{MCFA/S}$ in some cases (**Table 30**). These modifications also reduced the cell fitness and resulted in a higher product toxicity compared to a *S. cerevisiae* strain in Gajewski *et al.* (2017), which produced almost 4-fold more octanoic acid via mutated Fas1 having all the fermentation pathways intact.

Mth1 was mutated to increase the carbon flux to the mitochondria and expressed mitochondria-targeted variants of the rBOX to produce 1-butanol and butyric acid. However, expressing rBOX in the mitochondria (**Figure 35** and **Figure 37**) did not lead to higher butyric acid titres than in the cytosol (**Figure 14**). In addition, altering the mitochondrial NADH metabolism to improve the activity of the rBOX in that organelle resulted in a growth phenotype (**Figure 36**), which is not desired for large-scale. Therefore, further strain improvements should focus on the cytosol.

If we aim for a large-scale production process with strains using the rBOX, we need to make the large-scale fermentation economically feasible. In this work, the best $Y_{MCFA/S}$ are 0.0061

(**Table 30**), and the highest titres are 74.58 ± 0.39 mg/L of hexanoic acid for GDY27. Geno Inc. (former Genomatica Inc.) produced 1,4-butanediol in *E. coli* at large-scale with a Y_{PS}= 0.35 (g/g) (Burgard, Burk et al. 2016). DuPont produced 130 g/L of 1,3-propanediol in *E. coli* at large-scale with a Y_{PS}= 0.51 (g/g) (Nakamura and Whited 2003). Titres and yields at large-scale are usually higher than at lab-scale due to better controlled conditions. Nevertheless, titres above 5 g/L at lab-scale are usually desired to scale up a production process (Srinivasan and Smolke 2020). This titre requirement can vary depending on the value of the product. If we take as example the bulk chemical farnesene, Amyris Inc. already scaled up their strain once it reached 1- 1.2 g/L in 96 deep well plates and shake flasks (Meadows, Hawkins et al. 2016).

Overall, future strain engineering efforts in *S. cerevisiae* should focus on improving the pathways productivity in the cytosol and particularly in reducing the product toxicity of MCFA and MCFOH, a major limitation in this work. These strain engineering strategies could be accompanied by more efficient fermentation methods, preferably compatible with large-scale fermentation processes. As an example, using a dodecane overlay improves the extraction of longer MCFA (Zhu, Hu et al. 2020) and MCFOH (Henritzi, Fischer et al. 2018, Yan, Cordell et al. 2022) while favouring *in situ* recovery.

6 Deutsche Zusammenfassung

Mikroben sind die vielfältigsten lebenden Organismen auf der Erde. Ihre Vielfalt und weite Verbreitung haben zu unterschiedlichen Stoffwechselanpassungen geführt, die ihnen die Fähigkeit verleihen, unter verschiedenen Bedingungen zu leben, giftige Stoffe besser zu vertragen und Verbindungen mit unterschiedlicher chemischer Komplexität zu produzieren. Die mikrobielle Biotechnologie macht sich die Stoffwechselvielfalt der Mikroorganismen zunutze, um Produkte für verschiedene Industriezweige herzustellen, darunter Lebensmittel, Arzneimittel und Chemikalien. Heute gibt es eine Vielzahl von Produkten der mikrobiellen Biotechnologie, von Waschmitteln mit rekombinanten Proteasen über Impfstoffe gegen das Hepatitis-B-Virus bis hin zu Laktasepillen zur Behandlung von Laktoseintoleranz. Die mikrobielle Produktion von Massenchemikalien wie Alkoholen oder Säuren stellt jedoch nach wie vor eine Herausforderung dar, da die Ausbeute gering und die Kosten im Vergleich zur Herstellung dieser Verbindungen durch chemische Synthese hoch sind.

Die chemische Industrie ist ein bedeutender Energieverbraucher und Kohlendioxid-Emittent. Darüber hinaus verursachen einige der in dieser Industrie verwendeten Extraktionsverfahren aus pflanzlichen Komponenten dauerhafte Schäden an natürlichen Ökosystemen, wie z.B. die Extraktion mittelkettiger Fettsäuren (MCFA). MCFA sind Carbonsäuren mit Kohlenwasserstoffketten mit sechs bis zehn Kohlenstoffatomen. Sie werden in der chemischen Industrie als Ausgangsstoffe für Biokraftstoffe, als flüchtige Ester für die Lebensmittelindustrie, als Ausgangsstoffe für Tenside in der analytischen Chemie oder als Polymervorstufen für Materialien mit verbesserten Lagereigenschaften verwendet. Sie werden jedoch aus Kokos- und Palmöl und -saat gewonnen, wofür große Monokulturen von Kokos- und Palmenbäumen notwendig sind. Aus diesen Gründen ist die mikrobielle Produktion von MCFA von großem Interesse.

In der Natur werden Fettsäuren hauptsächlich über die Fettsäurebiosynthese (FAB) hergestellt. Die reverse β-Oxidation (rBOX) ist jedoch ein energieeffizienterer Weg als die FAB. Im Gegensatz zur FAB, bei der ein Acetyl-CoA zunächst unter Verwendung von ATP in die Elongationseinheit Malonyl-CoA umgewandelt wird, wird bei der rBOX Acetyl-CoA direkt als Elongationseinheit verwendet. Der rBOX-Weg besteht aus vier Reaktionen, die in jedem Zyklus zur Verlängerung eines Acyl-CoA-Moleküls um zwei Kohlenstoffeinheiten führen. Der Stoffwechselweg beginnt mit einer nicht-decarboxylativen Claisen-Kondensationsreaktion, die durch eine Thiolase katalysiert wird. In dieser Reaktion gibt Acetyl-CoA zwei Kohlenstoffeinheiten an ein Acyl-CoA-Molekül ab, wodurch ein β-Ketoacyl-CoA entsteht. Das β-Ketoacyl-CoA wird anschließend durch eine β-Hydroxyacyl-CoA-Dehydrogenase in einer NADH-verbrauchenden Reaktion zu 3-Hydroxyacyl-CoA reduziert. Das 3-Hydroxyacyl-CoA

wird dann durch eine Enoyl-CoA-Hydratase zu trans-Δ2-Enoyl-CoA dehydriert. Schließlich wird die Doppelbindung am α-Kohlenstoff des trans-Δ2-Enoyl-CoA durch eine trans-Enoyl-CoA-Reduktase reduziert, wodurch ein Acyl-CoA-Molekül entsteht und NAD^+ regeneriert wird. Dieses Acyl-CoA-Molekül kann für einen neuen Elongationszyklus benutzt, von einem Terminationsenzym verwendet oder in einem anderen Stoffwechselweg verarbeitet werden, um eine Vielzahl von Produkten wie Alkohole, Säuren, Polyketide oder flüchtige Ester zu erzeugen.

Saccharomyces cerevisiae ist ein robuster Mikroorganismus, der eine höhere Toleranz gegenüber toxischen Verbindungen aufweist als viele andere industrielle Organismen und sich in der Biotechnologie gut etabliert hat. Diese Hefe dient als industrieller Produzent von hochwertigen Produkten wie Impfstoffen und Arzneimitteln, aber auch von Produkten mit geringem Wert wie Ethanol. Darüber hinaus ist sie aufgrund ihrer genetischen Zugänglichkeit der ideale Organismus für die Einführung neuer Stoffwechselmerkmale zur Erhöhung der Produktionstiter.

In dieser Arbeit wurde der rBOX-Stoffwechselweg in *S. cerevisiae* exprimiert und der Stoffwechsel dieser Hefe so manipuliert, dass sie MCFA und mittelkettige Fettalkohole (MCFOH) produziert. In vorherigen Arbeiten führte die Expression der rBOX in *S. cerevisiae* zu 1-Butanol mit vier Kohlenstoffatomen als Produkt mit den besten Titern und zu Hexanoyl-CoA mit sechs Kohlenstoffatomen, dem Produkt aus zwei Zyklen der rBOX, als längstes Produkt. Im ersten Teil dieser Arbeit wurden drei Strategien des *Metabolic Engineering* kombiniert, um die Länge der Produkte aus der Expression der rBOX im Cytosol zu erweitern: (1) Es wurde ein Plattform-Produktionsstamm mit einem optimierten NADH-Metabolismus entwickelt, (2) verschiedene Enzymkombinationen des rBOX Stoffwechselweges, die zu den gewünschten Produkten führten, wurden gescreent, und (3) die Eliminierung konkurrierender Reaktionen und die Optimierung der Fermentationsbedingungen wurden getestet. Anschließend wurde der resultierende Stamm verwendet, um zwei verschiedene MCFOH-synthetisierende Enzyme zu testen und die Produktpalette um MCFOH zu erweitern. Im zweiten Teil der Arbeit wurde die Kompartimentierung der Stoffwechselwege in den Mitochondrien untersucht, um die Aktivität der rBOX zu verbessern.

Im ersten Ansatz wurde die Verfügbarkeit von NADH für den Stoffwechselweg optimiert. Die Oxidation von NADH ist ein wichtiger Treiber des rBOX Stoffwechselweges. Im Wildtyp von *S. cerevisiae* wird das in der Glykolyse produzierte NADH jedoch hauptsächlich durch Ethanol- und Glycerin-Gärung zu NAD^+ reoxidiert. Um die Konkurrenz um NADH aus den Fermentationsreaktionen zu reduzieren, wurde ein Alkoholdehydrogenase-defizienter Stamm, VSY0 (Δ*adh1-5*), verwendet. In diesem Stamm wurde die Expression von zwei rBOX-Wegvarianten mit entweder ^{Cn}bktB aus *Cupriavidus necator* oder nativem *ERG10* als Thiolase

verglichen. Beide Varianten enthielten ^{Ca}hbd und ^{Ca}crt aus *Clostridium acetobutylicum* als β-Hydroxyacyl-CoA-Dehydrogenase bzw. Enoyl-CoA-Hydratase und ^{Td}Ter aus *Treponema denticola* als trans-Enoyl-CoA-Reduktase. Das Experiment ergab hohe Glycerin- und Buttersäuregehalte, was darauf hindeutet, dass ein erheblicher Teil des NADH durch die Glycerinfermentation oxidiert wurde. Die Deletion von *GPD2*, der wichtigsten Glycerinphosphatdehydrogenase, wodurch der Stamm GDY15 (Δ*adh1-5,* Δ*gpd2*) entstand, verbesserte den Wachstumsphänotyp und verringerte die Glycerinproduktion,. Die Deletion von *GPD2* erhöhte die Stoffwechselaktivität, verdoppelte den Buttersäuretiter und erhöhte den Hexansäuretiter um 59 %. Die Hexansäure erreichte jedoch nur eine Konzentration von 2 mg/L und Buttersäure blieb das Hauptprodukt der rBOX.

Die zweite Strategie konzentrierte sich auf die Erprobung neuer Kombinationen von Enzymen zur Verbesserung der MCFA-Produktion in GDY15, einem Stamm mit erhöhtem cytosolischem NADH. ^{Cn}BktB wurde als Thiolase in allen Varianten des Stoffwechselwegs verwendet, die von Plasmiden in GDY15 exprimiert wurden. Die Produkte des Stoffwechselweges wurden durch die Expression der β-Hydroxyacyl-CoA-Dehydrogenasen ^{Ca}*hbd* oder ^{Yl}*HAD* (*Y. lipolytica*) auf Buttersäure beschränkt. Andererseits war die Expression von ^{Cn}*paaH1* (*C. necator*) wesentlich für die Produktion von MCFA. Durch die Kombination von ^{Cn}*bktB*, ^{Cn}*paaH1*, ^{Ca}*crt* und ^{Td}*ter* wurde zum ersten Mal Hexansäure als Hauptprodukt produziert (≈ 30 mg/L). Octansäure wurde erstmals mit der rBOX in *S. cerevisiae* durch die Kombination von ^{Cn}*bktB*, ^{Cn}*paaH1* und ^{Td}*ter* mit den Enoyl-CoA-Reduktasen ^{Cn}*crt2* (*C. necator*) oder ^{Yl}*ECH* (*Y. lipolytica*) hergestellt und wurde zum Hauptprodukt dieser rBOX-Variante. Ähnliche Titer von Octansäure (≈ 40 mg/L) wurden entweder mit ^{Cn}*crt2* oder ^{Yl}*ECH* erzielt, wobei das Verhältnis von Octansäure zu Hexansäure bei ^{Cn}*crt2* etwas höher war. Das Produktionsmuster wurde durch die getesteten trans-Enoyl-CoA-Reduktasen (^{Eg}*ter* oder ^{Td}*ter*) nicht beeinflusst, aber mit ^{Td}Ter wurden insgesamt höhere Produktionstiter beobachtet. Schließlich wurde festgestellt, dass die Oktansäure produzierenden Stämme schlechter wuchsen als die Hexansäure und Buttersäure produzierenden Stämme, was auf einen Zusammenhang zwischen der Länge der produzierten MCFA und der Toxizität schließen lässt.

Um die MCFA-Produktion weiter zu steigern, wurden verschiedene Ansätze getestet. Zunächst wurde die Verfügbarkeit der Vorstufe Butyryl-CoA durch Koexpression eines Octanoyl-CoA produzierenden Stoffwechselweges (^{Cn}*bktB*, ^{Cn}*paaH1*, ^{Cn}*crt2*, ^{Td}*ter*) mit einer Butyryl-CoA produzierenden Variante (*ERG10,* ^{Ca}*hbd,* ^{Ca}*crt*, ^{Td}*ter*) auf Plasmiden und im Stamm GDY15 erhöht. Diese Strategie führte zu einem Anstieg des Hexansäuretiters um 23 %, während die Produktion von Octansäure und Decansäure nicht beeinflusst wurde. Das Hauptprodukt dieses Ansatzes war jedoch Buttersäure. Im zweiten Ansatz wurden die kurzkettigen Acyl-CoA-Thioesterasen *TES1* und die mittelkettige Fettsäureacyl-CoA-Synthetase *FAA2*

ausgeschaltet, um die Konkurrenz um Butyryl-CoA bzw. den Abbau der produzierten Fettsäuren zu verhindern. Die MCFA- oder Buttersäure-Titer wurden jedoch durch die Deletion von *TES1* oder *FAA2* nicht beeinflusst. Im dritten Ansatz wurde die Produktion von MCFA in synthetischem Medium (SM), einem gleichmäßig gepufferten (YPD-20 mM) oder einem stark gepufferten komplexen Medium (YPD-100 mM) verglichen. Für diesen Vergleich wurden die Hexansäure produzierenden Varianten (^{Cn}*bktB*, ^{Cn}*paaH1*, ^{Ca}*crt*, ^{Td}*ter*) und die Oktansäure produzierenden Varianten (^{Cn}*bktB*, ^{Cn}*paaH1*, ^{Cn}*crt2 or* ^{Yl}*ECH*, ^{Td}*ter*) in das Genom von GDY15 integriert. Die höchsten MCFA-Titer nach 50 Stunden wurden durch die Integration der Varianten in das Genom und die Fermentation in YPD-100 mM erzielt. Bei dem Hexansäure produzierenden Stamm wurde ein Titer von ≈ 75 mg/L Hexansäure erreicht, während bei den Octansäure produzierenden Stämmen GDY28 und GDY29 ein Titer von ≈ 60 mg/L Octansäure erreicht wurde. In beiden Fällen handelt es sich um die höchsten Titer von Hexan- und Octansäure, die in *S. cerevisiae* mit der rBOX berichtet wurden. Die Buttersäuretiter waren jedoch auch in YPD-100 mM erhöht, mit ≈ 60 mg/L in GDY27 und ≈ 40 mg/L in den Octansäure produzierenden Stämmen, was auf eine Verbesserung der Produktspezifität schließen lässt. Außerdem wurde bei den Octansäure produzierenden Stämmen erneut ein verringertes Wachstum beobachtet.

Die Expression von zwei dualen Acyl-CoA-Reduktasen/Alkohol-Dehydrogenasen (ACR/ADH), ^{Ca}*adhE2* aus *Clostridium acetobutylicum* und die mutmaßliche ACR/ADH ^{Ec}*eutE* aus *Escherichia coli*, wurde getestet, um die Produktpalette des Stoffwechselweges zu mittelkettigen Fettalkoholen (MCFOH) zu erweitern. Beide Enzyme wurden durch Plasmide in dem Octanoyl-CoA produzierenden Stamm GDY29 exprimiert. Zum ersten Mal wurden 1-Hexanol und 1-Octanol mit diesen Enzymen in *S. cerevisiae* produziert. Die Titer waren jedoch niedrig (unter 10 mg/L bzw. 2 mg/L) und 1-Butanol war in beiden Fällen das Hauptprodukt mit Titern über 80 mg/L. Dies zeigt die Präferenz dieser beiden Enzyme für Butyryl-CoA. Die MCFA-Titer sanken bei Expression von ^{Ca}AdhE2 oder ^{Ec}EutE, was wahrscheinlich auf die Konkurrenz der rBOX um Butyryl-CoA zurückzuführen ist. Ein interessanter Ansatz ist der Test von Carbonsäurereduktasen (CARs), da diese Fettsäuren zu Aldehyden reduzieren können, die wiederum durch endogene oder heterologe Alkoholdehydrogenasen weiter zu Fettalkoholen reduziert werden können. Damit wäre die Konkurrenz zu den Zwischenprodukten in der rBOX ausgeschaltet.

Im zweiten Teil dieser Arbeit wurde die Kompartimentierung der rBOX in den Mitochondrien von *S. cerevisiae* untersucht. Die Mitochondrien verfügen über hohe Acetyl-CoA-Konzentrationen und ein reduzierendes Milieu, das für die NADH-verbrauchenden Reaktionen in der rBOX geeignet ist. Daher sollte dieses Organell genutzt werden, um die Aktivität und die Titer des Stoffwechselweges zu verbessern. Zu diesem Zweck wurde (1) der

Glucosestoffwechsel so verändert, dass der Kohlenstoffffluss in die Mitochondrien verlagert wurde, und (2) eine Butyryl-CoA-produzierende rBOX-Variante gezielt in die Mitochondrien eingeführt, wobei die Produktion von 1-Butanol und Buttersäure als Konzeptnachweis diente.

Der Crabtree-Effekt ist die Bevorzugung der Fermentation gegenüber der Atmung, um unter aeroben Bedingungen Energie zu erzeugen. In Hefe ist der Crabtree-Effekt stark mit der Aufnahme von Hexosen verbunden. Daher wurde im ersten Ansatz die Regulation von Mth1, einem Transkriptionsfaktor, der die Expression von Hexosetransportern steuert, verändert, um den Crabtree-Effekt in *S. cerevisiae* zu beseitigen und den Kohlenstoffffluss zu den Mitochondrien zu erhöhen. Das Wachstum des resultierenden Stammes GDY1 (∆*adh1-5,* $MTH1_{\Delta 169\text{-}393}$) erholte sich auf WT-Niveau und die Fermentation wurde unter semi-aeroben Bedingungen mit hohem Glukosegehalt deutlich reduziert. Eine ähnliche Verringerung des Crabtree-Effekts wurde beim ∆*adh1-5,* ∆*gpd2*-Stamm GDY15 beobachtet. Allerdings war die Wachstumserholung nicht so ausgeprägt wie beim GDY1-Stamm. Durch die Kombination beider Deletionen (GDY2: ∆*adh1-5,* ∆*gpd2,* $MTH1_{\Delta 169\text{-}393}$) wurde die Glycerinproduktion reduziert, das Wachstum jedoch nicht beeinträchtigt. Die Alkoholacyltransferase *EAT1* aus *Kluyveromyces marxianus* wurde in den Mitochondrien der verschiedenen Stämme exprimiert, um den erhöhten Kohlenstoffffluss zu den Mitochondrien zu validieren. Isoamylacetat wird von Eat1 aus Acetyl-CoA und Isoamylalkohol synthetisiert, einem Produkt des Aminosäurestoffwechsels in den Mitochondrien. Höhere Isoamylacetattiter wurden bei Stämmen mit der Mutation $MTH1_{\Delta 169\text{-}393}$ beobachtet.

Im zweiten Ansatz wurden schwache oder starke Promotoren verwendet, um verschiedene Butyryl-CoA-produzierende Varianten zu exprimieren, und die *MTH1*-Mutantenstämme GDY1 und GDY2 wurden als Expressionsplattformen verwendet. ACR/ADH ^{Ec}*eutE* und ^{Ca}*adhE2* wurden in den Mitochondrien (^{Ca}$adhE2_{MT}$ und ^{Ec}$eutE_{MT}$) einzeln oder kombiniert exprimiert, um 1-Butanol zu produzieren. Die starke Expression aller Enzyme war toxisch für die Zellen, und die höchsten Buttersäuretiter (≈ 50 mg/L) in den Mitochondrien aus der rBOX wurden durch die schwache Expression von $ERG10_{MT}$ ^{Ca}hbd_{MT}, ^{Ca}crt_{MT}, ^{Td}ter_{MT}, ^{Ec}$eutE_{MT}$ und ^{Ca}$adhE2_{MT}$ erhalten. Anschließend wurde die Expression der mitochondrialen NADH-Oxidase *NDI1* herunterreguliert, um die Konkurrenz um mitochondriales NADH zu verringern. Diese Herunterregulierung führte zu den höchsten 1-Butanol-Titern bei der Expression des Signalwegs in den Mitochondrien. Allerdings führte die Herunterregulierung von *NDI1* auch zu einem unerwünschten *Petite*-Phänotyp. In diesem *NDI1*-herunterregulierten Stamm wurden die besten 1-Butanol-Titer (≈ 5 mg/L) durch starke Expression von $ERG10_{MT}$ und ^{Td}ter_{MT} und durch schwache Expression von ^{Ca}hbd_{MT}, ^{Ca}crt_{MT} und ^{Ca}$adhE2_{MT}$ erhalten.

Zusammenfassend lässt sich sagen, dass in dieser Arbeit erstmals erfolgreich Hexan- und Oktansäure in *S. cerevisiae* mit der rBOX hergestellt werden konnte. Darüber hinaus wurden

für einige in der rBOX verwendete Enzyme neue Substratspezifitäten entdeckt. Dennoch sollten weitere *Metabolic Engineering*-Strategien eingesetzt werden, um die Produktspezifität zu verbessern und die Produkttoxizität zu verringern. Weiterhin wurde der Kohlenstoffffluss zu den Mitochondrien erhöht, indem *S. cerevisiae* in eine Crabtree-negative Hefe umgewandelt wurde, und die rBOX wurde erfolgreich in den Mitochondrien kompartimentiert. Allerdings schränkt die Konkurrenz durch mitochondriale NADH- und Acetyl-CoA-verbrauchende Reaktionen, von denen einige für die Lebensfähigkeit der Zellen unerlässlich sind, die Verwendung dieser Organelle für die rBOX ein.

7 References

1. Aguilera-Méndez, A., C. Fernández-Lainez, I. Ibarra-González, C. Fernandez-Mejia, H. Hayashi, B. Do, M. H. Ahmed, L. Bettendorff, K. Shibata, T. Fukuwatari, D. L. Lildballe, T. Yagi, M. Rychlik, C. Sanchez-Moreno, R. Agarwal, F. Ahmed, J. R. Guyton, F. Bamonti, R. Prakash, J. Dierkes, C. Antoniades, Y. Kohda, S. Fushinobu, C. Fernandez-Mejia, D. Gaso-Sokac, J. Zempleni, A. Lebiedzinska, S. H. Lee, N. M. Zahr, H. Zielinski, M. A. Segundo, R. Goldschmidt, M. S. Thakur, T. Apeland, A. S. Hazell, A. Szutowicz, J. Ishihara, A. Chango, K. Koyama, J. Luo, C. M. Gomes, D. Woollard, M. Zielinska-Dawidziak, T. Nitto, G. Sanna, J.-a. A. Ho, D. P. Perrone, A. Chango, K. Shibata, C. Antoniades, P. Chen and R. Clarke (2012). The Chemistry and Biochemistry of Niacin (B3). B Vitamins and Folate: Chemistry, Analysis, Function and Effects. V. R. Preedy, The Royal Society of Chemistry**:** 0.
2. Ahn, J. H., H. Seo, W. Park, J. Seok, J. A. Lee, W. J. Kim, G. B. Kim, K.-J. Kim and S. Y. Lee (2020). "Enhanced succinic acid production by Mannheimia employing optimal malate dehydrogenase." Nature Communications **11**(1): 1970.
3. Ahuatzi, D., A. Riera, R. Pela´ez, P. Herrero and F. Moreno (2007). "Hxk2 Regulates the Phosphorylation State of Mig1 and Therefore Its Nucleocytoplasmic Distribution*." Journal of Biological Chemistry **282**(7): 4485-4493.
4. Akhtar, M. K., H. Dandapani, K. Thiel and P. R. Jones (2015). "Microbial production of 1-octanol: A naturally excreted biofuel with diesel-like properties." Metab Eng Commun **2**: 1-5.
5. Akhtar, M. K., N. J. Turner and P. R. Jones (2013). "Carboxylic acid reductase is a versatile enzyme for the conversion of fatty acids into fuels and chemical commodities." Proc Natl Acad Sci U S A **110**(1): 87-92.
6. Akyalçın, S. and M. R. Altıokka (2012). "Kinetics of esterification of acetic acid with 1-octanol in the presence of Amberlyst 36." Applied Catalysis A: General **429-430**: 79-84.
7. Al-Saryi, N. A., M. Y. Al-Hejjaj, C. W. T. van Roermund, G. E. Hulmes, L. Ekal, C. Payton, R. J. A. Wanders and E. H. Hettema (2017). "Two NAD-linked redox shuttles maintain the peroxisomal redox balance in Saccharomyces cerevisiae." Scientific Reports **7**(1): 11868.
8. Almgren, M. and S. Rangelov (2004). "Spontaneously formed nonequilibrium vesicles of cetyltrimethylammonium bromide and sodium octyl sulfate in aqueous dispersions." Langmuir **20**(16): 6611-6618.
9. Anderson, A. J., T. D. Jackson, D. A. Stroud and D. Stojanovski (2019). "Mitochondria-hubs for regulating cellular biochemistry: emerging concepts and networks." Open Biol **9**(8): 190126.
10. Andorfer, M. C., L. R. F. Backman, P. L. Li, E. C. Ulrich and C. L. Drennan (2021). "Rescuing activity of oxygen-damaged pyruvate formate-lyase by a spare part protein." Journal of Biological Chemistry **297**(6): 101423.
11. André, A. C., L. Debande and B. S. Marteyn (2021). "The selective advantage of facultative anaerobes relies on their unique ability to cope with changing oxygen levels during infection." Cell Microbiol **23**(8): e13338.
12. Ansell, R., K. Granath, S. Hohmann, J. M. Thevelein and L. Adler (1997). "The two isoenzymes for yeast NAD+-dependent glycerol 3-phosphate dehydrogenase encoded by GPD1 and GPD2 have distinct roles in osmoadaptation and redox regulation." EMBO J **16**(9): 2179-2187.
13. Aouida, M., M. Rubio-Texeira, J. M. Thevelein, R. Poulin and D. Ramotar (2013). "Agp2, a member of the yeast amino acid permease family, positively regulates polyamine transport at the transcriptional level." PLoS One **8**(6): e65717.
14. Ashok, B., K. Nanthagopal, V. Anand, K. M. Aravind, A. K. Jeevanantham and S. Balusamy (2019). "Effects of n-octanol as a fuel blend with biodiesel on diesel engine characteristics." Fuel **235**: 363-373.
15. Aslankoohi, E., M. N. Rezaei, Y. Vervoort, C. M. Courtin and K. J. Verstrepen (2015). "Glycerol production by fermenting yeast cells is essential for optimal bread dough fermentation." PLoS One **10**(3): e0119364.
16. Atsumi, S., A. F. Cann, M. R. Connor, C. R. Shen, K. M. Smith, M. P. Brynildsen, K. J. Chou, T. Hanai and J. C. Liao (2008). "Metabolic engineering of Escherichia coli for 1-butanol production." Metab Eng **10**(6): 305-311.
17. Avalos, J. L., G. R. Fink and G. Stephanopoulos (2013). "Compartmentalization of metabolic pathways in yeast mitochondria improves the production of branched-chain alcohols." Nat Biotechnol **31**(4): 335-341.

18. Baeshen, N. A., M. N. Baeshen, A. Sheikh, R. S. Bora, M. M. Ahmed, H. A. Ramadan, K. S. Saini and E. M. Redwan (2014). "Cell factories for insulin production." Microb Cell Fact **13**: 141.
19. Bakker, B. M., C. Bro, P. Kötter, M. A. Luttik, J. P. van Dijken and J. T. Pronk (2000). "The mitochondrial alcohol dehydrogenase Adh3p is involved in a redox shuttle in Saccharomyces cerevisiae." J Bacteriol **182**(17): 4730-4737.
20. Bakker, B. M., K. M. Overkamp, A. J. van Maris, P. Kotter, M. A. Luttik, J. P. van Dijken and J. T. Pronk (2001). "Stoichiometry and compartmentation of NADH metabolism in Saccharomyces cerevisiae." FEMS Microbiol Rev **25**(1): 15-37.
21. Barker, H. A., M. D. Kamen and B. T. Bornstein (1945). "The Synthesis of Butyric and Caproic Acids from Ethanol and Acetic Acid by Clostridium Kluyveri." Proc Natl Acad Sci U S A **31**(12): 373-381.
22. Baumann, L., T. Doughty, V. Siewers, J. Nielsen, E. Boles and M. Oreb (2021). "Transcriptomic response of Saccharomyces cerevisiae to octanoic acid production." FEMS Yeast Research **21**(2).
23. Beber, M. E., M. G. Gollub, D. Mozaffari, K. M. Shebek, Avi I. Flamholz, R. Milo and E. Noor (2021). "eQuilibrator 3.0: a database solution for thermodynamic constant estimation." Nucleic Acids Research **50**(D1): D603-D609.
24. Behera, B. C. (2020). "Citric acid from Aspergillus niger: a comprehensive overview." Crit Rev Microbiol **46**(6): 727-749.
25. Bekers, K. M., J. J. Heijnen and W. M. van Gulik (2015). "Determination of the in vivo NAD:NADH ratio in Saccharomyces cerevisiae under anaerobic conditions, using alcohol dehydrogenase as sensor reaction." Yeast **32**(8): 541-557.
26. Bergman, A., V. Siewers, J. Nielsen and Y. Chen (2016). "Functional expression and evaluation of heterologous phosphoketolases in Saccharomyces cerevisiae." AMB Express **6**(1): 115.
27. Bhattacharya, S., B. D. Esquivel and T. C. White (2018). "Overexpression or Deletion of Ergosterol Biosynthesis Genes Alters Doubling Time, Response to Stress Agents, and Drug Susceptibility in Saccharomyces cerevisiae." mBio **9**(4): 10.1128/mbio.01291-01218.
28. Bideaux, C., S. Alfenore, X. Cameleyre, C. Molina-Jouve, J. L. Uribelarrea and S. E. Guillouet (2006). "Minimization of glycerol production during the high-performance fed-batch ethanolic fermentation process in Saccharomyces cerevisiae, using a metabolic model as a prediction tool." Appl Environ Microbiol **72**(3): 2134-2140.
29. Biebl, H. (1999). CLOSTRIDIUM | Clostridium Acetobutylicum. Encyclopedia of Food Microbiology. R. K. Robinson. Oxford, Elsevier**:** 445-451.
30. Bokulich, N. A. and C. W. Bamforth (2013). "The microbiology of malting and brewing." Microbiol Mol Biol Rev **77**(2): 157-172.
31. Boos, F., L. Krämer, C. Groh, F. Jung, P. Haberkant, F. Stein, F. Wollweber, A. Gackstatter, E. Zöller, M. van der Laan, M. M. Savitski, V. Benes and J. M. Herrmann (2019). "Mitochondrial protein-induced stress triggers a global adaptive transcriptional programme." Nat Cell Biol **21**(4): 442-451.
32. Borrull, A., G. Lopez-Martinez, M. Poblet, R. Cordero-Otero and N. Rozes (2015). "New insights into the toxicity mechanism of octanoic and decanoic acids on Saccharomyces cerevisiae." Yeast **32**(5): 451-460.
33. Bourgarel, D., C. C. Nguyen and M. Bolotin-Fukuhara (1999). "HAP4, the glucose-repressed regulated subunit of the HAP transcriptional complex involved in the fermentation-respiration shift, has a functional homologue in the respiratory yeast Kluyveromyces lactis." Mol Microbiol **31**(4): 1205-1215.
34. Bro, C., B. Regenberg and J. Nielsen (2004). "Genome-wide transcriptional response of a Saccharomyces cerevisiae strain with an altered redox metabolism." Biotechnol Bioeng **85**(3): 269-276.
35. Burgard, A., M. J. Burk, R. Osterhout, S. Van Dien and H. Yim (2016). "Development of a commercial scale process for production of 1,4-butanediol from sugar." Current Opinion in Biotechnology **42**: 118-125.
36. Canelas, A. B., W. M. van Gulik and J. J. Heijnen (2008). "Determination of the cytosolic free NAD/NADH ratio in Saccharomyces cerevisiae under steady-state and highly dynamic conditions." Biotechnol Bioeng **100**(4): 734-743.
37. Cantu, D. C., Y. Chen and P. J. Reilly (2010). "Thioesterases: a new perspective based on their primary and tertiary structures." Protein Sci **19**(7): 1281-1295.

38. Cardenas, J. and N. A. Da Silva (2016). "Engineering cofactor and transport mechanisms in Saccharomyces cerevisiae for enhanced acetyl-CoA and polyketide biosynthesis." Metabolic Engineering **36**: 80-89.
39. Carman, G. M. and G. S. Han (2011). "Regulation of phospholipid synthesis in the yeast Saccharomyces cerevisiae." Annu Rev Biochem **80**: 859-883.
40. Celińska, E. and W. Grajek (2009). "Biotechnological production of 2,3-butanediol—Current state and prospects." Biotechnology Advances **27**(6): 715-725.
41. Chacinska, A., C. M. Koehler, D. Milenkovic, T. Lithgow and N. Pfanner (2009). "Importing mitochondrial proteins: machineries and mechanisms." Cell **138**(4): 628-644.
42. Chen, J. and R. Gonzalez (2023). "Engineering Escherichia coli for selective 1-decanol production using the reverse β-oxidation (rBOX) pathway." Metabolic Engineering **79**: 173-181.
43. Chen, Y., F. Li, J. Guo, G. Liu, X. Guo and D. Xiao (2014). "Enhanced ethyl caproate production of Chinese liquor yeast by overexpressing EHT1 with deleted FAA1." J Ind Microbiol Biotechnol **41**(3): 563-572.
44. Cheon, Y., J. S. Kim, J. B. Park, P. Heo, J. H. Lim, G. Y. Jung, J. H. Seo, J. H. Park, H. M. Koo, K. M. Cho, J. B. Park, S. J. Ha and D. H. Kweon (2014). "A biosynthetic pathway for hexanoic acid production in Kluyveromyces marxianus." J Biotechnol **182-183**: 30-36.
45. Cherry, J. M., E. L. Hong, C. Amundsen, R. Balakrishnan, G. Binkley, E. T. Chan, K. R. Christie, M. C. Costanzo, S. S. Dwight, S. R. Engel, D. G. Fisk, J. E. Hirschman, B. C. Hitz, K. Karra, C. J. Krieger, S. R. Miyasato, R. S. Nash, J. Park, M. S. Skrzypek, M. Simison, S. Weng and E. D. Wong (2012). "Saccharomyces Genome Database: the genomics resource of budding yeast." Nucleic Acids Res **40**(Database issue): D700-705.
46. Choi, E. S., J. H. Sohn and S. K. Rhee (1994). "Optimization of the expression system using galactose-inducible promoter for the production of anticoagulant hirudin in Saccharomyces cerevisiae." Applied Microbiology and Biotechnology **42**(4): 587-594.
47. Chou, K. Y., J. Y. Lee, K. B. Kim, E. Kim, H. S. Lee and H. Y. Ryu (2023). "Histone modification in Saccharomyces cerevisiae: A review of the current status." Comput Struct Biotechnol J **21**: 1843-1850.
48. Claros, M. G. and P. Vincens (1996). "Computational method to predict mitochondrially imported proteins and their targeting sequences." Eur J Biochem **241**(3): 779-786.
49. Clomburg, J. M., S. C. Contreras, A. Chou, J. B. Siegel and R. Gonzalez (2017). "Combination of type II fatty acid biosynthesis enzymes and thiolases supports a functional beta-oxidation reversal." Metab Eng **45**: 11-19.
50. Cooper, G. M. (2000). "The Cell: A Molecular Approach. Sunderland (MA) Sinauer Associates." Structure and Organization of Actin Filaments.
51. Crabtree, H. G. (1929). "Observations on the carbohydrate metabolism of tumours." Biochem J **23**(3): 536-545.
52. Croft, T., P. Venkatakrishnan and S.-J. Lin (2020). "NAD+ Metabolism and Regulation: Lessons From Yeast." Biomolecules **10**(2): 330.
53. Dai, Z., M. Huang, Y. Chen, V. Siewers and J. Nielsen (2018). "Global rewiring of cellular metabolism renders Saccharomyces cerevisiae Crabtree negative." Nature Communications **9**(1): 3059.
54. Day, M. (2013). "Yeast petites and small colony variants: for everything there is a season." Adv Appl Microbiol **85**: 1-41.
55. de Castro, E., C. J. Sigrist, A. Gattiker, V. Bulliard, P. S. Langendijk-Genevaux, E. Gasteiger, A. Bairoch and N. Hulo (2006). "ScanProsite: detection of PROSITE signature matches and ProRule-associated functional and structural residues in proteins." Nucleic Acids Res **34**(Web Server issue): W362-365.
56. de Smidt, O., J. C. du Preez and J. Albertyn (2012). "Molecular and physiological aspects of alcohol dehydrogenases in the ethanol metabolism of Saccharomyces cerevisiae." FEMS Yeast Res **12**(1): 33-47.
57. Dekishima, Y., E. I. Lan, C. R. Shen, K. M. Cho and J. C. Liao (2011). "Extending carbon chain length of 1-butanol pathway for 1-hexanol synthesis from glucose by engineered Escherichia coli." J Am Chem Soc **133**(30): 11399-11401.
58. Dellomonaco, C., J. M. Clomburg, E. N. Miller and R. Gonzalez (2011). "Engineered reversal of the beta-oxidation cycle for the synthesis of fuels and chemicals." Nature **476**(7360): 355-359.
59. den Brave, F., A. Gupta and T. Becker (2021). "Protein Quality Control at the Mitochondrial Surface." Frontiers in Cell and Developmental Biology **9**.

60. Deparis, Q., A. Claes, M. R. Foulquié-Moreno and J. M. Thevelein (2017). "Engineering tolerance to industrially relevant stress factors in yeast cell factories." FEMS Yeast Res **17**(4).
61. Dong, C., Z. Shi, L. Huang, H. Zhao, Z. Xu and J. Lian (2021). "Cloning and characterization of a panel of mitochondrial targeting sequences for compartmentalization engineering in Saccharomyces cerevisiae." Biotechnol Bioeng **118**(11): 4269-4277.
62. Duman-Özdamar, Z. E., V. A. P. Martins Dos Santos, J. Hugenholtz and M. Suarez-Diez (2022). "Tailoring and optimizing fatty acid production by oleaginous yeasts through the systematic exploration of their physiological fitness." Microb Cell Fact **21**(1): 228.
63. Duncan, J. D., M. E. Setati and B. Divol (2023). "Redox cofactor metabolism in Saccharomyces cerevisiae and its impact on the production of alcoholic fermentation end-products." Food Research International **163**: 112276.
64. Duran, L., J. M. López and J. L. Avalos (2020). "¡Viva la mitochondria!: harnessing yeast mitochondria for chemical production." FEMS Yeast Research **20**(6).
65. Eaglesfield, R. and K. Tokatlidis (2021). "Targeting and Insertion of Membrane Proteins in Mitochondria." Frontiers in Cell and Developmental Biology **9**.
66. Ehrenworth, A. M., M. A. Haines, A. Wong and P. Peralta-Yahya (2017). "Quantifying the efficiency of Saccharomyces cerevisiae translocation tags." Biotechnol Bioeng **114**(11): 2628-2636.
67. Elbahloul, Y. and A. Steinbuchel (2009). "Large-scale production of poly(3-hydroxyoctanoic acid) by Pseudomonas putida GPo1 and a simplified downstream process." Appl Environ Microbiol **75**(3): 643-651.
68. Elgersma, Y., C. W. van Roermund, R. J. Wanders and H. F. Tabak (1995). "Peroxisomal and mitochondrial carnitine acetyltransferases of Saccharomyces cerevisiae are encoded by a single gene." Embo j **14**(14): 3472-3479.
69. Emanuelsson, O., S. Brunak, G. von Heijne and H. Nielsen (2007). "Locating proteins in the cell using TargetP, SignalP and related tools." Nat Protoc **2**(4): 953-971.
70. Engler, C., R. Kandzia and S. Marillonnet (2008). "A one pot, one step, precision cloning method with high throughput capability." PLoS One **3**(11): e3647.
71. Fendt, S. M. and U. Sauer (2010). "Transcriptional regulation of respiration in yeast metabolizing differently repressive carbon substrates." BMC Syst Biol **4**: 12.
72. Feng, X., J. Lian and H. Zhao (2015). "Metabolic engineering of Saccharomyces cerevisiae to improve 1-hexadecanol production." Metab Eng **27**: 10-19.
73. Fiaux, J., Z. P. Cakar, M. Sonderegger, K. Wüthrich, T. Szyperski and U. Sauer (2003). "Metabolic-flux profiling of the yeasts Saccharomyces cerevisiae and Pichia stipitis." Eukaryot Cell **2**(1): 170-180.
74. Fillet, S., J. Gibert, B. Suárez, A. Lara, C. Ronchel and J. L. Adrio (2015). "Fatty alcohols production by oleaginous yeast." Journal of Industrial Microbiology and Biotechnology **42**(11): 1463-1472.
75. Fontaine, L., I. Meynial-Salles, L. Girbal, X. Yang, C. Croux and P. Soucaille (2002). "Molecular characterization and transcriptional analysis of adhE2, the gene encoding the NADH-dependent aldehyde/alcohol dehydrogenase responsible for butanol production in alcohologenic cultures of Clostridium acetobutylicum ATCC 824." J Bacteriol **184**(3): 821-830.
76. Frey, C. N. (1930). "History and development of the mordern yeast industry." Industrial & Engineering Chemistry **22**(11): 1154-1162.
77. Fukasawa, Y., J. Tsuji, S. C. Fu, K. Tomii, P. Horton and K. Imai (2015). "MitoFates: improved prediction of mitochondrial targeting sequences and their cleavage sites." Mol Cell Proteomics **14**(4): 1113-1126.
78. Gajewski, J., R. Pavlovic, M. Fischer, E. Boles and M. Grininger (2017). "Engineering fungal de novo fatty acid synthesis for short chain fatty acid production." Nat Commun **8**: 14650.
79. Galdieri, L., T. Zhang, D. Rogerson, R. Lleshi and A. Vancura (2014). "Protein acetylation and acetyl coenzyme a metabolism in budding yeast." Eukaryot Cell **13**(12): 1472-1483.
80. Gallage, Nethaji J. and Birger L. Møller (2015). "Vanillin–Bioconversion and Bioengineering of the Most Popular Plant Flavor and Its De Novo Biosynthesis in the Vanilla Orchid." Molecular Plant **8**(1): 40-57.
81. Gancedo, J. M. (2008). "The early steps of glucose signalling in yeast." FEMS Microbiol Rev **32**(4): 673-704.
82. García-Campusano, F., V. H. Anaya, L. Robledo-Arratia, H. Quezada, H. Hernández, L. Riego and A. González (2009). "ALT1-encoded alanine aminotransferase plays a central role in the metabolism of alanine in Saccharomyces cerevisiae." Can J Microbiol **55**(4): 368-374.
83. Generoso, W. C., M. Gottardi, M. Oreb and E. Boles (2016). "Simplified CRISPR-Cas genome editing for Saccharomyces cerevisiae." J Microbiol Methods **127**: 203-205.

84. Gibson, D. G., L. Young, R. Y. Chuang, J. C. Venter, C. A. Hutchison, 3rd and H. O. Smith (2009). "Enzymatic assembly of DNA molecules up to several hundred kilobases." Nat Methods **6**(5): 343-345.
85. Ginsberg, J. and A. C. Society (2008). Development of Deep-tank Fermentation: Pfizer Inc : June 12, 2008 : a National Historic Chemical Landmark, American Chemical Society.
86. Goffeau, A., B. G. Barrell, H. Bussey, R. W. Davis, B. Dujon, H. Feldmann, F. Galibert, J. D. Hoheisel, C. Jacq, M. Johnston, E. J. Louis, H. W. Mewes, Y. Murakami, P. Philippsen, H. Tettelin and S. G. Oliver (1996). "Life with 6000 genes." Science **274**(5287): 546, 563-547.
87. Gomes, F., F. R. Palma, M. H. Barros, E. T. Tsuchida, H. G. Turano, T. G. P. Alegria, M. Demasi and L. E. S. Netto (2017). "Proteolytic cleavage by the inner membrane peptidase (IMP) complex or Oct1 peptidase controls the localization of the yeast peroxiredoxin Prx1 to distinct mitochondrial compartments." Journal of Biological Chemistry **292**(41): 17011-17024.
88. Grabowska, D. and A. Chelstowska (2003). "The ALD6 gene product is indispensable for providing NADPH in yeast cells lacking glucose-6-phosphate dehydrogenase activity." J Biol Chem **278**(16): 13984-13988.
89. Gray, M. W. (2012). "Mitochondrial evolution." Cold Spring Harb Perspect Biol **4**(9): a011403.
90. Grote, A., K. Hiller, M. Scheer, R. Münch, B. Nörtemann, D. C. Hempel and D. Jahn (2005). "JCat: a novel tool to adapt codon usage of a target gene to its potential expression host." Nucleic Acids Research **33**(suppl_2): W526-W531.
91. Grunstein, M. (1997). "Histone acetylation in chromatin structure and transcription." Nature **389**(6649): 349-352.
92. Gulevich, A. Y., A. Y. Skorokhodova, A. Stasenko, R. Shakulov and V. Debabov (2016). "Metabolic engineering of Escherichia coli for 1, 3-butanediol biosynthesis through the inverted fatty acid β-oxidation cycle." Applied biochemistry and microbiology **52**: 15-22.
93. Guo, Z. P., L. Zhang, Z. Y. Ding, Z. X. Wang and G. Y. Shi (2011). "Improving ethanol productivity by modification of glycolytic redox factor generation in glycerol-3-phosphate dehydrogenase mutants of an industrial ethanol yeast." J Ind Microbiol Biotechnol **38**(8): 935-943.
94. Habich, M., S. L. Salscheider and J. Riemer (2019). "Cysteine residues in mitochondrial intermembrane space proteins: more than just import." Br J Pharmacol **176**(4): 514-531.
95. Hagman, A., T. Säll and J. Piškur (2014). "Analysis of the yeast short-term Crabtree effect and its origin." The FEBS Journal **281**(21): 4805-4814.
96. Hahn-Hägerdal, B., K. Karhumaa, C. U. Larsson, M. Gorwa-Grauslund, J. Görgens and W. H. van Zyl (2005). "Role of cultivation media in the development of yeast strains for large scale industrial use." Microbial Cell Factories **4**(1): 31.
97. Hammer, S. K. and J. L. Avalos (2017). "Harnessing yeast organelles for metabolic engineering." Nat Chem Biol **13**(8): 823-832.
98. Hammer, S. K., Y. Zhang and J. L. Avalos (2020). "Mitochondrial Compartmentalization Confers Specificity to the 2-Ketoacid Recursive Pathway: Increasing Isopentanol Production in Saccharomyces cerevisiae." ACS Synth Biol **9**(3): 546-555.
99. Hase, T., U. Müller, H. Riezman and G. Schatz (1984). "A 70-kd protein of the yeast mitochondrial outer membrane is targeted and anchored via its extreme amino terminus." Embo j **3**(13): 3157-3164.
100. Hassing, E. J., P. A. de Groot, V. R. Marquenie, J. T. Pronk and J. G. Daran (2019). "Connecting central carbon and aromatic amino acid metabolisms to improve de novo 2-phenylethanol production in Saccharomyces cerevisiae." Metab Eng **56**: 165-180.
101. Henritzi, S., M. Fischer, M. Grininger, M. Oreb and E. Boles (2018). "An engineered fatty acid synthase combined with a carboxylic acid reductase enables de novo production of 1-octanol in Saccharomyces cerevisiae." Biotechnol Biofuels **11**: 150.
102. Hiltunen, J. K., A. M. Mursula, H. Rottensteiner, R. K. Wierenga, A. J. Kastaniotis and A. Gurvitz (2003). "The biochemistry of peroxisomal β-oxidation in the yeast Saccharomyces cerevisiae." FEMS Microbiology Reviews **27**(1): 35-64.
103. Hiltunen, J. K., M. S. Schonauer, K. J. Autio, T. M. Mittelmeier, A. J. Kastaniotis and C. L. Dieckmann (2009). "Mitochondrial fatty acid synthesis type II: more than just fatty acids." J Biol Chem **284**(14): 9011-9015.
104. Hirata, D. and T. Hiroi (1991). "Genes That Cause Overproduction of Isoamyl Alcohol by Increased Gene-Dosage Effect in Saccharomyces cerevisiae." Agricultural and Biological Chemistry **55**(4): 919-924.
105. Hiser, L., M. E. Basson and J. Rine (1994). "ERG10 from Saccharomyces cerevisiae encodes acetoacetyl-CoA thiolase." J Biol Chem **269**(50): 31383-31389.

106. Hitschler, J. and E. Boles (2019). "De novo production of aromatic m-cresol in Saccharomyces cerevisiae mediated by heterologous polyketide synthases combined with a 6-methylsalicylic acid decarboxylase." Metab Eng Commun **9**: e00093.
107. Hoffmeister, M., M. Piotrowski, U. Nowitzki and W. Martin (2005). "Mitochondrial trans-2-enoyl-CoA reductase of wax ester fermentation from Euglena gracilis defines a new family of enzymes involved in lipid synthesis." J Biol Chem **280**(6): 4329-4338.
108. Holstein, S. A. and R. J. Hohl (2004). "Isoprenoids: remarkable diversity of form and function." Lipids **39**(4): 293-309.
109. Hu, Y., Z. Zhu, D. Gradischnig, M. Winkler, J. Nielsen and V. Siewers (2020). "Engineering carboxylic acid reductase for selective synthesis of medium-chain fatty alcohols in yeast." Proceedings of the National Academy of Sciences **117**(37): 22974-22983.
110. Hu, Y., Z. Zhu, J. Nielsen and V. Siewers (2019). "Engineering Saccharomyces cerevisiae cells for production of fatty acid-derived biofuels and chemicals." Open Biol **9**(5): 190049.
111. Hu, Z., B. He, L. Ma, Y. Sun, Y. Niu and B. Zeng (2017). "Recent Advances in Ergosterol Biosynthesis and Regulation Mechanisms in Saccharomyces cerevisiae." Indian J Microbiol **57**(3): 270-277.
112. Hubmann, G., S. Guillouet and E. Nevoigt (2011). "Gpd1 and Gpd2 fine-tuning for sustainable reduction of glycerol formation in Saccharomyces cerevisiae." Appl Environ Microbiol **77**(17): 5857-5867.
113. Inui, H., K. Miyatake, Y. Nakano and S. Kitaoka (1984). "Fatty acid synthesis in mitochondria of Euglena gracilis." Eur J Biochem **142**(1): 121-126.
114. Ishihama, Y., T. Schmidt, J. Rappsilber, M. Mann, F. U. Hartl, M. J. Kerner and D. Frishman (2008). "Protein abundance profiling of the Escherichia coli cytosol." BMC Genomics **9**: 102.
115. Iwata, M., Y. Lee, T. Yamashita, T. Yagi, S. Iwata, A. D. Cameron and M. J. Maher (2012). "The structure of the yeast NADH dehydrogenase (Ndi1) reveals overlapping binding sites for water- and lipid-soluble substrates." Proc Natl Acad Sci U S A **109**(38): 15247-15252.
116. Janßen, H. J. and A. Steinbüchel (2014). "Fatty acid synthesis in Escherichia coli and its applications towards the production of fatty acid based biofuels." Biotechnology for Biofuels **7**(1): 7.
117. Jarboe, L. R., L. A. Royce and P. Liu (2013). "Understanding biocatalyst inhibition by carboxylic acids." Front Microbiol **4**: 272.
118. Jeon, B. S., O. Choi, Y. Um and B.-I. Sang (2016). "Production of medium-chain carboxylic acids by Megasphaera sp. MH with supplemental electron acceptors." Biotechnology for Biofuels **9**(1): 129.
119. Jeon, B. S., O. Choi, Y. Um and B. I. Sang (2016). "Production of medium-chain carboxylic acids by Megasphaera sp. MH with supplemental electron acceptors." Biotechnol Biofuels **9**: 129.
120. Jia, H., T. Chen, J. Qu, M. Yao, W. Xiao, Y. Wang, C. Li and Y. Yuan (2020). "Collaborative subcellular compartmentalization to improve GPP utilization and boost sabinene accumulation in Saccharomyces cerevisiae." Biochemical Engineering Journal **164**: 107768.
121. Jordá, T. and S. Puig (2020). "Regulation of Ergosterol Biosynthesis in Saccharomyces cerevisiae." Genes (Basel) **11**(7).
122. Judge, A. and M. S. Dodd (2020). "Metabolism." Essays Biochem **64**(4): 607-647.
123. Kang, S., H. Kim, B. S. Jeon, O. Choi and B. I. Sang (2022). "Chain elongation process for caproate production using lactate as electron donor in Megasphaera hexanoica." Bioresour Technol **346**: 126660.
124. Karim, A. S., K. A. Curran and H. S. Alper (2013). "Characterization of plasmid burden and copy number in Saccharomyces cerevisiae for optimization of metabolic engineering applications." FEMS Yeast Res **13**(1): 107-116.
125. Kayikci, O. and J. Nielsen (2015). "Glucose repression in Saccharomyces cerevisiae." FEMS Yeast Res **15**(6).
126. Khan, S., M. W. Ullah, R. Siddique, G. Nabi, S. Manan, M. Yousaf and H. Hou (2016). "Role of Recombinant DNA Technology to Improve Life." Int J Genomics **2016**: 2405954.
127. Khosla, C. (2009). "Structures and mechanisms of polyketide synthases." J Org Chem **74**(17): 6416-6420.
128. Kiessling, T., M. Hinzmann, L. Mederake, S. Dittmann, D. Brennecke, M. Böhm-Beck, K. Knickmeier and M. Thiel (2023). "What potential does the EU Single-Use Plastics Directive

have for reducing plastic pollution at coastlines and riversides? An evaluation based on citizen science data." Waste Manag **164**: 106-118.
129. Kim, J. W., Y. G. Lee, S. J. Kim, Y. S. Jin and J. H. Seo (2019). "Deletion of glycerol-3-phosphate dehydrogenase genes improved 2,3-butanediol production by reducing glycerol production in pyruvate decarboxylase-deficient Saccharomyces cerevisiae." J Biotechnol **304**: 31-37.
130. Kim, S., J. M. Clomburg and R. Gonzalez (2015). "Synthesis of medium-chain length (C6-C10) fuels and chemicals via beta-oxidation reversal in Escherichia coli." J Ind Microbiol Biotechnol **42**(3): 465-475.
131. Kim, S. and R. Gonzalez (2018). "Selective production of decanoic acid from iterative reversal of beta-oxidation pathway." Biotechnol Bioeng **115**(5): 1311-1320.
132. Kim, S. and J.-S. Hahn (2015). "Efficient production of 2,3-butanediol in Saccharomyces cerevisiae by eliminating ethanol and glycerol production and redox rebalancing." Metabolic Engineering **31**: 94-101.
133. Kim, S. G., S. Jang, J. H. Lim, B. S. Jeon, J. Kim, K. H. Kim, B. I. Sang and G. Y. Jung (2018). "Optimization of hexanoic acid production in recombinant Escherichia coli by precise flux rebalancing." Bioresour Technol **247**: 1253-1257.
134. Klaus, M. and M. Grininger (2018). "Engineering strategies for rational polyketide synthase design." Natural Product Reports **35**(10): 1070-1081.
135. Klug, L. and G. Daum (2014). "Yeast lipid metabolism at a glance." FEMS Yeast Research **14**(3): 369-388.
136. Knight, M. J., I. D. Bull and P. Curnow (2014). "The yeast enzyme Eht1 is an octanoyl-CoA:ethanol acyltransferase that also functions as a thioesterase." Yeast **31**(12): 463-474.
137. Kolkman, A., P. Daran-Lapujade, A. Fullaondo, M. M. Olsthoorn, J. T. Pronk, M. Slijper and A. J. Heck (2006). "Proteome analysis of yeast response to various nutrient limitations." Mol Syst Biol **2**: 2006 0026.
138. Koonin, E. V. (2010). "The origin and early evolution of eukaryotes in the light of phylogenomics." Genome Biol **11**(5): 209.
139. Kozak, B. U., H. M. van Rossum, K. R. Benjamin, L. Wu, J.-M. G. Daran, J. T. Pronk and A. J. A. van Maris (2014). "Replacement of the Saccharomyces cerevisiae acetyl-CoA synthetases by alternative pathways for cytosolic acetyl-CoA synthesis." Metabolic Engineering **21**: 46-59.
140. Kozak, B. U., H. M. van Rossum, K. R. Benjamin, L. Wu, J. M. Daran, J. T. Pronk and A. J. van Maris (2014). "Replacement of the Saccharomyces cerevisiae acetyl-CoA synthetases by alternative pathways for cytosolic acetyl-CoA synthesis." Metab Eng **21**: 46-59.
141. Kozak, B. U., H. M. van Rossum, M. A. Luttik, M. Akeroyd, K. R. Benjamin, L. Wu, S. de Vries, J. M. Daran, J. T. Pronk and A. J. van Maris (2014). "Engineering acetyl coenzyme A supply: functional expression of a bacterial pyruvate dehydrogenase complex in the cytosol of Saccharomyces cerevisiae." mBio **5**(5): e01696-01614.
142. Kozak, B. U., H. M. van Rossum, M. S. Niemeijer, M. van Dijk, K. Benjamin, L. Wu, J. M. Daran, J. T. Pronk and A. J. van Maris (2016). "Replacement of the initial steps of ethanol metabolism in Saccharomyces cerevisiae by ATP-independent acetylating acetaldehyde dehydrogenase." FEMS Yeast Res **16**(2): fow006.
143. Krink-Koutsoubelis, N., A. C. Loechner, A. Lechner, H. Link, C. M. Denby, B. Vogeli, T. J. Erb, S. Yuzawa, T. Jakociunas, L. Katz, M. K. Jensen, V. Sourjik and J. D. Keasling (2018). "Engineered Production of Short-Chain Acyl-Coenzyme A Esters in Saccharomyces cerevisiae." ACS Synth Biol **7**(4): 1105-1115.
144. Krishnan, A., B. A. McNeil and D. T. Stuart (2020). "Biosynthesis of Fatty Alcohols in Engineered Microbial Cell Factories: Advances and Limitations." Frontiers in Bioengineering and Biotechnology **8**.
145. Krivoruchko, A., Y. Zhang, V. Siewers, Y. Chen and J. Nielsen (2015). "Microbial acetyl-CoA metabolism and metabolic engineering." Metabolic Engineering **28**: 28-42.
146. Kruis, A. J., A. C. Bohnenkamp, B. Nap, J. Nielsen, A. E. Mars, R. H. Wijffels, J. van der Oost, S. W. M. Kengen and R. A. Weusthuis (2020). "From Eat to trEat: engineering the mitochondrial Eat1 enzyme for enhanced ethyl acetate production in Escherichia coli." Biotechnol Biofuels **13**: 76.
147. Kruis, A. J., B. Gallone, T. Jonker, A. E. Mars, I. M. H. van Rijswijck, J. C. M. Wolkers-Rooijackers, E. J. Smid, J. Steensels, K. J. Verstrepen, S. W. M. Kengen, J. van der Oost and R. A. Weusthuis (2018). "Contribution of Eat1 and Other Alcohol Acyltransferases to Ester Production in Saccharomyces cerevisiae." Front Microbiol **9**: 3202.

148. Kruis, A. J., M. Levisson, A. E. Mars, M. van der Ploeg, F. Garces Daza, V. Ellena, S. W. M. Kengen, J. van der Oost and R. A. Weusthuis (2017). "Ethyl acetate production by the elusive alcohol acetyltransferase from yeast." Metab Eng **41**: 92-101.
149. Kumar, S., N. Kumar and S. Ul-Islam (2022). Role of Microbes in Industrial Products and Processes, John Wiley & Sons.
150. Kümmel, A., J. C. Ewald, S.-M. Fendt, S. J. Jol, P. Picotti, R. Aebersold, U. Sauer, N. Zamboni and M. Heinemann (2010). "Differential glucose repression in common yeast strains in response to HXK2 deletion." FEMS Yeast Research **10**(3): 322-332.
151. la-Rosa, J. D. P., M. A. García-Ramírez, A. C. Gschaedler-Mathis, A. I. Gómez-Guzmán, J. R. Solís-Pacheco and O. González-Reynoso (2021). "Estimation of metabolic fluxes distribution in Saccharomyces cerevisiae during the production of volatile compounds of Tequila." Math Biosci Eng **18**(5): 5094-5113.
152. Lakshmanan, J., A. L. Mosley and S. Ozcan (2003). "Repression of transcription by Rgt1 in the absence of glucose requires Std1 and Mth1." Curr Genet **44**(1): 19-25.
153. Lamers, D., N. van Biezen, D. Martens, L. Peters, E. van de Zilver, N. Jacobs-van Dreumel, R. H. Wijffels and C. Lokman (2016). "Selection of oleaginous yeasts for fatty acid production." BMC Biotechnol **16**(1): 45.
154. Lan, E. I., Y. Dekishima, D. S. Chuang and J. C. Liao (2013). "Metabolic engineering of 2-pentanone synthesis in Escherichia coli." AIChE Journal **59**(9): 3167-3175.
155. Leavell, M. D., D. J. McPhee and C. J. Paddon (2016). "Developing fermentative terpenoid production for commercial usage." Current Opinion in Biotechnology **37**: 114-119.
156. Leber, C., J. W. Choi, B. Polson and N. A. Da Silva (2016). "Disrupted short chain specific beta-oxidation and improved synthase expression increase synthesis of short chain fatty acids in Saccharomyces cerevisiae." Biotechnol Bioeng **113**(4): 895-900.
157. Lee, M. E., W. C. DeLoache, B. Cervantes and J. E. Dueber (2015). "A Highly Characterized Yeast Toolkit for Modular, Multipart Assembly." ACS Synth Biol **4**(9): 975-986.
158. Lee, S. Y., J. H. Park, S. H. Jang, L. K. Nielsen, J. Kim and K. S. Jung (2008). "Fermentative butanol production by Clostridia." Biotechnol Bioeng **101**(2): 209-228.
159. Lee, Y., O. Nasution, Y. M. Lee, E. Kim, W. Choi and W. Kim (2017). "Overexpression of PMA1 enhances tolerance to various types of stress and constitutively activates the SAPK pathways in Saccharomyces cerevisiae." Appl Microbiol Biotechnol **101**(1): 229-239.
160. Legras, J. L., C. Erny, C. Le Jeune, M. Lollier, Y. Adolphe, C. Demuyter, P. Delobel, B. Blondin and F. Karst (2010). "Activation of two different resistance mechanisms in Saccharomyces cerevisiae upon exposure to octanoic and decanoic acids." Appl Environ Microbiol **76**(22): 7526-7535.
161. Leis, R., M. J. de Castro, C. de Lamas, R. Picáns and M. L. Couce (2020). "Effects of Prebiotic and Probiotic Supplementation on Lactase Deficiency and Lactose Intolerance: A Systematic Review of Controlled Trials." Nutrients **12**(5).
162. Leonardi, R. and S. Jackowski (2007). "Biosynthesis of Pantothenic Acid and Coenzyme A." EcoSal Plus **2**(2).
163. Levi, P. G. and J. M. Cullen (2018). "Mapping Global Flows of Chemicals: From Fossil Fuel Feedstocks to Chemical Products." Environ Sci Technol **52**(4): 1725-1734.
164. Lian, J., R. Jin and H. Zhao (2016). "Construction of plasmids with tunable copy numbers in Saccharomyces cerevisiae and their applications in pathway optimization and multiplex genome integration." Biotechnology and Bioengineering **113**(11): 2462-2473.
165. Lian, J., T. Si, N. U. Nair and H. Zhao (2014). "Design and construction of acetyl-CoA overproducing Saccharomyces cerevisiae strains." Metabolic Engineering **24**: 139-149.
166. Lian, J. and H. Zhao (2015). "Reversal of the beta-oxidation cycle in Saccharomyces cerevisiae for production of fuels and chemicals." ACS Synth Biol **4**(3): 332-341.
167. Lin, X. (2021). "The regulation of Saccharomyces cerevisiae Snf1 protein kinase on glucose utilization is in a glucose-dependent manner." Curr Genet **67**(2): 245-248.
168. Liu, P., A. Chernyshov, T. Najdi, Y. Fu, J. Dickerson, S. Sandmeyer and L. Jarboe (2013). "Membrane stress caused by octanoic acid in Saccharomyces cerevisiae." Appl Microbiol Biotechnol **97**(7): 3239-3251.
169. Ljungdahl, P. O. and B. Daignan-Fornier (2012). "Regulation of amino acid, nucleotide, and phosphate metabolism in Saccharomyces cerevisiae." Genetics **190**(3): 885-929.
170. Lobs, A. K., C. Schwartz, S. Thorwall and I. Wheeldon (2018). "Highly Multiplexed CRISPRi Repression of Respiratory Functions Enhances Mitochondrial Localized Ethyl Acetate Biosynthesis in Kluyveromyces marxianus." ACS Synth Biol **7**(11): 2647-2655.
171. Luo, X., M. A. Reiter, L. d'Espaux, J. Wong, C. M. Denby, A. Lechner, Y. Zhang, A. T. Grzybowski, S. Harth, W. Lin, H. Lee, C. Yu, J. Shin, K. Deng, V. T. Benites, G. Wang, E. E. K.

Baidoo, Y. Chen, I. Dev, C. J. Petzold and J. D. Keasling (2019). "Complete biosynthesis of cannabinoids and their unnatural analogues in yeast." Nature **567**(7746): 123-126.
172. Luttik, M. A., K. M. Overkamp, P. Kotter, S. de Vries, J. P. van Dijken and J. T. Pronk (1998). "The Saccharomyces cerevisiae NDE1 and NDE2 genes encode separate mitochondrial NADH dehydrogenases catalyzing the oxidation of cytosolic NADH." J Biol Chem **273**(38): 24529-24534.
173. Luttik, M. A., K. M. Overkamp, P. Kötter, S. de Vries, J. P. van Dijken and J. T. Pronk (1998). "The Saccharomyces cerevisiae NDE1 and NDE2 genes encode separate mitochondrial NADH dehydrogenases catalyzing the oxidation of cytosolic NADH." J Biol Chem **273**(38): 24529-24534.
174. Lv, X., F. Wang, P. Zhou, L. Ye, W. Xie, H. Xu and H. Yu (2016). "Dual regulation of cytoplasmic and mitochondrial acetyl-CoA utilization for improved isoprene production in Saccharomyces cerevisiae." Nature Communications **7**(1): 12851.
175. Lynd, L. R., M. S. Laser, D. Bransby, B. E. Dale, B. Davison, R. Hamilton, M. Himmel, M. Keller, J. D. McMillan, J. Sheehan and C. E. Wyman (2008). "How biotech can transform biofuels." Nature Biotechnology **26**(2): 169-172.
176. Machado, H. B., Y. Dekishima, H. Luo, E. I. Lan and J. C. Liao (2012). "A selection platform for carbon chain elongation using the CoA-dependent pathway to produce linear higher alcohols." Metab Eng **14**(5): 504-511.
177. MacKenzie, J. A. and R. M. Payne (2007). "Mitochondrial protein import and human health and disease." Biochim Biophys Acta **1772**(5): 509-523.
178. Maeda, I., S. Delessert, S. Hasegawa, Y. Seto, S. Zuber and Y. Poirier (2006). "The peroxisomal Acyl-CoA thioesterase Pte1p from Saccharomyces cerevisiae is required for efficient degradation of short straight chain and branched chain fatty acids." J Biol Chem **281**(17): 11729-11735.
179. Mahoney, R. R. (1997). Lactose: Enzymatic Modification. Advanced Dairy Chemistry Volume 3: Lactose, water, salts and vitamins. P. F. Fox. Boston, MA, Springer US**:** 77-125.
180. Malina, C., C. Larsson and J. Nielsen (2018). "Yeast mitochondria: an overview of mitochondrial biology and the potential of mitochondrial systems biology." FEMS Yeast Research **18**(5).
181. Malina, C., R. Yu, J. Björkeroth, E. J. Kerkhoven and J. Nielsen (2021). "Adaptations in metabolism and protein translation give rise to the Crabtree effect in yeast." Proc Natl Acad Sci U S A **118**(51).
182. Maloney, F. P., L. Gerwick, W. H. Gerwick, D. H. Sherman and J. L. Smith (2016). "Anatomy of the beta-branching enzyme of polyketide biosynthesis and its interaction with an acyl-ACP substrate." Proc Natl Acad Sci U S A **113**(37): 10316-10321.
183. Margulis, L. (1970). "Origin of eukaryotic cells: evidence and research implications for a theory of the origin and evolution of microbial, plant, and animal cells on the Precambrian earth." (No Title).
184. Marrakchi, H., Y. M. Zhang and C. O. Rock (2002). "Mechanistic diversity and regulation of Type II fatty acid synthesis." Biochem Soc Trans **30**(Pt 6): 1050-1055.
185. Marres, C. A., S. de Vries and L. A. Grivell (1991). "Isolation and inactivation of the nuclear gene encoding the rotenone-insensitive internal NADH: ubiquinone oxidoreductase of mitochondria from Saccharomyces cerevisiae." Eur J Biochem **195**(3): 857-862.
186. Martin, W. and M. Mentel (2010) "The Origin of Mitochondria." Nature Education **3**.
187. Martinez-Munoz, G. A. and P. Kane (2017). "Vacuolar and plasma membrane proton pumps collaborate to achieve cytosolic pH homeostasis in yeast." J Biol Chem **292**(19): 7743.
188. Matsuda, F., C. Furusawa, T. Kondo, J. Ishii, H. Shimizu and A. Kondo (2011). "Engineering strategy of yeast metabolism for higher alcohol production." Microb Cell Fact **10**: 70.
189. Meadows, A. L., K. M. Hawkins, Y. Tsegaye, E. Antipov, Y. Kim, L. Raetz, R. H. Dahl, A. Tai, T. Mahatdejkul-Meadows, L. Xu, L. Zhao, M. S. Dasika, A. Murarka, J. Lenihan, D. Eng, J. S. Leng, C.-L. Liu, J. W. Wenger, H. Jiang, L. Chao, P. Westfall, J. Lai, S. Ganesan, P. Jackson, R. Mans, D. Platt, C. D. Reeves, P. R. Saija, G. Wichmann, V. F. Holmes, K. Benjamin, P. W. Hill, T. S. Gardner and A. E. Tsong (2016). "Rewriting yeast central carbon metabolism for industrial isoprenoid production." Nature **537**(7622): 694-697.
190. Mehrer, C. R., M. R. Incha, M. C. Politz and B. F. Pfleger (2018). "Anaerobic production of medium-chain fatty alcohols via a beta-reduction pathway." Metab Eng **48**: 63-71.
191. Meijaard, E., J. F. Abrams, D. Juffe-Bignoli, M. Voigt and D. Sheil (2020). "Coconut oil, conservation and the conscientious consumer." Curr Biol **30**(16): 3274-3275.

192. Meijaard, E., T. M. Brooks, K. M. Carlson, E. M. Slade, J. Garcia-Ulloa, D. L. A. Gaveau, J. S. H. Lee, T. Santika, D. Juffe-Bignoli, M. J. Struebig, S. A. Wich, M. Ancrenaz, L. P. Koh, N. Zamira, J. F. Abrams, H. H. T. Prins, C. N. Sendashonga, D. Murdiyarso, P. R. Furumo, N. Macfarlane, R. Hoffmann, M. Persio, A. Descals, Z. Szantoi and D. Sheil (2020). "The environmental impacts of palm oil in context." Nat Plants **6**(12): 1418-1426.
193. Melo, A. M., T. M. Bandeiras and M. Teixeira (2004). "New insights into type II NAD(P)H:quinone oxidoreductases." Microbiol Mol Biol Rev **68**(4): 603-616.
194. Membrillo-Hernandez, J., P. Echave, E. Cabiscol, J. Tamarit, J. Ros and E. C. Lin (2000). "Evolution of the adhE gene product of Escherichia coli from a functional reductase to a dehydrogenase. Genetic and biochemical studies of the mutant proteins." J Biol Chem **275**(43): 33869-33875.
195. Miyakawa, I. (2017). "Organization and dynamics of yeast mitochondrial nucleoids." Proc Jpn Acad Ser B Phys Biol Sci **93**(5): 339-359.
196. Mossmann, D., C. Meisinger and F. N. Vögtle (2012). "Processing of mitochondrial presequences." Biochimica et Biophysica Acta (BBA) - Gene Regulatory Mechanisms **1819**(9): 1098-1106.
197. Mühlenhoff, U. and R. Lill (2000). "Biogenesis of iron–sulfur proteins in eukaryotes: a novel task of mitochondria that is inherited from bacteria." Biochimica et Biophysica Acta (BBA)-Bioenergetics **1459**(2-3): 370-382.
198. Nakamura, C. E. and G. M. Whited (2003). "Metabolic engineering for the microbial production of 1,3-propanediol." Curr Opin Biotechnol **14**(5): 454-459.
199. Nakamura, C. E. and G. M. Whited (2003). "Metabolic engineering for the microbial production of 1,3-propanediol." Current Opinion in Biotechnology **14**(5): 454-459.
200. Nandy, S. K. and R. K. Srivastava (2018). "A review on sustainable yeast biotechnological processes and applications." Microbiological Research **207**: 83-90.
201. Nanthagopal, K., R. S. Kishna, A. E. Atabani, A. a. H. Al-Muhtaseb, G. Kumar and B. Ashok (2020). "A compressive review on the effects of alcohols and nanoparticles as an oxygenated enhancer in compression ignition engine." Energy Conversion and Management **203**: 112244.
202. Nevoigt, E. and U. Stahl (1997). "Osmoregulation and glycerol metabolism in the yeast Saccharomyces cerevisiae." FEMS Microbiol Rev **21**(3): 231-241.
203. Nielsen, J., C. B. Tillegreen and D. Petranovic (2022). "Innovation trends in industrial biotechnology." Trends Biotechnol **40**(10): 1160-1172.
204. Nissen, T. L., M. Anderlund, J. Nielsen, J. Villadsen and M. C. Kielland-Brandt (2001). "Expression of a cytoplasmic transhydrogenase in Saccharomyces cerevisiae results in formation of 2-oxoglutarate due to depletion of the NADPH pool." Yeast **18**(1): 19-32.
205. Nogae, I. and M. Johnston (1990). "Isolation and characterization of the ZWF1 gene of Saccharomyces cerevisiae, encoding glucose-6-phosphate dehydrogenase." Gene **96**(2): 161-169.
206. Olzhausen, J., M. Grigat, L. Seifert, T. Ulbricht and H. J. Schüller (2021). "Increased biosynthesis of acetyl-CoA in the yeast Saccharomyces cerevisiae by overexpression of a deregulated pantothenate kinase gene and engineering of the coenzyme A biosynthetic pathway." Appl Microbiol Biotechnol **105**(19): 7321-7337.
207. Olzhausen, J., S. Schubbe and H. J. Schuller (2009). "Genetic analysis of coenzyme A biosynthesis in the yeast Saccharomyces cerevisiae: identification of a conditional mutation in the pantothenate kinase gene CAB1." Curr Genet **55**(2): 163-173.
208. Orij, R., J. Postmus, A. Ter Beek, S. Brul and G. J. Smits (2009). "In vivo measurement of cytosolic and mitochondrial pH using a pH-sensitive GFP derivative in Saccharomyces cerevisiae reveals a relation between intracellular pH and growth." Microbiology (Reading) **155**(Pt 1): 268-278.
209. Orita, I., G. Unno, R. Kato and T. Fukui (2022). "Biosynthesis of Polyhydroxyalkanoate Terpolymer from Methanol via the Reverse β-Oxidation Pathway in the Presence of Lanthanide." Microorganisms **10**(1): 184.
210. Otterstedt, K., C. Larsson, R. M. Bill, A. Stahlberg, E. Boles, S. Hohmann and L. Gustafsson (2004). "Switching the mode of metabolism in the yeast Saccharomyces cerevisiae." EMBO Rep **5**(5): 532-537.
211. Ottone, C., C. Bernal, N. Serna, A. Illanes and L. Wilson (2018). "Enhanced long-chain fatty alcohol oxidation by immobilization of alcohol dehydrogenase from S. cerevisiae." Appl Microbiol Biotechnol **102**(1): 237-247.
212. Oud, B., C. L. Flores, C. Gancedo, X. Zhang, J. Trueheart, J. M. Daran, J. T. Pronk and A. J. van Maris (2012). "An internal deletion in MTH1 enables growth on glucose of

pyruvate-decarboxylase negative, non-fermentative Saccharomyces cerevisiae." Microb Cell Fact **11**: 131.
213. Ozcan, S., T. Leong and M. Johnston (1996). "Rgt1p of Saccharomyces cerevisiae, a key regulator of glucose-induced genes, is both an activator and a repressor of transcription." Mol Cell Biol **16**(11): 6419-6426.
214. P.G Roosphashree, S. S. S., N.S Kumari (2022). "Effect of medium chain fatty acid in human health and disease." Journal of Functional Foods **92**.
215. Pal, S., D. H. Park and B. V. Plapp (2009). "Activity of yeast alcohol dehydrogenases on benzyl alcohols and benzaldehydes: characterization of ADH1 from Saccharomyces carlsbergensis and transition state analysis." Chem Biol Interact **178**(1-3): 16-23.
216. Palomino, A., P. Herrero and F. Moreno (2005). "Rgt1, a glucose sensing transcription factor, is required for transcriptional repression of the HXK2 gene in Saccharomyces cerevisiae." Biochem J **388**(Pt 2): 697-703.
217. Pan, D., C. Lindau, S. Lagies, N. Wiedemann and B. Kammerer (2018). "Metabolic profiling of isolated mitochondria and cytoplasm reveals compartment-specific metabolic responses." Metabolomics **14**(5): 59.
218. Papapetridis, I., M. Goudriaan, M. Vázquez Vitali, N. A. de Keijzer, M. van den Broek, A. J. A. van Maris and J. T. Pronk (2018). "Optimizing anaerobic growth rate and fermentation kinetics in Saccharomyces cerevisiae strains expressing Calvin-cycle enzymes for improved ethanol yield." Biotechnol Biofuels **11**: 17.
219. Papapetridis, I., M. Goudriaan, M. Vázquez Vitali, N. A. de Keijzer, M. van den Broek, A. J. A. van Maris and J. T. Pronk (2018). "Optimizing anaerobic growth rate and fermentation kinetics in Saccharomyces cerevisiae strains expressing Calvin-cycle enzymes for improved ethanol yield." Biotechnology for Biofuels **11**(1): 17.
220. Paramasivan, K. and S. Mutturi (2022). "Recent advances in the microbial production of squalene." World Journal of Microbiology and Biotechnology **38**(5): 91.
221. Parapouli, M., A. Vasileiadis, A. S. Afendra and E. Hatziloukas (2020). "Saccharomyces cerevisiae and its industrial applications." AIMS Microbiol **6**(1): 1-31.
222. Partridge, J. D., G. Sanguinetti, D. P. Dibden, R. E. Roberts, R. K. Poole and J. Green (2007). "Transition of Escherichia coli from Aerobic to Micro-aerobic Conditions Involves Fast and Slow Reacting Regulatory Components*." Journal of Biological Chemistry **282**(15): 11230-11237.
223. Patinios, C., L. Lanza, I. Corino, M. C. R. Franssen, J. Van der Oost, R. A. Weusthuis and S. W. M. Kengen (2020). "Eat1-Like Alcohol Acyl Transferases From Yeasts Have High Alcoholysis and Thiolysis Activity." Frontiers in Microbiology **11**.
224. Peyraud, R., P. Kiefer, P. Christen, S. Massou, J. C. Portais and J. A. Vorholt (2009). "Demonstration of the ethylmalonyl-CoA pathway by using 13C metabolomics." Proc Natl Acad Sci U S A **106**(12): 4846-4851.
225. Pfeiffer, T. and A. Morley (2014). "An evolutionary perspective on the Crabtree effect." Front Mol Biosci **1**: 17.
226. Piper, P., Y. Mahe, S. Thompson, R. Pandjaitan, C. Holyoak, R. Egner, M. Muhlbauer, P. Coote and K. Kuchler (1998). "The pdr12 ABC transporter is required for the development of weak organic acid resistance in yeast." EMBO J **17**(15): 4257-4265.
227. Rapaport, D. and W. Neupert (1999). "Biogenesis of Tom40, core component of the TOM complex of mitochondria." J Cell Biol **146**(2): 321-331.
228. Reboredo, F. H., F. C. Lidon, J. C. Ramalho and M. F. Pessoa (2017). "The forgotten implications of low oil prices on biofuels." Biofuels, Bioproducts and Biorefining **11**(4): 625-632.
229. Reid, M. F. and C. A. Fewson (1994). "Molecular characterization of microbial alcohol dehydrogenases." Crit Rev Microbiol **20**(1): 13-56.
230. Reifenberger, E., E. Boles and M. Ciriacy (1997). "Kinetic characterization of individual hexose transporters of Saccharomyces cerevisiae and their relation to the triggering mechanisms of glucose repression." Eur J Biochem **245**(2): 324-333.
231. Reifenrath, M. and E. Boles (2018). "A superfolder variant of pH-sensitive pHluorin for in vivo pH measurements in the endoplasmic reticulum." Sci Rep **8**(1): 11985.
232. Rigouin, C., C. Croux, V. Borsenberger, M. Ben Khaled, T. Chardot, A. Marty and F. Bordes (2018). "Increasing medium chain fatty acids production in Yarrowia lipolytica by metabolic engineering." Microbial Cell Factories **17**(1): 142.
233. Ro, D.-K., E. M. Paradise, M. Ouellet, K. J. Fisher, K. L. Newman, J. M. Ndungu, K. A. Ho, R. A. Eachus, T. S. Ham, J. Kirby, M. C. Y. Chang, S. T. Withers, Y. Shiba, R. Sarpong and

J. D. Keasling (2006). "Production of the antimalarial drug precursor artemisinic acid in engineered yeast." Nature **440**(7086): 940-943.
234. Roberts, T. M., H. M. Kaltenbach and F. Rudolf (2020). "Development and optimisation of a defined high cell density yeast medium." Yeast **37**(5-6): 336-347.
235. Rodriguez, S., C. M. Denby, T. Van Vu, E. E. Baidoo, G. Wang and J. D. Keasling (2016). "ATP citrate lyase mediated cytosolic acetyl-CoA biosynthesis increases mevalonate production in Saccharomyces cerevisiae." Microb Cell Fact **15**: 48.
236. Rout, S., S. Oeljeklaus, A. Makki, J. Tachezy, B. Warscheid and A. Schneider (2021). "Determinism and contingencies shaped the evolution of mitochondrial protein import." Proceedings of the National Academy of Sciences **118**(6): e2017774118.
237. Roy, A., D. Jouandot, 2nd, K. H. Cho and J. H. Kim (2014). "Understanding the mechanism of glucose-induced relief of Rgt1-mediated repression in yeast." FEBS Open Bio **4**: 105-111.
238. Royce, L. A., P. Liu, M. J. Stebbins, B. C. Hanson and L. R. Jarboe (2013). "The damaging effects of short chain fatty acids on Escherichia coli membranes." Appl Microbiol Biotechnol **97**(18): 8317-8327.
239. Runguphan, W. and J. D. Keasling (2014). "Metabolic engineering of Saccharomyces cerevisiae for production of fatty acid-derived biofuels and chemicals." Metab Eng **21**: 103-113.
240. Saerens, S. M., F. R. Delvaux, K. J. Verstrepen and J. M. Thevelein (2010). "Production and biological function of volatile esters in Saccharomyces cerevisiae." Microb Biotechnol **3**(2): 165-177.
241. Saerens, S. M., K. J. Verstrepen, S. D. Van Laere, A. R. Voet, P. Van Dijck, F. R. Delvaux and J. M. Thevelein (2006). "The Saccharomyces cerevisiae EHT1 and EEB1 genes encode novel enzymes with medium-chain fatty acid ethyl ester synthesis and hydrolysis capacity." J Biol Chem **281**(7): 4446-4456.
242. Sakihama, Y., R. Hidese, T. Hasunuma and A. Kondo (2019). "Increased flux in acetyl-CoA synthetic pathway and TCA cycle of Kluyveromyces marxianus under respiratory conditions." Scientific Reports **9**(1): 5319.
243. Salvy, P. and V. Hatzimanikatis (2021). "Emergence of diauxie as an optimal growth strategy under resource allocation constraints in cellular metabolism." Proceedings of the National Academy of Sciences **118**(8): e2013836118.
244. San-Valero, P., A. Fernandez-Naveira, M. C. Veiga and C. Kennes (2019). "Influence of electron acceptors on hexanoic acid production by Clostridium kluyveri." J Environ Manage **242**: 515-521.
245. Sarris, D. and S. Papanikolaou (2016). "Biotechnological production of ethanol: Biochemistry, processes and technologies." Engineering in Life Sciences **16**(4): 307-329.
246. Sayyed, U. M. H. and R. Mahalakshmi (2022). "Mitochondrial protein translocation machinery: From TOM structural biogenesis to functional regulation." Journal of Biological Chemistry **298**(5): 101870.
247. Schadeweg, V. and E. Boles (2016a). "n-Butanol production in Saccharomyces cerevisiae is limited by the availability of coenzyme A and cytosolic acetyl-CoA." Biotechnol Biofuels **9**: 44.
248. Schadeweg, V. and E. Boles (2016b). "Increasing n-butanol production with Saccharomyces cerevisiae by optimizing acetyl-CoA synthesis, NADH levels and trans-2-enoyl-CoA reductase expression." Biotechnol Biofuels **9**: 257.
249. Schmidt, O., N. Pfanner and C. Meisinger (2010). "Mitochondrial protein import: from proteomics to functional mechanisms." Nature reviews Molecular cell biology **11**(9): 655-667.
250. Schuurmans, J. M., S. L. Rossell, A. van Tuijl, B. M. Bakker, K. J. Hellingwerf and M. J. Teixeira de Mattos (2008). "Effect of hxk2 deletion and HAP4 overexpression on fermentative capacity in Saccharomyces cerevisiae." FEMS Yeast Research **8**(2): 195-203.
251. Segawa, M., C. Wen, I. Orita, S. Nakamura and T. Fukui (2019). "Two NADH-dependent (S)-3-hydroxyacyl-CoA dehydrogenases from polyhydroxyalkanoate-producing Ralstonia eutropha." J Biosci Bioeng **127**(3): 294-300.
252. Shaigani, P., D. Awad, V. Redai, M. Fuchs, M. Haack, N. Mehlmer and T. Brueck (2021). "Oleaginous yeasts- substrate preference and lipid productivity: a view on the performance of microbial lipid producers." Microbial Cell Factories **20**(1): 220.
253. Shakya, V. P. S., W. A. Barbeau, T. Xiao, C. S. Knutson, M. H. Schuler and A. L. Hughes (2021). "A nuclear-based quality control pathway for non-imported mitochondrial proteins." eLife **10**: e61230.

254. Shen, C. R., E. I. Lan, Y. Dekishima, A. Baez, K. M. Cho and J. C. Liao (2011). "Driving forces enable high-titer anaerobic 1-butanol synthesis in Escherichia coli." Appl Environ Microbiol **77**(9): 2905-2915.
255. Shevchuk, N. A., A. V. Bryksin, Y. A. Nusinovich, F. C. Cabello, M. Sutherland and S. Ladisch (2004). "Construction of long DNA molecules using long PCR-based fusion of several fragments simultaneously." Nucleic Acids Research **32**(2): e19-e19.
256. Slater, S., K. L. Houmiel, M. Tran, T. A. Mitsky, N. B. Taylor, S. R. Padgette and K. J. Gruys (1998). "Multiple beta-ketothiolases mediate poly(beta-hydroxyalkanoate) copolymer synthesis in Ralstonia eutropha." J Bacteriol **180**(8): 1979-1987.
257. Sofinska, B., Witko, Dryzek, Harazna, Witko, Kryzciak-Czerwenka, Guzik (2018). "Structural, topographical, and mechanical characteristics of purified polyhydroxyoctanoate polymer." Journal of applied polymer science **136**(4).
258. Srinivasan, P. and C. D. Smolke (2020). "Biosynthesis of medicinal tropane alkaloids in yeast." Nature **585**(7826): 614-619.
259. Srivastava, V., K. N. Nand, A. Ahmad and R. Kumar (2023). "Yeast-Based Virus-like Particles as an Emerging Platform for Vaccine Development and Delivery." Vaccines (Basel) **11**(2).
260. Steen, E. J., R. Chan, N. Prasad, S. Myers, C. J. Petzold, A. Redding, M. Ouellet and J. D. Keasling (2008). "Metabolic engineering of Saccharomyces cerevisiae for the production of n-butanol." Microb Cell Fact **7**: 36.
261. Steen, E. J., Y. Kang, G. Bokinsky, Z. Hu, A. Schirmer, A. McClure, S. B. Del Cardayre and J. D. Keasling (2010). "Microbial production of fatty-acid-derived fuels and chemicals from plant biomass." Nature **463**(7280): 559-562.
262. Stojiljkovic, I., A. J. Baumler and F. Heffron (1995). "Ethanolamine utilization in Salmonella typhimurium: nucleotide sequence, protein expression, and mutational analysis of the cchA cchB eutE eutJ eutG eutH gene cluster." J Bacteriol **177**(5): 1357-1366.
263. Südfeld, C., A. Kiyani, H. Buckens, M. Hubáček, R. H. Wijffels, M. J. Barbosa and S. D'Adamo (2022). "Accumulation of medium chain fatty acids in Nannochloropsis oceanica by heterologous expression of Cuphea palustris thioesterase FatB1." Algal Research **64**: 102665.
264. Swenson, S. A., C. M. Moore, J. R. Marcero, A. E. Medlock, A. R. Reddi and O. Khalimonchuk (2020). "From Synthesis to Utilization: The Ins and Outs of Mitochondrial Heme." Cells **9**(3).
265. Swiegers, J. H., N. Dippenaar, I. S. Pretorius and F. F. Bauer (2001). "Carnitine-dependent metabolic activities in Saccharomyces cerevisiae: three carnitine acetyltransferases are essential in a carnitine-dependent strain." Yeast **18**(7): 585-595.
266. Tahir, M. N., F. Shahbazi, S. Rondeau-Gagne and J. F. Trant (2021). "The biosynthesis of the cannabinoids." J Cannabis Res **3**(1): 7.
267. Takakubo, F., P. Cartwright, N. Hoogenraad, D. R. Thorburn, F. Collins, T. Lithgow and H. H. Dahl (1995). "An amino acid substitution in the pyruvate dehydrogenase E1 alpha gene, affecting mitochondrial import of the precursor protein." Am J Hum Genet **57**(4): 772-780.
268. Tan, Z., J. M. Clomburg and R. Gonzalez (2018). "Synthetic Pathway for the Production of Olivetolic Acid in Escherichia coli." ACS Synth Biol **7**(8): 1886-1896.
269. Tan, Z., J. M. Yoon, A. Chowdhury, K. Burdick, L. R. Jarboe, C. D. Maranas and J. V. Shanks (2018). "Engineering of E. coli inherent fatty acid biosynthesis capacity to increase octanoic acid production." Biotechnology for Biofuels **11**(1): 87.
270. Tarasava, K., S. H. Lee, J. Chen, M. Kopke, M. C. Jewett and R. Gonzalez (2022). "Reverse beta-oxidation pathways for efficient chemical production." J Ind Microbiol Biotechnol **49**(2).
271. Taura, F., S. Tanaka, C. Taguchi, T. Fukamizu, H. Tanaka, Y. Shoyama and S. Morimoto (2009). "Characterization of olivetol synthase, a polyketide synthase putatively involved in cannabinoid biosynthetic pathway." FEBS Lett **583**(12): 2061-2066.
272. Tehlivets, O., K. Scheuringer and S. D. Kohlwein (2007). "Fatty acid synthesis and elongation in yeast." Biochim Biophys Acta **1771**(3): 255-270.
273. Tehlivets, O., K. Scheuringer and S. D. Kohlwein (2007). "Fatty acid synthesis and elongation in yeast." Biochimica et Biophysica Acta (BBA) - Molecular and Cell Biology of Lipids **1771**(3): 255-270.
274. Teixeira, P. G., V. Siewers and J. Nielsen (2017). "Quantitative in vivo evaluation of the reverse β-oxidation pathway for fatty acid production in Saccharomyces cerevisiae." bioRxiv: 201616.

275. Thomas, K. C., S. H. Hynes and W. M. Ingledew (2002). "Influence of medium buffering capacity on inhibition of Saccharomyces cerevisiae growth by acetic and lactic acids." Appl Environ Microbiol **68**(4): 1616-1623.
276. Tokuhiro, K., N. Ishida, E. Nagamori, S. Saitoh, T. Onishi, A. Kondo and H. Takahashi (2009). "Double mutation of the PDC1 and ADH1 genes improves lactate production in the yeast Saccharomyces cerevisiae expressing the bovine lactate dehydrogenase gene." Appl Microbiol Biotechnol **82**(5): 883-890.
277. Tseng, H. C., C. H. Martin, D. R. Nielsen and K. L. Prather (2009). "Metabolic engineering of Escherichia coli for enhanced production of (R)- and (S)-3-hydroxybutyrate." Appl Environ Microbiol **75**(10): 3137-3145.
278. Turk, E. M., V. Das, R. D. Seibert and E. D. Andrulis (2013). "The mitochondrial RNA landscape of Saccharomyces cerevisiae." PLoS One **8**(10): e78105.
279. Ulery, T. L., S. H. Jang and J. A. Jaehning (1994). "Glucose repression of yeast mitochondrial transcription: kinetics of derepression and role of nuclear genes." Mol Cell Biol **14**(2): 1160-1170.
280. Vadali, R. V., G. N. Bennett and K. Y. San (2004). "Cofactor engineering of intracellular CoA/acetyl-CoA and its effect on metabolic flux redistribution in Escherichia coli." Metab Eng **6**(2): 133-139.
281. Van Dien, S. (2013). "From the first drop to the first truckload: commercialization of microbial processes for renewable chemicals." Curr Opin Biotechnol **24**(6): 1061-1068.
282. van Maris, A. J. A., B. M. Bakker, M. Brandt, A. Boorsma, M. J. Teixeira de Mattos, L. A. Grivell, J. T. Pronk and J. Blom (2001). "Modulating the distribution of fluxes among respiration and fermentation by overexpression of HAP4 in Saccharomyces cerevisiae." FEMS Yeast Research **1**(2): 139-149.
283. van Rossum, H. M., B. U. Kozak, M. S. Niemeijer, H. J. Duine, M. A. Luttik, V. M. Boer, P. Kötter, J. M. Daran, A. J. van Maris and J. T. Pronk (2016b). "Alternative reactions at the interface of glycolysis and citric acid cycle in Saccharomyces cerevisiae." FEMS Yeast Res **16**(3).
284. van Rossum, H. M., B. U. Kozak, M. S. Niemeijer, J. C. Dykstra, M. A. Luttik, J. M. Daran, A. J. van Maris and J. T. Pronk (2016a). "Requirements for Carnitine Shuttle-Mediated Translocation of Mitochondrial Acetyl Moieties to the Yeast Cytosol." mBio **7**(3).
285. van Rossum, H. M., B. U. Kozak, J. T. Pronk and A. J. A. van Maris (2016c). "Engineering cytosolic acetyl-coenzyme A supply in Saccharomyces cerevisiae: Pathway stoichiometry, free-energy conservation and redox-cofactor balancing." Metab Eng **36**: 99-115.
286. Vega, M., A. Riera, A. Fernández-Cid, P. Herrero and F. Moreno (2016). "Hexokinase 2 Is an Intracellular Glucose Sensor of Yeast Cells That Maintains the Structure and Activity of Mig1 Protein Repressor Complex." J Biol Chem **291**(14): 7267-7285.
287. Vinodkumar, V. and A. Karthikeyan (2022). "Effect of manifold injection of n-decanol on neem biodiesel fuelled CI engine." Energy **241**: 122856.
288. Vogeli, B., L. Schulz, S. Garg, K. Tarasava, J. M. Clomburg, S. H. Lee, A. Gonnot, E. H. Moully, B. R. Kimmel, L. Tran, H. Zeleznik, S. D. Brown, S. D. Simpson, M. Mrksich, A. S. Karim, R. Gonzalez, M. Kopke and M. C. Jewett (2022). "Cell-free prototyping enables implementation of optimized reverse beta-oxidation pathways in heterotrophic and autotrophic bacteria." Nat Commun **13**(1): 3058.
289. Vögtle, F. N., J. M. Burkhart, H. Gonczarowska-Jorge, C. Kücükköse, A. A. Taskin, D. Kopczynski, R. Ahrends, D. Mossmann, A. Sickmann, R. P. Zahedi and C. Meisinger (2017). "Landscape of submitochondrial protein distribution." Nat Commun **8**(1): 290.
290. Vogtle, F. N., S. Wortelkamp, R. P. Zahedi, D. Becker, C. Leidhold, K. Gevaert, J. Kellermann, W. Voos, A. Sickmann, N. Pfanner and C. Meisinger (2009). "Global analysis of the mitochondrial N-proteome identifies a processing peptidase critical for protein stability." Cell **139**(2): 428-439.
291. Vojcic, L., C. Pitzler, G. Körfer, F. Jakob, M. Ronny, K. H. Maurer and U. Schwaneberg (2015). "Advances in protease engineering for laundry detergents." N Biotechnol **32**(6): 629-634.
292. Vorapreeda, T., C. Thammarongtham, S. Cheevadhanarak and K. Laoteng (2012). "Alternative routes of acetyl-CoA synthesis identified by comparative genomic analysis: involvement in the lipid production of oleaginous yeast and fungi." Microbiology (Reading) **158**(Pt 1): 217-228.
293. Vowinckel, J., J. Hartl, H. Marx, M. Kerick, K. Runggatscher, M. A. Keller, M. Mülleder, J. Day, M. Weber, M. Rinnerthaler, J. S. L. Yu, S. K. Aulakh, A. Lehmann, D. Mattanovich, B. Timmermann, N. Zhang, C. D. Dunn, J. I. MacRae, M. Breitenbach and M. Ralser (2021).

"The metabolic growth limitations of petite cells lacking the mitochondrial genome." Nat Metab **3**(11): 1521-1535.
294. Waks, Z. and P. A. Silver (2009). "Engineering a synthetic dual-organism system for hydrogen production." Appl Environ Microbiol **75**(7): 1867-1875.
295. Wang, X. and X. J. Chen (2015). "A cytosolic network suppressing mitochondria-mediated proteostatic stress and cell death." Nature **524**(7566): 481-484.
296. Watanabe, S. and S. Tsujino (2022). "Applications of Medium-Chain Triglycerides in Foods." Front Nutr **9**: 802805.
297. Wehrs, M., D. Tanjore, T. Eng, J. Lievense, T. R. Pray and A. Mukhopadhyay (2019). "Engineering Robust Production Microbes for Large-Scale Cultivation." Trends in Microbiology **27**(6): 524-537.
298. Wei, C. B., S. H. Liu, Y. G. Liu, L. L. Lv, W. X. Yang and G. M. Sun (2011). "Characteristic aroma compounds from different pineapple parts." Molecules **16**(6): 5104-5112.
299. Weinert, B. T., V. Iesmantavicius, T. Moustafa, C. Schölz, S. A. Wagner, C. Magnes, R. Zechner and C. Choudhary (2014). "Acetylation dynamics and stoichiometry in Saccharomyces cerevisiae." Mol Syst Biol **10**(1): 716.
300. Wernig, F., L. Baumann, E. Boles and M. Oreb (2021). "Production of octanoic acid in Saccharomyces cerevisiae: Investigation of new precursor supply engineering strategies and intrinsic limitations." Biotechnol Bioeng **118**(8): 3046-3057.
301. Wernig, F., S. Born, E. Boles, M. Grininger and M. Oreb (2020). "Fusing alpha and beta subunits of the fungal fatty acid synthase leads to improved production of fatty acids." Sci Rep **10**(1): 9780.
302. Wess, J., M. Brinek and E. Boles (2019). "Improving isobutanol production with the yeast Saccharomyces cerevisiae by successively blocking competing metabolic pathways as well as ethanol and glycerol formation." Biotechnol Biofuels **12**: 173.
303. Westermann, B. and W. Neupert (2000). "Mitochondria-targeted green fluorescent proteins: convenient tools for the study of organelle biogenesis in Saccharomyces cerevisiae." Yeast **16**(15): 1421-1427.
304. White, S. W., J. Zheng, Y. M. Zhang and Rock (2005). "The structural biology of type II fatty acid biosynthesis." Annu Rev Biochem **74**: 791-831.
305. White, W. H., P. L. Gunyuzlu and J. H. Toyn (2001). "Saccharomyces cerevisiae is capable of de Novo pantothenic acid biosynthesis involving a novel pathway of beta-alanine production from spermine." J Biol Chem **276**(14): 10794-10800.
306. Wiltschi, B., T. Cernava, A. Dennig, M. Galindo Casas, M. Geier, S. Gruber, M. Haberbauer, P. Heidinger, E. Herrero Acero, R. Kratzer, C. Luley-Goedl, C. A. Müller, J. Pitzer, D. Ribitsch, M. Sauer, K. Schmölzer, W. Schnitzhofer, C. W. Sensen, J. Soh, K. Steiner, C. K. Winkler, M. Winkler and T. Wriessnegger (2020). "Enzymes revolutionize the bioproduction of value-added compounds: From enzyme discovery to special applications." Biotechnology Advances **40**: 107520.
307. Winzeler, E. A., D. D. Shoemaker, A. Astromoff, H. Liang, K. Anderson, B. Andre, R. Bangham, R. Benito, J. D. Boeke, H. Bussey, A. M. Chu, C. Connelly, K. Davis, F. Dietrich, S. W. Dow, M. El Bakkoury, F. Foury, S. H. Friend, E. Gentalen, G. Giaever, J. H. Hegemann, T. Jones, M. Laub, H. Liao, N. Liebundguth, D. J. Lockhart, A. Lucau-Danila, M. Lussier, N. M'Rabet, P. Menard, M. Mittmann, C. Pai, C. Rebischung, J. L. Revuelta, L. Riles, C. J. Roberts, P. Ross-MacDonald, B. Scherens, M. Snyder, S. Sookhai-Mahadeo, R. K. Storms, S. Véronneau, M. Voet, G. Volckaert, T. R. Ward, R. Wysocki, G. S. Yen, K. Yu, K. Zimmermann, P. Philippsen, M. Johnston and R. W. Davis (1999). "Functional characterization of the S. cerevisiae genome by gene deletion and parallel analysis." Science **285**(5429): 901-906.
308. Wu, J., Z. Wang, X. Duan, P. Zhou, P. Liu, Z. Pang, Y. Wang, X. Wang, W. Li and M. Dong (2019). "Construction of artificial micro-aerobic metabolism for energy- and carbon-efficient synthesis of medium chain fatty acids in Escherichia coli." Metab Eng **53**: 1-13.
309. Wu, J., N. Zhang, A. Hayes, K. Panoutsopoulou and S. G. Oliver (2004). "Global analysis of nutrient control of gene expression in Saccharomyces cerevisiae during growth and starvation." Proceedings of the National Academy of Sciences **101**(9): 3148-3153.
310. Wu, Z., X. Huang, R. Chen, X. Mao and X. Qi (2022). "The United States and China on the paths and policies to carbon neutrality." J Environ Manage **320**: 115785.
311. Xia, J., B. J. Sánchez, Y. Chen, K. Campbell, S. Kasvandik and J. Nielsen (2022). "Proteome allocations change linearly with the specific growth rate of Saccharomyces cerevisiae under glucose limitation." Nature Communications **13**(1): 2819.

312. Yamamoto, H., M. Esaki, T. Kanamori, Y. Tamura, S. Nishikawa and T. Endo (2002). "Tim50 is a subunit of the TIM23 complex that links protein translocation across the outer and inner mitochondrial membranes." Cell **111**(4): 519-528.
313. Yaman, H., B. Doğan, M. K. Yeşilyurt and D. Erol (2021). "Application of Higher-Order Alcohols (1-Hexanol-C6 and 1-Heptanol-C7) in a Spark-Ignition Engine: Analysis and Assessment." Arabian Journal for Science and Engineering **46**(12): 11937-11961.
314. Yan, Q., W. T. Cordell, M. A. Jindra, D. K. Courtney, M. K. Kuckuk, X. Chen and B. F. Pfleger (2022). "Metabolic engineering strategies to produce medium-chain oleochemicals via acyl-ACP:CoA transacylase activity." Nature Communications **13**(1): 1619.
315. Yan, Q. and B. F. Pfleger (2020). "Revisiting metabolic engineering strategies for microbial synthesis of oleochemicals." Metab Eng **58**: 35-46.
316. Yang, J., J. Zhang, Z. Zhu and G. Du (2021). "The challenges and prospects of Escherichia coli as an organic acid production host under acid stress." Applied Microbiology and Biotechnology **105**(21): 8091-8107.
317. Yang, N. J. and M. J. Hinner (2015). "Getting across the cell membrane: an overview for small molecules, peptides, and proteins." Methods Mol Biol **1266**: 29-53.
318. Yang, P., S. Jiang, S. Lu, S. Jiang, S. Jiang, Y. Deng, J. Lu, H. Wang and Y. Zhou (2022). "Ethanol yield improvement in Saccharomyces cerevisiae GPD2 Delta FPS1 Delta ADH2 Delta DLD3 Delta mutant and molecular mechanism exploration based on the metabolic flux and transcriptomics approaches." Microbial Cell Factories **21**(1): 160.
319. Yao, Z., Y. Guo, H. Wang, Y. Chen, Q. Wang, J. Nielsen and Z. Dai (2023). "A highly efficient transcriptome-based biosynthesis of non-ethanol chemicals in Crabtree negative Saccharomyces cerevisiae." Biotechnology for Biofuels and Bioproducts **16**(1): 37.
320. Yazdabadi, S. H., H. Farrokhpour and M. Tabrizchi (2021). "Using surfactants as matrix for the matrix-assisted laser desorption/ionization time of flight mass spectrometry (MALDI-TOF-MS) of amino acids: Sodium dodecyl sulfate (SDS) and sodium octyl sulfate (SOS)." Biophys Chem **278**: 106667.
321. Yee, D. A., A. B. DeNicola, J. M. Billingsley, J. G. Creso, V. Subrahmanyam and Y. Tang (2019). "Engineered mitochondrial production of monoterpenes in Saccharomyces cerevisiae." Metab Eng **55**: 76-84.
322. Yocum, H. C., S. Bassett and N. A. Da Silva (2022). "Enhanced production of acetyl-CoA-based products via peroxisomal surface display in Saccharomyces cerevisiae." Proc Natl Acad Sci U S A **119**(48): e2214941119.
323. Yoo, M., G. Bestel-Corre, C. Croux, A. Riviere, I. Meynial-Salles and P. Soucaille (2015). "A Quantitative System-Scale Characterization of the Metabolism of Clostridium acetobutylicum." mBio **6**(6): e01808-01815.
324. Yoo, M., C. Croux, I. Meynial-Salles and P. Soucaille (2016). "Elucidation of the roles of adhE1 and adhE2 in the primary metabolism of Clostridium acetobutylicum by combining in-frame gene deletion and a quantitative system-scale approach." Biotechnol Biofuels **9**: 92.
325. Yuan, J., X. Chen, P. Mishra and C. B. Ching (2017). "Metabolically engineered Saccharomyces cerevisiae for enhanced isoamyl alcohol production." Appl Microbiol Biotechnol **101**(1): 465-474.
326. Yuan, J. and C.-B. Ching (2016). "Mitochondrial acetyl-CoA utilization pathway for terpenoid productions." Metabolic Engineering **38**: 303-309.
327. Yuan, Y., Y. Chen, S. Yan, Y. Liang, Y. Zheng and L. Dongdong (2013). "Molecular cloning and characterisation of an acyl carrier protein thioesterase gene (CocoFatB1) expressed in the endosperm of coconut (Cocos nucifera) and its heterologous expression in Nicotiana tabacum to engineer the accumulation of different fatty acids." Funct Plant Biol **41**(1): 80-86.
328. Zhang, D. L., S. M. Jennings, G. W. Robinson and C. D. Poulter (1993). "Yeast Squalene Synthase: Expression, Purification, and Characterization of Soluble Recombinant Enzyme." Archives of Biochemistry and Biophysics **304**(1): 133-143.
329. Zhang, J., A. t. Pierick, H. M. van Rossum, R. Maleki Seifar, C. Ras, J.-M. Daran, J. J. Heijnen and S. Aljoscha Wahl (2015). "Determination of the Cytosolic NADPH/NADP Ratio in Saccharomyces cerevisiae using Shikimate Dehydrogenase as Sensor Reaction." Scientific Reports **5**(1): 12846.
330. Zhang, M., S. Kurita, I. Orita, S. Nakamura and T. Fukui (2019). "Modification of acetoacetyl-CoA reduction step in Ralstonia eutropha for biosynthesis of poly(3-hydroxybutyrate-co-3-hydroxyhexanoate) from structurally unrelated compounds." Microb Cell Fact **18**(1): 147.

331. Zhang, Y., Z. Dai, A. Krivoruchko, Y. Chen, V. Siewers and J. Nielsen (2015). "Functional pyruvate formate lyase pathway expressed with two different electron donors in Saccharomyces cerevisiae at aerobic growth." FEMS Yeast Research **15**(4).
332. Zhang, Y., M. Su, Y. Chen, Z. Wang, J. Nielsen and Z. Liu (2023). "Engineering yeast mitochondrial metabolism for 3-hydroxypropionate production." Biotechnology for Biofuels and Bioproducts **16**(1): 64.
333. Zhang, Y., M. Su, Z. Wang, J. Nielsen and Z. Liu (2022). "Rewiring regulation on respiro-fermentative metabolism relieved Crabtree effects in Saccharomyces cerevisiae." Synth Syst Biotechnol **7**(4): 1034-1043.
334. Zhao, H., X. Zhou and Y. H. Zhou (2020). "Hepatitis B vaccine development and implementation." Hum Vaccin Immunother **16**(7): 1533-1544.
335. Zhao, L., Y. Huang, L. Lu, W. Yang, T. Huang, Z. Lin, C. Lin, H. Kwan, H. L. X. Wong, Y. Chen, S. Sun, X. Xie, X. Fang, H. Yang, J. Wang, L. Zhu and Z. Bian (2018). "Saturated long-chain fatty acid-producing bacteria contribute to enhanced colonic motility in rats." Microbiome **6**(1): 107.
336. Zheng, L. Y., G. M. Sun, Y. G. Liu, L. L. Lv, W. X. Yang, W. F. Zhao and C. B. Wei (2012). "Aroma volatile compounds from two fresh pineapple varieties in China." Int J Mol Sci **13**(6): 7383-7392.
337. Zhou, Y. J., N. A. Buijs, Z. Zhu, J. Qin, V. Siewers and J. Nielsen (2016). "Production of fatty acid-derived oleochemicals and biofuels by synthetic yeast cell factories." Nature communications **7**(1): 11709.
338. Zhu, Z., Y. Hu, P. G. Teixeira, R. Pereira, Y. Chen, V. Siewers and J. Nielsen (2020). "Multidimensional engineering of Saccharomyces cerevisiae for efficient synthesis of medium-chain fatty acids." Nature Catalysis **3**(1): 64-74.
339. Zhu, Z., Y. J. Zhou, A. Krivoruchko, M. Grininger, Z. K. Zhao and J. Nielsen (2017). "Expanding the product portfolio of fungal type I fatty acid synthases." Nat Chem Biol **13**(4): 360-362.

8 Appendix

I – Abbreviations

% - percent
∆ - deletion of a gene
ºC – degrees (Celsius)
µg – micrograms
µM - micromolar
µL – microlitres
AAD – Acetylating aldehyde dehydrogenase
ADS – Amorphadiene synthase
ADP – Adenosine diphosphate
AcALD – Acetaldehyde
ACR – Acyl-CoA reductase
ACL – ATP-citrate lyase
ACS1/2 – Acetyl-CoA synthase
ADH – Alcohol dehydrogenase
ALD – Acetaldehyde dehydrogenase
ALE – Adaptative laboratory evolution
AMP – Adenosine monophosphate
ATP – Adenosine triphosphate
1,3BPG – 1,3-biphosphoglycerate
BLAST – Basic local alignment search tool
bp - Base pairs
C-II – Succinate dehydrogenase (Complex II of the ETC)
C-III – Complex III of the ETC
C-IV – Cytochrome C oxidase (Complex IV of the ETC)
C-V – Complex V of the ETC
CAR – Carboxylic acid reductase
CIT – Citrate
CIT1 – Citrate synthase
CloNat – Nourseothricin resistance cassette
CoA – Coenzyme A
CytC – Cytochrome C
ddH_2O – de-ionized water
DHAP – Dihydroxy-acetone-phosphate
DNA – Deoxyribonucleic acid
E4P – Erythrose-4-phosphate
e^- – Electrons
EAT1 – Ethanol:acetyltransferase
ECH – Enoyl-CoA hydratase/isomerase
EI – Electron ionization
ETC – Electron transport chain
ENO1/2 - Enolase
F1,6P – Fructose-1,6-biphosphate
F6P – Fructose-6-phosphate
FAB – Fatty-acid biosynthesis
FAME – Fatty acid methyl ester
FBA1 - Fructose 1,6-bisphosphate aldolase
FID – Flame ionization detector
FUM – Fumarate
g – Grams
G1P – Glycerol-1-phosphate
G3P – Glycerol-3-phosphate
G418 – Geneticin
G6P – Glucose-6-phosphate
GA3P – Glyceraldehyde-3-phosphate
GC – Gas chromatography
GND1/2 – 6-phosphogluconate dehydrogenase
GPD – Glycerol-3-phosphate dehydrogenase
GPM1 – Phosphoglycerate mutase
GSMM – Genome-scale metabolic model
h – Hours
H^+ - Protons
HIS3 – Imidazoleglycerol-phosphate dehydratase gene (for histidine-based auxotrophic selection)
***HOR2* –** Glycerol-3-phosphatase
HPLC – High-performance liquid chromatography
HXK2 – Hexokinase 2
HXT – Hexose transporter(s)
HygR – Hygromycin resistance cassette
3-HBD – 3-hydroxyacyl-CoA dehydrogenase
IM – Inner membrane of the mitochondria
IMP – Mitochondrial inner membrane peptidase system
IMS – Intermembrane space of the mitochondria
KanMX – Geneticin resistance cassette
Kb – Kilobases
KEGG – Kyoto Encyclopedia of Genes and Genomes database
L – litres
LB – Lysogeny broth (cultivation medium)
LDH – Lactate dehydrogenase
LEU2 - Beta-isopropylmalate dehydrogenase gene (for leucine-based auxotrophic selection)
M – molar
MCFA – Medium-chain fatty acid
MCFOH – Medium-chain fatty alcohol
MEP – Mevalonate pathway
mg – milligrams
min – minutes
mL – millilitres
mM – millimolar
MS – Mass spectrometry
mtDNA – Mitochondrial DNA
MTS – Mitochondrial targeting sequence
ng – nanograms
nm – nanometres
NAD^+ / $NADH^+$ – Nicotinamide adenine dinucleotide (oxidised/ reduced)
$NADP^+$ / $NADPH^+$ – Nicotinamide adenine dinucleotide phosphate (oxidised/ reduced)
NDE1 - NADH:ubiquinone oxidoreductase (outer mitochondrial membrane)
NDI1 - NADH:ubiquinone oxidoreductase (inner mitochondrial membrane)
O_2 – Oxygen

OAA – Oxaloacetate
OM – Outer membrane space of the mitochondria
3PG – 3-phosphoglycerate
2PG – 2-phosphoglycerate
PAM - ATP-driven presequence translocase-associated motor
PLA – Poly-lactic acid
PCR – Polymerase chain reaction
PEG – Polyethyleneglycol
PEP – Phosphoenolpyruvate
PDC – Pyruvate decarboxylase
PDH – Pyruvate dehydrogenase complex
PFL – Pyruvate formate lyase
PFK1/2 – Phosphofructokinase
PGK1 – 3-phosphoglycerate kinase
PK – Phosphoketolase
POI – Product of interest
PP_i – Inorganic pyrophosphate
PPP – Pentose phosphate pathway
PTA – Phosphotransacetylase
PYK2 – Pyruvate kinase
PYR – Pyruvate
rBOX – Reverse β-oxidation pathway
***RHR2* –** Glycerol-3-phosphatase
RKI1 – Ribose-5-phosphate ketol-isomerase
RNA – Ribonucleic acid
R5P – R bose-5-phosphate
Ru5P – Ribulose-5-phosphate
RPE1 – D-ribulose-5-phosphate 3-epimerase
rpm – revolutions per minute
RT – Room temperature
S7P – Sedoheptulose-7-phosphate
SCD – Synthetic complete medium with dextrose
SCG_{-URA} – Synthetic complete medium with galactose and without uracil
SCFA – Short-chain fatty acids
SCFOH – Short-chain fatty alcohols
SM – Synthetic medium
SUCC – Succinate
TAL1 – Transaldolase
TDH3 - Glyceraldehyde-3-phosphate dehydrogenase
TER – *Trans*-enoyl-CoA reductase
TCA – Tricarboxylic acid cycle (Kreb's Cycle)
TKL1/2 – Transketolase
TPI - Triose phosphate isomerase
U – Units of enzymatic activity
Ub – Ubiquinone/ubiquinol
URA3 – Orotidine-5'-phosphate decarboxylase gene (for uracil-based auxotrophic selection)
V – volts
v/v – volume per volume
w/v – weight per volume
xg – g-force (relative centrifugal force)
Xu5P – Xylulose-5-phosphate
YPD – Yeast, peptone, and dextrose
YPD-20 mM – YPD buffered with 20 mM phosphate buffer
YPD-100 mM – YPD buffered with 100 mM phosphate buffer
$Y_{MCFA/S}$ – Yield of medium-chain fatty acids on glucose (g/g)
$Y_{MCFA/X}$ – Yield of medium-chain fatty acids on biomass (g/g)
$Y_{MCFOH/S}$ – Yield of medium-chain fatty alcohols on glucose (g/g)
$Y_{BUT/S}$ – Yield of butyrate on glucose (g/g)
$Y_{BUT/X}$ – Yield of butyrate on biomass (g/g)
$Y_{HEX/S}$ – Yield of hexanoic acid on glucose (g/g)
$Y_{HEX/X}$ – Yield of hexanoic acid on biomass (g/g)
$Y_{OCT/S}$ – Yield of octanoic acid on glucose (g/g)
$Y_{OCT/X}$ – Yield of octanoic acid on biomass (g/g)
$Y_{DEC/S}$ – Yield of decanoic acid on glucose (g/g)
$Y_{DEC/X}$ – Yield of decanoic acid on biomass (g/g)
$Y_{ETOH/S}$ – Yield of ethanol on glucose (g/g)
$Y_{GLY/S}$ – Yield of glycerol on glucose (g/g)
$Y_{X/S}$ – Yield of biomass on glucose (g/g)
ZWF1 – Glucose-6-phosphate dehydrogenase

II – Sequencing Primers

Table 37. Oligonucleotides used for sequencing during this study.

Primer name	Sequence (5'→ 3')	Comments	source
GDPseq1	GTTAGCAGACAAAACGTTAC	mtATP9 (from ERG10)	*This study*
GDPseq2	TCCGGTCGTACAGATGAAC	Envy GFP (rev)	*This study*
GDPseq3	CGCTGCTACTGGTATTGATG	AdhE2 (end part)	*This study*
GDPseq4	CTTGTAGTTCCCGTCATCTTTG	mtGFP/ATP9tag (pVT100mU)	*This study*
GDPseq5	CCTATCAACCCAATCTGTTC	Envy GFP (end part)	*This study*
GDPseq17	ACAGAATCCACATGGGTGTTAC	BktB	*This study*
GDPseq18	CTTGTCGTCGAACAAGTGAG	Cas9 gap	*This study*
GDPseq19	CTCACGCACACTGGAATGAATG	pRPL3	*This study*
GDPseq20	GTGCGTTTTCCTCTACAGTTG	Crt rev	*This study*
GDPseq21	ATCCATCTTTCCCAGTCTTC	Ter	*This study*
GDPseq22	CGGTCAAACTGTTTTGGTTGATG	Erg10	*This study*
GDPseq24	CTTCAACTGGATCCTTACCAATAG	Hbd mid, start and Promoter	*This study*
GDPseq25	CTTGAACATGGCTGCTGATTG	Hbd mid, end and Term	*This study*
GDPseq26	CACCAGCAGCAATCAATCTCTT	EutE mid, start, promoter	*This study*
GDPseq27	TTACCTTGTTGAACCAAGCTATTG	EutE mid, end, terminator	*This study*
GDPseq28	TGTTGGTTGGTCAAGCTATCTTC	OLS mid, end, terminator	*This study*
GDPseq29	GTATGGGCACAGACAACCTAAAC	Forward F3 scar	*This study*
GDPseq30	CGACTGTGTGGAGCTTTATTCAC	Reverse F5 scar	*This study*
GDPseq31	AAGTGAATAAAGCTCCACACAGTC	Forward F5 scar	*This study*
GDPseq32	CACACACTGGCTTAAGATGAC	Forward F2 scar	*This study*
GDPseq33	GTCATCTTAAGCCAGTGTGTG	Reverse F2 scar	*This study*
GDPseq34	TAGACTACCCATGAGTCACAATG	Forward F4 scar	*This study*
GDPseq35	CATTGTGACTCATGGGTAGTCTAC	Reverse F4 scar	*This study*
GDPseq36	GTTCGTAACATCTCTGTAACTGC	Reverse FE scar	*This study*
GDPseq45	GTGACACTGACGTTGCTATC	Bktb fwd	*This study*
GDPseq49	CTGACAAGGCTTCTGCTTTGG	PaaH1 fwd	*This study*
GDPseq50	GCTTCGTTGATCATTGGACAC	PaaH1 rv	*This study*
GDPseq51	GAACGACGCTTTGATGGACG	Crt2 fwd	*This study*
GDPseq52	GCGTCCATCATTCTAGAAGTC	Crt2 rv	*This study*
GDPseq53	CTGCTGGTGCTGACATCAAG	Crt(Yl) fwd	*This study*
GDPseq54	CTTTGAGTACCACCAGCACC	Crt(Yl) rv	*This study*
GDPseq55	CTGCTGTTGCTGACGTTGAC	Fw YlHAD	*This study*
GDPseq56	GGCATCAAGATTCTGTTAGCC	Rv YlHAD	*This study*
GDPseq57	GCTCAAGTTTCTGGTGACGAC	BktB fwd 4	*This study*
Vsp157	TTTCGTTGTCGAACTTACC	Erg10 mid-section	*V. Schadeweg*
Vsp162	CACCGAAACCTGGGG	Crt start + Promoter	*V. Schadeweg*
Vsp313	CCGTCTTGAAGCCATTCGG	Ter end + Terminator	*V. Schadeweg*
Vsp316	GGTGACAACGGTTTGACC	EutE (mid)	*V. Schadeweg*
Vsp317	GCTGAACACCCATTCGC	EutE (end)- Terminator	*V. Schadeweg*

Vsp170	TGTTAGAAGCGTGAGCC	AdhE2 (mid)	*V. Schadeweg*
Vsp171	GGTAATCTTGTTAACGTAACCC	AdhE2 (mid2)	*V. Schadeweg*
Vsp172	TGTCAGCGTTAATAGCACC	AdhE2 (mid3)	*V. Schadeweg*
Vsp173	CGTCGTGGTCAATAATACC	AdhE2 start - Promoter	*V. Schadeweg*

III – Reverse β-oxidation genes

Table 38. Codon-optimized DNA sequences of the reverse β-oxidation genes used in this study. The native mitochondrial tags in ^{Yl}Had and ^{Yl}Ech are <u>underlined</u>.

Erg10 (S. cerevisiae)
ATGTCTCAAAACGTTTACATTGTTTCTACTGCTAGAACCCCAATTGGTTCTTTCCAAGGTTCTTT GTCCTCCAAGACCGCTGTTGAATTGGGTGCTGTTGCTTTGAAGGGTGCTTTGGCTAAGGTTCC AGAATTGGATGCTTCCAAGGATTTCGACGAAATTATTTTCGGTAACGTTTTGTCTGCTAACTTGG GTCAAGCTCCAGCTAGACAAGTTGCTTTGGCTGCTGGTTTGTCTAACCACATCGTTGCTTCTAC CGTTAACAAGGTCTGTGCTTCCGCTATGAAGGCTATCATTTTGGGTGCTCAATCCATCAAGTGT GGTAACGCTGATGTTGTCGTTGCTGGTGGTTGTGAATCTATGACTAACGCTCCATACTACATGC CAGCTGCTAGAGCTGGTGCTAAGTTCGGTCAAACTGTTTTGGTTGATGGTGTCGAAAGAGATG GTTTGAACGATGCTTACGATGGTTTGGCTATGGGTGTTCACGCTGAAAAGTGTGCTAGAGATTG GGATATTACTAGAGAACAACAAGACAACTTCGCTATCGAATCCTACCAAAAGTCTCAAAAGTCT CAAAAGGAAGGTAAGTTCGACAACGAAATTGTTCCAGTTACCATTAAGGGTTTCAGAGGTAAGC CAGATACTCAAGTCACCAAGGACGAAGAACCAGCTAGATTGCACGTTGAAAAGTTGAGATCTG CTAGAACTGTTTTCCAAAAGGAAAACGGTACTGTTACTGCTGCTAACGCTTCTCCAATCAACGA TGGTGCTGCTGCTGTCATCTTGGTTTCCGAAAAGGTTTTGAAGGAAAAGAACTTGAAGCCATTG GCTATTATCAAGGGTTGGGGTGAAGCTGCTCACCAACCAGCTGATTTCACCTGGGCTCCATCT TTGGCTGTTCCAAAGGCTTTGAAGCACGCTGGTATCGAAGACATCAACTCTGTTGATTACTTCG AATTCAACGAAGCTTTCTCTGTTGTCGGTTTGGTTAACACTAAGATTTTGAAGTTGGACCCATCT AAGGTTAACGTTTACGGTGGTGCTGTTGCTTTGGGTCACCCATTGGGTTGTTCTGGTGCTAGA GTTGTTGTTACCTTGTTGTCCATCTTGCAACAAGAAGGTGGTAAGATCGGTGTTGCTGCTATTT GTAACGGTGGTGGTGGTGCTTCCTCTATTGTCATTGAAAAGATTTAA
BktB (C. necator)
ATGACTAGAGAAGTTGTTGTTGTTTCTGGTGTTAGAACTGCTATCGGTACTTTCGGTGGTTCTTT GAAGGACGTTGCTCCAGCTGAATTGGGTGCTTTGGTTGTTAGAGAAGCTTTGGCTAGAGCTCA AGTTTCTGGTGACGACGTTGGTCACGTTGTTTTCGGTAACGTTATCCAAACTGAACCAAGAGAC ATGTACTTGGGTAGAGTTGCTGCTGTTAACGGTGGTGTTACTATCAACGCTCCAGCTTTGACTG TTAACAGATTGTGTGGTTCTGGTTTGCAAGCTATCGTTTCTGCTGCTCAAACTATCTTGTTGGGT GACACTGACGTTGCTATCGGTGGTGGTGCTGAATCTATGTCTAGAGCTCCATACTTGGCTCCA GCTGCTAGATGGGGTGCTAGAATGGGTGACGCTGGTTTGGTTGACATGATGTTGGGTGCTTTG CACGACCCATTCCACAGAATCCACATGGGTGTTACTGCTGAAAACGTTGCTAAGGAATACGAC ATCTCTAGAGCTCAACAAGACGAAGCTGCTTTGGAATCTCACAGAAGAGCTTCTGCTGCTATCA AGGCTGGTTACTTCAAGGACCAAATCGTTCCAGTTGTTTCTAAGGGTAGAAAGGGTGACGTTAC TTTCGACACTGACGAACACGTTAGACACGACGCTACTATCGACGACATGACTAAGTTAAGGCC AGTTTTCGTTAAGGAAAACGGTACTGTTACTGCTGGTAACGCTTCTGGTTTGAACGACGCTGCT GCTGCTGTTGTTATGATGGAAAGAGCTGAAGCTGAAAGAAGAGGTTTGAAGCCATTGGCTAGA TTGGTTTCTTACGGTCACGCTGGTGTTGACCCAAAGGCTATGGGTATCGGTCCAGTTCCAGCT ACTAAGATCGCTTTGGAAAGAGCTGGTTTGCAAGTTTCTGACTTGGACGTTATCGAAGCTAACG AAGCTTTCGCTGCTCAAGCTTGTGCTGTTACTAAGGCTTTGGGTTTGGACCCAGCTAAGGTTAA CCCAAACGGTTCTGGTATCTCTTTGGGTCACCCAATCGGTGCTACTGGTGCTTTGATCACTGTT AAGGCTTTGCACGAATTGAACAGAGTTCAAGGTAGATACGCTTTGGTTACTATGTGTATCGGTG GTGGTCAAGGTATCGCTGCTATCTTCGAAAGAATCTAA
***Hbd* (*C. acetobutylicum*)**

ATGAAGAAGGTTTGTGTTATTGGTGCTGGTACTATGGGTTCTGGTATTGCTCAAGCTTTCGCTG
CTAAGGGTTTCGAAGTTGTTTTGAGAGATATTAAGGATGAATTCGTTGATAGAGGTTTGGATTTC
ATCAACAAGAACTTGTCTAAGTTGGTTAAGAAGGGTAAGATTGAAGAAGCTACTAAGGTTGAAA
TCTTGACTAGAATTTCCGGTACCGTTGACTTGAACATGGCTGCTGATTGTGATTTGGTTATTGAA
GCTGCTGTTGAAAGAATGGATATTAAGAAGCAAATTTTCGCTGACTTGGACAACATTTGTAAGC
CAGAAACCATTTTGGCTTCTAACACCTCTTCTTTGTCTATTACCGAAGTTGCTTCTGCTACTAAG
AGGCCAGATAAGGTTATTGGTATGCACTTCTTCAACCCAGCTCCAGTTATGAAGTTGGTTGAAG
TTATTAGAGGTATTGCTACCTCTCAAGAAACTTTCGATGCTGTTAAGGAAACCTCTATTGCTATT
GGTAAGGATCCAGTTGAAGTTGCTGAAGCTCCAGGTTTCGTTGTTAACAGAATTTTGATTCCAA
TGATTAACGAAGCTGTTGGTATTTTGGCTGAAGGTATTGCTTCTGTTGAAGACATTGATAAGGC
TATGAAGTTGGGTGCTAACCACCCAATGGGTCCATTGGAATTGGGTGATTTCATTGGTTTGGAT
ATTTGTTTGGCTATTATGGATGTTTTGTACTCTGAAACTGGTGATTCTAAGTACAGACCACACAC
CTTGTTGAAGAAGTACGTTAGAGCTGGTTGGTTGGGTAGAAAGTCTGGTAAGGGTTTCTACGAT
TACTCTAAGTAA

Had (Y. lipolytica)

ATGTTCAGATTGACTACTGCTAGAATCGCTTCTGTTAGAGGTTTCTCTACTTCTGCTTCTTTGTC
TAAGAAGGTTGACTCTTTGTCTGTTATCGGTGCTGGTCAAATGGGTTTGGGTATCGCTTTGGTT
GCTGCTAACAAGGCTGGTTTGCAAGTTAACTTGATCGACGCTAACCAAGGTGCTTTGGACAAG
GGTTTGAAGTTCATGGACAAGTTGTTGGAAAAGGACGTTGGTAAGGGTAGATTGACTTCTGAC
GAAGCTCAAGCTGTTAGAGGTAGAGTTACTGGTCACACTAACTTGCAATCTGCTGTTGCTGACG
TTGACATGATCATCGAAGCTGTTCCAGAAATCCCAAAGTTGAAGTTCGACATCTTCAGAGACTT
GAACGAATGGACTCAAAAGGACACTATCTTGGCTACTAACACTTCTTCTATCTCTATCACTAAGA
TCGCTGCTGCTGCTGGTGCTGGTGCTCCAAGAGTTATCTCTGCTCACTTCATGAACCCAGTTC
CAGTTCAAAAGGGTGTTGAAATCATCACTGGTTTGCAAACTTCTCCAGAAACTTTGGCTACTAC
TTTGGAAGTTGTTAAGAGAATGGGTAAGATCCCATCTATCTCTAAGGACTCTCCAGGTTTCTTG
GCTAACAGAATCTTGATGCCATACATCAACGAAGCTATCATCACTTTGGAAACTGGTGTTGGTG
AAAAGGAAGACATCGACAACATCTTGAAGAACGGTTGTGCTATGCCAATGGGTCCATTGGCTTT
GGCTGACTTCATCGGTTTGGACACTTGTTTGGCTATCATGAGAGTTTTGTACGAAGACACTGGT
GACTCTAAGTACAGACCATCTGTTTTGTTGAACAAGTACGTTGACGCTGGTTGGTTGGGTAAGA
AGTCTGGTAAGGGTTTCTACGACTACTAA

***PaaH1* (*C. necator*)**

ATGTCTATCAGAACTGTTGGTATCGTTGGTGCTGGTACTATGGGTAACGGTATCGCTCAAGCTT
GTGCTGTTGTTGGTTTGAACGTTGTTATGGTTGACATCTCTGACGCTGCTGTTCAAAAGGGTGT
TGCTACTGTTGCTTCTTCTTTGGACAGATTGATCAAGAAGGAAAAGTTGACTGAAGCTGACAAG
GCTTCTGCTTTGGCTAGAATCAAGGGTTCTACTTCTTACGACGACTTGAAGGCTACTGACATCG
TTATCGAAGCTGCTACTGAAAACTACGACTTGAAGGTTAAGATCTTGAAGCAAATCGACGGTAT
CGTTGGTGAAAACGTTATCATCGCTTCTAACACTTCTTCTATCTCTATCACTAAGTTGGCTGCTG
TTACTTCTAGAGCTGACAGATTCATCGGTATGCACTTCTTCAACCCAGTTCCAGTTATGGCTTTG
GTTGAATTGATCAGAGGTTTGCAAACTTCTGACACTACTCACGCTGCTGTTGAAGCTTTGTCTA
AGCAATTGGGTAAGTACCCAATCACTGTTAAGAACTCTCCAGGTTTCGTTGTTAACAGAATCTT
GTGTCCAATGATCAACGAAGCTTTCTGTGTTTTGGGTGAAGGTTTGGCTTCTCCAGAAGAAATC
GACGAAGGTATGAAGTTGGGTTGTAACCACCCAATCGGTCCATTGGCTTTGGCTGACATGATC
GGTTTGGACACTATGTTGGCTGTTATGGAAGTTTTGTACACTGAATTCGCTGACCCAAAGTACA
GACCAGCTATGTTGATGAGAGAAATGGTTGCTGCTGGTTACTTGGGTAGAAAGACTGGTAGAG
GTGTTTACGTTTACTCTAAGTAA

Ech (*Y. lipolytica*)

ATGACTGTTCACCACAGAACTGAAATGTTGAGAACTATCAGATCTTCTTCTAGATTGGGTGTTA
GAGCTATGTCTACTGCTGCTACTAGAAGAGCTGCTCAAATCGGTTTCCACACTAGAGTTCCAAC
TGTTGTTACTAAGGCTCCAACTTTGAGAATGCAAACTACTCCATTCTCTTCTTCTGCTCCAGCTC
AAACTTTCGGTGACAAGAAGTACGAACACATCTTGACTTCTACTCCAGTTCCAAAGGTTGCTTT
GGTTACTTTGAACAGACCAAAGGCTTTGAACGCTTTGTGTACTCCATTGATCAAGGAATTGAAC
GAAGCTTTGCAAGCTGCTGACGCTGACCCAACTATCGGTGCTATCGTTTTGACTGGTTCTGAAA
AGTCTTTCGCTGCTGGTGCTGACATCAAGGAAATGAAGGACAAGACTGTTACTTCTGTTTTGAA
CGAAAACTTCATCGAAGAATGGGGTAACATGGCTAACATCAAGAAGCCAATCATCGCTGCTGTT
AACGGTTTCGCTTTGGGTGGTGGTTGTGAATTGGCTATGATGGCTGACATCATCTACGCTGGT
GCTAAGGCTAAGTTCGGTCAACCAGAAATCAAGTTGGGTGTTATCCCAGGTGCTGGTGGTACT
CAAAGATTGACTAGAGCTATCGGTTTGTACAGAGCTAACCACTACATCTTGACTGGTGAAATGT
TCACTGCTCAACAAGCTGCTGACTGGGGTTTGGCTGCTAAGGTTTACGAACCAGCTCAATTGG
TTGACGAATCTGTTAAGGCTGCTGCTCAAATCGCTTCTTACGGTCAATTGGCTGTTCAAGCTGC
TAAGGCTTCTGTTCACCAATCTGCTGAAGTTGGTTTGAGAGCTGGTTTGGAATTCGAAAGAGTT
AGATTCCACGGTTTGTTCGGTACTCACGACCAAAAGGAAGGTATGGCTGCTTTCGCTGAAAAG
AGAGAACCAAACTTCAAGAACGAATAA

Crt (C. acetobutylicum)

ATGGAATTGAACAACGTCATCTTGGAAAAGGAAGGTAAGGTTGCTGTTGTTACCATTAACAGAC
CAAAGGCTTTGAACGCTTTGAACTCTGATACCTTGAAGGAAATGGATTACGTTATTGGTGAAAT
TGAAAACGATTCTGAAGTTTTGGCTGTTATTTTGACTGGTGCTGGTGAAAAGTCTTTCGTTGCT
GGTGCTGATATTTCTGAAATGAAGGAAATGAACACCATTGAAGGTAGAAAGTTCGGTATTTTGG
GTAACAAGGTTTTCAGAAGATTGGAATTGTTGGAAAAGCCAGTTATTGCTGCTGTTAACGGTTT
CGCTTTGGGTGGTGGTTGTGAAATTGCTATGTCTTGTGATATTAGAATTGCTTCTTCTAACGCTA
GATTCGGTCAACCAGAAGTTGGTTTGGGTATTACCCCAGGTTTCGGTGGTACCCAAAGATTGT
CTAGATTGGTTGGTATGGGTATGGCTAAGCAATTGATTTTCACTGCTCAAAACATTAAGGCTGA
TGAAGCTTTGAGAATCGGTTTGGTTAACAAGGTTGTTGAACCATCTGAATTGATGAACACCGCT
AAGGAAATTGCTAACAAGATTGTTTCTAACGCTCCAGTTGCTGTTAAGTTGTCTAAGCAAGCTAT
TAACAGAGGTATGCAATGTGATATTGATACTGCTTTGGCTTTCGAATCTGAAGCTTTCGGTGAA
TGTTTCTCTACCGAAGATCAAAAGGATGCTATGACCGCTTTCATTGAAAAGAGAAAGATTGAAG
GTTTCAAGAACAGATAA

Crt2 (C. necator)

ATGCCATACGAAAACATCTTGGTTGAAACTAGAGGTAGAGTTGGTTTGGTTACTTTGAACAGAC
CAAAGGCTTTGAACGCTTTGAACGACGCTTTGATGGACGAATTGGGTGCTGCTTTGACTGCTTT
CGACCAAGACGAAGGTATCGGTGCTATCGTTATCACTGGTTCTGAAAGAGCTTTCGCTGCTGG
TGCTGACATCGGTATGATGGCTAAGTACTCTTTCATGGACGTTTACAAGGGTGACTACATCACT
AGAAACTGGGAAACTATCAGAAAGATCAGAAAGCCAGTTATCGCTGGTGTTGCTGGTTACGCT
TTGGGTGGTGGTTGTGAATTGGCTATGATGTGTGACATCATCATCGCTGCTGACTCTGCTAAGT
TCGGTCAACCAGAAGTTAAGTTGGGTACTATGCCAGGTGCTGGTGGTACTCAAAGATTGCCAA
GAGCTGTTTCTAAGGCTAAGGCTATGGACTTGTGTTTGACTTCTAGAATGATGGACGCTGCTGA
AGCTGAAAGATCTGGTTTGGTTTCTAGAGTTGTTCCAGCTGACAAGTTGTTGGACGAAGTTTTG
GCTGCTGCTGAAACTATCGCTGGTTTCTCTTTGCCAGTTGTTATGATGATCAAGGAATCTGTTA
ACGCTGCTTACGAAACTACTTTGGCTGAAGGTGTTCACTTCGAAAGAAGATTGTTCCACGCTAC
TTTCGCTTCTGAAGACCAAAAGGAAGGTATGGCTGCTTTCGTTGAAAAGAGATCTCCAAACTTC
CAACACAGATAA

Ter (T. denticola)

ATGATTGTTAAGCCAATGGTTAGAAACAACATTTGTTTGAACGCTCACCCACAAGGTTGTAAGA
AGGGTGTTGAAGATCAAATTGAATACACCAAGAAGAGAATTACCGCTGAAGTTAAGGCTGGTG
CTAAGGCTCCAAAGAACGTTTTGGTTTTGGGTTGTTCTAACGGTTACGGTTTGGCTTCTAGAAT
TACCGCTGCTTTCGGTTACGGTGCTGCTACTATCGGTGTTTCCTTCGAAAAGGCTGGTTCTGAA
ACCAAGTACGGTACCCCAGGTTGGTACAACAACTTGGCTTTCGACGAAGCTGCTAAGAGAGAA
GGTTTGTACTCCGTTACTATTGACGGTGACGCTTTCTCCGATGAAATCAAGGCTCAAGTTATCG
AAGAAGCTAAGAAGAAGGGTATTAAGTTCGATTTGATTGTTTACTCTTTGGCTTCTCCAGTTAGA
ACCGATCCAGACACCGGTATTATGCACAAGTCCGTCTTGAAGCCATTCGGTAAGACCTTCACC
GGTAAGACCGTCGATCCATTCACCGGTGAATTGAAGGAAATCTCCGCTGAACCAGCTAACGAT
GAAGAAGCTGCTGCTACCGTTAAGGTTATGGGTGGTGAAGACTGGGAAAGATGGATTAAGCAA
TTGTCTAAGGAAGGTTTGTTGGAAGAAGGTTGTATTACCTTGGCTTACTCCTACATCGGTCCAG
AAGCTACTCAAGCTTTGTACAGAAAGGGTACCATTGGTAAGGCTAAGGAACACTTGGAAGCTA
CTGCTCACAGATTGAACAAGGAAAACCCATCTATTAGAGCTTTCGTTTCTGTTAACAAGGGTTT
GGTTACCAGAGCTTCTGCTGTTATCCCAGTTATTCCATTGTACTTGGCTTCCTTGTTCAAGGTTA

TGAAGGAAAAGGGTAACCACGAAGGTTGTATCGAACAAATTACCAGATTGTACGCTGAAAGATT
GTACAGAAAGGACGGTACCATCCCAGTCGATGAAGAAAACAGAATCAGAATCGACGACTGGGA
ATTGGAAGAAGACGTTCAAAAGGCTGTTTCTGCTTTGATGGAAAAGGTTACCGGTGAAAACGCT
GAATCTTTGACCGACTTGGCTGGTTACAGACACGACTTCTTGGCTTCTAACGGTTTCGATGTTG
AAGGTATCAACTACGAAGCTGAAGTTGAAAGATTCGACAGAATTTAA

Ter (E. gracilis)

ATGGCTATGTTCACCACCACCGCTAAGGTCATCCAACCAAAGATTAGAGGTTTCATCTGTACCA
CCACCCACCCAATCGGTTGTGAAAAGAGAGTCCAAGAAGAAATCGCTTACGCTAGAGCTCACC
CACCAACCTCTCCAGGTCCAAAGAGAGTTTTGGTCATCGGTTGTTCTACCGGTTACGGTTTGTC
CACCAGAATCACCGCTGCTTTCGGTTACCAAGCTGCTACCTTGGGTGTTTTCTTGGCTGGTCCA
CCAACCAAGGGTAGACCAGCTGCTGCTGGTTGGTACAACACCGTTGCTTTCGAAAAGGCTGCT
TTGGAAGCTGGTTTGTACGCTAGATCTTTGAACGGTGACGCTTTCGACTCCACCACCAAGGCT
AGAACCGTCGAAGCTATCAAGAGAGACTTGGGTACCGTTGACTTGGTTGTTTACTCTATCGCTG
CTCCAAAGAGAACCGACCCAGCTACCGGTGTCTTGCACAAGGCTTGTTTGAAGCCAATCGGTG
CTACCTACACCAACAGAACTGTTAACACCGACAAGGCTGAAGTTACCGACGTTTCTATTGAACC
AGCTTCCCCAGAAGAAATCGCTGACACCGTTAAGGTTATGGGTGGTGAAGACTGGGAATTGTG
GATCCAAGCTTTGTCTGAAGCTGGTGTTTTGGCTGAAGGTGCTAAGACCGTTGCTTACTCCTAC
ATCGGTCCAGAAATGACCTGGCCAGTCTACTGGTCCGGTACCATCGGTGAAGCTAAGAAGGAC
GTTGAAAAGGCTGCTAAGAGAATCACCCAACAATACGGTTGTCCAGCTTACCCAGTTGTTGCTA
AGGCTTTGGTCACCCAAGCTTCTTCCGCTATCCCAGTTGTTCCATTGTACATCTGTTTGTTGTAC
AGAGTTATGAAGGAAAAGGGTACCCACGAAGGTTGTATCGAACAAATGGTTAGATTGTTGACC
ACCAAGTTGTACCCAGAAAACGGTGCTCCAATCGTCGATGAAGCTGGTAGAGTTAGAGTTGAT
GACTGGGAAATGGCTGAAGATGTTCAACAAGCTGTTAAGGACTTGTGGTCCCAAGTTTCTACTG
CTAACTTGAAGGACATCTCCGACTTCGCTGGTTACCAAACTGAATTCTTGAGATTGTTCGGTTT
CGGTATTGACGGTGTTGACTACGACCAACCAGTTGACGTTGAAGCTGACTTGCCATCTGCTGC
TCAACAATAA

AdhE2 (C. acetobutylicum)

ATGAAGGTTACCAACCAAAAGGAATTGAAGCAAAAGTTGAACGAATTGAGAGAAGCTCAAAAGA
AGTTCGCTACCTACACTCAAGAACAAGTTGATAAGATTTTCAAGCAATGTGCTATTGCTGCTGC
TAAGGAAAGAATTAACTTGGCTAAGTTGGCTGTTGAAGAAACCGGTATTGGTTTGGTTGAAGAT
AAGATTATTAAGAACCACTTCGCTGCTGAATACATTTACAACAAGTACAAGAACGAAAAGACTT
GTGGTATTATTGACCACGACGATTCTTTGGGTATTACCAAGGTTGCTGAACCAATTGGTATTGT
TGCTGCTATTGTTCCAACTACTAACCCAACTTCCACCGCTATTTTCAAGTCTTTGATTTCTTTGA
AGACCAGAAACGCTATTTTCTTCTCTCCACACCCAAGAGCTAAGAAGTCTACCATTGCTGCTGC
TAAGTTGATTTTGGATGCTGCTGTTAAGGCTGGTGCTCCAAAGAACATTATTGGTTGGATTGAT
GAACCATCTATTGAATTGTCTCAAGATTTGATGTCTGAAGCTGATATTATTTTGGCTACCGGTGG
TCCATCTATGGTTAAGGCTGCTTACTCTTCTGGTAAGCCAGCTATTGGTGTTGGTGCTGGTAAC
ACCCCAGCTATTATTGATGAATCTGCTGATATTGATATGGCTGTTTCTTCCATTATTTTGTCTAA
GACTTACGACAACGGTGTTATTTGTGCTTCTGAACAATCTATTTTGGTTATGAACTCTATTTACG
AAAAGGTTAAGGAAGAATTCGTTAAGAGAGGTTCTTACATTTTGAACCAAAACGAAATTGCTAA
GATTAAGGAAACTATGTTCAAGAACGGTGCTATTAACGCTGACATTGTTGGTAAGTCTGCTTAC
ATTATTGCTAAGATGGCTGGTATTGAAGTTCCACAAACTACCAAGATTTTGATTGGTGAAGTTCA
ATCTGTTGAAAAGTCTGAATTGTTCTCTCACGAAAAGTTGTCTCCAGTTTTGGCTATGTACAAGG
TTAAGGATTTCGATGAAGCTTTGAAGAAGGCTCAAAGATTGATTGAATTGGGTGGTTCTGGTCA
CACCTCTTCTTTGTACATTGATTCTCAAAACAACAAGGATAAGGTTAAGGAATTCGGTTTGGCTA
TGAAGACTTCTAGAACCTTCATTAACATGCCATCTTCTCAAGGTGCTTCTGGTGATTTGTACAAC
TTCGCTATTGCTCCATCTTTCACTTTGGGTTGTGGTACTTGGGGTGGTAACTCTGTTTCTCAAAA
CGTTGAACCAAAGCACTTGTTGAACATTAAGTCTGTTGCTGAAAGAAGAGAAAACATGTTGTGG
TTCAAGGTTCCACAAAAGATTTACTTCAAGTACGGTTGTTTGAGATTCGCTTTGAAGGAATTGAA
GGATATGAACAAGAAGAGAGCTTTCATTGTTACCGATAAGGATTTGTTCAAGTTGGGTTACGTT
AACAAGATTACCAAGGTTTTGGATGAAATTGATATTAAGTACTCTATTTTCACCGATATTAAGTCT
GATCCAACTATTGATTCTGTTAAGAAGGGTGCTAAGGAAATGTTGAACTTCGAACCAGATACTA
TTATCTCTATTGGTGGTGGTTCTCCAATGGATGCTGCTAAGGTTATGCACTTGTTGTACGAATA
CCCAGAAGCTGAAATTGAAAACTTGGCTATTAACTTCATGGATATTAGAAAGAGAATTTGTAACT
TCCCAAAGTTGGGTACCAAGGCTATTTCTGTTGCTATTCCAACCACTGCTGGTACCGGTTCTGA
AGCTACCCCATTCGCTGTTATTACTAACGATGAAACCGGTATGAAGTACCCATTGACTTCTTAC
GAATTGACCCCAAACATGGCTATTATTGATACTGAATTGATGTTGAACATGCCAAGAAAGTTGA
CCGCTGCTACTGGTATTGATGCTTTGGTTCACGCTATTGAAGCTTACGTTTCTGTTATGGCTAC
CGATTACACTGATGAATTGGCTTTGAGAGCTATTAAGATGATTTTCAAGTACTTGCCAAGAGCTT
ACAAGAACGGTACTAACGACATTGAAGCTAGAGAAAAGATGGCTCACGCTTCTAACATTGCTG

GTATGGCTTTCGCTAACGCTTTCTTGGGTGTTTGTCACTCTATGGCTCACAAGTTGGGTGCTAT
GCACCACGTTCCACACGGTATTGCTTGTGCTGTTTTGATTGAAGAAGTTATTAAGTACAACGCT
ACCGACTGTCCAACCAAGCAAACCGCTTTCCCACAATACAAGTCTCCAAACGCTAAGAGAAAG
TACGCTGAAATTGCTGAATACTTGAACTTGAAGGGTACTTCTGATACCGAAAAGGTTACCGCTT
TGATTGAAGCTATTTCTAAGTTGAAGATTGATTTGTCTATTCCACAAAACATTTCTGCTGCTGGT
ATTAACAAGAAGGATTTCTACAACACCTTGGATAAGATGTCTGAATTGGCTTTCGATGACCAAT
GTACCACCGCTAACCCAAGATACCCATTGATTTCTGAATTGAAGGATATCTACATTAAGTCTTTC
TAA

EutE (E. coli)

ATGAACCAACAAGATATTGAACAAGTTGTTAAGGCTGTTTTGTTGAAGATGCAATCTTCTGACAC
CCCATCCGCTGCTGTTCACGAAATGGGTGTTTTCGCTTCCTTGGATGACGCTGTTGCTGCTGC
TAAGGTCGCTCAACAAGGTTTGAAGTCTGTTGCTATGAGACAATTGGCTATTGCTGCTATTAGA
GAAGCTGGTGAAAAGCACGCTAGAGATTTGGCTGAATTGGCTGTCTCTGAAACCGGTATGGGT
AGAGTTGAAGATAAGTTCGCTAAGAACGTCGCTCAAGCTAGAGGTACCCCAGGTGTTGAATGT
TTGTCTCCACAAGTTTTGACTGGTGACAACGGTTTGACCTTGATTGAAAACGCTCCATGGGGTG
TTGTTGCTTCTGTTACCCCATCCACTAACCCAGCTGCTACCGTTATTAACAACGCTATCTCTTTG
ATTGCTGCTGGTAACTCTGTCATTTTCGCTCCACACCCAGCTGCTAAGAAGGTTTCCCAAAGAG
CTATTACCTTGTTGAACCAAGCTATTGTTGCTGCTGGTGGTCCAGAAAACTTGTTGGTTACTGTT
GCTAACCCAGATATCGAAACCGCTCAAAGATTGTTCAAGTTCCCAGGTATCGGTTTGTTGGTTG
TTACCGGTGGTGAAGCTGTTGTTGAAGCTGCTAGAAAGCACACCAACAAGAGATTGATTGCTG
CTGGTGCTGGTAACCCACCAGTTGTTGTTGATGAAACCGCTGACTTGGCTAGAGCTGCTCAAT
CCATCGTCAAGGGTGCTTCTTTCGATAACAACATCATTTGTGCTGACGAAAAGGTTTTGATTGTT
GTTGATTCTGTTGCTGATGAATTGATGAGATTGATGGAAGGTCAACACGCTGTTAAGTTGACCG
CTGAACAAGCTCAACAATTGCAACCAGTTTTGTTGAAGAACATCGACGAAAGAGGTAAGGGTA
CTGTCTCTAGAGACTGGGTTGGTAGAGATGCTGGTAAGATCGCTGCTGCTATCGGTTTGAAGG
TTCCACAAGAAACCAGATTGTTGTTCGTTGAAACCACCGCTGAACACCCATTCGCTGTTACTGA
ATTGATGATGCCAGTTTTGCCAGTCGTTAGAGTCGCTAACGTTGCTGATGCTATTGCTTTGGCT
GTTAAGTTGGAAGGTGGTTGTCACCACACCGCTGCTATGCACTCTAGAAACATCGAAAACATG
AACCAAATGGCTAACGCTATTGATACCTCTATTTTCGTTAAGAACGGTCCATGTATTGCTGGTTT
GGGTTTGGGTGGTGAAGGTTGGACCACCATGACCATCACCACCCCAACCGGTGAAGGTGTTA
CCTCTGCTAGAACCTTCGTCAGATTGAGAAGATGTGTTTTGGTCGATGCTTTCAGAATTGTTTAA

IV – *^{Ca}adhE2$_{MT}$* mutation in GDY20

Sequence alignment of *^{Ca}adhE2$_{MT}$* in plasmid GDV148 (*query*) against the sequenced *^{Ca}adhE2$_{MT}$* in GDY20 (*Sbjct*). In GDY20, there is frameshift deletion of two adenosine residues in positions 1346 and 1347.

```
Query  1     ATGTTAAGAATCAGATCACTCCTAAATAATAAGCGTGCCTTTTCGTCCACAGTCAGGACA  60
             ||||||||||||||||||||||||||||||||||||||||||||||||||||||||||||
Sbjct  1     ATGTTAAGAATCAGATCACTCCTAAATAATAAGCGTGCCTTTTCGTCCACAGTCAGGACA  60

Query  61    TTGAAGGTTACCAACCAAAAGGAATTGAAGCAAAAGTTGAACGAATTGAGAGAAGCTCAA  120
             ||||||||||||||||||||||||||||||||||||||||||||||||||||||||||||
Sbjct  61    TTGAAGGTTACCAACCAAAAGGAATTGAAGCAAAAGTTGAACGAATTGAGAGAAGCTCAA  120

Query  121   AAGAAGTTCGCTACCTACACTCAAGAACAAGTTGATAAGATTTTCAAGCAATGTGCTATT  180
             ||||||||||||||||||||||||||||||||||||||||||||||||||||||||||||
Sbjct  121   AAGAAGTTCGCTACCTACACTCAAGAACAAGTTGATAAGATTTTCAAGCAATGTGCTATT  180

Query  181   GCTGCTGCTAAGGAAAGAATTAACTTGGCTAAGTTGGCTGTTGAAGAAACCGGTATTGGT  240
             ||||||||||||||||||||||||||||||||||||||||||||||||||||||||||||
Sbjct  181   GCTGCTGCTAAGGAAAGAATTAACTTGGCTAAGTTGGCTGTTGAAGAAACCGGTATTGGT  240

Query  241   TTGGTTGAAGATAAGATTATTAAGAACCACTTCGCTGCTGAATACATTTACAACAAGTAC  300
             ||||||||||||||||||||||||||||||||||||||||||||||||||||||||||||
Sbjct  241   TTGGTTGAAGATAAGATTATTAAGAACCACTTCGCTGCTGAATACATTTACAACAAGTAC  300

Query  301   AAGAACGAAAAGACTTGTGGTATTATTGACCACGACGATTCTTTGGGTATTACCAAGGTT  360
             ||||||||||||||||||||||||||||||||||||||||||||||||||||||||||||
Sbjct  301   AAGAACGAAAAGACTTGTGGTATTATTGACCACGACGATTCTTTGGGTATTACCAAGGTT  360

Query  361   GCTGAACCAATTGGTATTGTTGCTGCTATTGTTCCAACTACTAACCCAACTTCCACCGCT  420
             ||||||||||||||||||||||||||||||||||||||||||||||||||||||||||||
Sbjct  361   GCTGAACCAATTGGTATTGTTGCTGCTATTGTTCCAACTACTAACCCAACTTCCACCGCT  420

Query  421   ATTTTCAAGTCTTTGATTTCTTTGAAGACCAGAAACGCTATTTTCTTCTCTCCACACCCA  480
             ||||||||||||||||||||||||||||||||||||||||||||||||||||||||||||
Sbjct  421   ATTTTCAAGTCTTTGATTTCTTTGAAGACCAGAAACGCTATTTTCTTCTCTCCACACCCA  480

Query  481   AGAGCTAAGAAGTCTACCATTGCTGCTGCTAAGTTGATTTTGGATGCTGCTGTTAAGGCT  540
             ||||||||||||||||||||||||||||||||||||||||||||||||||||||||||||
Sbjct  481   AGAGCTAAGAAGTCTACCATTGCTGCTGCTAAGTTGATTTTGGATGCTGCTGTTAAGGCT  540

Query  541   GGTGCTCCAAAGAACATTATTGGTTGGATTGATGAACCATCTATTGAATTGTCTCAAGAT  600
             ||||||||||||||||||||||||||||||||||||||||||||||||||||||||||||
Sbjct  541   GGTGCTCCAAAGAACATTATTGGTTGGATTGATGAACCATCTATTGAATTGTCTCAAGAT  600

Query  601   TTGATGTCTGAAGCTGATATTATTTTGGCTACCGGTGGTCCATCTATGGTTAAGGCTGCT  660
             ||||||||||||||||||||||||||||||||||||||||||||||||||||||||||||
Sbjct  601   TTGATGTCTGAAGCTGATATTATTTTGGCTACCGGTGGTCCATCTATGGTTAAGGCTGCT  660

Query  661   TACTCTTCTGGTAAGCCAGCTATTGGTGTTGGTGCTGGTAACACCCCAGCTATTATTGAT  720
             ||||||||||||||||||||||||||||||||||||||||||||||||||||||||||||
Sbjct  661   TACTCTTCTGGTAAGCCAGCTATTGGTGTTGGTGCTGGTAACACCCCAGCTATTATTGAT  720

Query  721   GAATCTGCTGATATTGATATGGCTGTTTCTTCCATTATTTTGTCTAAGACTTACGACAAC  780
             ||||||||||||||||||||||||||||||||||||||||||||||||||||||||||||
Sbjct  721   GAATCTGCTGATATTGATATGGCTGTTTCTTCCATTATTTTGTCTAAGACTTACGACAAC  780

Query  781   GGTGTTATTTGTGCTTCTGAACAATCTATTTTGGTTATGAACTCTATTTACGAAAAGGTT  840
             ||||||||||||||||||||||||||||||||||||||||||||||||||||||||||||
Sbjct  781   GGTGTTATTTGTGCTTCTGAACAATCTATTTTGGTTATGAACTCTATTTACGAAAAGGTT  840

Query  841   AAGGAAGAATTCGTTAAGAGAGGTTCTTACATTTTGAACCAAAACGAAATTGCTAAGATT  900
             ||||||||||||||||||||||||||||||||||||||||||||||||||||||||||||
Sbjct  841   AAGGAAGAATTCGTTAAGAGAGGTTCTTACATTTTGAACCAAAACGAAATTGCTAAGATT  900

Query  901   AAGGAAACTATGTTCAAGAACGGTGCTATTAACGCTGACATTGTTGGTAAGTCTGCTTAC  960
             ||||||||||||||||||||||||||||||||||||||||||||||||||||||||||||
Sbjct  901   AAGGAAACTATGTTCAAGAACGGTGCTATTAACGCTGACATTGTTGGTAAGTCTGCTTAC  960

Query  961   ATTATTGCTAAGATGGCTGGTATTGAAGTTCCACAAACTACCAAGATTTTGATTGGTGAA  1020
             ||||||||||||||||||||||||||||||||||||||||||||||||||||||||||||
Sbjct  961   ATTATTGCTAAGATGGCTGGTATTGAAGTTCCACAAACTACCAAGATTTTGATTGGTGAA  1020

Query  1021  GTTCAATCTGTTGAAAAGTCTGAATTGTTCTCTCACGAAAAGTTGTCTCCAGTTTTGGCT  1080
             ||||||||||||||||||||||||||||||||||||||||||||||||||||||||||||
Sbjct  1021  GTTCAATCTGTTGAAAAGTCTGAATTGTTCTCTCACGAAAAGTTGTCTCCAGTTTTGGCT  1080

Query  1081  ATGTACAAGGTTAAGGATTTCGATGAAGCTTTGAAGAAGGCTCAAAGATTGATTGAATTG  1140
             ||||||||||||||||||||||||||||||||||||||||||||||||||||||||||||
Sbjct  1081  ATGTACAAGGTTAAGGATTTCGATGAAGCTTTGAAGAAGGCTCAAAGATTGATTGAATTG  1140

Query  1141  GGTGGTTCTGGTCACACCTCTTCTTTGTACATTGATTCTCAAAACAACAAGGATAAGGTT  1200
             ||||||||||||||||||||||||||||||||||||||||||||||||||||||||||||
Sbjct  1141  GGTGGTTCTGGTCACACCTCTTCTTTGTACATTGATTCTCAAAACAACAAGGATAAGGTT  1200

Query  1201  AAGGAATTCGGTTTGGCTATGAAGACTTCTAGAACCTTCATTAACATGCCATCTTCTCAA  1260
             ||||||||||||||||||||||||||||||||||||||||||||||||||||||||||||
Sbjct  1201  AAGGAATTCGGTTTGGCTATGAAGACTTCTAGAACCTTCATTAACATGCCATCTTCTCAA  1260

Query  1261  GGTGCTTCTGGTGATTTGTACAACTTCGCTATTGCTCCATCTTTCACTTTGGGTTGTGGT  1320
             ||||||||||||||||||||||||||||||||||||||||||||||||||||||||||||
Sbjct  1261  GGTGCTTCTGGTGATTTGTACAACTTCGCTATTGCTCCATCTTTCACTTTGGGTTGTGGT  1320

Query  1321  ACTTGGGGTGGTAACTCTGTTTCTCAAAACGTTGAACCAAAGCACTTGTTGAACATTAAG  1380
             ||||||||||||||||||||||||  ||||||||||||||||||||||||||||||||||
Sbjct  1321  ACTTGGGGTGGTAACTCTGTTTCTC--AACGTTGAACCAAAGCACTTGTTGAACATTAAG  1378

Query  1381  TCTGTTGCTGAAAGAAGAGAAAACATGTTGTGGTTCAAGGTTCCACAAAAGATTTACTTC  1440
             ||||||||||||||||||||||||||||||||||||||||||||||||||||||||||||
Sbjct  1379  TCTGTTGCTGAAAGAAGAGAAAACATGTTGTGGTTCAAGGTTCCACAAAAGATTTACTTC  1438

Query  1441  AAGTACGGTTGTTTGAGATTCGCTTTGAAGGAATTGAAGGATATGAACAAGAAGAGAGCT  1500
             ||||||||||||||||||||||||||||||||||||||||||||||||||||||||||||
Sbjct  1439  AAGTACGGTTGTTTGAGATTCGCTTTGAAGGAATTGAAGGATATGAACAAGAAGAGAGCT  1498

Query  1501  TTCATTGTTACCGATAAGGATTTGTTCAAGTTGGGTTACGTTAACAAGATTACCAAGGTT  1560
             ||||||||||||||||||||||||||||||||||||||||||||||||||||||||||||
Sbjct  1499  TTCATTGTTACCGATAAGGATTTGTTCAAGTTGGGTTACGTTAACAAGATTACCAAGGTT  1558

Query  1561  TTGGATGAAATTGATATTAAGTACTCTATTTTCACCGATATTAAGTCTGATCCAACTATT  1620
             ||||||||||||||||||||||||||||||||||||||||||||||||||||||||||||
Sbjct  1559  TTGGATGAAATTGATATTAAGTACTCTATTTTCACCGATATTAAGTCTGATCCAACTATT  1618

Query  1621  GATTCTGTTAAGAAGGGTGCTAAGGAAATGTTGAACTTCGAACCAGATACTATTATCTCT  1680
             ||||||||||||||||||||||||||||||||||||||||||||||||||||||||||||
Sbjct  1619  GATTCTGTTAAGAAGGGTGCTAAGGAAATGTTGAACTTCGAACCAGATACTATTATCTCT  1678

Query  1681  ATTGGTGGTGGTTCTCCAATGGATGCTGCTAAGGTTATGCACTTGTTGTACGAATACCCA  1740
             ||||||||||||||||||||||||||||||||||||||||||||||||||||||||||||
Sbjct  1679  ATTGGTGGTGGTTCTCCAATGGATGCTGCTAAGGTTATGCACTTGTTGTACGAATACCCA  1738

Query  1741  GAAGCTGAAATTGAAAACTTGGCTATTAACTTCATGGATATTAGAAAGAGAATTTGTAAC  1800
             ||||||||||||||||||||||||||||||||||||||||||||||||||||||||||||
Sbjct  1739  GAAGCTGAAATTGAAAACTTGGCTATTAACTTCATGGATATTAGAAAGAGAATTTGTAAC  1798

Query  1801  TTCCCAAAGTTGGGTACCAAGGCTATTTCTGTTGCTATTCCAACCACTGCTGGTACCGGT  1860
             ||||||||||||||||||||||||||||||||||||||||||||||||||||||||||||
Sbjct  1799  TTCCCAAAGTTGGGTACCAAGGCTATTTCTGTTGCTATTCCAACCACTGCTGGTACCGGT  1858

Query  1861  TCTGAAGCTACCCCATTCGCTGTTATTACTAACGATGAAACCGGTATGAAGTACCCATTG  1920
             ||||||||||||||||||||||||||||||||||||||||||||||||||||||||||||
Sbjct  1859  TCTGAAGCTACCCCATTCGCTGTTATTACTAACGATGAAACCGGTATGAAGTACCCATTG  1918

Query  1921  ACTTCTTACGAATTGACCCCAAACATGGCTATTATTGATACTGAATTGATGTTGAACATG  1980
             ||||||||||||||||||||||||||||||||||||||||||||||||||||||||||||
Sbjct  1919  ACTTCTTACGAATTGACCCCAAACATGGCTATTATTGATACTGAATTGATGTTGAACATG  1978

Query  1981  CCAAGAAAGTTGACCGCTGCTACTGGTATTGATGCTTTGGTTCACGCTATTGAAGCTTAC  2040
             ||||||||||||||||||||||||||||||||||||||||||||||||||||||||||||
Sbjct  1979  CCAAGAAAGTTGACCGCTGCTACTGGTATTGATGCTTTGGTTCACGCTATTGAAGCTTAC  2038

Query  2041  GTTTCTGTTATGGCTACCGATTACACTGATGAATTGGCTTTGAGAGCTATTAAGATGATT  2100
             ||||||||||||||||||||||||||||||||||||||||||||||||||||||||||||
Sbjct  2039  GTTTCTGTTATGGCTACCGATTACACTGATGAATTGGCTTTGAGAGCTATTAAGATGATT  2098

Query  2101  TTCAAGTACTTGCCAAGAGCTTACAAGAACGGTACTAACGACATTGAAGCTAGAGAAAAG  2160
             ||||||||||||||||||||||||||||||||||||||||||||||||||||||||||||
Sbjct  2099  TTCAAGTACTTGCCAAGAGCTTACAAGAACGGTACTAACGACATTGAAGCTAGAGAAAAG  2158

Query  2161  ATGGCTCACGCTTCTAACATTGCTGGTATGGCTTTCGCTAACGCTTTCTTGGGTGTTTGT  2220
             ||||||||||||||||||||||||||||||||||||||||||||||||||||||||||||
Sbjct  2159  ATGGCTCACGCTTCTAACATTGCTGGTATGGCTTTCGCTAACGCTTTCTTGGGTGTTTGT  2218

Query  2221  CACTCTATGGCTCACAAGTTGGGTGCTATGCACCACGTTCCACACGGTATTGCTTGTGCT  2280
             ||||||||||||||||||||||||||||||||||||||||||||||||||||||||||||
Sbjct  2219  CACTCTATGGCTCACAAGTTGGGTGCTATGCACCACGTTCCACACGGTATTGCTTGTGCT  2278

Query  2281  GTTTTGATTGAAGAAGTTATTAAGTACAACGCTACCGACTGTCCAACCAAGCAAACCGCT  2340
             ||||||||||||||||||||||||||||||||||||||||||||||||||||||||||||
Sbjct  2279  GTTTTGATTGAAGAAGTTATTAAGTACAACGCTACCGACTGTCCAACCAAGCAAACCGCT  2338

Query  2341  TTCCCACAATACAAGTCTCCAAACGCTAAGAGAAAGTACGCTGAAATTGCTGAATACTTG  2400
             ||||||||||||||||||||||||||||||||||||||||||||||||||||||||||||
Sbjct  2339  TTCCCACAATACAAGTCTCCAAACGCTAAGAGAAAGTACGCTGAAATTGCTGAATACTTG  2398

Query  2401  AACTTGAAGGGTACTTCTGATACCGAAAAGGTTACCGCTTTGATTGAAGCTATTTCTAAG  2460
             ||||||||||||||||||||||||||||||||||||||||||||||||||||||||||||
Sbjct  2399  AACTTGAAGGGTACTTCTGATACCGAAAAGGTTACCGCTTTGATTGAAGCTATTTCTAAG  2458

Query  2461  TTGAAGATTGATTTGTCTATTCCACAAAACATTTCTGCTGCTGGTATTAACAAGAAGGAT  2520
             ||||||||||||||||||||||||||||||||||||||||||||||||||||||||||||
Sbjct  2459  TTGAAGATTGATTTGTCTATTCCACAAAACATTTCTGCTGCTGGTATTAACAAGAAGGAT  2518

Query  2521  TTCTACAACACCTTGGATAAGATGTCTGAATTGGCTTTCGATGACCAATGTACCACCGCT  2580
             ||||||||||||||||||||||||||||||||||||||||||||||||||||||||||||
Sbjct  2519  TTCTACAACACCTTGGATAAGATGTCTGAATTGGCTTTCGATGACCAATGTACCACCGCT  2578

Query  2581  AACCCAAGATACCCATTGATTTCTGAATTGAAGGATATCTACATTAAGTCTTTCTAA  2637
             ||||||||||||||||||||||||||||||||||||||||||||||||||||||||
Sbjct  2579  AACCCAAGATACCCATTGATTTCTGAATTGAAGGATATCTACATTAAGTCTTTCTAA  2635
```

V – GC-MS Chromatogram

GC chromatogram of strains CEN.PK2-1C **(A)**, GDY2.1 **(B)** and GDY15.1 **(C)** expressing $^{Km}EAT1_{MIT}$ (GDV156), $^{Km}EAT1_{CYT}$ (GDV157), and the empty vector control (EV). Ethyl acetate (EtAc, 1.93 min), 1-butanol (ButOH, 2. 34min), isoamyl alcohol (IsOH, 3.31 min), Iso-butylacetate (IsButAc, 4.15 min) and Isoamyl acetate (IsAc, 6.86 min). 25 mg/L of 1-butanol were used as normalization standard in each sample.

(A)

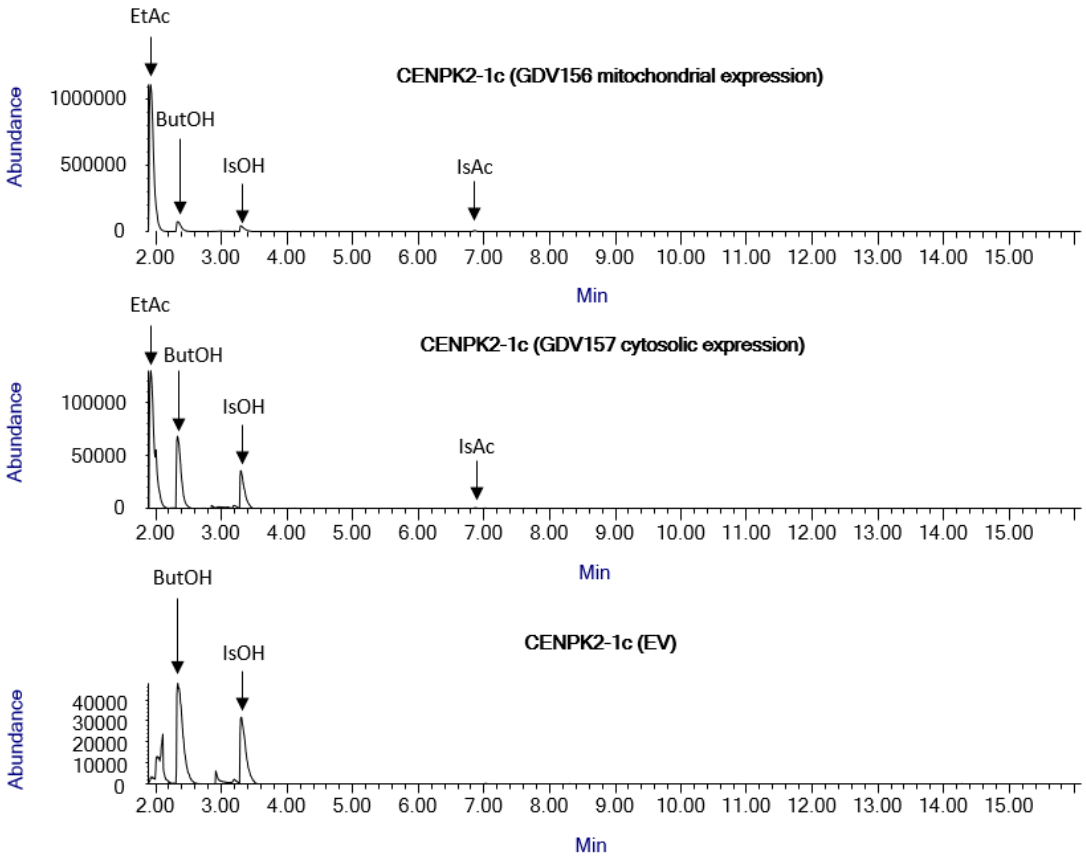

(B)

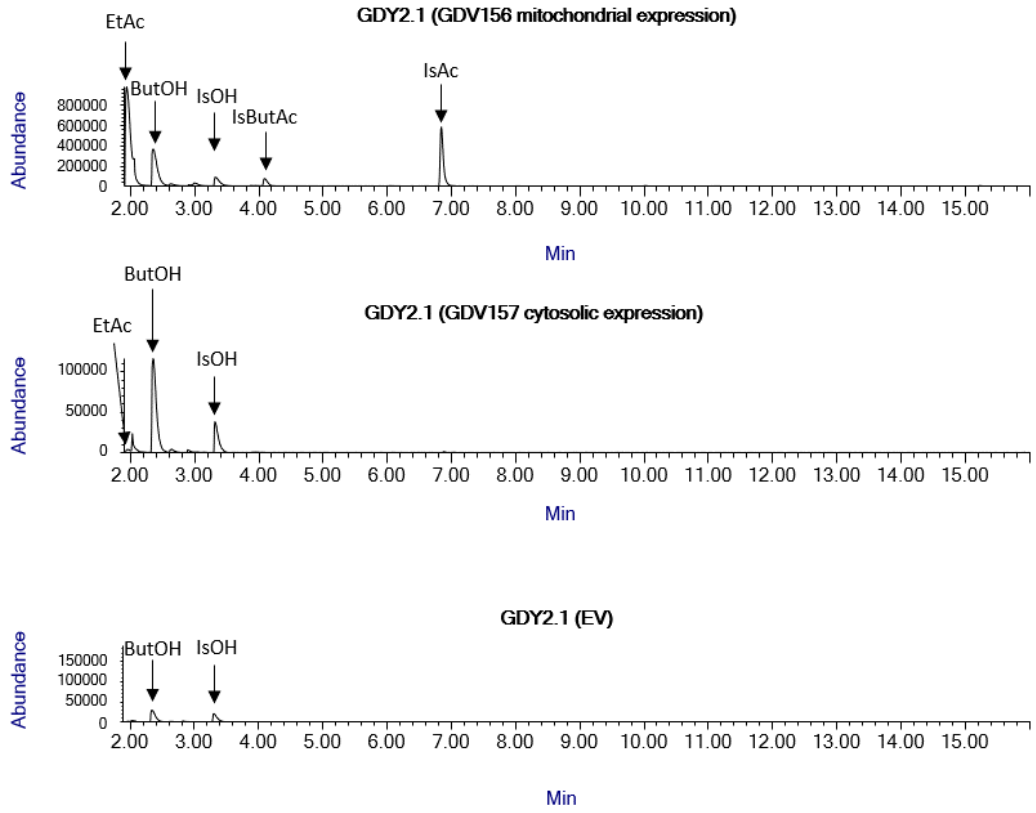
GDY2.1 (GDV156 mitochondrial expression)
EtAc
ButOH
IsOH
IsButAc
IsAc
Abundance
Min
GDY2.1 (GDV157 cytosolic expression)
GDY2.1 (EV)

(C)

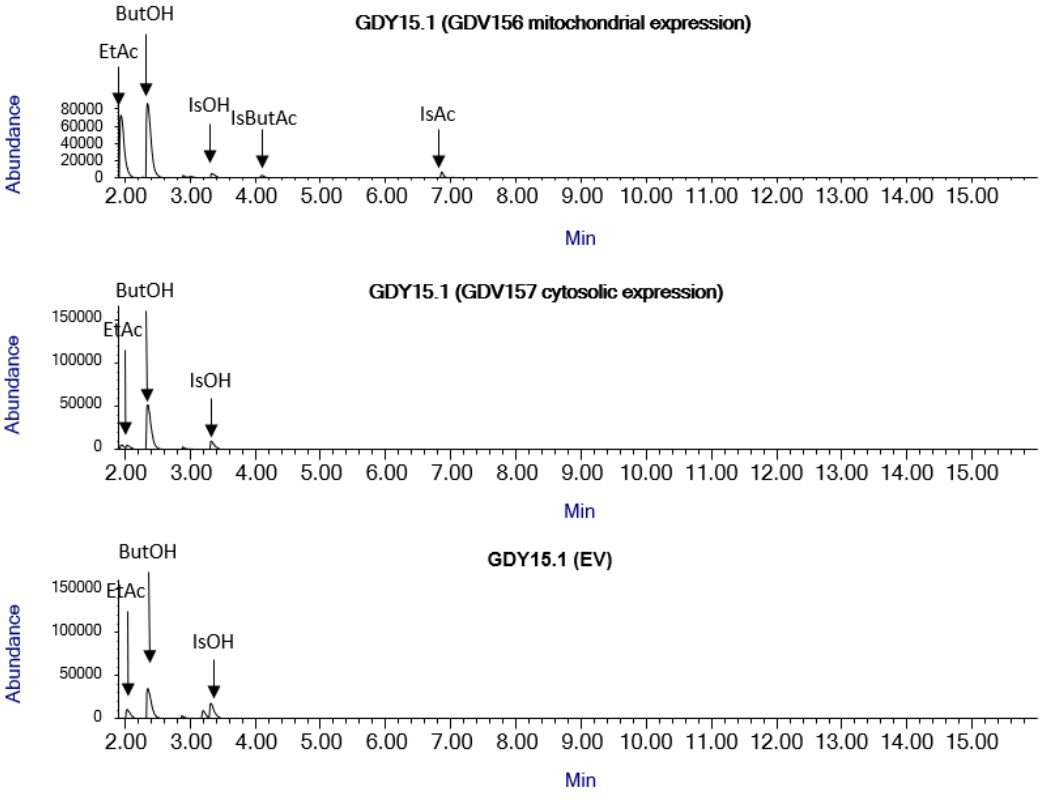
GDY15.1 (GDV156 mitochondrial expression)
ButOH
EtAc
IsOH
IsButAc
IsAc
Abundance
Min
GDY15.1 (GDV157 cytosolic expression)
GDY15.1 (EV)